

ADVANCED AIRSPACE

Free Flight

Flexible Super Sectors

Air/Ground Integration

Other Modes

Air/Ground Operations Centres

Completely Autonomous Systems

Collaborative Decision Making

Auto-Controller

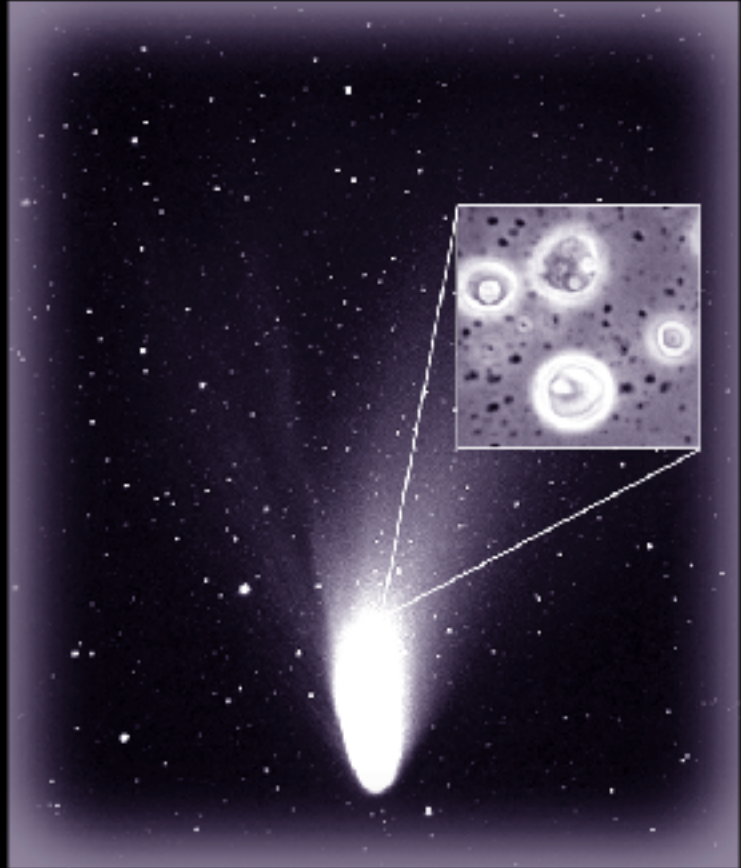
Unified Traffic Flow Management

Supervisory Manager Controller

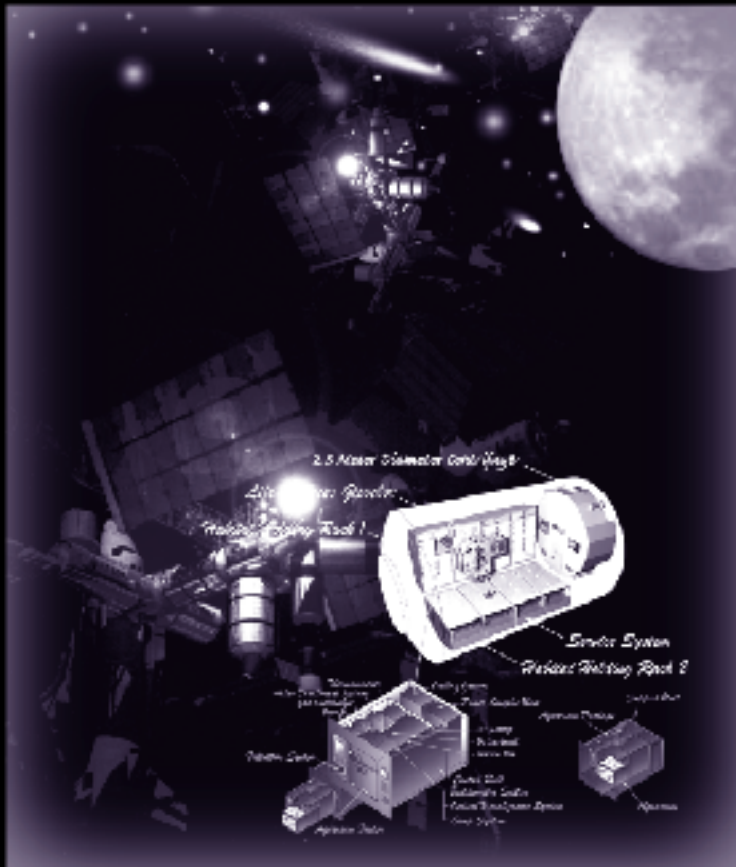
Active Exception Controller

Data Link

Voice



RESEARCH & TECHNOLOGY
NASA AMES RESEARCH CENTER



RESEARCH & TECHNOLOGY
NASA AMES RESEARCH CENTER

2000



NATIONAL AERONAUTICS AND SPACE ADMINISTRATION
AMES RESEARCH CENTER • MOFFETT FIELD, CALIFORNIA

NASA/TM-2001-210935

Notice

The use of trade names and manufacturers in this document does not constitute an official endorsement of such products or manufacturers, either expressed or implied, by the National Aeronautics and Space Administration.

Available from:

NASA Center for AeroSpace Information
7121 Standard Drive
Hanover, MD 21076-1320
(301) 621-0390

National Technical Information Service
5285 Port Royal Road
Springfield, VA 22161
(703) 487-4650

Foreword

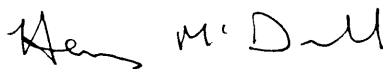
This report highlights the research accomplished during fiscal year 2000 by Ames Research Center scientists and engineers. The work is divided into accomplishments that support four of NASA's Strategic Enterprises: Aerospace Technology, Space Science, Biological and Physical Research, and Earth Science. The key purpose of this report is to communicate information to our stakeholders about the scope and diversity of Ames' mission and the nature of Ames research and technology activities.

Ames Research Center is making significant contributions to the Aerospace Technology Enterprise goals to revolutionize aviation, advance space transportation, pioneer technology innovation, and to commercialize technology. Ames has the Agency's lead role for basic research in Aviation Operations Systems, Information Systems Technology, and Rotorcraft. Ames is also the Lead Center for focused programs in Aviation System Capacity and High-Performance Computing and Communications. To perform these leadership roles, Ames maintains core competencies in information technology, nanotechnology, biotechnology, aerospace operation systems, and thermal protection systems technology.

Ames is recognized as a world leader in astrobiology, the study of life in the universe and of the chemical and physical forces and adaptations that influence life's origin, evolution, and destiny. Key areas of research include life in extreme environments, microbial mats, and the mechanisms of the origin of living systems. As NASA's lead in airborne astronomy, Ames astrophysicists carry out research in such areas as interstellar photochemistry, star and planetary formation, and the search for extrasolar planets. Ames supports the Office of Earth Science (OES) by conducting research in biogeochemical cycling, ecosystem dynamics, and the chemical and transport processes that determine atmospheric composition, dynamics, and climate. Ames' Airborne Sensor Facility provides remote sensing support for OES investigations, and for calibration and validation studies of the Earth Observing System (EOS). Ames supports the Office of Biological and Physical Research (OBPR) Enterprise by managing spaceflight programs, by operating unique ground facilities such as centrifuges, and by developing advanced biomedical technologies. Work continues on developing life-support capabilities for long-duration travel and habitation on other planets, as well as equipment to operate safely and effectively in microgravity.

Ames is also the Agency's Center of Excellence for Information Technology. The three cornerstones of Information Technology research at Ames are automated reasoning for autonomous systems, human-centered computing, and high performance computing and networking. The mission critical capabilities enabled by NASA's three cornerstones of Information Technology span all of NASA's strategic enterprises.

For further information on Ames' research and technology projects, please contact the person designated as the point of contact at the end of each article. For further information about the report itself, contact Dr. Stephanie Langhoff, Chief Scientist, Mail Stop 230-3, NASA Ames Research Center, Moffett Field, CA 94035. An electronic version of this report is available on the Ames home page.



Dr. Henry McDonald
Director, Ames Research Center



Aerospace Technology Enterprise

Overview	1
-----------------------	----------

REVOLUTIONIZE AVIATION

Future Air Traffic Management Concepts Evaluation Tool (FACET)	5
---	----------

Banavar Sridhar

Full-Immersion Air Traffic Control Tower Simulation	7
--	----------

Nancy S. Dorigi, Jim McClenahan

Direct-To Tool for En Route Controllers	8
--	----------

Heinz Erzberger, Dave McNally

Multi-Center Traffic Management Advisor	10
--	-----------

Tom Davis

Mitigating Runway Incursions with Cockpit Display Technology	11
---	-----------

Becky L. Hooey, David C. Foyle, Anthony D. Andre

Air Ground Integration Study	13
---	-----------

Sandy Lozito, Margaret-Anne Mackintosh, Karen DiMeo, Parimal Kopardekar

Enabling Cockpit-Based Self-Separation	15
---	-----------

Walter W. Johnson and Vernol Battiste

Aviation Performance Measuring System	17
--	-----------

Thomas R. Chidester

Performance Data Analysis and Reporting System	19
---	-----------

Irving C. Statler

New Contextual Data-Mining Technologies	22
--	-----------

Michael W. McGreevy

Alternative Perspectives on Traffic Risk	23
---	-----------

Jeannie Davison, Judith Orasanu

Evaluation of In-flight Alertness Management Technology	25
--	-----------

Melissa M. Mallis

Evaluating Stereo Displays for Manual Control	26
--	-----------

Mary K. Kaiser and Barbara Sweet

Active Final Approach Spacing Tool Development	28
---	-----------

John E. Robinson

An Analysis of the Radar Reflectivity of Aircraft Wake Vortices	29
--	-----------

Karim R. Shariff

Uncertainties in Prediction of Wake-Vortex Locations	30
---	-----------

Vernon Rossow

Remote Tower Sensor System	31
---	-----------

Yuri Gawdiak, Richard Papasin, Chris Leidich, David Maluf, Kevin Bass, Hoan Mai, Chris Berg, Peter Tran



Boeing 777 Landing Gear Noise Study	32
<i>Paul Soderman, Clif Horne</i>	
Joint Shipboard Helicopter Integration Process	34
<i>Dean Giovannetti</i>	
Intelligent Neural Flight and Propulsion Control System	36
<i>John Kaneshige, Karen Gundy-Burlet</i>	
Large Rotor Research Program	37
<i>Thomas R. Norman, Patrick M. Shinoda, Stephen A. Jacklin</i>	
V-22 Tilt Rotor Aeroacoustics	38
<i>Megan S. McCluer, Jeff L. Johnson, Larry A. Young</i>	
Tilt Rotor Descent Aerodynamics	40
<i>Mark D. Betzina</i>	
A Comparison of Transmission Vibration Responses from OH-58C and AH-1 Helicopters	41
<i>Edward M. Huff, Irem Y. Tumer, Marianne Mosher</i>	
Wind Turbine Calculations and Validation	43
<i>Robert M. Kufeld</i>	
Remote Access and Analysis of Aeronautics Data	44
<i>David Korsmeyer, Joan Walton</i>	
Remote Large Data Set Visualization	46
<i>David Ellsworth</i>	
Computational Simulation of High-Lift Wind-Tunnel Test	48
<i>Stuart E. Rogers</i>	
Parametric Powered-Lift Navier–Stokes Computations	50
<i>Neal M. Chaderjian, Scott Murman, Shishir Pandya, Jasim Ahmad</i>	

A D V A N C E S P A C E T R A N S P O R T A T I O N

Computational Fluid Dynamic Simulation of Space Shuttle Orbiter During Contingency Abort Maneuvers	52
<i>P. Papadopoulos, D. Prabhu, M. Wright, C. Davies, R. McDaniel, J. Brown, E. Venkatapathy, P. Wercinski</i>	
Automated Computational Fluid Dynamics for Large Test Matrices	54
<i>Michael Aftosmis, Marsha Berger, Shishir Pandya, John Melton</i>	
Highly Maneuverable Crew Transfer Vehicle Design Study	56
<i>James Reuther, David Kinney</i>	
Slender Hypersonic Aerothermodynamic Research Probe Ballistic Flight Experiment B2 .	58
<i>Don Ellerby, Sylvia Johnson</i>	
Shuttle Materials Resistant to Micrometeorite Orbital Debris	60
<i>Daniel B. Leiser, David A. Stewart</i>	
Subsurface Microsensors for Assisted Recertification of Thermal Protection Systems	63
<i>Frank S. Milos</i>	



ILab—Parameter Study Tool and IPG Portal	65
<i>Maurice Yarrow</i>	
Multithreading for Dynamic Unstructured Grid Applications.....	66
<i>Rupak Biswas</i>	
Overset Grid-Generation Software Package	68
<i>William Chan, Stuart Rogers</i>	
Multi-Level Parallel Computations of Unsteady Turbopump Flows.....	70
<i>Cetin Kiris, Dochan Kwak</i>	

P I O N E E R T E C H N O L O G Y I N N O V A T I O N

Flight Control Design for an Unmanned Rotorcraft Program with a Rapid Development Schedule	72
<i>Jason D. Colbourne, Mark B. Tischler</i>	
Vertical Lift Technology and NASA Revolutionary Concepts Program	73
<i>Larry A. Young, John F. Madden, Khanh Q. Nguyen</i>	
Mars Exploration Using Vertical-Lift Planetary Aerial Vehicles	75
<i>Larry A. Young, Michael R. Derby, Edwin W. Aiken</i>	
Ultrafast Beam Self-Switching by Using Coupled VCSELs	76
<i>Peter M. Goorjian, Cun-Zheng Ning</i>	
Multiscale Large-Eddy Simulation	78
<i>Alan A. Wray</i>	
Unstructured Large-Eddy Simulation Code for Simulation of Reacting Flows in Complex Geometries	79
<i>K. Mahesh, G. Constantinescu, S. Apte, G. Iaccarino, P. Moin</i>	
Physics and Models for Optoelectronics Simulation	80
<i>J. Li, S. H. Cheung, C. Z. Ning</i>	
Quantum Electronic Device Simulation in Two-Dimensions	82
<i>A. Svizhenko, M. P. Anantram, T. R. Govindan</i>	
Genetic Algorithm Aerodynamic Shape Optimization	83
<i>Terry L. Holst, Thomas H. Pulliam</i>	
Contributors to Three-Dimensional Perception of Sound	84
<i>Durand R. Begault, Elizabeth M. Wenzel</i>	
Bioelectric Keyboard and Joystick for Computer Control	86
<i>Kevin Wheeler, Chuck Jorgensen</i>	
Center for Turbulence Research: 2000 Summer Program	87
<i>P. Moin, N. N. Mansour, W. C. Reynolds</i>	
The Effects of Turbulence on Phytoplankton	88
<i>S. Ghosal, M. Rogers, A. Wray</i>	

Space Science Enterprise

Overview 91

ASTROPHYSICS

Identifying Polycyclic Aromatic Hydrocarbons in Space 95
Jesse Bregman, Pasquale Temi

The AIRES Far-Infrared Detector Array 96
Edwin Erickson, Jessie Dotson, Jam Farhoomand, Christopher Mason

The World’s Largest Grating 97
Michael R. Haas, James A. Baltz, Edwin F. Erickson, Emmett I. Quigley, David C. Scimeca

The SOFIA Water-Vapor Monitor 99
Thomas L. Roellig, Robert Cooper, Brian Shiroyama, Regina Flores, Lunming Yuen, Allan Meyer

New Interstellar Simulation Chamber Cavity Ring-Down Spectroscopy of
Interstellar Organic Materials 100
Farid Salama, Ludovic Biennier, Robert Walker, Lou Allamandola, Jim Scherer, Anthony O’Keefe

SPACE TECHNOLOGY

Carbon Nanotube Deposition and Growth Technique 102
Lance Delzeit

Low-Temperature Multiplexing Readouts for Airborne Astronomy 103
Jam Farhoomand

Guide Star Telescope Detector Assembly for Gravity Probe-B 104
John H. Goebel

Lightweight, High-Efficiency Pulse Tube Cryocooler 106
Peter Kittel, Louis J. Salerno

Protein Nanotechnology 107
Jonathan Trent

PLANETARY SCIENCE

The Radiative Signature of Europa Ice 109
Galina M. Chaban, Timothy J. Lee, Winifred M. Huo

Particle-Gas Dynamics in the Protoplanetary Nebula 110
J. N. Cuzzi, R. C. Hogan, A. R. Dobrovolskis

Planetary Rings 111
J. N. Cuzzi, I. Mosqueira, M. Showalter, F. Poulet

Vortex Evolution in a Protoplanetary Disk	113
<i>Sanford Davis</i>	
Liquid Water on Present-Day Mars?	115
<i>Robert M. Haberle</i>	
Measurement of Meteor Impact Experiments Using Three-Component Particle Image Velocimetry	116
<i>James T. Heineck, Peter H. Schultz</i>	
The Center for Star Formation Studies	118
<i>D. Hollenbach, K. R. Bell, G. Laughlin</i>	
The Formation and Dynamics of Planetary Systems	119
<i>Gregory Laughlin</i>	
Stability of Upsilon Andromedae's Planetary System	120
<i>Jack J. Lissauer, Eugenio Rivera</i>	
The Organic Refractory Material in the Diffuse Interstellar Medium: Mid-Infrared Spectroscopic Constraints	121
<i>Yvonne J. Pendleton, Louis J. Allamandola</i>	
Theoretical Predictions of the Opacity of Methane	122
<i>David Schwenke</i>	
Cratering Rates on Synchronously Rotating Satellites	123
<i>Kevin Zahnle, Paul Schenk</i>	
 E X O B I O L O G Y	
A Greenhouse Co-Laboratory	124
<i>Brad Bebout, Richard Keller</i>	
CHEMIN: A Mineralogical Instrument for Mars Exploration	126
<i>David F. Blake</i>	
Sugar-Related Compounds in Meteorites	127
<i>George Cooper, Novelle Kimmich, Josh Sarinana, Katrina Brabham, Laurence Garrel, Warren Belisle</i>	
Effects of Disturbance on Microbial Communities	129
<i>Ken Cullings</i>	
Structure and Functions of Protocells	130
<i>Andrew Pohorille, Michael A. Wilson</i>	
Microbial Ecosystem Structure	132
<i>Lee Prufert-Bebout</i>	
Ringdown Cavity for Isotopic Ratio Measurements of Carbon and Oxygen	133
<i>Todd Sauke, Joe Becker</i>	
Prebiotic Peptide Synthesis	134
<i>Arthur L. Weber</i>	

Biological and Physical Research Enterprise

Overview 137

FUNDAMENTAL SPACE BIOLOGY

Dietary Salt Sensitivity and Bone in a Spaceflight Model 139
Sara B. Arnaud

Effect of Age and Activity Level on Bone Mass and Distribution 140
Tammy Cleek, Robert Whalen

BIOASTRONAUTICS RESEARCH

NASA Virtual GloveboX (VGX): Advanced Astronaut Training and Simulation System
for the International Space Station 142
Jeffrey D. Smith, Richard Boyle

ADVANCED LIFE SUPPORT

Advanced Life Support Power Reduction 144
Cory K. Finn

Solid-State Compressor for Space Station Oxygen Recovery 146
John Finn

Development of a Waste Processing Incinerator for Life Support 148
John W. Fisher

Development of the Vapor Phase Catalytic Ammonia
Removal Process 149
Michael Flynn, Bruce Borchers

Earth Science Enterprise

Overview 153

ECOSYSTEM SCIENCE AND TECHNOLOGY BRANCH

Automated Processing of Terrestrial Satellite Imagery Using Bayesian Methods 156
Chris Hlavka, Peter Cheeseman, John Stutz, Robert Slye

Biomass Burning Losses of Carbon Estimated from Ecosystem Modeling and Satellite
Data Analysis for the Brazilian Amazon Region 158
Christopher Potter, Vanessa Brooks Genovese, Steven Klooster, Matthew Bobo, Alicia Torregrosa

New Technology Developed and Tested for Disaster Management and Mitigation 158
James Brass, Vincent Ambrosia, Robert Higgins

VINTAGE: Viticultural Integration of NASA Technologies for Assessment of the Grapevine Environment	159
---	------------

L. Johnson, V. Vanderbilt, M. Bobo

ATMOSPHERIC CHEMISTRY AND DYNAMICS BRANCH

Airborne Tracking Sunphotometry	161
--	------------

*Philip B. Russell, Beat Schmid, John M. Livingston, Jens Redemann, Robert Bergstrom,
James Eilers, Richard Kolyer, Duane Allen, Dawn McIntosh, Jill Bauman*

Analysis of Polar Stratospheric Clouds from Advanced Very-High-Resolution Radiometer Measurements	163
--	------------

Kathy L. Pagan, R. Stephen Hipskind

Asian Pollution at the California Coast, and African Plumes in the Mid-Pacific: High Resolution CO Simulations Reveal Unexpectedly Long Transports	165
---	------------

Robert B. Chatfield

Dominant Presence of Oxygenated Organic Species in the Remote Southern Pacific Troposphere	168
---	------------

H. Singh and Y. Chen

ER-2 and DC-8 Meteorological Measurement Systems	168
---	------------

*T. Paul Bui, Stuart W. Bowen, Cecilia Chang, Jonathan Dean-Day, Leonhard Pfister,
Antonio A. Trias*

Open Path Diode Laser Hygrometer (DLH) Instrument for Tropospheric and Stratospheric Water Vapor Studies	169
---	------------

James R. Podolske

The Argus Instrument.....	170
----------------------------------	------------

Max Loewenstein, Hansjürg Jost, James Podolske, Jeff Greenblatt

Transport and Meteorological Analysis	172
--	------------

Leonhard Pfister, Henry B. Selkirk, Marion J. Legg

Hypervalent Chlorine Nitrates: Implications for Stratospheric Chlorine Chemistry	174
---	------------

Timothy J. Lee

ATMOSPHERIC PHYSICS BRANCH

Aerosol Radiative Forcing of Asian Continental Outflow	176
---	------------

Rudolf F. Poeschel and Anthony W. Strawa

Analysis of SOLVE Observations of PSCs and Implications for the Evolution of the Arctic Vortex	177
---	------------

Katja Drdla

Global Aerosol Climatology Project	178
---	------------

Peter Pilewskie, Warren Gore, and Larry Pezzolo

In-Situ Measurement of Particle Extinction	179
---	------------

Anthony W. Strawa and Rudolf F. Poeschel

The Runaway Greenhouse Effect on Earth and Other Planets	180
---	------------

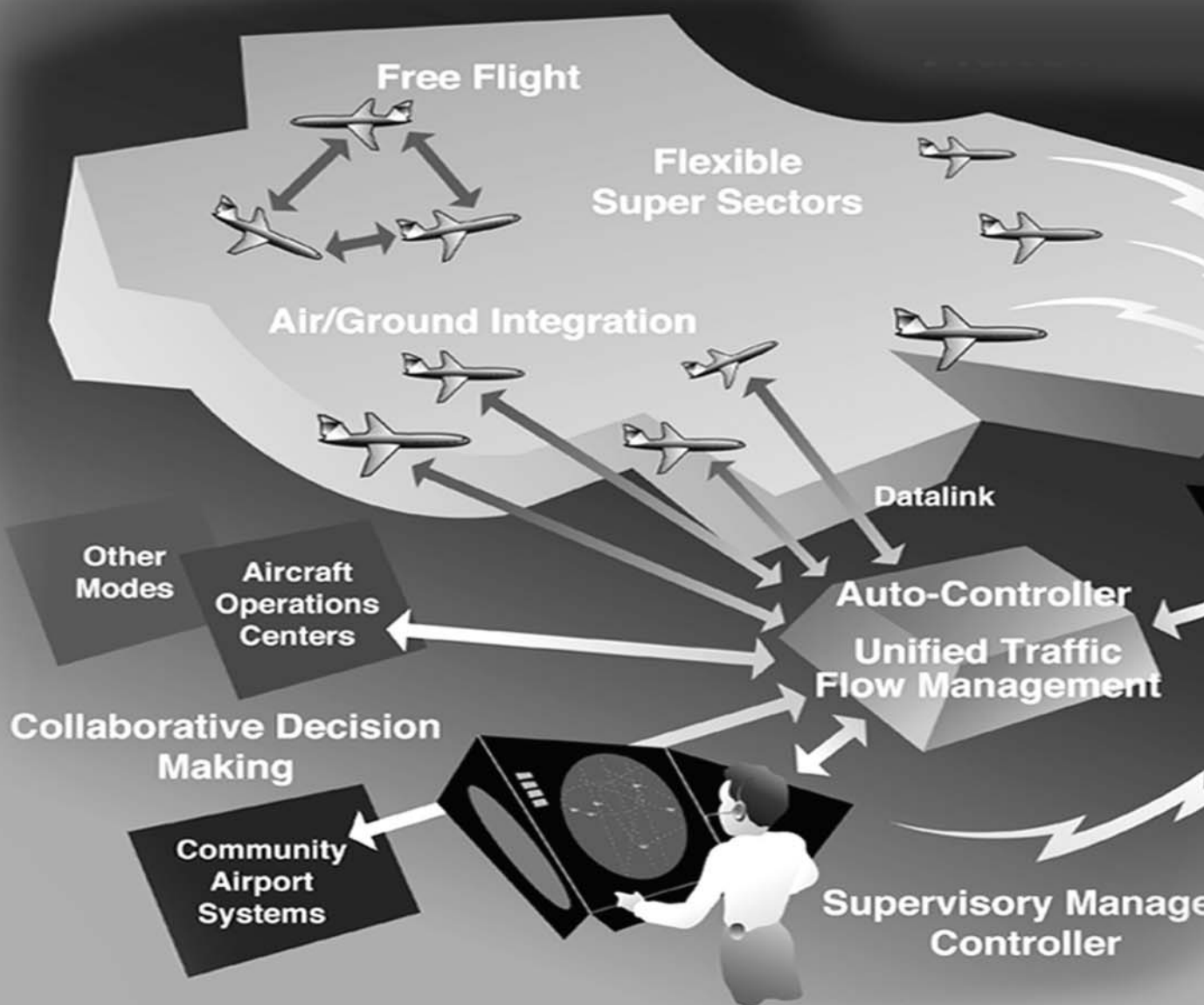
Maura Rabbette, Peter Pilewskie, Christopher McKay, and Richard Young

Three-Dimensional Simulations of Polar Stratospheric Cloud Formation	182
---	------------

Eric Jensen



Aerospace Technology Enterprise





Overview

NASA's mission for Aerospace Technology (AT) Enterprise is to pioneer the identification, development, application, and commercialization of high-payoff aeronautics and space transportation technologies. The Enterprise's research and technology programs promote economic growth and contribute to national security through advances that will lead to a safe and efficient national aviation system, affordable and reliable space transportation, and improved information management systems.

Research and development conducted by the AT Enterprise is led by individual NASA Research Centers according to primary roles and core competencies. Ames Research Center (ARC) utilizes its core competencies and its unique expertise areas to lead research and technology development activities to achieve the AT Enterprise goals, which are to

- Revolutionize Aviation: Enable a safe and environmentally friendly expansion of aviation
- Advance Space Transportation: Create a safe, affordable highway through the air and into space
- Pioneer Technology Innovation: Enable a revolution in aerospace systems
- Commercialize Technology: Extend the benefit of NASA's research and technology

The AT Enterprise manages through a carefully defined set of technology areas that are aligned with designated Center Missions. Lead Centers have the responsibility to manage the implementation and execution phases of technology programs. In order to achieve this mission, NASA has designated Ames Research

Center as the Center of Excellence for Information Technology and has delegated to Ames the lead role for basic research in Aviation Operations Systems, Information Systems Technology, and Rotorcraft. Ames is also the NASA Lead Center for focused programs in Aviation System Capacity and High-Performance Computing and Communications. To perform these leadership roles, Ames maintains Agency leads in the core competencies of information technology, biotechnology, nanotechnology, and aerospace operations systems, with unique expertise areas in rotorcraft and thermal protection systems.

The plans and goals of the AT Enterprise directly support national policies in both aeronautics and space; those policies are documented in “Goals for a National Partnership in Aeronautics Research and Technology” and the “National Space Transportation Policy,” respectively. The following paragraphs highlight Ames Research Center’s accomplishments in FY01 toward achieving the goals of the Enterprise.

Revolutionize Aviation

Air transportation has become an essential component of the economic progress of the United States. Efficient aviation operations assist in domestic industrial progress and help U.S. businesses to compete in the global marketplace. Aviation products are also a major contributor to a positive U.S. industrial balance of trade. Projections linked to world economic growth suggest that air travel demand will triple over the next 20 years. To preserve the Nation’s economic health and the welfare of the traveling public, NASA must provide technology advances for safer, cleaner, quieter, and more affordable air travel. Ames has unsurpassed expertise in key disciplines

that are requisite to addressing these challenges. Those disciplines include human-centered air traffic management automation tools, innovative rotorcraft and short takeoff vehicles, integrated design-automation tools, and technologies for managing and communicating information on every level. Ames maintains key national facilities that are crucial for performing the basic and applied research needed to support the U.S. aerospace industry. These efforts are all part of Ames’ contribution to increased safety, reduced noise, increased capacity, and increased mobility objectives.

Airlines and businesses lose billions of dollars annually from delays and lost productivity owing to weather and traffic congestion in the current airspace system. Under the Aviation System Capacity program, Ames has developed air traffic management decision-support tools such as the Active Final Approach Spacing Tool (aFAST) component of the Center/ TRACON Automation System (CTAS). The success of the CTAS system has led to widespread FAA acceptance of the system including plans to field CTAS at numerous major airports across the country. During FY00, the implementation of these tools was continued at several U.S. sites under the FAA’s “Free Flight Phase 1” program. The Direct-To Tool for En Route Controllers received rave reviews after airport tests. The predictions, analyses, and measurements of wake-vortex locations trailing aircraft have been advanced through a number of different approaches. The unique suite of tools that Ames offers was expanded this year with the increased use of Future Flight Central, a simulated Aircraft Control Tower used by airports to study and evaluate operational concepts. Information technology advancements were applied to these challenges through remote large data-set visualization, remote access and analysis of aeronautical data, and

advancing computations for wind tunnel test and data analysis.

While increasing aviation system capacity and affordability, Ames is improving flight safety with innovative research in new aircraft crew-station designs and display systems and human-centered air traffic controller station design. In addition, advanced neural network control systems promise the ability to autonomously reconfigure a vehicle so that it can survive the failure of virtually any of its systems. An example of this reconfiguration capability was flight tested in conjunction with the Dryden Flight Research Center.

A major challenge to deploying rotorcraft vehicles to alleviate air traffic congestion is noise abatement. Ames projects are providing revolutionary technology advances in aero-acoustics including higher harmonic control (HHC) for blade-vortex interaction noise reduction, phased microphone array technology, and development of a Tilt Rotor Aero-acoustic Model (TRAM). Some early results indicate the possibility of reducing noise from the rotor by a factor of 4 at certain frequencies through the use of HHC. Noise from aircraft landing gear has also been analyzed this year, leading to similar opportunities for noise reduction.

Advance Space Transportation

Low-cost space access is key to realizing the commercial potential of space and to greatly expanding space research and exploration. Through integration of aviation technologies and flight operation principles with commercial launch vehicles, a tenfold reduction in the cost of placing payloads in low-Earth orbit is anticipated within the next decade. High reliability and rapid turnaround are the first steps to increased confidence in delivering payloads on time with fewer ground crews.

NASA has initiated research on a broad spectrum of technology advancements that have the potential to reduce costs well beyond the initial reusable launch vehicle goals. Involved are new technologies and the integration of aeronautical principles such as air-breathing propulsion and advanced structures. This will enable a cost-to-orbit measured in hundreds, not thousands, of dollars per pound. Additional innovative work in interplanetary spacecraft thermal protection and autonomous vehicle systems promises to decrease the mass of interplanetary spacecraft while dramatically improving their reliability and performance.

Ames is developing new thermal protection systems that will enable radical improvements in vehicle entry performance. If forced to de-orbit in an emergency, current spacecraft, such as the space shuttle, have very limited cross-range capability; consequently, the crew has very few available emergency landing sites. Dramatic improvements in thermal protection technology, such as the materials to enable the use of sharp leading edges, will allow radically different aerodynamic shapes that will lead to dramatic improvements in cross-range capability. A flight experiment of some of these materials was conducted, and is yielding data that will improve our understanding of the ways in which these new materials must be developed and applied to aerospace vehicles. Full vehicle systems analysis has been performed to measure the improved safety that can be achieved given increased cross-range. Advanced micro-sensor technology and intelligent vehicle health management research will provide order-of-magnitude decreases in the cost and time required to inspect and refurbish reusable launch vehicles. These Ames technologies are at the heart of system-wide improvements in the launch-to-low-Earth-orbit space transportation market.

Aviation and space transportation have been exciting and challenging areas of scientific and engineering endeavor since their inception. The basic aerospace paradigm is shifting from large hardware developments to information-based design and data system management. As NASA's Center of Excellence for Information Technology, Ames Research Center's contribution will continue to grow throughout the remainder of this century and into the next. Specific accomplishments this year include work in advancing grid-generation tools and applications.

Pioneer Technology Innovation

NASA's charter is to explore high-risk technology areas that can revolutionize aerospace systems and create new markets for U.S. industry. The technology challenges for NASA include eliminating the barriers to affordable and environmentally friendly high-speed travel, expanding general aviation, and accelerating the application of technology advances to increase design confidence and decrease design cycle time.

Next-generation design tools will revolutionize the aviation industry. The impact will benefit all four AT Enterprise goals, contributing to every technology objective. Ames' aerospace and information technology research programs are developing aerospace-vehicle design tools

that integrate the design system with performance analysis and high-accuracy computational and wind tunnel performance testing. These Ames-developed systems have demonstrated order-of-magnitude improvements in the time required to develop and validate a successful design. Research at Ames in information technology will elevate the power of computing tools to artificial domain experts through application of fuzzy logic, neural networks, and other new artificial intelligence methods. New tools will integrate multidisciplinary product teams, linking design, operations, and training databases to dramatically cut design cycle times and improve operational efficiency. Ames' accomplishments include applying neural networks and genetic algorithms for real-time reconfiguration of integrated flight controls to alleviate system failure events, genetic algorithms for aerodynamic shape optimization, and development of flight controls for unmanned rotorcraft. Innovation in vertical-lift technologies, and conceptual development of the application of vertical-lift vehicles for planetary exploration progressed this year. Work is under way to identify and understand the factors that contribute to the three-dimensional perception of sound. Additionally, in FY00 Ames made significant strides in the development and application of nanotechnology, including demonstrating the ability to manufacture carbon nanotubes.

REVOLUTIONIZE AVIATION

Future Air Traffic Management Concepts Evaluation Tool (FACET)

Banavar Sridhar

The air transportation system is on the verge of gridlock, with delays and cancelled flights reaching all time highs. To understand the causes of these problems and to identify the potential benefit of new technologies or procedures, Ames has taken the first step in developing a system-level modeling and simulation capability referred to as Future ATM (Air Traffic Management) Concepts Evaluation Tool (FACET). FACET provides a flexible simulation environment for exploring, developing, and evaluating advanced ATM concepts.

FACET simulates system-wide air traffic operations over the contiguous United States, utilizing models of aircraft performance, weather, and airspace features to synthesize aircraft trajectories. Figure 1 shows the various input sources, main components, and some of the applications of FACET. FACET's modular software architecture strikes an appropriate balance between flexibility and fidelity. This innovative feature enables FACET to model airspace operations at the national level and to process over 5,000 aircraft on a single desktop computer for a variety of operating systems. The software architecture of FACET successfully blends two programming languages, "Java" for the graphical user interfaces and "C" for the underlying computational engine, with state-of-the-art software development practices. These two features are essential ingredients to the portability and versatility of FACET.

As shown in figure 1, four advanced air traffic management (ATM) concepts have been successfully evaluated with FACET. A fifth application, system-wide optimization, is under development. A flight-deck-based conflict-detection and resolution-feasibility study

showed that free maneuvering operations (a key element of free flight) are not adversely affected by the decentralization of control authority associated with self-separation. The direct-to routing analysis indicated that national deployment of a newly developed Ames controller decision support tool, Direct-To, could result in cost savings of \$200 million per year. The Playbook Evaluation Tool is a first step in developing advanced traffic-flow management techniques for aircraft rerouting and airspace redesign. FACET has also been used to study the integration of aircraft and space launch vehicle operations in the U.S. National Airspace System. Those in the Advanced Space Transportation Program expect the number of reusable and other space launch vehicles to increase significantly over the next decade. The FAA Office of Commercial Space Transportation has requested FACET to evaluate the FAA's future Space and Air Traffic Management System (SATMS).

Figure 2 is an example of a FACET display mode. The display shows current aircraft locations, Center boundaries, and changes to aircraft routes. This together with numerous other graphic interface capabilities allows the researcher to quickly assess the results of a specific analysis or study.

The capabilities of FACET have been demonstrated to a large and diverse group of ATM experts from industry, academia, and the government; the feedback received to date has been overwhelmingly positive. A patent application for FACET is being prepared. Several organizations have requested and received a copy of the FACET software for collaborative work under a NASA Non-Disclosure Agreement.

FACET has become a powerful ATM simulation tool with the capability to evolve into a decision support tool for Traffic Flow Management. The FACET development approach—to build and expand functionality as needed while meeting the requirements and schedule of a

focused program—has produced a versatile ATM tool at a very low cost.

Point of Contact: Banavar Sridhar
(650) 604-5450
bsridhar@mail.arc.nasa.gov

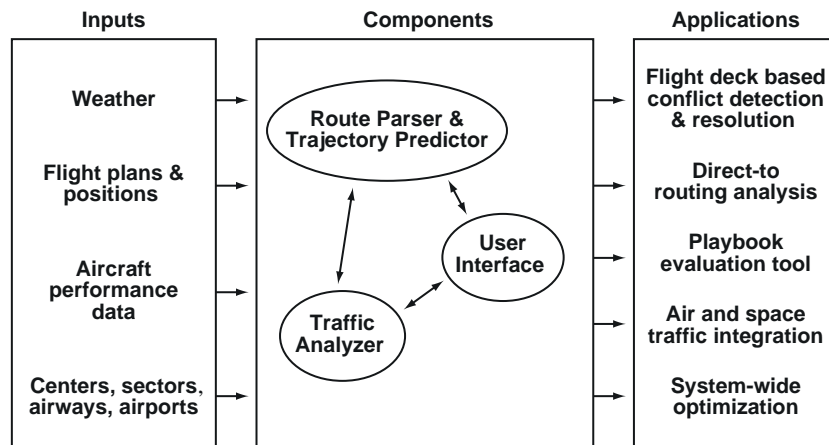


Fig. 1. FACET architecture.

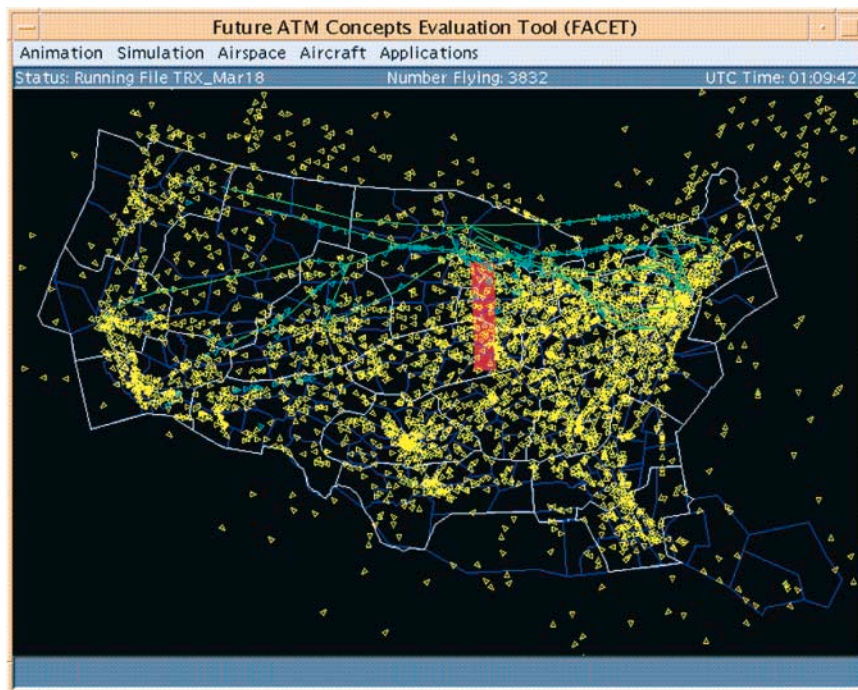


Fig. 2. Modeling of TFM concepts using FACET.

Full-Immersion Air Traffic Control Tower Simulation

Nancy S. Dorigi, Jim McClenahan

NASA's FutureFlight Central is the world's first full-scale, full-immersion airport-surface simulation environment in which the safety and efficiency of new technologies and procedures can be researched, developed, and evaluated under various airport conditions. Construction of this innovative new Ames facility was completed and the facility formally dedicated with a ribbon-cutting ceremony on 13 December 1999.

FutureFlight Central (FFC) consists of a two-story physical structure replicating a full-scale air traffic control tower, including work areas to support pilots, ramp controllers, and airport operators along with FFC simulation engineers, software developers, and researchers. It is equipped with air traffic control simulation software components and a digital voice, a simulated radio/telephone/intercom system, a data communication network, and audiovisual equipment to support the simulations. The tower cab (fig. 1) features programmable user

displays and a virtually seamless, visual display system consisting of screens and projectors that provide a 360-degree out-the-window field of view driven by the air traffic control simulation software and image generators.

The FFC staff successfully completed the first simulation for a paying customer when the Boeing Corporation completed a human factors study in the facility at the end of May 2000. For this very first simulation in the FFC, Boeing gave the FFC staff extremely high marks in its debrief survey. The staff received scores of 10 out of a possible 10 on every item except two, on which it received scores of 9.

In June 2000, San Francisco International Airport entered into an agreement with FFC to simulate and preview new tower locations associated with its potential runway reconfiguration. And in August 2000, Los Angeles International Airport and United Airlines



Fig. 1. FutureFlight Central air traffic control tower cab.

signed a contract to include FFC in a joint study of runway incursions. These major U.S. airports are the first to benefit from Future-Flight Central, a world-class airport operations simulation facility designed to advance the safety, efficiency, and cost effectiveness of

current and future airport procedures, design, and technologies.

Point of Contact: Nancy Dorigi
(650) 604-3258
ndorigi@mail.arc.nasa.gov

Direct-To Tool for En Route Controllers

Heinz Erzberger, Dave McNally

A new tool that helps air traffic controllers improve the efficiency of trajectories has been developed by researchers at Ames Research Center. The tool, called Direct-To, identifies all the aircraft in a region of airspace that can reduce their time of flight by choosing more direct routes than those originally planned. It was designed to help reduce routing inefficiencies resulting from the fixed highway-in-the-sky route structure and other operational constraints imposed by air traffic control. The software for the tool has been completed and was integrated into the Center-TRACON Automation System (CTAS), which comprises a suite of tools for air traffic controllers. The tool is scheduled for operational tests in mid-year 2001 at the Fort Worth Air Route Traffic Control Center. In preparation for the field test, the tool has been operated at Ames in shadow mode with live air traffic data received from the Fort Worth Center. It has also undergone extensive simulator evaluations with controllers in the loop.

The algorithm in Direct-To first computes four-dimensional trajectories along the planned flight plan routes for all aircraft tracked by radar in a Center's airspace. Then it computes a direct-to trajectory, also referred to as a great circle route, to a trial direct-to way point on the aircraft's flight plan. Finally, it compares the times of the original and the direct-to trajectories leading to the trial direct-to way point

where the two trajectories rejoin. If the direct-to trajectory shows at least a 1-minute time saving over the original trajectory, the aircraft is added to the Direct-To list. This list, which is displayed on the controller's monitor, contains the identifiers of all such aircraft found by the algorithm, ordered by the amount of the time saving, with aircraft showing the greatest saving placed at the top. In addition to finding all aircraft eligible for direct-to flight plan changes, the algorithm analyzes the proposed direct-to route for potential conflicts. If a conflict is predicted to occur, the time to the conflict is added to the list.

The controller interface for Direct-To is based on graphical user interface techniques incorporated in personal computers. It makes extensive use of point-and-click mouse inputs and on-screen graphics and buttons to minimize controller workload. For example, it requires only two mouse clicks to make a direct-to flight plan change, rather than the more than 10 keystrokes a controller has to enter to make the same change in today's system. This reduction in workload, combined with the accurate identification of the most time-saving and conflict-free direct-to trajectories, will make it possible for controllers to issue direct-to clearances to pilots more frequently, thereby yielding substantial cost savings to aircraft operators.

An estimate of the time and cost saving expected from use of the tool has been obtained by running the tool in shadow mode with live traffic input from the Fort Worth Center for a period of several months. It shows a potential saving of about 1,500 minutes of flying time per day. It is equivalent to a saving of 2.5 minutes for the average aircraft eligible for a direct-to clearance. This translates to yearly cost savings of about \$15,000,000 for airlines operating in the Fort Worth Center's airspace. If the tool were implemented at all en route centers in the continental U.S. airspace, the operating cost savings could exceed \$150,000,000. A patent application for the Direct-To tool has been filed with the Patent and Trademark Office.

The figure shows a screen photo of a controller display, which superimposes Direct-To tool

information on a plan view radar display. Ampersands indicate the location of radar targets. Three aircraft are on the Direct-To list, located in the upper right. The controller has selected flight SCX61, which is a departure out of DFW, as a candidate for a direct-to clearance to the fix TXO, with a time saving of 2.6 minutes. The green "OK's" indicate that no conflicts are expected for any of the direct-to-eligible aircraft on the list. The panel at the bottom provides information generated by the Trial Planner. It contains the "ACCEPT" button the controller clicks to confirm the clearance. The direct-to trajectory to TXO is shown in yellow, and the flight plan trajectory with its detour to the south is shown in white.

Point of Contact: Heinz Erzberger
(650) 604-5425
herzberger@mail.arc.nasa.gov

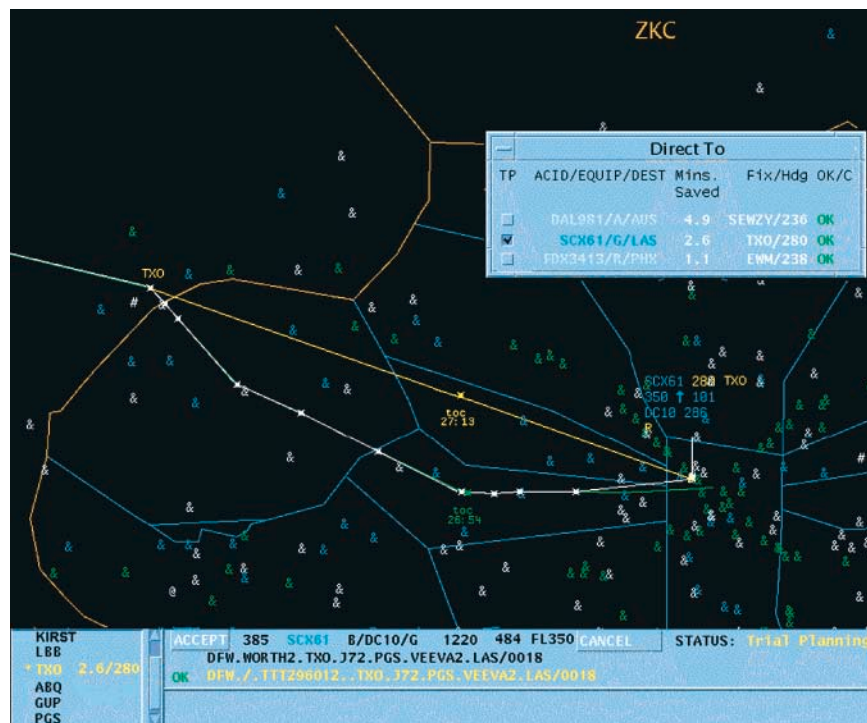


Fig. 1. Photo of Controller display showing Direct-To tool.

Multi-Center Traffic Management Advisor

Tom Davis

The primary objective of Multi-Center Traffic Management Advisor (McTMA) is to improve the capacity at busy airports that are controlled by more than one Center. This is a common situation in the U.S. Northeast Corridor. Capacity increases are expected as a result of improving the flow of traffic into the airport through better coordination between the facilities. The research and development will initially focus on arrivals to Philadelphia International Airport. As illustrated in the figure, two en route Centers, New York and Washington, feed the Philadelphia terminal area ((TRACON) Terminal Radar Approach Control) and airport, with additional significant interactions with Cleveland and Boston Centers.

Multi-Center TMA is a major extension of the Ames-developed Traffic Management Advisor (TMA) that is currently being deployed as part of the Federal Aviation Administration's

(FAA's) Free Flight Phase 1 Program. The TMA is a decision support tool that assists en route traffic managers and controllers in predicting, planning, and controlling arrival air traffic into busy terminal areas. TMA predicts arrival traffic demand, generates efficient arrival schedules to fully utilize a busy airport's capacity, and issues advisories to controllers that aid them in meeting the TMA-generated schedule. The NASA-developed TMA has been operational on a daily basis at the Ft. Worth en route Center for nearly 4 years. The FAA's Free Flight Phase 1 Program is deploying TMAs to seven additional en route Centers. All of the TMA deployments have focused on facilities where a single Center manages arrivals.

The extension of TMA to a multi-Center environment requires the design, development, and evaluation in simulation and field-test of a multi-facility software architecture and of operational procedures for the collaboration, management, and control of arrival traffic. In order to enhance the technical expertise and ultimate success of the McTMA project, two programmatic efforts were put into place. First, Ames Research Center entered into a cooperative agreement with the Mitre Corporation's Center for Advanced Aviation System Development (CAASD) to conduct joint research on McTMA concepts. The CAASD is a federally funded research and development center that supports the FAA. Second, NASA developed a multi-facility software architecture concept that is the basis of a 4-year, \$14 million contract award to Computer Sciences Corporation for the software development of McTMA.

To date, field site surveys of Cleveland, New York, Washington, and Boston Centers and Philadelphia TRACON were conducted in order to understand current operational



Fig. 1. Northeast Corridor map.

procedures and to develop operational concepts for McTMA. Ames researchers used the knowledge gained in the site surveys to adapt TMA to Philadelphia and the surrounding Centers. Ames then conducted a series of real-time simulations—utilizing air traffic controllers and traffic managers from all of the affected facilities—of the arrival traffic feeding through the en route Centers into the Philadelphia TRACON. The results of the simulations defined the requirements for the system software architecture and the arrival traffic scheduling algorithms. Additionally, it was confirmed that because of the narrow geometry of many of the sectors, as well as crossing traffic bound for other busy East Coast airports, delay absorption would need to be allocated sector-by-sector. It was also determined that some delay would have to be

absorbed by sectors much farther upstream from the airport than expected. This is caused by the limited delay capacity of much of the airspace.

Additional simulations are planned and will be conducted at Ames and at the FAA's Technical Center over the next year. These simulations will be followed by an operational field test, beginning in early 2002 and lasting through 2004. Following successful completion of the McTMA field trials, the system will be handed off to the FAA for further deployment to selected sites throughout the United States.

Point of Contact: Tom Davis
(650) 604-5438
tdavis@mail.arc.nasa.gov

Mitigating Runway Incursions with Cockpit Display Technology

Becky L. Hooey, David C. Foyle, Anthony D. Andre

Between 1988 and 2000 the U.S. Runway Safety Program Office (ATP-20) reported 3,420 runway incursions; 48% of these incursions were caused by pilots deviating from taxi clearances issued to them by air traffic control (ATC). Research at Ames Research Center has been conducted to identify the factors that contribute to these incidents and to develop cockpit display technologies to mitigate these and other errors in order to increase runway safety while simultaneously increasing efficiency.

Two full-mission surface-operations simulation studies were conducted in the Advanced Concept Flight Simulator (ACFS) at Ames. The ACFS was equipped with the Taxiway Navigation and Situation Awareness (T-NASA) display suite, which is composed of an electronic moving map (EMM) and a head-up display (HUD) to be used during taxi (see

fig. 1). The EMM presented an over-the-shoulder perspective view of the airport surface, location of own-ship in real time, and the taxi route clearance, textually and

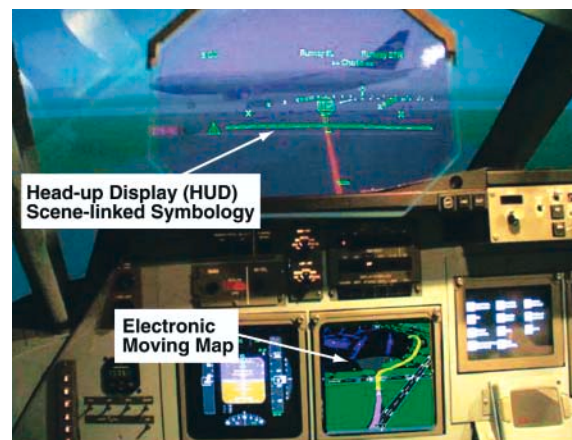


Fig. 1. The T-NASA System consists of an electronic moving map and a head-up display depicting the cleared taxi route transmitted via data-link ATC.

graphically. The HUD presented local guidance information via scene-linked symbols depicting the centerline and edges of the cleared taxiways. The ACFS was also equipped with advanced data-link technology that transmitted an electronic record of all ATC communications to the cockpit.

The simulations revealed that pilots committed navigation errors on 17% of land-and-taxi-to-gate trials in simulated low-visibility and night conditions. These navigation errors occurred as often during night conditions as during low-visibility conditions. An analysis of these navigation errors revealed three distinct classes of errors: (1) planning errors (formulating an erroneous understanding of the taxi route), (2) decision errors (making an incorrect turn choice at a taxiway intersection), and (3) execution errors (incorrectly maneuvering through an intersection).

Each class of errors had a unique set of contributing factors and mitigating solutions (see fig. 2). Planning errors occurred most often because of miscommunication between pilots and ATC. Technologies such as data-link and the T-NASA EMM that provide clear, unambiguous, and readily available representations

of the clearance were shown to mitigate these errors. Decision errors occurred because of high operational demands, as well as because of inadequate navigational awareness. The T-NASA HUD and EMM in combination reduced the number of these errors by providing pilots both global navigational awareness and local control guidance. Finally, execution errors were caused by inadequate or confusing environmental cues such as complex taxiway geometry, confusing signs and markings, and the “sea-of-blue lights” phenomenon (that is, the blue taxi lights form a confusing pattern when viewed off axis). The T-NASA HUD disambiguated the external environment cues and reduced the frequency of errors.

These studies revealed three classes of navigation errors: planning, decision, and execution. Further, it was shown that cockpit display technologies (such as T-NASA) that address these contributing factors can augment pilots’ cognitive, decision making, and perceptual abilities, thereby resulting in fewer navigation errors and increased runway safety.

Point of Contact: Becky L. Hooey
(650) 604-2399
bhooey@mail.arc.nasa.gov


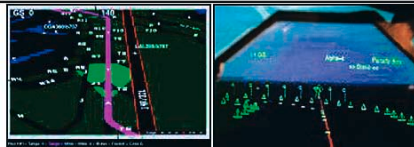

<p>PLANNING ERRORS (Miscommunication / misunderstanding route) Datalink (left) and T-NASA EMM (right) mitigate taxi route planning errors by enhancing Pilot-ATC communication & understanding of clearance.</p>	 <p>The image shows two side-by-side cockpit displays. The left display is a Datalink interface showing a text-based communication with ATC: 'NASA 227: Taxi to Concourse C via A, T, A10.' Below the text are 'Accept' and 'Reject' buttons. The right display is the T-NASA EMM (Enhanced Mission Manager) showing a graphical representation of the airport taxiway layout with a highlighted route in green.</p>
<p>DECISION ERRORS (Making an incorrect turn decision) Together the T-NASA EMM (left) and HUD (right) mitigate decision errors by enhancing navigational awareness, and lowering workload.</p>	 <p>The image shows two side-by-side cockpit displays. The left display is the T-NASA EMM showing a graphical view of the taxiway intersection with a green route. The right display is the HUD (Head-Up Display) showing a graphical view of the taxiway intersection with a green route and various navigational cues.</p>
<p>EXECUTION ERRORS (Errors in maneuvering through an intersection) The T-NASA HUD mitigates execution errors by disambiguating complex taxiway geometry and confusing airport signage and markings.</p>	 <p>The image shows a single cockpit display of the T-NASA HUD, which provides a clear, unambiguous graphical representation of the taxiway geometry and markings, helping to disambiguate complex airport signage and markings.</p>

Fig. 2. The T-NASA cockpit displays mitigate navigation errors during surface operations, increasing taxi efficiency and safety.

Air Ground Integration Study

Sandy Lozito, Margaret-Anne Mackintosh, Karen DiMeo, Parimal Kopardekar

A simulation was conducted to examine the effect of shared air/ground authority when each is equipped with enhanced traffic- and conflict-alerting systems. The potential benefits of an advanced air traffic management (ATM) concept referred to as “free flight” include improved safety through enhanced conflict detection and resolution capabilities, increased flight-operations management, and better decision-making tools for air traffic controllers and flight crews. One element of the free-flight concept suggests shifting aircraft separation responsibility from air traffic controllers to flight crews, thereby creating an environment with “shared-separation” authority.

During FY00, NASA, the Federal Aviation Administration (FAA), and the Volpe National

Transportation Systems Center completed the first integrated, high-fidelity, real-time, human-in-the-loop simulation. A number of related accomplishments contributed to the successful completion of this effort: (1) linking Ames simulation facilities on the West Coast with those of the FAA William J. Hughes Technical Center (WJHTC) on the East Coast; (2) developing a prototype cockpit display of traffic information with alerting logic (CDTI-AL) which served as a flight crew decision support tool (figs. 1, 2); and (3) incorporating the User Request Evaluation Tool (URET) developed by MITRE Corporation for the air traffic controllers.

The simulation, conducted over a 4-week period, involved 6 line pilots; 12 certified



Fig. 1. Flight deck cockpit display of traffic (CDTI) showing an impending conflict with DAL152.

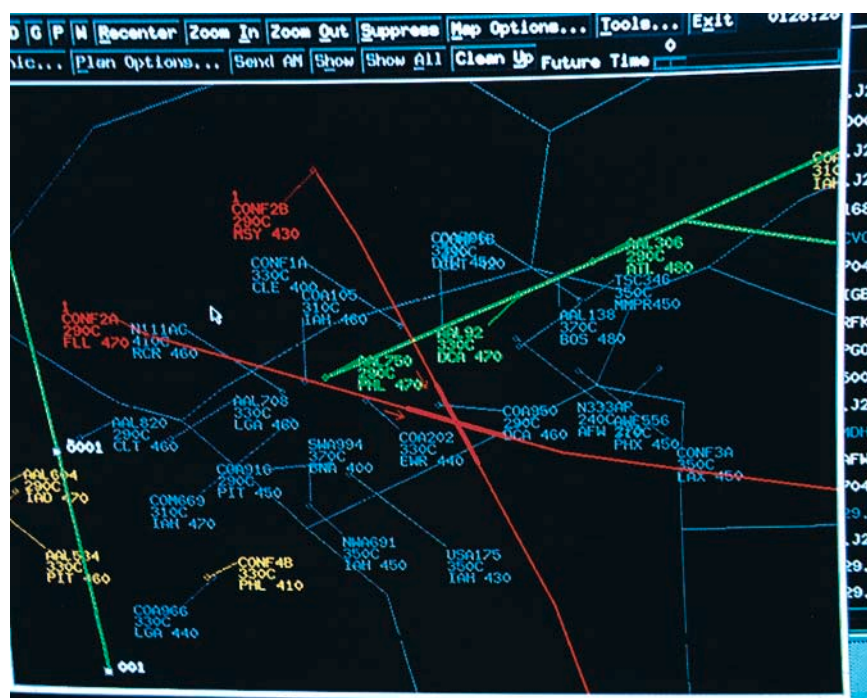


Fig. 2. Flight deck cockpit display of traffic (CDTI) depicting predictor tools to enable conflict detection awareness.

professional controllers, who served as participants; and 4 operations supervisors, who served as subject matter experts and observers. Two Memphis Air Route Traffic Control Centers (ARTCC) were emulated in the experiment. Four test conditions were defined by level of controller and flight crew shared-separation responsibilities and associated procedures. Standard separation rules of 5 nautical miles horizontal or 1,000/2,000 feet vertical (as appropriate) were observed throughout. All flight crews and controllers experienced all four conditions. Objective ground-side data included communications, separation errors, URET alerts and trial plans, closest point of approach, traffic density, and number of free-flight cancellations. Objective air-side data consisted of communications, separation errors, CDTI-AL alerts, closest point of approach, and number of free-flight cancellations. Subjective ground-side and air-side data consisted of workload and situation awareness ratings and comments about shared-

separation experiences, traffic realism, and other details. Expert observers recorded critical observations.

The controllers expressed concern about the feasibility of shared-separation as simulated in this study and its potential effect on flight safety. They reported higher workload, they preferred to resolve conflicts earlier than pilots did, and they tended to cancel free-flight when they perceived that pilots were delaying resolution of the conflict. However, their level of situation awareness was high across all conditions. Pilots preferred shared-separation conditions, particularly the one affording them the highest level of separation responsibility (SS:L2). They rated both shared-separation conditions as being relatively safer than current operations and as providing more situation awareness.

This research helped to facilitate the technical connection and collaboration between multiple organizations. It also demonstrated some of

the advantages of exploring free flight and shared-separation authority in a full-mission study environment.

Point of Contact: Sandy Lozito
(650) 604-0008
slozito@mail.arc.nasa.gov

Enabling Cockpit-Based Self-Separation

Walter W. Johnson and Vernol Battiste

Data from capacity studies suggest that the National Airspace System (NAS) will reach its capacity limits with the current centralized Air Traffic Control (ATC) system within the next 2 decades. The goals of this effort were to design and develop prototypes of flight deck tools to support airborne management of separation and to evaluate the feasibility of shifting flight deck and ATC roles and responsibilities relating to the management of separation. The concept of Free Flight introduces many challenges for aviation operations in the air and on the ground. Of considerable concern is the plan to move from centralized control and responsibility for aircraft separation to decentralized control and distributed responsibility.

Because of the impending NAS overload, research on distributed air-ground concepts has been undertaken to identify and develop air-ground concepts to ensure that free-flight operations are implemented successfully. The underlying concept evaluated in this effort was based on three principles: (1) aircraft pilots should always broadcast intent information in the form of current flight plans; (2) all flight plans should be deconflicted to the maximum extent possible (in this case out to a range of 120 nautical miles); and (3) the interface for flightpath replanning tools should be graphical and impose low workload.

A full-mission air-ground simulation was conducted in the Ames' Crew Vehicle Systems Research Facility in support of this effort. Its goal was to evaluate the effect of advanced

displays with intent information (for example, four-dimensional (4-D) flight plans) on flight crew and ATC performance during limited free-flight operations. To assess the value of 4-D intent information, flight crews performed real-time, strategic flightpath replanning with and without access to graphically presented 3-D flight plan information about surrounding traffic during en route operations. To support the replanning task, flight crews used an enhanced cockpit situation display (CSD) that depicted surrounding traffic, a dynamic 4-D predictor symbology, and tools that alerted the crew to impending losses of separation (fig. 1). The conflict-alert tool was color-coded (blue, white, and green) to reflect aircraft and portions of flight plans that were above, at, or below own-ship altitude. The CSD also contained a graphical route assessment and replanning tool used to develop alternative (deconflicted) flight plans (fig. 2). Once developed, modified flight plans were submitted electronically for approval and, upon approval, automatically loaded into the autopilot and data linked to all surrounding traffic. The study also examined two levels of ATC authority: (1) Limited Authority, at which level ATC intervened only when a loss of separation was imminent; and (2) Full Authority, at which level ATC ran the sector as they would normally.

The results suggest that flight crews with advanced 4-D flight plan information can perform strategic self-separation during operations in densely populated traffic environments. And, when ATC remains in the information

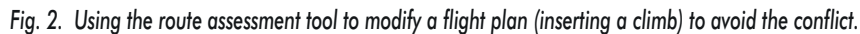


Fig. 1. Detection of a conflict on the CSD.

and approval loop, strategic self-separation performed by flight crews is not disruptive to normal ATC sector operations. The results also showed that crews with access to 4-D flight plan information were more efficient, made smaller deviations for traffic and fewer total flight plan modifications, and experienced lower workload. Crew evaluations of 3-D

and 4-D traffic information, of the display declutter features, and of the advanced flight replanning tools were very positive, although the input devices (knobs/dials or touch pads) were not as highly rated as the display itself.

Point of Contact: Walter W. Johnson
(650) 604-3667
wjohnson@mail.arc.nasa.gov



Thomas R. Chidester

limits for a given phase of flight. These current programs are referred to as Flight Operational Quality Assurance (FOQA, or MOQA in the military).

But this process uses only a portion of the data. It scans large quantities of data to extract and make understandable a small number of predefined events. As a result, there is far more potential information in these data sets, information that could help operators understand and enhance the safety, reliability, and economics of their flight operations. The challenge is to find and cull out—from the mass of data

generated by aircraft systems and collected by data recorders—the key information that can be used for these other purposes. Scanning, analyzing, and reporting must be automated to produce meaningful information for the human analyst to act upon.

APMS implemented several key tools for this process in FY00, and FOQA vendors commercialized two of them. With its first airline partner, Alaska Airlines, APMS implemented five new analysis tools:

1. *Special Event Processing System* assists the FOQA analyst in analyzing, decision-making, decision-tracking, reporting, communicating, and recording for future reference information related to flight exceedances.
2. *Report Generator* assists FOQA managers in charting counts and rates of exceedances or special events through automated generation of uniform, high-quality, graphical reports of flight data trends.

3. *Graphics Viewer* assists the FOQA analyst in interpreting and verifying exceedances or special events by displaying the data traces of a specific flight in great detail for a period of minutes surrounding the event as depicted (fig. 1).

4. *Routine-Events* presents the distribution of flight parameters around “check points” that occur within each flight and are tied to standard operating procedures. This allows the FOQA analyst to make an immediate and obvious comparison of actual line-operation performance and operator-specified standard procedures.

5. *Pattern Search* enables the FOQA analyst to search any portion of the database for any specified pattern of flight parameters. This allows exploratory analysis of flight parameters that may be associated with precursors of exceedances or special events.

FOQA vendors implemented two of these tools in their commercially available software

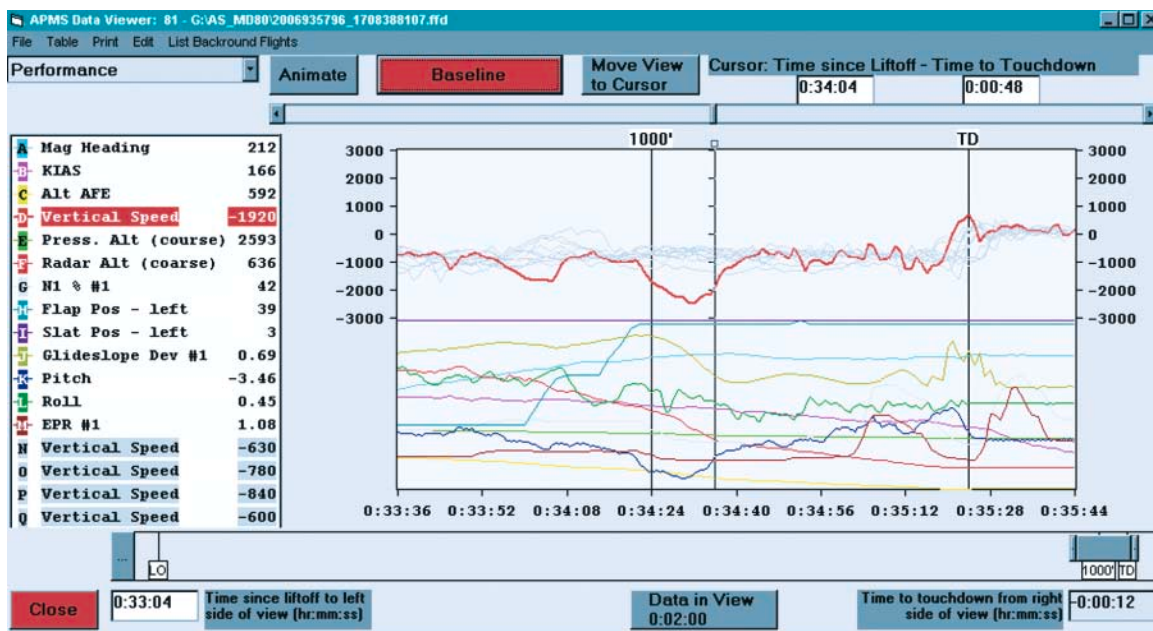


Fig. 1. The APMS Graphics Viewer.

packages in accordance with the terms of Space Act Agreements with their organizations. The Flight Data Company Ltd. (now Spirent-Heathrow) implemented the Report Generator in its Ground Replay and Analysis Facility. Teledyne Controls implemented

Routine Events in its Flight Data Replay and Analysis System (FLDRAS).

Point of Contact: Thomas Chidester
(650) 604-6007
tchidester@mail.arc.nasa.gov

Performance Data Analysis and Reporting System

Irving C. Statler

The Performance Data Analysis and Reporting System (PDARS) provides decision makers with a comprehensive, accurate, and insightful method for routinely monitoring the operational health, performance, and safety of the National Airspace System (NAS). The purpose of PDARS is to provide the technological developments that will enable a cultural change from the current reactive approach, of identifying and alleviating life-threatening aviation conditions and events, to a more proactive approach, while still meeting the projected requirements of increasing air traffic. PDARS pursues this objective by establishing a capability for facility-level managers to monitor air traffic control performance in the NAS, identifying and analyzing operational performance problems, and designing and evaluating improvements. PDARS incorporates innovative technology for the real-time collection and rapid processing of large volumes of complex data, and state-of-the-art tools for extracting, presenting and visualizing information such as radar flight tracks.

Six FAA facilities representing a microcosm of the NAS—Southern California and San Francisco Bay TRACONs (Terminal Radar Approach Controls), Los Angeles and Oakland

Centers, the Western-Pacific Region, and the System Command Center were selected to participate in an operational evaluation of the concept and tools. An initial PDARS prototype was implemented and fielded at the six sites. Data were accessed daily from all sites, processed overnight, and reports delivered routinely to all six facilities each morning. Examples of the displays and reports appear in figures 1 and 2, respectively. FAA personnel have been trained on PDARS, and both the system and its reports are being used on a day-to-day basis.

PDARS accomplished several key milestones in this process in FY00, including the completion, evaluation, and demonstration of a prototype network, generation of daily reports, and the design review and delivery of the first upgrades to the capabilities of the prototype network. Both informal feedback and a formal design review yielded positive comments on the prototype, guidance for where to pursue upgrades, and a drive to expand the capability to other facilities.

Point of Contact: Irving C. Statler
(650) 604-6654
istatler@mail.arc.nasa.gov

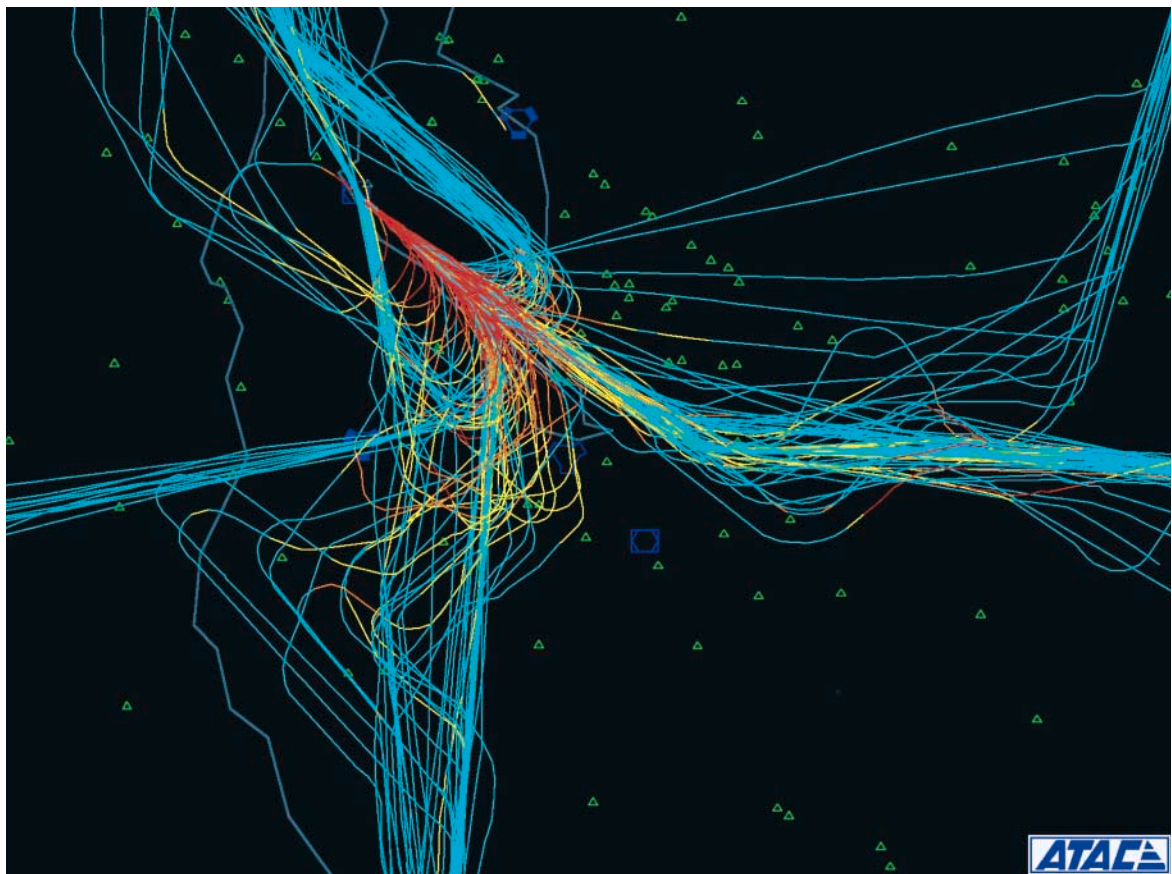


Fig. 1. Graphical depiction of traffic flow over time.

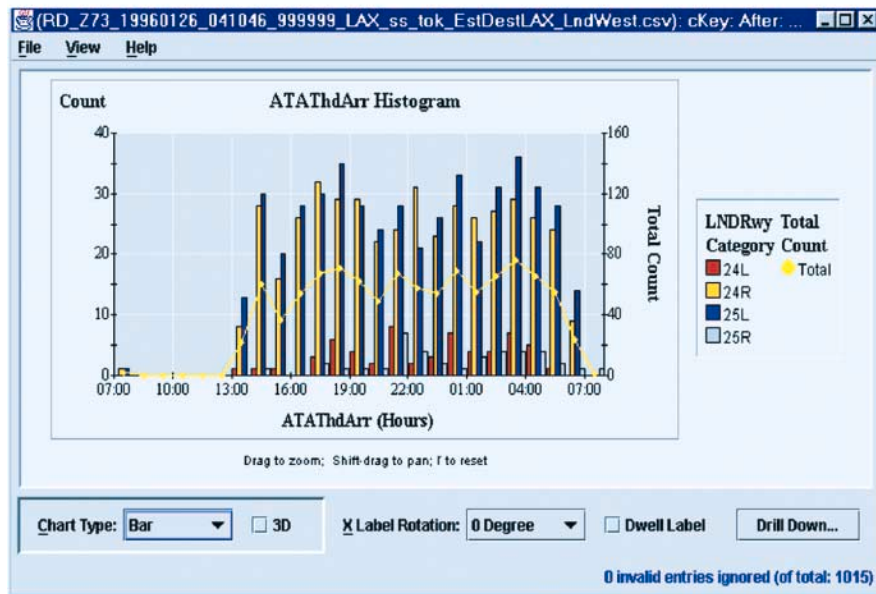
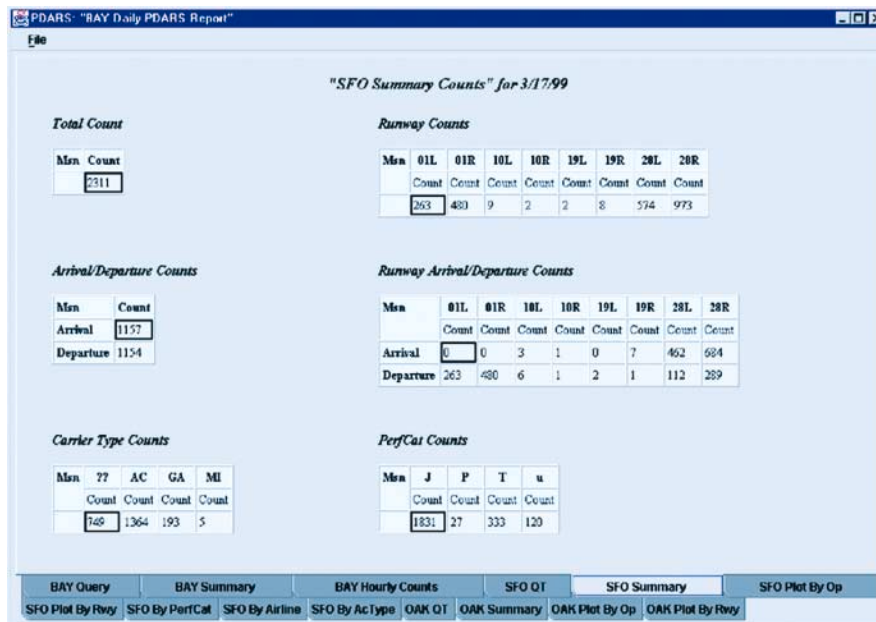


Fig. 2. Examples of data summaries.

New Contextual Data-Mining Technologies

Michael W. McGreevy

Four new contextual data-mining technologies have been developed and tested and are in the process of being patented and commercialized by Ames. The methods were developed as part of NASA's effort to dramatically reduce the potential for commercial aviation accidents by modeling and monitoring safety-related incidents in the National Airspace System (NAS). Specifically, this work provides a new set of information technologies that automatically interpret the contextual structure of incident and accident reports to develop detailed, computable models. These models represent the domain of commercial aviation operations, the situations described, and the concerns of the incident and accident reporters. These new methods provide greatly improved information retrieval from large databases of unstructured text.

The four new data-mining methods, collectively called QUORUM/Perilog, are keyword-in-context search, phrase search, phrase generation, and phrase discovery. These methods build upon a common core of contextual analysis, modeling, and relevance-ranking of text. QUORUM/Perilog keyword-in-context search retrieves text, such as incident narratives, that contain one or more user-specified keywords in typical or selected contexts, and ranks the narratives on their relevance to the keywords in context. It displays those narratives with their relevant sections highlighted, and also displays the criteria used to determine relevance. QUORUM/Perilog phrase search retrieves narratives that contain one or more user-specified phrases, even hundreds of phrases, and ranks the narratives on their relevance to the phrases. It displays the narratives with the phrases highlighted, and also shows near-matches to the query phrases. QUORUM/Perilog phrase generation creates a list of phrases, from the database of text, that contain a user-specified word or phrase.

QUORUM/Perilog phrase discovery finds phrases that are related to topics of interest. For example, a query on the topic of "fatigue" produces results including: "rest period," "reduced rest," "crew rest," "continuous duty," "crew scheduling," "duty period," "rest periods," "reserve or standby," and many others. Phrase discovery is useful for gaining a better understanding of the topics contained in a database. In addition, phrase generation and phrase discovery are particularly useful for finding query phrases for input to QUORUM/Perilog phrase search.

The new data-mining methods have been successfully tested on the tens of thousands of narrative incident reports in the database of the Aviation Safety Reporting System (ASRS). The ASRS is a national clearinghouse of aviation safety incident reports supported by the FAA and managed by NASA. The new technologies completed this year will support system-wide ASRS analyses for government, industry, and academic researchers.

The new data-mining methods are applicable to a wide variety of text, and several analyses have been done as demonstrations. For example, one analysis involved reports of safety-related incidents that occurred during ground maintenance of the space shuttle. In addition, a sample of incidents from the electric power generation industry was analyzed.

Commercialization of the four new data-mining methods began with the submission of four formal invention disclosures. The Ames Commercial Technology Office (CTO) reviewed the disclosures, and also hired contractors to conduct a search for prior art and an analysis of the commercial potential of the new technologies. Encouraged by the results, the CTO established a contract with an outside law firm to write four patent applications. The

four patent applications are based on nine “inventive concepts,” each of which could be an independent patent if the intent were to maximize the number of patents, as is often done in start-up companies. The writing of the patent applications was still in progress at the end of FY00. After approval by Ames and NASA Headquarters, completed applications are submitted to the United States Patent Office. Meanwhile, the CTO is developing a commercial licensing strategy for the new technologies.

The new methods have been documented in the paper, “Searching the ASRS database using QUORUM Keyword Search, Phrase Search, Phrase Generation, and Phrase Discovery.” The paper has been approved for publication pending submission of the patent applications.

Point of Contact: Michael W. McGreevy
(650) 604-5784
mmcgreevy@mail.arc.nasa.gov

Alternative Perspectives on Traffic Risk

Jeannie Davison, Judith Orasanu

A study was conducted to identify differences in the ways airline pilots and air traffic controllers might perceive risks and resolve problems in simulated traffic and control environments. Pilots and controllers are faced routinely with situations requiring them to make decisions that affect flight safety. Critical elements in decision making include recognizing cues that indicate some change in the circumstances and assessing the situation to ensure that effective decisions are made and appropriately implemented. Pilots and air traffic controllers perceive and respond differently to risks associated with operations in the National Airspace System (NAS). These differences contribute to miscommunications and increased aviation risks.

We examined whether air traffic controllers and airline pilots differ in their perceptions of risk (or threat) associated with varying traffic configurations and different air traffic control (ATC) environments (existing rules vs. free flight). The concept of free flight involves development of a more flexible ATC system, allowing user-preferred routing and flight crew self-separation in the en route portion of flight. A second goal of the study was to examine

whether the two groups would respond differently (that is, choose different maneuvering options) as a function of role, ATC environment, and varying traffic conditions.

Scenarios of evolving en route traffic situations were presented on a desktop computer to 32 airline pilots and 32 air traffic controllers. Participants indicated the amount of risk they perceived in individual snapshots displayed sequentially to represent evolving traffic scenarios. A sample of the display used in the study is shown in figure 1. In addition, participants indicated their preferred response to each situation by selecting maneuvering options.

Analyses revealed that risk perception was affected more by features of individual traffic situations than by either the participant’s role (pilot or air traffic controller) or the operative ATC environment (existing rules or free flight). The proximity of conflicting traffic had the greatest effect on the controllers’ ratings of risk, with the nearest proximity traffic scenarios being rated as significantly higher in risk than the far-proximity scenarios. For pilots, uncertainty appeared to be the primary factor in risk ratings. Pilots assigned the



Fig. 1. Example of a display showing an evolving traffic scenario.

highest risk ratings to the scenarios in which they had most difficulty making accurate judgments concerning where their flightpath would cross that of another aircraft. In addition, controllers assigned their highest risk ratings to scenarios with high-density/descending traffic, whereas pilots assigned their lowest risk ratings to these same scenarios. These risk ratings correspond to the maneuvers that participants indicated they would prefer to make in response to perceived conflicts. Controllers preferred to use horizontal maneuvers (heading changes to left or right) rather than vertical or combination maneuvers (climbing or descending turns). Pilots on the other hand were equally likely to use horizontal, vertical, and combination maneuvers to resolve perceived conflicts.

Risk perception is a key component in decision making, especially in dynamic environments such as space and aviation. As systems grow in complexity and diversity of participants, those responsible for regulation, procedures, and operations must be aware of differences in risk perception between the various users. They also must be sensitive to differences in users' preferred strategies for resolving perceived conflicts. Results from this study will assist in developing new regulations and procedures for the evolving air traffic management system and guiding the design of new traffic displays and separation standards.

Point of Contact: Jeannie Davison
(650) 604-1357
jdavison@mail.arc.nasa.gov

Evaluation of In-flight Alertness Management Technology

Melissa M. Mallis

An objective approach for detecting the presence of drowsiness and fatigue on the flight deck was demonstrated in a full-mission simulation. Long, uneventful flights in modern aircraft are characterized by (1) extensive monitoring because of high levels of aircraft system automation, (2) physical inactivity, (3) a requirement to remain vigilant for low-frequency occurrences, (4) dim light levels, (5) steady background noise, (6) reduced social and cognitive interaction, and (7) limited environmental manipulations. Together these factors create a context in which underlying sleepiness is likely to manifest itself in the form of compromised vigilance, reduced alertness, and impaired performance. Flying at night while fatigued is further complicated by the fact that individuals are poor at judging their own level of sleepiness, often reporting high levels of alertness even though physiological measures may suggest extreme sleepiness.

A controlled cockpit simulator study was conducted to evaluate the feasibility and utility of an on-line, human-centered, objective monitoring technology for tracking alertness-drowsiness and to evaluate the effectiveness of fatigue-related feedback on the alertness, neurobehavioral performance, and behavior of flight crews during a simulated, long-haul, nighttime flight. The alertness-drowsiness monitoring technology used is based on the PERCLOS metric: the proportion of time subjects exhibit slow eye closures. This metric has been validated in the laboratory as being highly accurate in detecting drowsiness-induced performance lapses. In the past, however, eye closures have been scored subjectively by a human rater. In this study, we used a fully-automated, video-based system using infrared retinal reflectance to measure PERCLOS objectively. The automated PERCLOS system, developed by the Carnegie

Mellon Research Institute, is shown in figure 1. In addition, the effects of feedback on subsequent alertness, neurobehavioral performance, and behavior were evaluated. Thus, this study was the first demonstration of the potential usefulness of an on-line, human-centered, objective monitoring technology capable of detecting reduced vigilance (hypovigilance) and providing feedback on the flight deck.



Fig. 1. Unobtrusive, on-line, automated, biobehaviorally based PERCLOS systems mounted in the cockpit of the Boeing 747-400 simulator.

Twelve two-man crews consisting of 28 healthy male adults familiar with glass cockpits, flew 6-hour, uneventful, nighttime flights in the Ames 747-400 FAA-certified, Level D flight simulator. Each flight was divided into four counterbalanced segments. In half of these segments, PERCLOS feedback was available on a light emitting diode (LED) display by indicator lights that illuminated as eye closure durations increased, or by a human voice message. The first-generation PERCLOS system implemented in the study consisted of online, computer analysis of video images of the subject's eyes using small cameras with infrared illumination sources mounted on the flight deck (fig. 2). Measures of psychomotor



Fig. 2. The automated PERCLOS system captures two infrared images of the eye using a small camera with associated optics mounted in the flight deck. The two images are processed and reduced to a single image which is evaluated online for degree of eyelid closure.

vigilance performance, subjective sleepiness, continuous brain wave activity (electroencephalography, EEG), and continuous eye

movement activity (electrooculography, EOG) were collected throughout the flight.

A PERCLOS-based alertness monitoring technology on the flight deck has potential as an on-line noninvasive alertness system for pilots who may encounter challenges in high homeostatic drive and circadian rhythm disruption. An on-line, human-centered, objective monitoring technology may be used as a backup for crew members who have integrated in-flight napping or activity break policies in their standard operating procedures. This type of technology can also potentially be implemented in environments that have fewer than three crew members during flight operations.

Point of Contact: Melissa M. Mallis
(650) 604-3654
mmallis@mail.arc.nasa.gov

Evaluating Stereo Displays for Manual Control

Mary K. Kaiser and Barbara Sweet

The current study was conducted to evaluate the relative benefits of stereo presentation versus higher update rates for controlling simulated vehicle motion. Visual displays are used to convey critical control information to pilots of aircraft and space vehicles. Recent developments in display technology enable the use of stereo displays, but these displays incur significant costs. In addition to increasing the complexity of system hardware and software, stereo necessarily decreases the spatial or temporal resolution of the display, since the two required fields (one for each eye) must be interlaced temporally or spatially. In the past, analysis tools were developed to examine which visual cues are required to support manual control tasks. This year, we applied this tool to determine whether stereo displays

improved operators' control of motion in depth (as in a docking task), given that stereo halves the update rate of the display.

The model of the depth control task is shown in Figure 1. It was previously demonstrated that stereo disparity provides a more useful cue for position than for motion, leading to the prediction that stereo would prove more useful when operators control vehicle rate (i.e., change in position) than acceleration (i.e., change in motion). In the experiments, pilots performed both kinds of control tasks while viewing either stereo or non-stereo displays at two different update rates.

Results indicated that pilots performed significantly better with stereo on the rate-control task, but gained no benefit from stereo on the

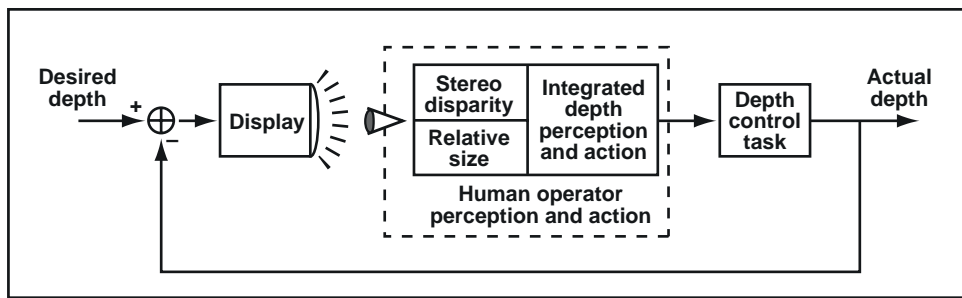


Fig. 1. Model of an operator depth control task.

acceleration-control task. As can be seen in Figure 2, operators had smaller errors (as measured by depth rms) with stereo displays in the rate control task (top panel), but not in the acceleration control task (bottom panel). These findings validated the model's predictions and the utility of the analysis tools.

The research provides an effective demonstration that the specification of critical visual cues is task specific. Thus, display designers need to consider the nature of the operators' task in order to make an intelligent selection of visual interface parameters. The design issue is not to determine whether or not stereoscopic displays are useful, but rather to determine where and when stereo provides control information more effectively than other types of cues. The analysis tools support such determinations, for stereo as well as other display parameters (e.g., update rate, resolution, contrast), enabling designers to optimize displays for specific missions.

Point of Contact: Mary K. Kaiser
(650) 604-4448
mkaiser@mail.arc.nasa.gov

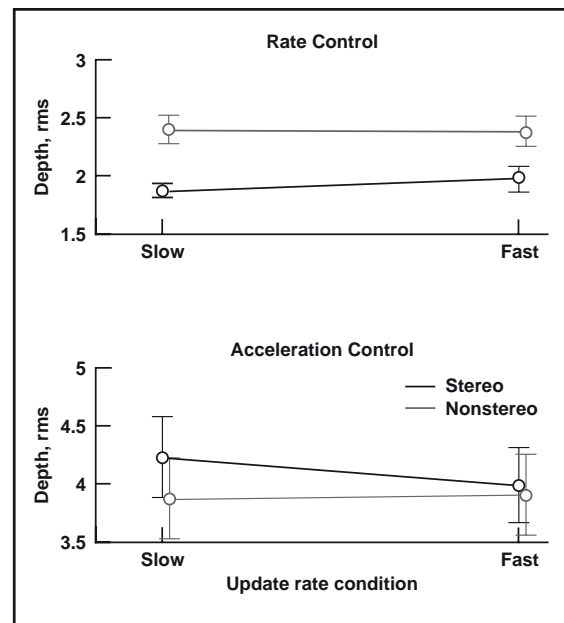


Fig. 2. Pilots' control performance on Rate Control (top panel) and Acceleration Control (bottom panel) tasks.

Active Final Approach Spacing Tool Development

John E. Robinson

The throughput of the nation's busiest airports could be improved by more precisely spacing aircraft on final approach. More accurate final approach spacing ensures that the aircraft are safely separated, but that no avoidable gaps exist in the traffic flow. Ames Research Center and the Federal Aviation Administration (FAA) are continuing to design, develop, and plan deployment of a software-based decision support tool (DST), called the Final Approach Spacing Tool (FAST), to increase airport throughput. An early version of this DST, known as *Passive* FAST (pFAST) provides runway assignments and relative landing orders and is being deployed as part of the FAA Free Flight Phase 1 Program. Current research is focused on developing a future version of this DST, known as *Active* FAST (aFAST) that will allow air traffic controllers to achieve more accurate final approach spacing by providing heading, speed, and altitude commands.

Because of the extremely dynamic nature of air traffic situations, providing advisories to air traffic controllers requires a system whose decisions are reliable yet flexible. As a result, the aFAST system incorporates elements of fuzzy reasoning and rule-based decision making. Using these technologies, the basic implementation of a concurrent scheduling algorithm and a knowledge-based conflict-detection and resolution algorithm have been completed. These algorithms form the foundation of the aFAST system. They determine safe and efficient trajectories for arrival traffic by simultaneously sequencing aircraft along flightpath segments and by resolving all predicted conflicts among those aircraft. A patent application for these algorithms is

being pursued in order to investigate their suitability for private and international ATC environments.

In order to evaluate the performance of the aFAST system, an innovative approach for its simulation was developed. Previous DSTs have focused, almost exclusively, on human-in-the-loop simulations to track the progress of their development, since no other reliable method of executing the advisories was available. The aFAST system will use a three-tiered testing process consisting of trajectory tracking, advisory tracking, and human-in-the-loop simulation. During trajectory tracking, aFAST uses its own solution trajectories to simulate radar tracks. The aircraft's initial positions that are used to determine an initial solution trajectory are specified in order to represent a complex traffic flow. Subsequently, each solution trajectory is used to simulate the next aircraft position, which is used to determine the next solution trajectory. This scenario allows the stability and performance of the aFAST system to be analyzed in an environment free of both prediction and flight technical errors. During advisory tracking, aFAST electronically issues its advisories to an independent Pseudo Aircraft Simulation (PAS). PAS automatically executes these maneuvers using its own independent set of aircraft and atmospheric models. This scenario is suitable for investigating the effects of prediction errors. Finally, during human-in-the-loop simulations, air traffic controllers issue advisories to human pseudo-pilots that respond using PAS. This most realistic scenario can be used to study the effects of both prediction and flight technical errors, as well as to explore the usability and

suitability of active advisories for achieving more accurate final approach spacing.

The aFAST system has used trajectory tracking to control several hours of flights to an airport with a single arrival runway. During these intentionally busy traffic scenarios, the aFAST system achieved safe and precise separation of the aircraft. In the near term, work will focus on the trajectory tracking and advisory tracking

methods of testing. These techniques will be used to (1) quantify the aFAST system's sensitivity to prediction and flight technical errors and (2) assess the benefits of active advisories. Finally, preparation for more complex multi-runway scenarios will begin.

Point of Contact: John Robinson
(650) 604-0873,
jerobinson@mail.arc.nasa.gov

An Analysis of the Radar Reflectivity of Aircraft Wake Vortices

Karim R. Shariff

Large aircraft shed strong vortices in their wakes which pose a hazard to following aircraft. Therefore, during landings in bad weather (that is, under instrument flight conditions) strict spacing is maintained between aircraft. These spacings are usually too conservative, and it has been estimated that several billion dollars could be saved annually by the airlines if the spacing could be reduced by 2 kilometers (km) from the current separations of 5.5 to 11 km. The objective of this work was to assess the potential of ground-based radar for detecting the vortices.

What is needed is a wake sensor that is relatively inexpensive, has long range, requires little or no maintenance, and works in all weather conditions. No sensor currently meets these requirements. Because the pressure in the eye of an aircraft vortex is low (and thus has a low index of refraction), the air in the eye reflects radio waves. A scattering analysis revealed that the peak reflectivity occurs at a frequency near 50 megahertz (MHz) (see fig. 1) and is strong enough that a vortex could

be detected at a range of 3 km with an average power of about 400 watts. A frequency of 50 MHz has several advantages: (1) clutter from rain and fog is not an issue and so the system would work in all weathers; (2) inexpensive and low-maintenance radars already operate at 50 MHz for measuring atmospheric winds and they could be modified to track vortices; and (3) if the system is supplemented with sound waves to enhance reflectivity (via the so-called Radio Acoustic Sounding System technique), the required sound frequency is low enough that attenuation of the sound wave (which would limit range) is not a problem. The main disadvantage of the system is size of the antenna system. A typical set-up might have a 10 by 10 array of small TV-like antennas spaced 3 meters apart on the ground. Such a system cannot be physically pointed. Rather, phase differences would be utilized for pointing.

A provisional patent has been filed and a flight test is being planned to verify the predicted reflectivity near 50 MHz.

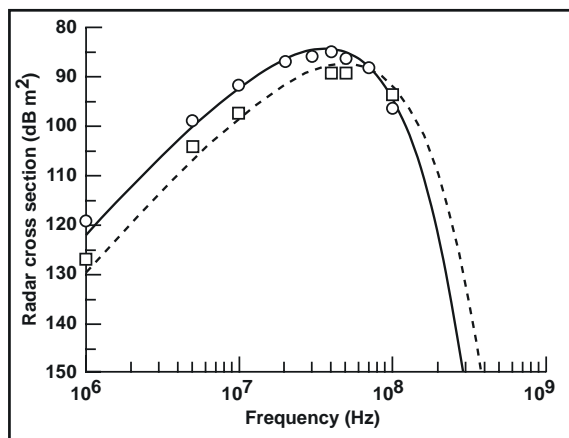


Fig. 1. Predicted radar cross-section (RCS) of aircraft vortices. The symbols show the results of a scattering analysis implemented computationally. The curves show the results of a simple but approximate analytical formula. Solid line and circle symbol: Vortex RCS for B-747 class aircraft. Dotted line and square symbol: Vortex RCS for DC-8 class aircraft. This figure is for a range of 1 km. Note that since aircraft vortices are not a point target, the RCS is a function of range and so the plotted results should not be used for other ranges.

Point of Contact: Karim Shariff
(650) 604-5361
shariff@nas.nasa.gov

Uncertainties in Prediction of Wake-Vortex Locations

Vernon Rossow

The capacity of many of the nation's airports is now limited by procedures that require sufficient separation distances between arrival and departures to prevent a trailing aircraft from encountering the vortex wake of a preceding aircraft. Vortex wakes must be avoided because, during the first few minutes of their duration, they contain intense swirling motions that can cause encountering aircraft to roll uncontrollably, and possibly crash. Considerable research is under way to better predict the location of vortices (shed by the leading aircraft) so that the trailing aircraft can avoid the hazardous region without excessive spacing. The objective of the work at Ames is to determine the principal sources of uncertainty associated with predicting the trailing aircraft's position relative to the vortex wakes being shed by the leading aircraft, and the effect that these uncertainties have on the spacing requirements between the two aircraft.

The primary factors that need to be considered in any computation directed at determining a vortex position relative to a trailing aircraft are

(1) the location of the wake-generating aircraft's flightpath, because it establishes the beginning location of the vortex wake; (2) the self-induced descent velocity of the vortex pair; (3) the size and location of the wake-hazardous region; (4) the wind velocity along the flightpath of each aircraft, and its variation with time; and (5) the location of the following aircraft's flightpath. The flightpath of the trailing aircraft must be included, because it is an important factor in determining the probability of an encounter. With the exception of the self-induced descent velocity of the vortex pair, all of these factors contain enough uncertainty to significantly affect the probability of a hazardous encounter for a given set of procedures and spacings for aircraft on arrival or departure at an airport.

Numerical simulation of a wide variety of arrival operations was used to study the effect of these uncertainties on the probability of a wake encounter by a following aircraft. In the study, the size of the hazardous region and the level of uncertainties in the winds along the

flightpath were varied to determine their effect on encounter probability. The uncertainty in the position of the leading and trailing aircraft was also varied in the study to cover the various levels of location accuracy achievable with the conventional instrument landing system, and with the significant improvement in the location accuracy achievable with the Local Area Augmentation System (LAAS). The LAAS is a landing-guidance system that is based on the Global Positioning Satellite System (GPSS). These simulation studies demonstrated that by implementing a more accurate aircraft positioning system based on GPSS and improving the wind measurements along the flightpath of the wake-generating aircraft, a significant reduction could be realized in the probability of a wake-vortex encounter by a trailing aircraft. That is, for the

same procedures currently in use, the foregoing improvements would translate into a potential reduction in spacing, while maintaining safety margins that are the same or greater than those in current use. The study also suggests that the proposed reduction in uncertainties may provide an ability to develop radically new and much more effective wake-vortex avoidance procedures that would not be possible with the current system at airports. For example, it may be possible to safely arrange a sequence of multiple flight corridors to airports that have a large landing surface area, instead of separate runways that accommodate only single flight corridors.

Point of Contact: Vernon J. Rossow
(650) 604-4570
vrossow@mail.arc.nasa.gov

Remote Tower Sensor System

Yuri Gawdiak, Richard Papasin, Chris Leidich, David Maluf, Kevin Bass, Hoan Mai, Chris Berg, Peter Tran

The Remote Tower Sensor System (RTSS) is a proof-of-concept prototype being developed by Ames Research Center in collaboration with the Federal Aviation Administration (FAA) and the National Oceanic and Atmospheric Administration (NOAA). Once fully installed, the system will greatly help San Francisco International Airport (SFO) improve predictions of landing conditions during weather transition periods by providing a better understanding of the formation and dissipation of clouds, weather, and wind currents in and around the airport approach zone. The project utilizes live video that is accessible over a secure Internet site. The camera system employs advanced image processing technologies to help controllers and forecasters understand and predict critical weather situations.

RTSS is leveraging off the existing Airport Approach Zone Camera System (AAZCS) project of real-time weather observations at SFO.

In FY00 the RTSS team set up a portable remote tower sensor test bed on the roof of building 269 at Ames (see fig. 1). Once testing is completed, this portable remote tower will be deployed at Half Moon Bay Airport as the first "virtual tower system" that will integrate real-time airport data in support of operations at airports without towers. Some of the key components consist of an ultrasonic wind sensor, air-temperature and relative humidity sensor, barometric pressure sensor, solar panels, wireless Ethernet, PTZ (Pan-Tilt-Zoom) motion camera, web access and logging.

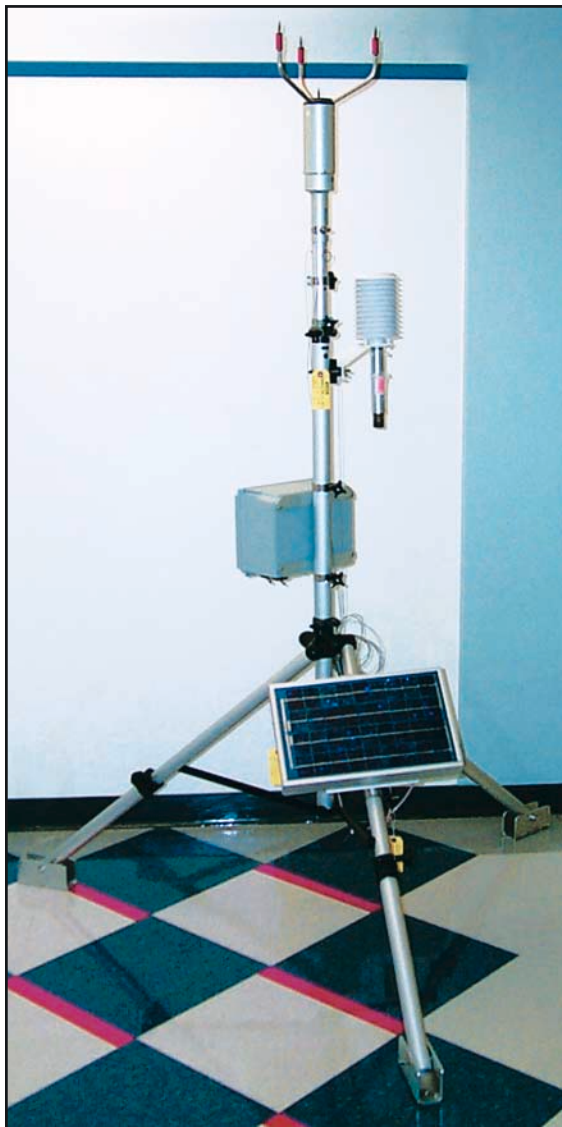


Fig 1. The Portable Remote Tower Sensor Test Bed.

On 3 March 2000 digital cameras were brought on-line at the Seattle/Tacoma (SEATAC) Tower, permitting for the first time, real-time monitoring of airport operations/weather for the tower management and TRACON.

A third part of the system came into being in June 2000 when the RTSS team set up an infrared camera test bed at SFO to measure and quantify weather-related visibility owing to low-cloud dissipation and fog surrounding the airport. The 4-day test consisted of installing the forward-looking infrared (FLIR) Alpha Indigo infrared camera system and a dual-mode visible/infrared camera onto the lower portion of the air-traffic control (ATC) tower, collecting and recording high-resolution video feeds from the cameras, and analyzing the data. RTSS can be utilized at both airports without towers as well as at major airport hubs for synthetic vision augmentation or local as well as remote low/zero visibility operations.

Point of Contact: Yuri Gawdiak
(650) 604-4765
ygawdiak@mail.arc.nasa.gov

Boeing 777 Landing Gear Noise Study

Paul Soderman, Clif Horne

As an integral part of NASA's goal to reduce aircraft noise, efforts are under way to develop the technology to measure and attenuate airframe noise generated by various components of transport aircraft. Noise caused by approach-deployed landing gear on modern

transport aircraft is comparable to that from other airframe noise sources (excluding the engines). Total airframe noise is comparable to engine noise on approach. To understand and alleviate the problem, Ames Research Center personnel, in collaboration with

Langley Research Center personnel, recently completed the first wind-tunnel study of a 26%-scale model of a Boeing 777 landing gear (fig. 1).

Using a 70-element phased microphone array developed at Ames, detailed noise maps and spectra were obtained from the 26%-scale landing-gear model in the Ames 7- by 10-Foot Wind Tunnel. Using a novel microphone assembly recessed behind a Kevlar cover flush with the wind-tunnel wall, flow noise about the array microphone was minimized, allowing landing-gear noise sources as small as 6 millimeters to be identified (23 millimeters full scale). A typical phased microphone array image of the measured noise sources is shown in figure 2. Over 50 configurations were studied, starting with a baseline six-wheel

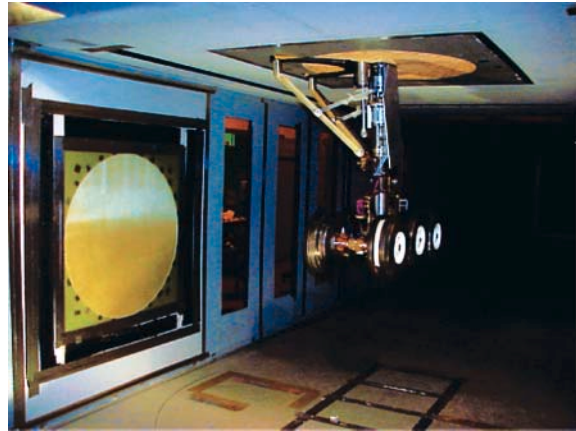


Fig. 1. Scale model of Boeing 777 landing gear in the Ames 7- by 10-Foot Wind Tunnel.

bogey, which included complex stereolithographic plastic struts, hoses, wire harness, brakes, gear door, etc., to model the flight article as

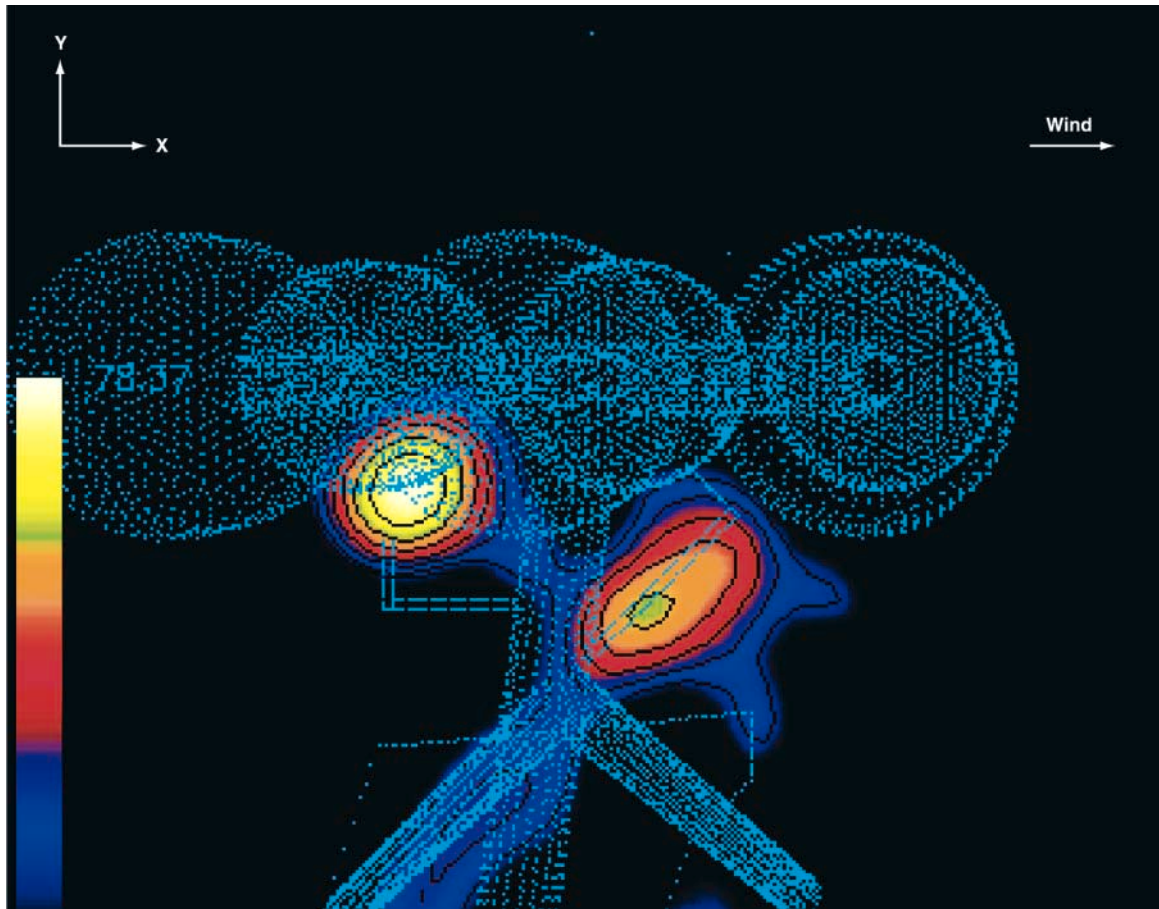


Fig. 2. Phased microphone array image of noise sources.

accurately as possible. Yaw and truck angles were varied. Various combinations of parts were removed from the baseline to rank-order noise sources. In addition, a full-faired bogey, and a simple tube and wheel mockup were evaluated. Preliminary data analysis indicates that the faired landing gear generated considerably less noise than the unmodified gear and, though full fairings may not be commercially practical, the data represent a probable lower limit of landing gear noise. The simplified tube and wheel geometry also generated less noise than the unmodified gear. Noise directivity for both flyover and sideline were obtained by mounting the landing gear model from the test section floor, ceiling, and wall. Different noise sources were important in different directions. Because drag is an important benefit of landing gear, drag data from the wind-tunnel balance will be correlated with acoustic data. Wake flow velocities were mapped to aid efforts at

Langley Research Center to model landing-gear wakes and potential interactions with high-lift systems.

The 26%-scale landing-gear model was designed to attach to the 26%-scale STAR wing, scheduled for testing in the Ames 40- by 80-Foot Wind Tunnel by the end of FY01. In collaboration with Boeing, Langley Research Center, and others, Ames researchers will measure airframe flyover noise and surface wing pressures with and without the landing gear deployed in simulated approach conditions. Various noise control devices will be evaluated. The data will be collected using the Ames phased microphone array.

Point of Contact: P. Soderman/C. Horne
(650) 604-6675/(650) 604-4571
psoderman@mail.arc.nasa.gov
chorne@mail.arc.nasa.gov

Joint Shipboard Helicopter Integration Process

Dean Giovannetti

Ames Research Center has designed, developed, integrated, and put into operation a state-of-the-art full-motion simulator for the Joint Shipboard Helicopter Integration Process (JSHIP) program. JSHIP is a Joint Military Test and Evaluation program, sponsored by the Office of the Secretary of Defense (OSD) to develop and test the processes and mechanisms that facilitate joint helicopter and ship operations. JSHIP has teamed with Ames Research Center to develop a man-in-the-loop simulator that replicates the dynamic interface of an LHA-class ship and a UH-60A Blackhawk helicopter. The objective was to develop a simulator capable of being used to define wind-over-deck (WOD) launch and recovery flight

scenarios providing increased interoperability of helicopter units not specifically designed to go aboard Navy ships.

The project required identifying, analyzing, and developing a simulation system to support the definition of helicopter/shipboard launch and recovery envelopes. Key simulation components included a compact, low-cost, wide-field-of-view, night-vision-capable, cross-cockpit visual system; a low-cost, high-resolution, PC-based image generator; integration of a four-axis dynamic seat shaker; a motion-rated simulator cab capable of operating on NASA's Vertical Motion Simulator (VMS) motion system; a visual database



Fig. 1. Simulator cab with external visual scene.

capable of simulating accurate ship and deck motions; a three-dimensional textured ocean and other visual effects; and a ship dynamics model, with airwake, representing various wind and ocean states. Figure 1 shows the simulator cab interior with the visual presentation of the ship and sea.

The new visual display system was designed to provide a 220-degree horizontal x 70-degree vertical, night-vision-goggle-compatible, continuous out-the-window field of view. This system provided all the benefits of a spherical screen at one-fifth the cost. The system consists of five off-the-shelf, high output cathode ray tube (CRT) projectors combined with custom mirrors and rear projection screens. The complete visual projection package is extremely compact and fully motion-rated to 3 g's.

The major challenge and enhancement to the simulation was the development of a wind-over-deck airwake model for a ship with a large superstructure on one side of the landing

deck. This airwake, which is highly complex and varies drastically depending on the direction of the incoming wind, is one of the most critical elements a pilot must deal with while landing a helicopter on a ship. To address this critical issue, an unsteady airwake model, developed using computational fluid dynamics (CFD) technology, was integrated into the simulation. This innovation has allowed, for the first time, an accurate representation of the wake problem. The mathematical model integrates airwake forces at 24 different points on the helicopter, including the segments of each rotor blade, the fuselage, horizontal and vertical tail, and the tail rotor. Additionally, ship-motion, landing gear, cross-coupling and engine transient dynamics were incorporated in the model.

The new simulation system provides an outstanding platform for developing WOD launch and recovery flight envelopes that will increase interoperability of helicopter units not specifically designed to go aboard Navy ships. Additionally, the system has tremendous

commercial market application in developing helicopter procedures for offshore oil platforms and inner city skyscrapers where turbulence is a major problem.

Point of Contact: D. Giovannetti
(650) 604-3871
dgiovannet@mail.arc.nasa.gov

Intelligent Neural Flight and Propulsion Control System

John Kaneshige, Karen Gundy-Burlet

The NeuroEngineering Laboratory at Ames Research Center develops flight control software that utilizes neural networks to compensate for failures resulting from control surface damage or system malfunctions. A neural network is software that works through pattern recognition, and thus is able to “learn” from sensory input, resulting in systems that can adapt to changes in their external circumstances. Neural networks have been the subject of theoretical and applied research since the early 1960s. They have been applied to a wide range of problems: from investment analysis to the control of modem equipment.

Modern commercial aircraft are among the safest transportation systems ever designed. But even with their track record of successful operation, aircraft remain vulnerable to failures of flight-control systems, whether because of accidents or equipment malfunctions. Post-accident analyses of catastrophic flight-control accidents show that stricken aircraft usually retain some working control surfaces at the time of the crash. Given enough time, a skilled pilot can determine how to compensate for the loss of a control surface, but there is usually not enough time during such an emergency for a pilot to determine the nature of the failure and learn how to compensate for it.

In 1983 a mid-air collision in the Sinai resulted in the loss of nearly all of one wing from an

F-15. Even under these dire circumstances, the pilot actually managed to land the disabled aircraft successfully, demonstrating that control of such badly damaged aircraft is possible. Is it possible to develop software that is capable of relearning the flight behavior of a damaged aircraft? Can the resulting “knowledgeable system” adapt the control of the aircraft in a way that effectively compensates for changing aircraft behavior that arises as a result of serious damage? A first-generation neural flight-control system is currently being tested on a modified F-15 aircraft at NASA’s Dryden Flight Research Center to answer these questions (fig. 1).

Commercial aircraft pose a different challenge than do military aircraft, a result of their inherently more stable designs and the



Fig. 1. F-15 ACTIVE Aircraft.

relatively benign environments in which they operate. Commercial transports are also less maneuverable, however, which means that when severe damage occurs the results can be catastrophic. An analysis of recent transport aircraft accidents shows that in many cases, engines are still operational at the time of the crash. So with this in mind, a second-generation neural flight-control system was developed and integrated with another piece of NASA software, Propulsion Controlled Aircraft (PCA). PCA manipulates engine throttles, thereby enabling the aircraft to be maneuvered and flown without the use of the control surfaces in a limited flight envelope.

The combined Intelligent Neural Flight and Propulsion Control System (INFPCS) utilizes engine control with whatever remaining control surfaces are operational. INFPCS was successfully demonstrated in the Advanced Concepts Flight Simulator at Ames over a period of 5 weeks in FY00 (fig. 2). This achievement paved the way for this technology to advance to a flight-test phase.

In addition to enhancing aircraft safety, neural flight control offers benefits during software



Fig. 2. The Advanced Concepts Flight Simulator at Ames Research Center.

design and development. Neural networks can enable the development of flight controllers for new aircraft in significantly less time than it currently takes, thereby saving enormous expense during the design and development process.

Point of Contact: Guy Power
(650) 604-5989
gpower@mail.arc.nasa.gov

Large Rotor Research Program

Thomas R. Norman, Patrick M. Shinoda, Stephen A. Jacklin

A significant operational milestone for NASA's Rotorcraft Program was met in FY00 with the installation and initial testing of a UH-60 Blackhawk rotor on the Large Rotor Test Apparatus (LRTA) in the 80- by 120-Foot Wind Tunnel at Ames Research Center. This installation (see fig. 1) is the culmination of a development program undertaken to provide a unique national capability for testing moderate-to-large helicopter and tilt rotors in the National Full-Scale Aerodynamics Complex (NFAC). The initial LRTA testing included

operating the LRTA (without blades) at speeds up to 100 knots and hover testing of the UH-60 up to full rotor speed and at 15,000 pounds of thrust. These test efforts demonstrated the structural integrity of the LRTA and verified operation of all LRTA measurement systems. With the successful culmination of these efforts, it is clear that the LRTA is ready to become the workhorse facility for NASA's large-rotor experimental programs. The first program to use the LRTA is a joint NASA/Army/Sikorsky/German effort to determine

the benefits of individual blade control (IBC) for noise and vibration reduction, and for performance improvement.

The LRTA is a wind-tunnel test stand designed for testing helicopter and tilt rotors up to 50,000 pounds of thrust and 6,000 horsepower. Developed jointly by NASA and the U.S. Army, the LRTA provides unique operational capabilities. These include the ability to measure both steady and oscillatory rotor hub loads using a five-component balance and instrumented flex-coupling, and to provide conventional collective and cyclic pitch control, as well as dynamic high-frequency blade-pitch control.

Point of Contact: Tom Norman
(650) 604-6653
tnorman@mail.arc.nasa.gov

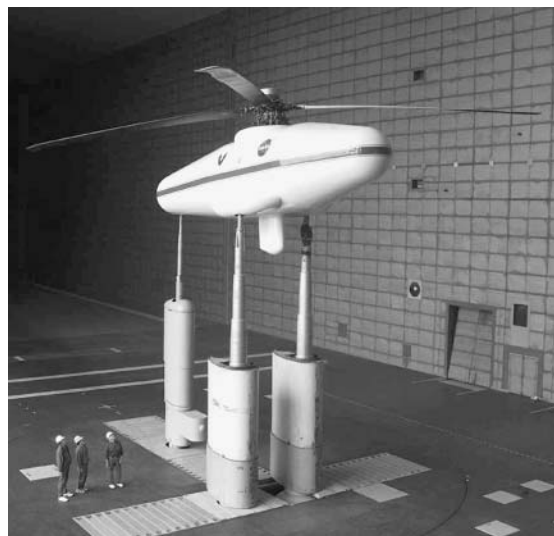


Fig. 1. Large Rotor Test Apparatus in the Ames 80- by 120-Foot Wind Tunnel.

V-22 Tilt Rotor Aeroacoustics

Megan S. McCluer, Jeff L. Johnson, Larry A. Young

The Full-Span Tilt Rotor Aeroacoustics Model (TRAM) is a nominal quarter-scale representation of the V-22 aircraft. The main objectives of the Full-Span TRAM are to investigate aeromechanics of tilt rotors, provide a comprehensive database for validating tilt-rotor analyses, and to support future tilt-rotor designs. It is a dual-rotor-powered model with extensive instrumentation for measurement of structural and aerodynamic loads unique to tilt rotors. Helicopter data trends cannot properly be extrapolated to proprotors or tilt-rotor wakes because tilt-rotor blade geometry and aerodynamic behavior are significantly different. The TRAM, having the first dynamic pressure-instrumented tilt-rotor blades, will provide the only available unsteady air loads data set that can validate tilt-rotor computational codes and will likely be used for many years.

The TRAM is a unique tilt-rotor research platform and a heavily instrumented wind-tunnel test stand. Rotor structural loads are monitored and recorded for safety of flight and for information on blade dynamic behavior. Left and right rotor balance and fuselage balance loads are monitored for safety of flight and for analysis of vehicle and rotor performance. Static pressure taps on the wing can be used to determine rotor/wing interactional effects. Rotor blade dynamic pressures and acoustics are recorded to determine the relationship between air loads and rotor noise magnitude and directivity. Tilt-rotor wake measurements also provide information about noise generation and propagation and can be used to improve computational wake models and noise predictions. Laser light sheet (LLS) flow

visualization and particle image velocimetry (PIV) flow measurements describe the wake geometry. All of these measurements will make the Full-Span TRAM database a unique and valuable asset with which computational codes can be validated and future designs can be compared.

The Full-Span TRAM was tested in Ames Research Center's 40- by 80-Foot Wind Tunnel from October through December 2000. Figure 1 is a photograph of the model installed in the test section. Rotor and vehicle performance measurements were taken in addition to wing pressures, acoustics, and flow visualization. Hover, forward flight, and airframe aerodynamic runs were performed. Helicopter-mode data were acquired during angle-of-attack and thrust sweeps for a variety of tunnel speeds and model configurations. Nondimensional performance data were acquired for three different tunnel speeds and for four different rotor-tip-path plane angles. Laser light sheet photographs suggest dual-tip vortex formation at low thrust conditions as shown in figure 2. Data from the Full-Span TRAM test will be compared with previously acquired isolated-rotor TRAM data. These results have implications for future tilt-rotor designs and will be shared with U.S. rotorcraft companies. Additional tilt-rotor aeromechanics testing using the TRAM is planned in collaboration with industry.

The Full-Span TRAM has been established as a valuable national asset for collaborative tilt-rotor research. Comprehensive data reduction



Fig. 1. The Full-Span Tilt Rotor Aeroacoustic Model (TRAM) in the Ames 40- by 80-Foot Wind Tunnel.



Fig. 2. Full-Span Tilt Rotor Aeroacoustic Model (TRAM) wake investigation (view from behind left rotor looking upstream at advancing blade). Negative tip loading produces counterrotating vortex pair, ($CT = 0.009$, Advance Ratio = 0.15).

and analysis of the 40- by 80-Foot Wind Tunnel test results will continue. Boeing and the Defense Advanced Research Projects Agency (DARPA) are sponsoring additional testing of the TRAM in the Ames 80- by 120-Foot Wind Tunnel in late 2001.

Point of Contact: Megan McCluer
(650) 604-0010
mmccluer@mail.arc.nasa.gov

Tilt Rotor Descent Aerodynamics

Mark D. Betzina

A small-scale experimental investigation was conducted in the Ames 80- by 120-Foot Wind Tunnel with the objective of studying the aerodynamic characteristics of a tilt rotor at high descent angles in helicopter mode. When helicopter rotors descend vertically or at high descent angles, they can enter a flow condition called the vortex ring state (VRS). VRS occurs when the descent velocity approaches the induced rotor-wake velocity, allowing recirculation of the wake through the rotor disk. VRS is characterized by rotor thrust loss and thrust oscillations. It can be dangerous, because the descent rate accelerates as the rotor thrust declines, and the helicopter may not have sufficient power available to slow the descent. Helicopter pilots typically avoid VRS by limiting descent rate at low forward speeds.

Tilt rotors have unique characteristics that are different from those of helicopter rotors, including higher disk loading, higher blade twist, and interactions between the two rotor wakes and with the wing. But no prior research had been done to determine if these characteristics cause tilt rotors to respond differently in VRS. Therefore, specific objectives of the current study were to determine the region of the flight envelope where VRS occurs and to determine if tilt rotors behave differently from helicopter rotors in VRS.

A single, 4-foot-diameter, three-bladed rotor, with twist and solidity similar to those of current tilt-rotor aircraft, was tested with an image plane to simulate the mean effect of a second rotor. Rotor performance data were obtained over a wide range of simulated flight conditions from horizontal flight to vertical descent.

Figure 1 shows the collective pitch required to maintain a constant rotor thrust coefficient as a

function of descent angle at an advance ratio of 0.08. The required rotor power has the same trend as the collective pitch. Large increases in collective pitch and power are required at descent angles between 40 and 60 degrees because of the thrust reduction that occurs in VRS. This thrust reduction was found to begin at descent angles between 20 and 40 degrees, depending on the collective pitch and advance ratio. This behavior could affect a tilt-rotor aircraft's response to the flight controls in VRS. Flight control simulations are required to determine the significance of these effects on aircraft controllability.

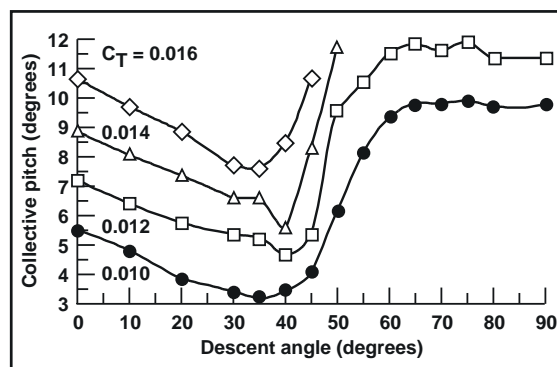


Fig. 1. Collective pitch required to maintain constant rotor thrust.

Rotor thrust fluctuations accompany the mean thrust reductions in VRS. Figure 2 shows the magnitude of the rotor thrust fluctuations, the larger symbols indicating larger fluctuations. The data are plotted on a graph of normalized descent velocity versus normalized horizontal velocity, indicating the region of the flight envelope where thrust fluctuations occur. As shown, significant thrust fluctuations are found at descent angles of 30 degrees and higher. The largest thrust fluctuations, up to 52% of the mean thrust, occur in the shaded region at descent angles between 50 and 80 degrees. The fluctuations have a very low frequency and

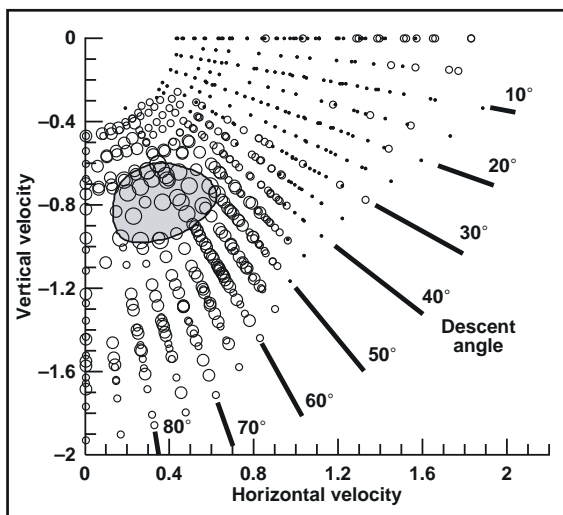


Fig. 2. Oscillatory rotor thrust magnitudes.

could cause low-frequency thrust and roll fluctuations in tilt-rotor aircraft operating in VRS.

Although these characteristics are generally similar to those of helicopter rotors, the data indicate that tilt rotors may experience larger thrust reductions and greater thrust fluctuations than single helicopter rotors. Because the image plane may not accurately represent the effects of a second rotor, further research is required to determine these characteristics for two side-by-side rotors.

Point of Contact: Mark Betzina
(650) 604-5106
mbetzina@mail.arc.nasa.gov

A Comparison of Transmission Vibration Responses from OH-58C and AH-1 Helicopters

Edward M. Huff, Irem Y. Tumer, Marianne Mosher

As part of NASA's overall goal to improve aviation safety, fundamental research is being conducted to support the development of systems that monitor critical rotating components, such as those found in helicopter gearboxes and aircraft engines. Damage detection based on observed patterns of surface vibration requires insight into the statistical properties of complex signals that are produced by interacting elements within the system, as well as the effects of in-flight maneuvering.

Table 1 shows the tendency of vibration signals to remain constant (i.e., stationary) over 34-second recording intervals. The extent of nonstationarity is dependent on both maneuver state and aircraft type, which other evidence suggests are related to vehicle weight and engine torque variations. Hence, these findings provide an essential link for developing damage-detection algorithms that are not

deceived by nonstationarity into making costly "false-alarms."

In FY2000 we conducted the first flight tests of the Ames' OH-58C aircraft and made comparisons of vibratory signals with an identical transmission tested at the NASA Glenn Helicopter Transmission Facility. Table 2 shows the results of an effort to parse signal energy for transmission component sources from these two tests. This work reveals similarities and differences between real flight and test rig vibration signals, information that is necessary to develop damage-detection algorithms with low false-alarm rates and high fault detection. Work in this area was reported at the American Helicopter Society Annual National Forum in 2000.

Point of Contact: Edward Huff
(650) 604-4870
ehuff@mail.arc.nasa.gov

Table 1. Stationarity for OH-58 and AH-1

Maneuver	Stationary Records, percent	
	OH-58 Kiowa	AH-1 Cobra
A. Forward flight, low speed	70.8	55.6
B. Forward flight, high speed	65.3	61.1
C. Sideward flight left	12.5	22.2
D. Sideward flight right	9.7	31.9
E. Forward climb, low power	50.0	97.0
F. Forward descent, low power	16.7	68.1
H. Hover	30.2	80.2
I. Hover turn left	11.1	59.7
J. Hover turn right	15.3	36.1
K. Coordinated turn left	79.2	80.6
L. Coordinated turn right	83.3	80.6
M. Forward climb, high power	65.3	86.1
N. Forward descent, high power	22.2	72.2
Average stationarity	40.6	64.2

Table 2. OH-58C and Test Rig Spectral Variance Components

Source	OH-58c Aircraft Average 4 Radial Channels				OH-58c Test Rig Sensor #3 Radial			
	Variance MS	df	Percent Total	MS	Variance MS	df	Percent Total	MS
Planetary	17.98	70	17.48		23.38	70	13.79	
Pinion - gear	15.86	18	15.42		30.14	18	17.77	
Engine	22.29	6	21.68					
<i>Residual Variance</i>	46.70	8098	45.42		116.07	8104	68.44	
Total Mean Square (MS)	102.83	8192	100.00		169.59	8192	100.00	

Wind Turbine Calculations and Validation

Robert M. Kufeld

The computation of the aerodynamic performance, flow separation, and dynamic stall on a rotating wing or blade continues to challenge the rotorcraft designer. Compressibility, stall delay, rapid change of angle of attack, dynamic stall, wake interaction, and flow unsteadiness are problems unique to rotors. Extensive research and testing to improve the calculations have been conducted over the years to help solve these problems as they relate to rotorcraft. This past year a partnership was initiated between the National Renewable Energy Laboratory and Ames to apply

computational fluid dynamics (CFD) and comprehensive computation tools developed for rotorcraft to the study of wind turbines.

CFD performance calculations (see fig. 1) were made of a research horizontal-axis wind turbine (HAWT) using a compressible Reynolds-averaged Navier-Stokes equations code using overset grids (OVERFLOW code version 1.6ap-rotorcraft) and a comprehensive vortex lattice method code (CAMRAD II). The results were compared with measurements collected during a full-scale wind tunnel test of

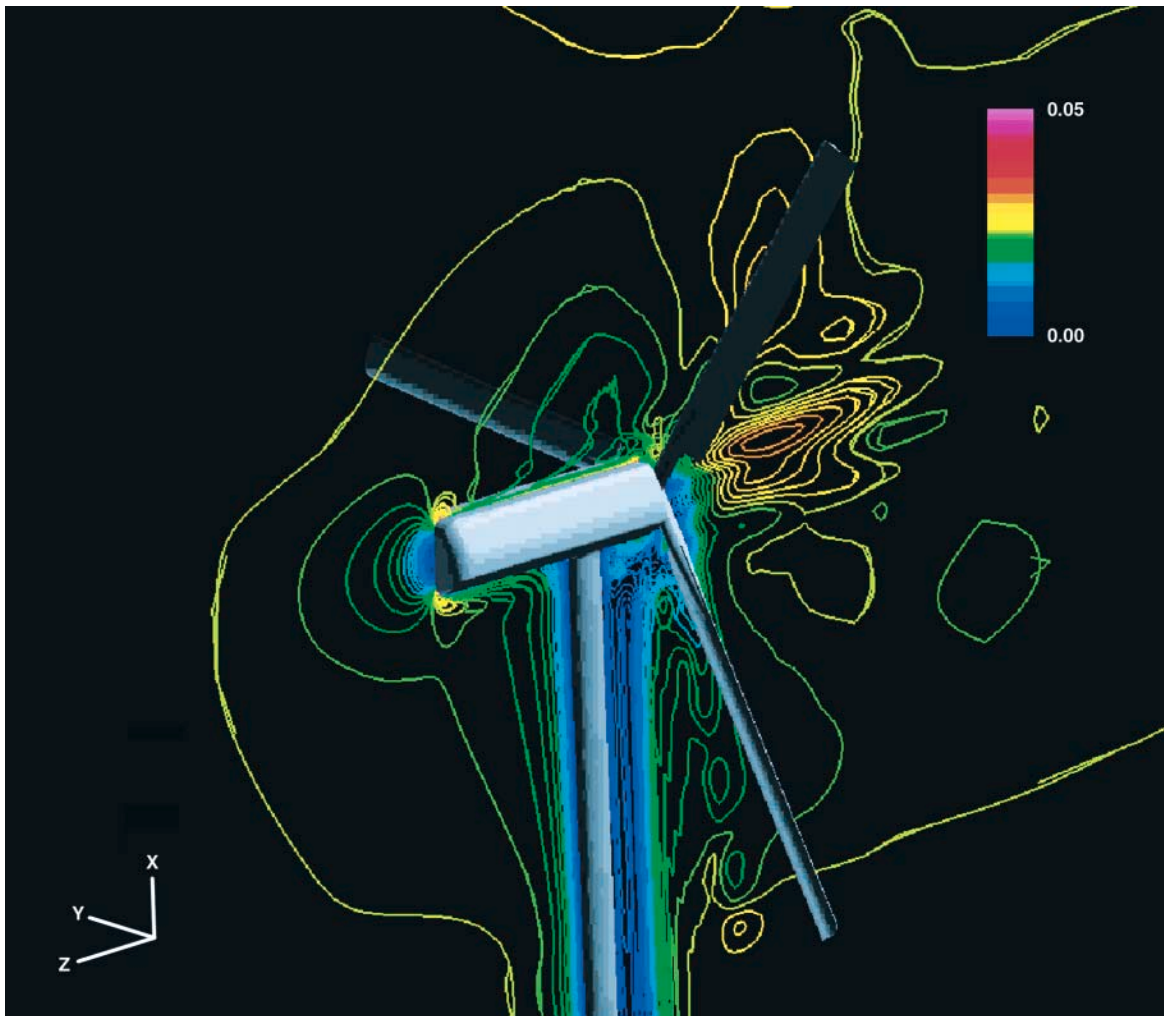


Fig. 1. Velocity contours for the complete rotor-tower-nacelle configuration as calculated by OVERFLOW.



Fig. 2. The research wind turbine inside the 80- by 120-Foot Wind Tunnel expelling smoke for wake visualization; airspeed = 7 m/sec, blade pitch = 3 degrees, yaw angle = 0.0 degrees.

the research wind turbine in the NASA Ames Full-Scale Aerodynamic Complex (80- by 120-Foot Wind Tunnel) (Fig. 2).

The research wind turbine was 10 meters (m) in diameter, turned at 72 revolutions per minute (rpm), and could generate 20 kilowatts (kW) of power. The turbine was highly instrumented with over 150 pressure transducers, strain gages, and motion sensors to identify its operational state. Easily reconfigured with both blade-pitch and nacelle azimuth control, the research wind turbine was tested in many different operational variations. Nominal testing was at airspeeds between 5 and 25 meters per second (m/sec) with a few test points recorded at 40 m/sec.

Point of Contact R. Kufeld
(650) 604-5664
rkufeld@mail.arc.nasa.gov

Remote Access and Analysis of Aeronautics Data

David Korsmeyer, Joan Walton

The DARWIN system has been developed in conjunction with new computational and experimental test technologies to provide remote access to the integrated knowledge generated from these independent systems. Version 2.5 of the DARWIN system for remote access to and analysis of aeronautics data was completed and deployed at the Ames wind tunnels in December 1999. The new and improved version was used by the Wind Tunnel Operations Division to support one of the first tests in the newly modernized 11- by 11-Foot Transonic Wind Tunnel in early January 2000.

The deployment of DARWIN version 2.5 at the Ames wind tunnels concluded a year of work by the DARWIN development team on implementing enhancements to the DARWIN system. The major new feature of this release

is a completely redesigned database schema. Building on 3 years of experience with the original database and on feedback from collaborators at NASA Langley, Eglin Air Force Base, and Arnold Engineering Development Center, the team developed a schema that can store values for a wide range of variables and thus flexibly capture information from disparate wind-tunnel test entries. All components of the DARWIN system, including the client, administrator, and database loader, were completely reworked to take advantage of the new database schema.

In addition to the new database, other features of this release include an improved client user interface and ability to review data from additional tunnel instrumentation suites, such as Video Model Deformation (VMD), Temperature Sensitive Paint (TSP), and Mini Tufts

(see fig. 1). It also includes the capability to manage and cross-plot associated computation fluid dynamics (CFD) results with the experimental data. The new DARWIN administrator allows wind-tunnel support personnel to manage the system without requiring assistance from the development team. Finally, the automated database loading system now takes a standard file format (netCDF) as input so that

accepting information produced by other data acquisition systems is easier.

Completion of the 11-foot LB435 Calibration Test in the 11- by 11-Foot Transonic Wind Tunnel marked the first support of a live wind-tunnel test entry using DARWIN version 2.5. All aspects of the system performed as advertised, including the client application, the

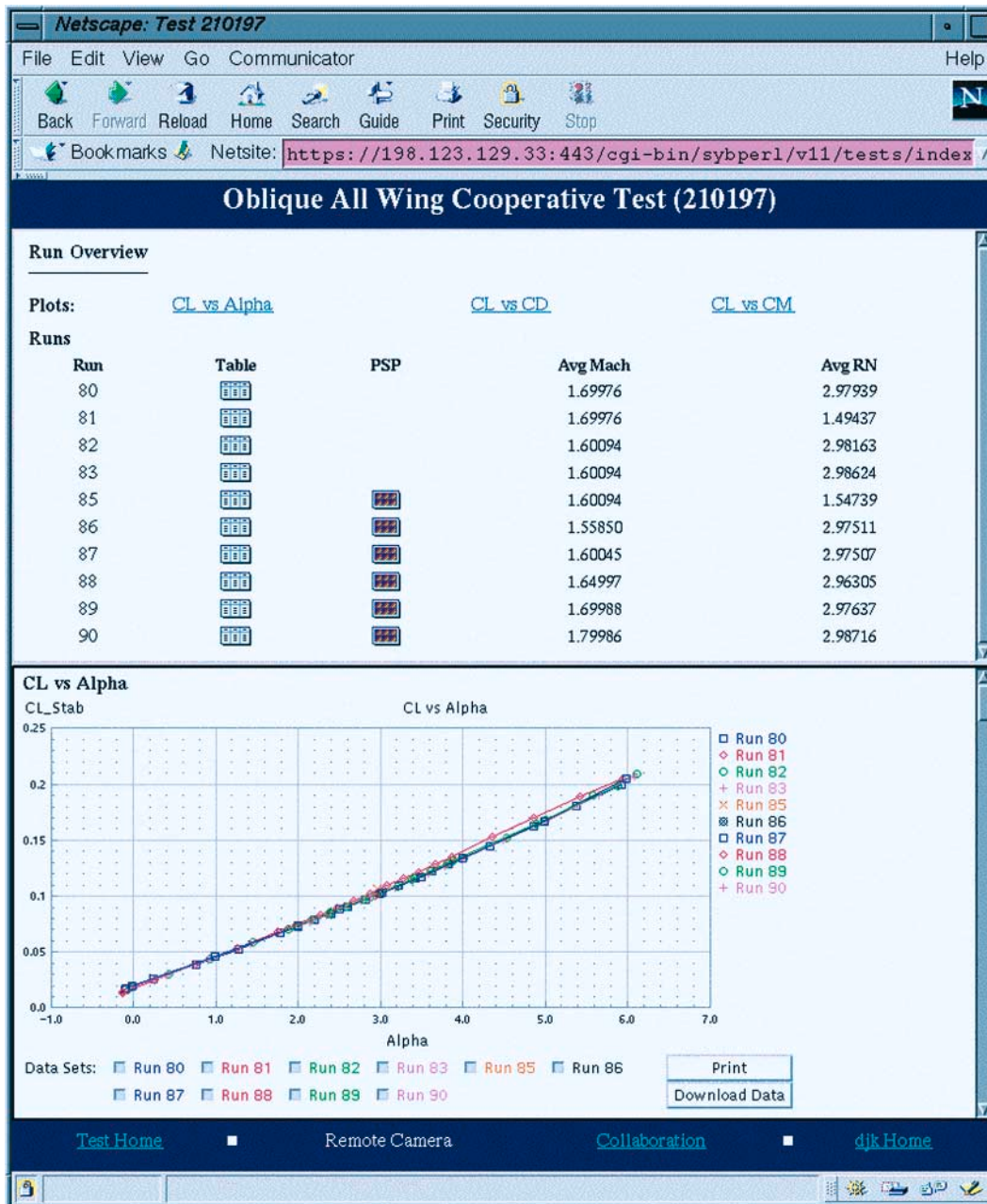


Fig. 1. The Darwin system screen showing the oblique all wing cooperative test (210197).

automated database loader, and the administrator application. The Wind Tunnel Operations staff made a few feature requests, which were addressed and implemented within a week or two of receipt. During the LB435 test, values for 119 variables were collected at 19,684 points in time, resulting in approximately 2.2 million recorded values. The DARWIN database now holds close to 20 million values across 18 wind-tunnel tests.

Deployment of DARWIN version 2.5 at Ames allows wind-tunnel customers, including NASA and university researchers, the U.S. military, and commercial aircraft manufacturers, to access wind-tunnel test data from

remote locations. Test data are available in near real time while tests are in progress and can be compared against archival tests already in the database. The DARWIN system lowers the cost of wind-tunnel tests by reducing travel requirements and providing rapid data analysis capabilities. Advances made in the version 2.5 release facilitate DARWIN support of the Unitary Plan Wind Tunnels and the National Full-Scale Aerodynamics Complex, and also pave the way for adoption of the DARWIN system at NASA Langley Research Center.

Point of Contact: David Korsmeyer
(650) 604-3144
dkorsmeyer@mail.arc.nasa.gov

Remote Large Data Set Visualization

David Ellsworth

Simulations run on large parallel systems produce data sets that contain hundreds of megabytes to terabytes of data. The researchers producing these data sets prefer to visualize them using their personal workstations. High-end PC workstations currently have the computation and graphics power to perform these visualizations. However, these workstations do not have sufficient memory to completely load large data sets. This research, which enables the use of personal workstations for visualizing data sets that are too large to be stored on personal workstations, will increase the productivity of researchers who are pushing the limits of simulations by producing very large data sets.

Because personal workstations have limited memory, out-of-core visualization techniques must be used. These techniques calculate the visualization with only a fraction of the data set resident in memory. In addition, many data sets are so large that they can only fit on central file servers. Since most file servers do

not have significant extra central processing unit (CPU) and memory capacity, remote out-of-core visualization is required.

Our earlier research developed an out-of-core visualization technique called application-controlled demand paging. This technique loads the data required by the visualization algorithm from disk into main memory as necessary. The technique works well because most visualization algorithms only use a small fraction of the entire data set. The overall speed typically increases as the user interacts with the data set, since previously loaded data are retained if possible. This means that the overall speed will soon approach the speed that would be seen if the entire data set were loaded into memory.

However, the original implementation of out-of-core visualization using demand paging did not try to perform computation, disk access, or network access at the same time. When the implementation detected that data must be

read, it stopped the calculation and waited for the data to be read from disk. If the data was read from disk on a remote server, the network transfer time increased the delay.

The new algorithm overlaps the computation, disk access, and network transfer by dividing the visualization into a number of tasks. When one task must wait for data to be retrieved from disk, a scheduling algorithm runs another task to keep the processor busy. The data retrieval from local or remote disk proceeds independently while the requesting task waits.

The new algorithm is general enough to support a variety of visualization techniques. The visualization techniques do have to be modified so that the work can be divided into a number of smaller tasks. However, this is the same as modifying the visualization so it can

be run in parallel, which is useful in itself and is likely to have already been performed.

Figure 1 shows one data set that was visualized using the new algorithm. This figure shows the Harrier jet flying slowly 30 feet off the ground with spherical particles showing the path of the jet exhaust. This large (107 gigabyte, 1,600 time-step) data set was produced by Ames researchers during their investigation of the cause of oscillations seen during landing.

Figure 2 has timings that show the improved performance of the new algorithm. It shows the time required to compute the entire 1,600-frame animation when data were read from a remote system over a 800-Mbit/second HIPPI network. Both the local and remote systems were SGI Onyx systems. The chart compares the performance seen using the standard



Fig 1. Simulation of the Harrier flying 30 feet above the ground.

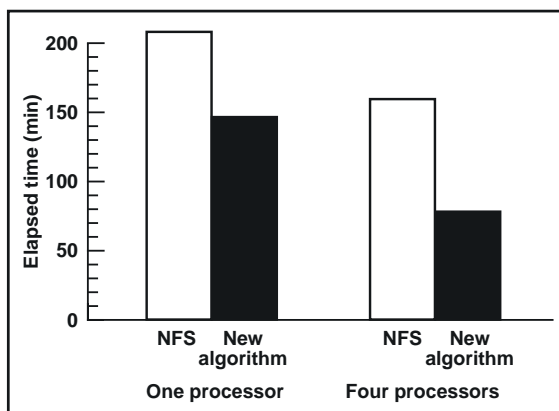


Fig 2. Improved performance of the new algorithm compared to using NFS, for one and four processors.

Network File System protocol to retrieve the data against the time using the new algorithm. When using one processor, the time decreased from 207 minutes to 146 minutes, a 30% decrease. When four local processors were used, the time decreased by more than half, from 159 to 77 minutes.

Point of Contact: David Ellsworth
(650) 604-0721
ellsworth@nas.nasa.gov

Computational Simulation of High-Lift Wind-Tunnel Test

Stuart E. Rogers

The modeling requirements for validating viscous computational fluid dynamic simulations of a high-lift trapezoidal wing were investigated. This wing has a full-span slat and a full-span flap, and has been tested extensively in the Ames 12-Foot Pressure Wind Tunnel. Because of the size of the wing, there are significant facility effects in the data from the 12-foot wind tunnel. The objective of the work was to quantify the effect of wind-tunnel walls, and to develop a computational model that would effectively simulate this effect.

Two different computational models of the test facility—differing in fidelity—were developed and tested. The first of these is a complete viscous simulation of all surfaces within the 12-foot wind-tunnel test section. This computational model more than doubles the cost of computing the flow over the trapezoidal wing, as compared to simulating free-air conditions. The second model of the wind-tunnel test section was a highly simplified straight duct, whose wall was treated as an inviscid surface. The surfaces used in this second model are shown in figure 1. Simulations with the second

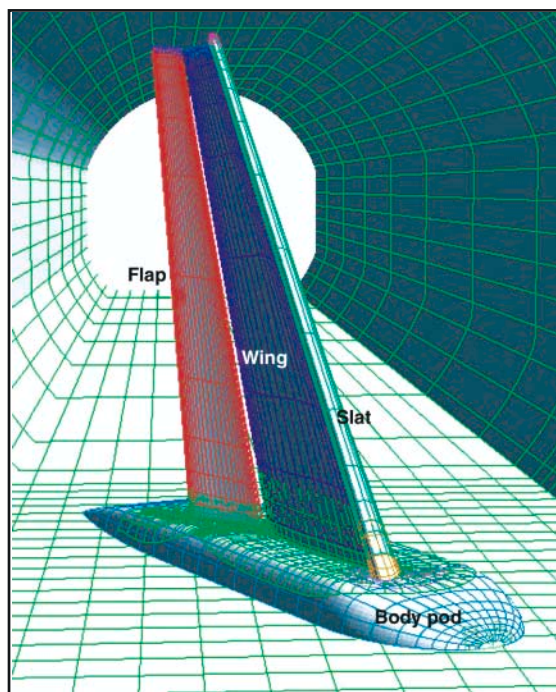


Fig. 1. Surfaces of the trapezoidal wing and simplified wind-tunnel test section.

model required the same computational time and memory as a free-air simulation.

The computed results were compared with experimental lift, drag, and surface pressure data. The results showed that the simplified inviscid model of the test section performed as well as the high-fidelity, viscous test-section model. Computed results generally compared very well with the experimental data at all but the highest angles of attack. Figure 2 is a plot of the lift coefficient versus angle of attack for the computational simulations and experimental results. The computed results include lift from both of the wind-tunnel models, as well as a free-air simulation. The experimental

results include the original uncorrected data, and data which include theoretical corrections to exclude the effect of the wind-tunnel walls. A comparison of computational results from both free-air and wind-tunnel simulations at the same lift condition indicated that it was necessary to simulate the wind-tunnel in order to perform validation using the 12-foot wind-tunnel experimental data.

Point of Contact: Stuart E. Rogers
(650) 604-4481
rogers@nas.nasa.gov

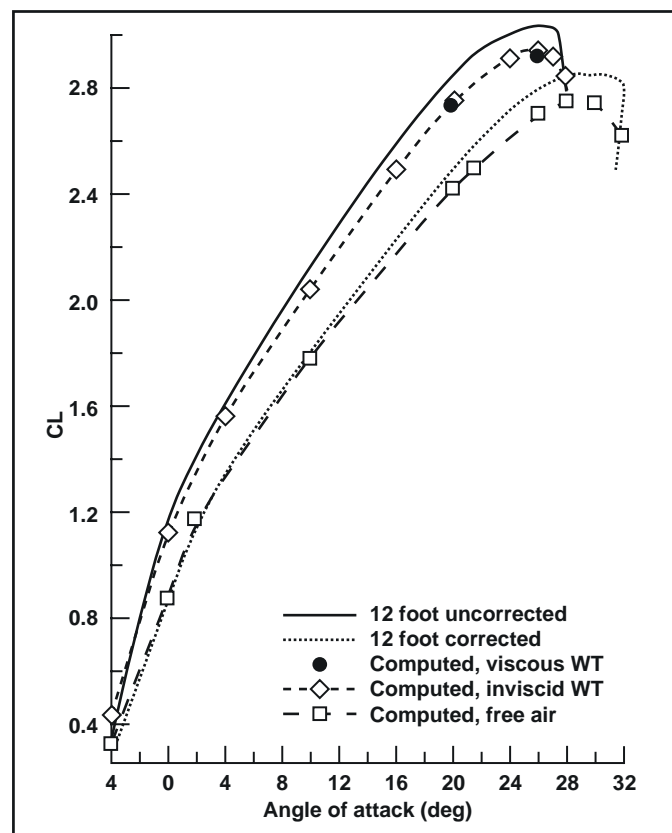


Fig. 2. Lift coefficient versus angle of attack.

Parametric Powered-Lift Navier–Stokes Computations

Neal M. Chaderjian, Scott Murman, Shishir Pandya, Jasim Ahmad

The goal of this work is to enable the computation of large numbers of unsteady high-fidelity flow simulations for a YAV-8B Harrier aircraft in ground effect by improving the solution process and taking advantage of NASA parallel supercomputers. The YAV-8B Harrier aircraft can take off and land vertically, or utilize short runways by directing its four exhaust nozzles toward the ground. Transition to forward flight is achieved by rotating these nozzles into a horizontal position.

The success and unique capabilities of the Harrier have prompted the design of a powered-lift version of the Joint Strike Fighter (JSF). Directing the exhaust nozzles toward the ground results in very complex and time-dependent flows consisting of ground vortices, jet flows along the ground plane, and hot jet fountains that impact the underside of the vehicle. The high-speed jet flows cause low pressures underneath the vehicle, resulting in loss of lift (suck-down effect). Moreover, hot gas ingestion (HGI) by the inlets can result in a sudden reduction in thrust (powered lift).

Safe flight operations near the ground are dependent on understanding and avoiding these problematic conditions. Time-accurate Reynolds-averaged Navier–Stokes (RANS) computations to date have focused on simplified geometries such as single or multiple jets in cross flow, delta wings with jets in ground effect, and a single Harrier RANS solution in ground effect. Two key obstacles remain in simulating these flows, the need for improved accuracy and the need for faster solution methods. This research focuses on faster solution methods, a key requirement for improving solution accuracy and enabling flow

simulations for powered-lift vehicles in ground effect in a more routine manner.

Forty-five time-accurate RANS flow simulations using the OVERFLOW-MLP code have been computed with a free-stream velocity $V = 33$ knots, an angle of attack range of 4–12 degrees with 1-degree increments, a height range of 10–30 feet with 5-foot increments, and a Reynolds number based on the body length of $Re = 15.2$ million. Because of the danger of gas injection and the suck-down effect, a Harrier pilot will not ordinarily maintain a constant altitude of less than 30 feet when operating at very low speeds or hover flight conditions. However, typical aerodynamic models require the static stability derivatives, or forces and moments, near the ground to simulate takeoff and landing scenarios. Therefore static computations have been carried out in this height range.

PERL scripts have been developed to automate the grid generation, numerical flow simulation, and data analysis processes. A Unix-based directory structure is used to store the thousands of files (over a terabyte) generated by these solutions. The user simply specifies the flow parameters, and the scripts automatically store and retrieve the data files. The current 45-solution database was generated using a NASA 512 processor 400-megahertz/R12000 Silicon Graphics Origin 2000 single-image computer. A typical flow simulation consisted of running nine cases concurrently using 16 processors per case, for a total of 144 processors. The number of cases and processors is arbitrary, depending on the computational resources. A nine-case run typically requires 14,000 node-hours.

Figure 1 shows two snapshots from a streak-line animation when the Harrier is 30 feet above the ground. The flow particles are colored by temperature, where red is hot and blue is cool. The ground vortex was found to vary in size with a frequency of 0.478 Hertz. Experimental measurements for a jet in crossflow found similar low frequencies. These very low frequencies require several seconds of real-time flow simulations. At this height, the inlet does not ingest any hot gasses. Figure 2 is a snapshot from a streak-line animation when the Harrier is only 10 feet above the ground. The ground vortex and its core are identified in the figure. The flow particles are rendered by small spheres and colored by temperature. The jet fountain forms a second vortex in front of the ground vortex, which is ingested by the inlet. Thus, HGI is a problem at this height. The long-term goal is to use this new capability, together with neural networks, to generate a stability and control database for a powered-lift vehicle in ground effect.

Point of Contact: Neal M. Chaderjian
(650) 604-4472
nchaderjian@mail.arc.nasa.gov

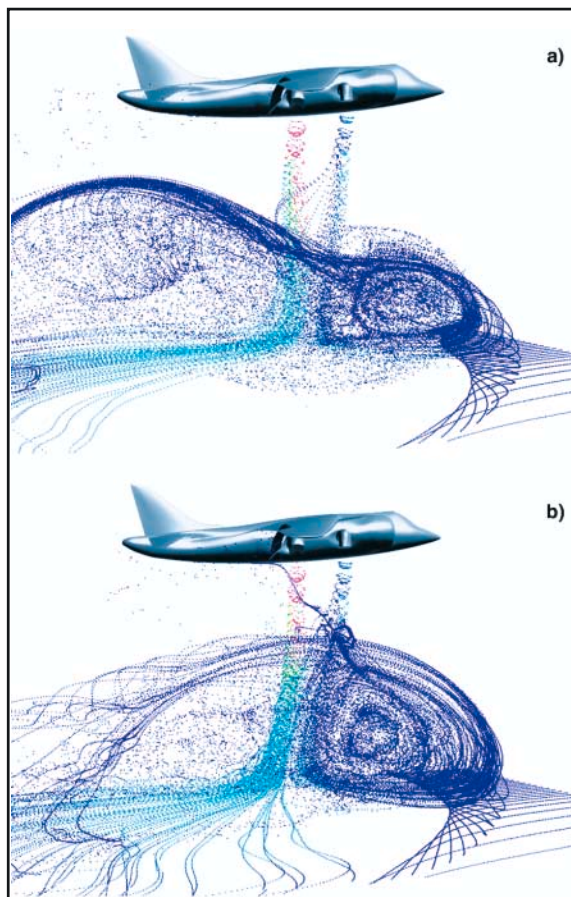


Fig. 1. Streak-line animation showing time variation of ground vortex size: height = 30 feet.

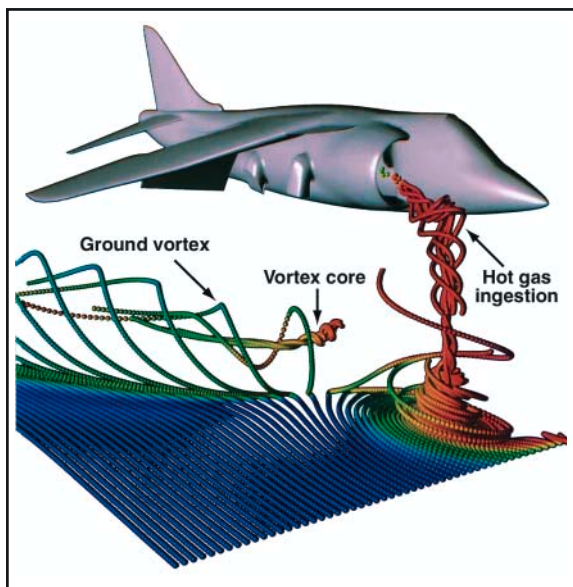


Fig. 2. Streak-line animation showing ground vortex and hot gas ingestion: height = 10 feet.

Computational Fluid Dynamic Simulation of Space Shuttle Orbiter During Contingency Abort Maneuvers

P. Papadopoulos, D. Prabhu, M. Wright, C. Davies, R. McDaniel, J. Brown, E. Venkatapathy, P. Wercinski

To improve the safety of the space shuttle orbiter (SSO), NASA is reexamining return-to-launch-site and transatlantic abort scenarios. Ames Research Center, in partnership with Boeing Reusable Space Systems (BRSS) and Johnson Space Center (JSC), has used computational fluid dynamics (CFD) to estimate the aerodynamic loads that would be experienced by the SSO during these abort maneuvers, for which very limited information exists relating to surface pressure distributions. Ames provided 38 cases that cover the Mach number range from 3.5 to 15, angle of attack range of 20 to 60 degrees, three elevon/body-flap combinations, and two speed-brake deflections. Additionally, five benchmark cases were computed and compared with data from the Orbiter Aerodynamic Data Book (OADB), which is the rigorous standard of SSO aerodynamics.

To accommodate the variety of control-surface deflections, the grid-generation strategy implemented by Ames was to build an initial "master" volume grid with topological characteristics that allowed replacement of localized volume grids around the control surfaces without changing the rest of the grid. The resulting volume grid consists of 38 zones with approximately 2 million grid points. CFD computations were performed using the General Aerodynamics Simulation Program (GASP). The overall strategy implemented to compute the contingency abort flight conditions used methods derived from the X-33

program. Automation tools were developed for setting up the cases, checking for convergence and quality, computing surface pressure and hinge-moment data, and postprocessing the results in a format useful for aerodynamic and structural analysis. Figure 1 shows an example of a computed solution. Flooded color contours of the surface pressure coefficient are shown at conditions of Mach 15, angle of attack 50 degrees, and inboard and outboard elevons at 10 degrees trailing-edge down. This flight condition (and most of the other cases simulated) are beyond the nominal flight envelope for the shuttle but are potential contingency abort trajectory flight conditions.

An SSO aerodynamics panel was convened at JSC to review the computations and to determine their acceptability for abort assessment. The details of the CFD process, comparisons with the OADB for integrated forces and moments, and comparisons with pressure data from available ground and flight measurements were presented to the SSO aerodynamics panel. The computations agreed very well over a range of Mach numbers from 3.5 to 15.0 and of vehicle attitude ranging from 20 to 60 degrees. In a limited number of cases, differences existed between the predicted aerodynamic coefficients and the OADB data. Analysis of the CFD simulations in these cases showed unique flow physics related to the growth of the subsonic region on the windward side of the vehicle. The combined effects of Mach number and real-gas flow physics were

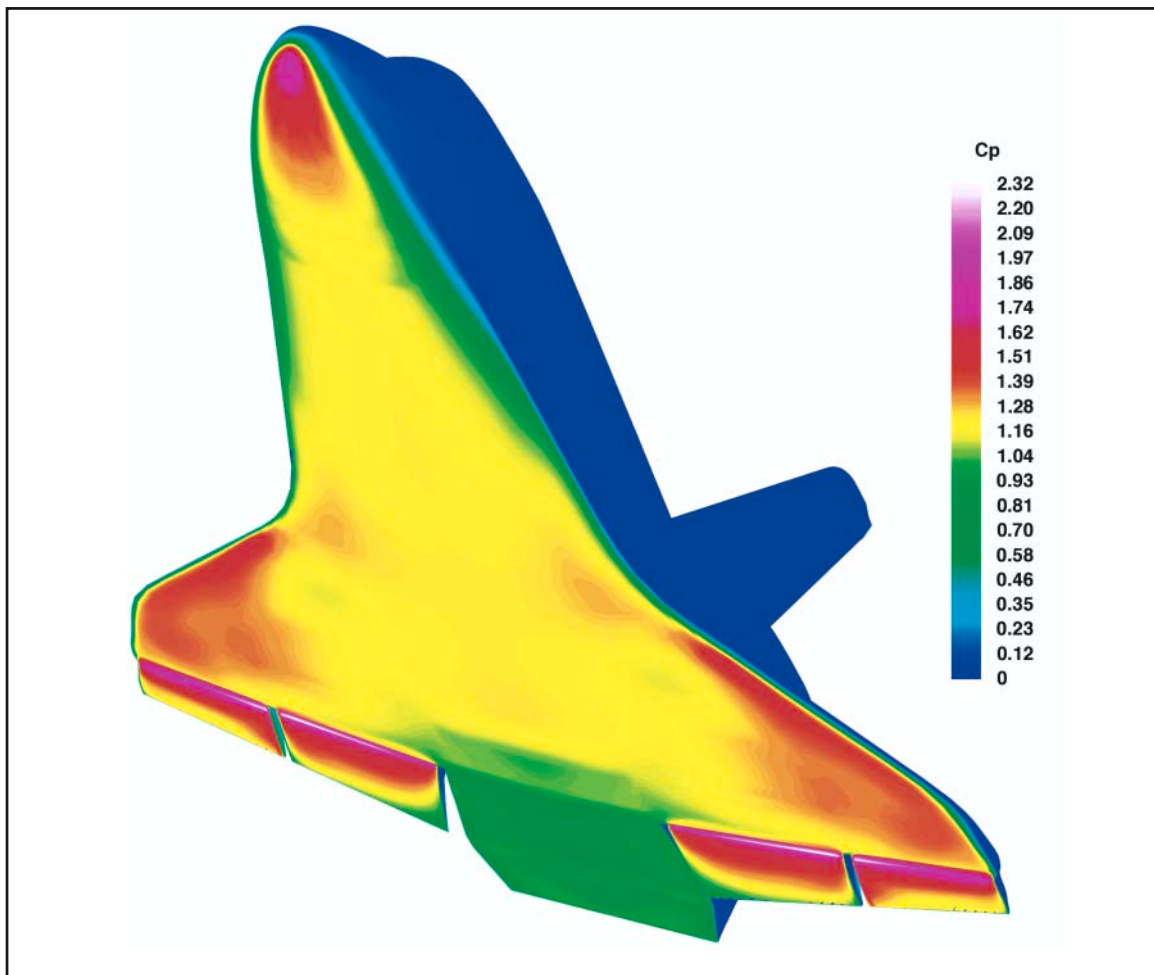


Fig. 1. Surface pressure coefficient distribution at Mach 15, 50-degree angle of attack, and elevons at 10 degrees trailing-edge down.

identified as the reason for the differences. Analysis was presented to substantiate these observations. Review of the historical development of the OADB, and in-depth analysis of the CFD solutions have led the SSO aerodynamics panel to favor the CFD solutions in the high Mach number and angle-of-attack regime. The overall good agreement between the CFD predictions and the OADB has led the Shuttle Program to accept the CFD predictions as the

basis for the Orbiter Contingency Abort Data Base, an extension for the current OADB. The detailed pressure distributions generated at key abort conditions will be used as the basis for evaluating the capability of the SSO during specific abort scenarios.

Point of Contact: P. Papadopoulos
(650) 604-3477
ppapadopoulos@mail.arc.nasa.gov

Automated Computational Fluid Dynamics for Large Test Matrices

Michael Aftosmis, Marsha Berger, Shishir Pandya, John Melton

The “virtual flight” and preliminary design of conceptual vehicles require running hundreds or even thousands of aerodynamic simulations. Practical computation of such large test matrices places a premium on automation of the entire simulation process and on automated control of data flow and job execution. In recent years, Cartesian mesh methods have made rapid strides toward the goal of fully automated aerodynamic analysis. Based on this technology, Ames researchers, with partners from the Courant Institute (New York University), have developed systems for automatically running the extremely large matrices of simulations required for preliminary design and virtual flight. When design permutations or control surface deflections modify the shape of a vehicle, the system automatically generates the new geometry, remeshes the design, and runs simulations covering a wide range of flight conditions to populate the test matrix. This capability allows users to evaluate a proposed design over its entire flight envelope, rather than at only a single flight condition. It also provides detailed information about vehicle stability and control and has been used in support of virtual flight by populating an aerodynamic database for Ames’ Vertical Motion Simulator.

Traditional structured and unstructured approaches to computational fluid dynamics (CFD) rely upon body-fitted meshes to discretize the space surrounding a vehicle. Since the mesh must be fitted to the geometry, meshing is generally an interactive process and can consume several months of the CFD cycle. In contrast, Ames’ Cartesian approach is based on the use of nonbody-fitted Cartesian cells. These cells are free to arbitrarily intersect the vehicle, and such intersections are accurately

accounted for by using techniques from computational geometry. Fundamentally, the approach trades the case-specific problem of generating a body-fitted mesh for the more general problem of computing and characterizing intersections of the cells touching the body. This generality means that analysts need not be concerned with details of the surface geometry and leads directly to automation.

With mesh generation, a fully automatic process, analysts are free to control the simulation from a more macroscopic level. A typical simulation matrix may study the effects of a deflection of a control surface (flap, aileron, rudder, etc.) over a range of Mach numbers and angles of attack. For example, testing a configuration with five different flap deflections, each at five Mach numbers, five angles of attack, and five sideslip angles produces a test matrix with 625 cases ($5 \times 5 \times 5 \times 5 = 625$).

The upper left frame in figure 1 shows a recent example of a space shuttle configuration with 20 separate components and 13 moveable control surfaces. The lower left frame gives an overview of a typical multilevel Cartesian mesh containing approximately 2 million cells. The three frames at the right of the figure show the mesh system’s automatic response to deflection of the main body-flap to 0, 15, and 30 degrees. The system will automatically deflect the control surface, regenerate the mesh, and run each new case over a specified sweep of Mach number, angle of attack, and sideslip.

The automated run system drives Ames’ Cart3D inviscid simulation software package. It includes tools for surface preprocessing, mesh generation, flow solution, and postprocessing. Recent in-house examples with

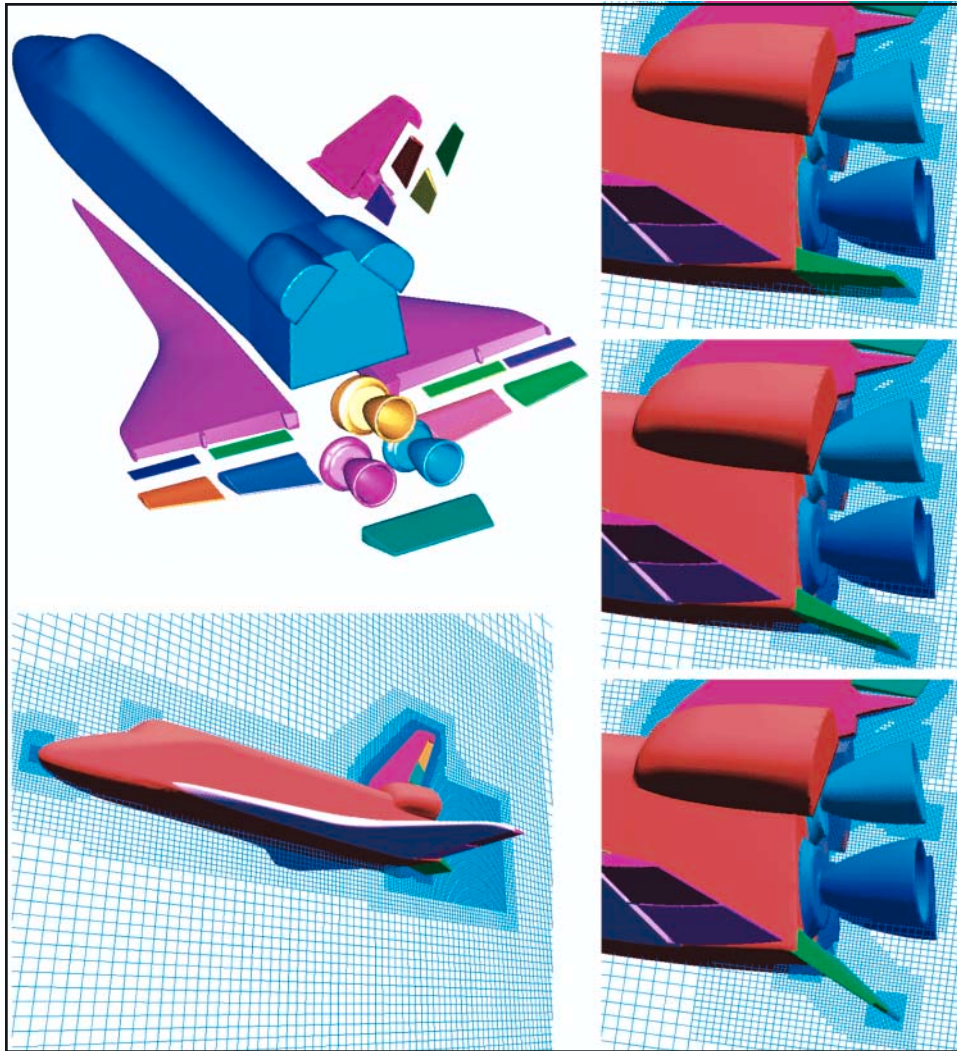


Fig. 1.(a) A recent example of a space shuttle configuration with 20 separate components and 13 moveable surfaces; (b) an overview of a typical multilevel Cartesian mesh containing approximately 2 million cells; and (c) the three frames show the mesh system's automatic response to deflection of the main body-flap to 0, 15, and 30 degrees.

configurations such as these have populated test matrices of over 400 cases in under 24 hours without dedicated computing time. External users in the Department of Defense (DoD) have reported running over 1,200 cases/day on dedicated computers. Cart3D has been distributed to over 80 sites, including four NASA Centers, several DoD and Department of Energy laboratories, as well as various sites

within U.S. industry and academia. The package runs on computers ranging from simple desktops to high-performance parallel platforms and is being commercialized through the Ames Commercial Technology Office.

Point of contact: Michael Aftosmis
650-604-4499
aftosmis@nas.nasa.gov
<http://www.nas.nasa.gov/~aftosmis/cart3d/>

Highly Maneuverable Crew Transfer Vehicle Design Study

James Reuther, David Kinney

The Highly Maneuverable Crew Transfer Vehicle (CTV) design study was undertaken to explore the effects of sharp leading edges on future reusable aerospace vehicles as part of NASA's Advanced Space Transportation Program (ASTP). More streamlined shapes should provide significant performance advantages during hypersonic flight by reducing the drag caused by the large bow shock present on blunt shapes. These performance improvements lead to significant increases in mission safety. Exploiting these advantages has been inhibited by the fact that exposing a sharp leading edge to the hostile conditions experienced during atmospheric reentry drives surface temperatures higher than can be tolerated by traditional materials. Fortunately, materials research under way at NASA Ames has led to the development of a new class of ultrahigh-temperature ceramics (UHTC) that can repeatedly survive such conditions.

Under the SHARP-CTV study project, a new CTV concept vehicle was designed that required a combination of existing tools, new analysis techniques, and new optimization processes. New methods included improving predictions of the temperature and heat flux around a sharp leading edge and the ability to calculate optimal cross-range and abort trajectories that included aerothermal performance constraints (APC). These methods were used in combination with an existing space vehicle conceptual design code called HAVOC. Aerodynamic predictions with HAVOC were benchmarked with advanced computational fluid dynamic (CFD) codes and limited wind-tunnel testing.

The SHARP-CTV-V5 design shows dramatic improvements over the blunt-nosed HL-20 in reentry cross-range and abort-safety while

meeting all other required capabilities. The team ran hundreds of low- and high-fidelity CFD analyses, optimized numerous trajectories, and constructed a low-speed wind-tunnel model to verify vehicle landing capabilities.

The improvements in performance and safety are illustrated by considering a typical due east (28-degree inclination) launch from the Kennedy Space Center (KSC). Calculations were carried out for both the HL-20 and SHARP-V5 in which it was assumed that a Titan III launch vehicle carried the CTVs to orbit. During nominal reentry or on launch abort, the CTV becomes a glider. In the case of 28-degree launch abort, the glide maneuver originates over the mid-Atlantic. Improved aerodynamics dramatically improves the capability of the vehicle to reach a greater number of alternative landing sites. In the case of HL-20, a booster failure that occurs between 64 and 390 seconds after launch results in the need to ditch into the Atlantic. For SHARP-CTV-V5 the Atlantic ditching window for a 28-degree inclination launch is from 64 to 218 seconds. The ground tracks of these abort scenarios are shown in figure 1. As shown in figure 2, similar calculations for a 51-degree (International Space Station, ISS, orbit) inclination launch from KSC produces an even more dramatic effect. HL-20 has a North Atlantic Ocean ditch window of between 355 and 403 seconds. By comparison, SHARP-CTV-V5 can always safely make an airport landing regardless of the time of booster failure.

The reduction in aerodynamic drag at hypersonic speeds not only assists in the abort safety capability but also improves the entry cross-range capability. Since ISS is at a 51-degree inclination orbit, depending on the orbital track

it is in, it may follow a ground track that takes it very far from the continental United States. If a CTV is to serve as an alternative ISS emergency escape system, it is a highly desirable capability to be able to land within the continental United States during a single orbit, irrespective of the ISS orbital track. The cross-range measures the distance away from the ground track that a vehicle is able to obtain. For HL-20 the cross-range is optimized to be 1,360 nautical miles (n.mi.), whereas for the

SHARP-CTV-V5 the optimized cross range is 3,500 n.mi. The difference between these two numbers implies that SHARP-CTV-V5 will always be able to perform the within-one-orbit escape mission, while the HL-20 would only be able to do it about half the time.

Point of Contact: James Reuther
(650) 604-1516
jreuther@mail.arc.nasa.gov

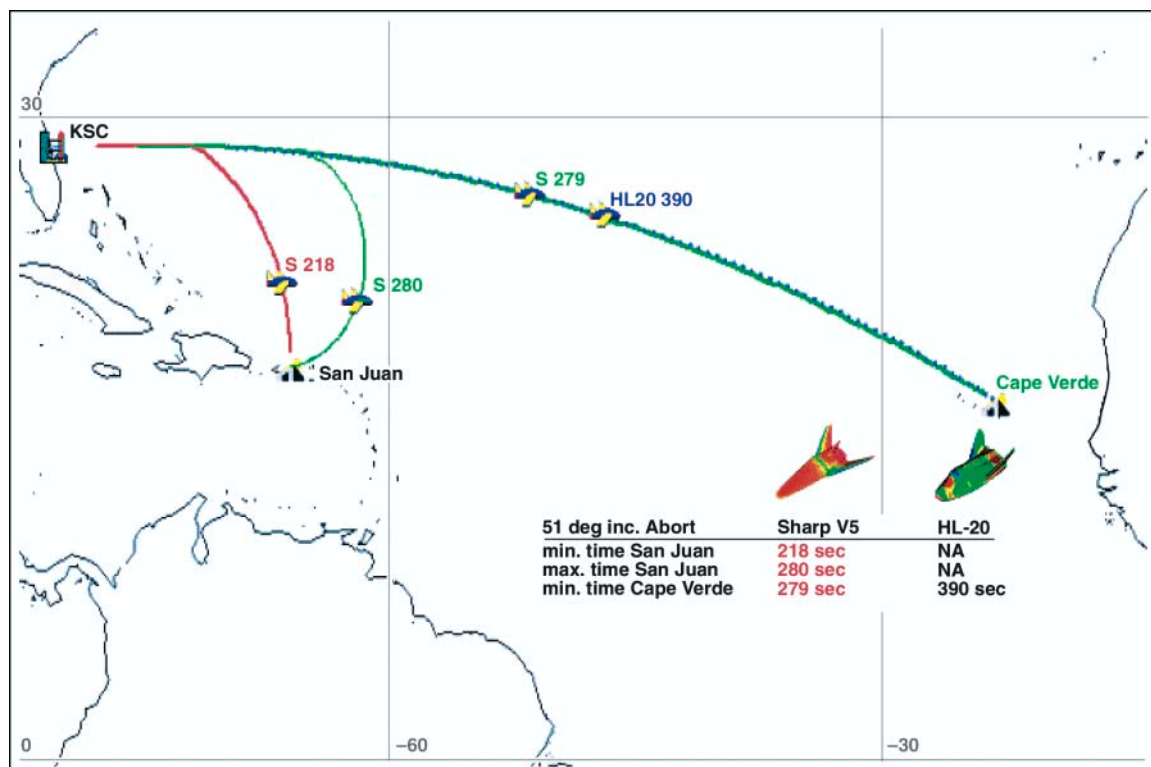


Fig. 1. Simulated ascent booster failure for both HL-20 and SHARP-V5 on a 28-degree inclination orbit.

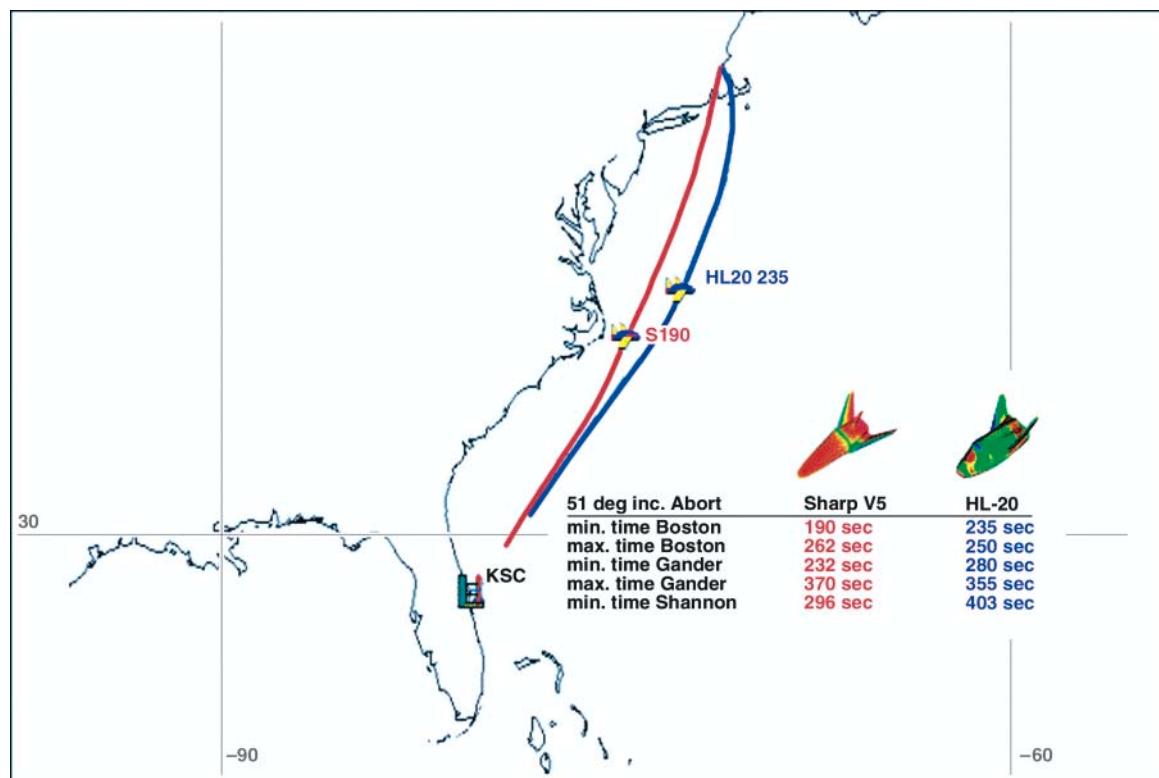


Fig. 2. Simulated ascent booster failure for both HL-20 and SHARP-V5 on a 51-degree inclination orbit.

Slender Hypersonic Aerothermodynamic Research Probe Ballistic Flight Experiment B2

Don Ellerby, Sylvia Johnson

The Slender Hypersonic Aerothermodynamic Research Probe Ballistic Flight Experiment B2 (SHARP-B2) was the second ballistic flight experiment in which the behavior of ultrahigh-temperature ceramic composite (UHTC) materials in a hypersonic flight environment was investigated. As in SHARP-B1, the SHARP-B2 flight experiment was a collaborative effort of Ames Research Center, Sandia National Laboratories, and the U.S. Air Force. The primary objective of the SHARP-B2 flight experiment was to investigate the aerothermal and thermal structural performance of the

UHTC materials near their aerothermal performance constraints, for example, their maximum single-use and multiple-use temperatures. A secondary objective was to recover the UHTC components to observe their condition after a hypersonic ballistic reentry.

Ames is investigating UHTC materials as an enabling technology for the development of reusable launch vehicles with sharp leading edges. Vehicles with sharp leading edges are desirable because of their potential for significant improvements in aerodynamic performance, lift-to-drag ratio (L/D), compared with

the current reusable launch vehicle, the space shuttle orbiter, which has a relatively blunt leading edge. The enhanced aerodynamic performance of a vehicle with sharp leading edges will lead to improved crew safety by increasing the window during ascent when a safe abort to ground can be performed and by increasing the cross-range of the vehicle, thus increasing the number of landing sites available during descent.

Significantly higher heating occurs on sharp leading edges during hypersonic flight than on blunt leading edges like those on the space shuttle. Therefore, if launch vehicles with sharp leading edges are to be used, new materials capable of withstanding these high temperatures must be developed. UHTCs are a family of ceramic materials with very high melting temperatures and good oxidation resistance in reentry environments. Ground-based arc-jet testing has demonstrated the potential of these materials in reusable applications at temperatures approaching 4,000°F; thus they offer the potential to develop passively cooled sharp leading edges.

The components flown on SHARP-B2 were much closer in geometry to what would be considered a sharp leading edge (see fig. 1)

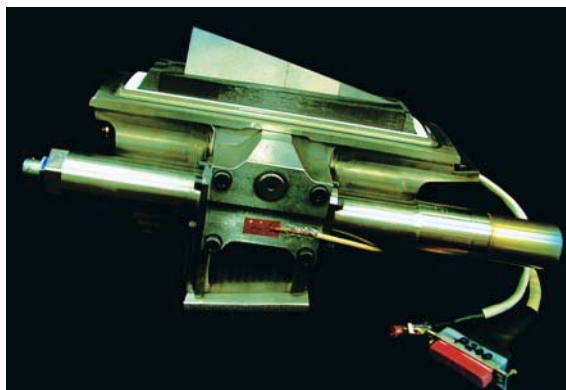


Fig. 1. UHTC strake.

than the axisymmetric nose tip flown on SHARP-B1. The strakes, as the UHTC components are referred to, are made of three segments, and each segment is composed of a different UHTC material, thus making it possible to investigate the performance of three different materials during a single flight experiment. Four strakes were equally spaced around the reentry vehicle and were split into two pairs; one strake in each pair was instrumented with sensors to measure the temperature within the strakes. The temperature was then correlated with the vehicle's altitude and velocity and compared with preflight predictions. The strakes were designed so each pair would be retracted at a specified altitude.

Figure 2 shows the SHARP-B2 mission scenario. The reentry vehicle was carried on a Minuteman III and was launched from Vandenberg Air Force Base on 28 September 2000. During reentry the strake pairs were retracted at predetermined heights based on aerothermal predictions of when the aft sections of the strakes would reach their multi- and single-use temperature limits. A parachute was then deployed to minimize the impact velocity in the Kwajalein atoll lagoon in the west Pacific. The reentry vehicle, with the retracted strakes, was then recovered.

The SHARP-B2 flight experiment provided a tremendous amount of data on both the strakes' aerothermal environment as well as the thermal and mechanical properties of the UHTC materials. Postflight analysis is providing invaluable information for future flight experiments. Recovery of the strakes demonstrates the need for postflight characterization of flight articles to facilitate materials development.

Point of Contact: Donald Ellerby
(650) 604-2811
dellerby@mail.arc.nasa.gov

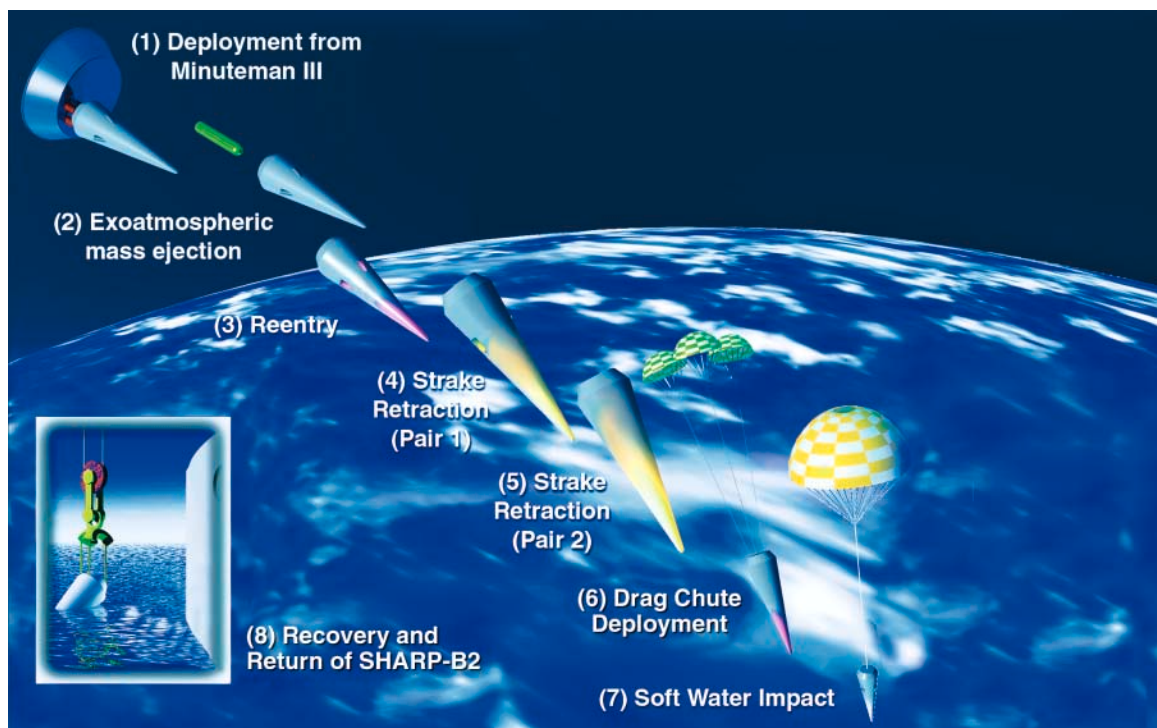


Fig. 2. SHARP-B2 flight experiment mission scenario (28 Sept. 2000).

Shuttle Materials Resistant to Micrometeorite Orbital Debris

Daniel B. Leiser, David A. Stewart

This research and development program was initiated to improve the micrometeorite orbital debris (MMOD) resistance of the belly tiles on the shuttle orbiter. More specifically, it was started to establish a means for substantially improving the damage resistance and MMOD characteristics of the RCG/LI-900 shuttle baseline tile. This improvement would result in a substantially reduced amount of damage and therefore less repair between flights as observed in the toughened unipiece fibrous insulator (TUFI)/AETB tiles (fig. 1) flown in the base heat shield. The goal was to obtain a more MMOD-resistant low-density insulation with thermal conductivity equivalent to that of LI-900 so that the “new” tile could replace the baseline tile on a one-for-one basis.

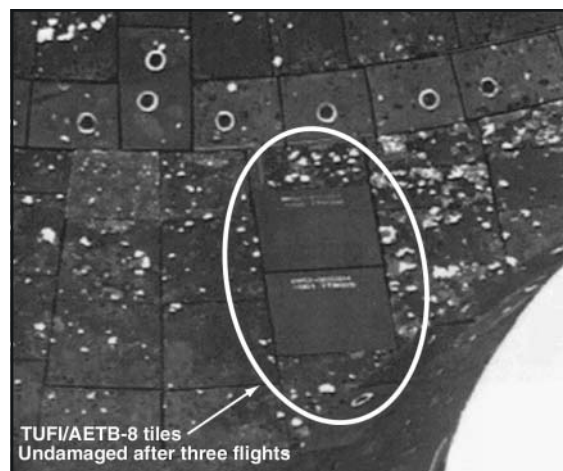


Fig. 1. Shuttle Flight Testing of LI-900/RCG vs AETB-8/TUFI in base heat shield.

For a short-term solution, this was accomplished by developing a new surface treatment for the LI-900 that takes advantage of the Ames technology developed previously and designated as TUF1, which has the desired improved damage resistance. The program used components that minimally changed significant properties of the surface-treatment composite developed (that is, thermal expansion coefficient, thermochemical stability, and processing temperature) while at the same time developing a new functionally gradient tough tile. A prototype of this material has been produced successfully, its damage resistance has been determined, and its microstructural stability has been demonstrated. Although it has the desired thermal conductivity, since it uses LI-900, the substrate is still mechanically weak.

A longer-term solution also in the initial phases of development uses AETB-8 as the insulation substrate. This substrate is significantly stronger than the LI-900 substrate and is more compatible with the TUF1 surface treatment. The solution involves developing a technique to reduce the “effective” thermal conductivity of TUF1/AETB-8 to a point where it is no longer an issue relative to using it as a substitute for an LI-900 tile on the orbiter. The modified TUF1/AETB-8 developed with a lower thermal conductivity and the improved damage resistance and MMOD characteristics of TUF1 would therefore be applicable to the orbiter as a direct substitute. The first modified AETB-8 substrates have been produced. One of the authors’ (Stewart) engineering model for the thermal conductivity of the composite material,

has successfully predicted the thermal response of both the LI-900 and low-conductivity AETB tiles with RCG- or TUF1-treated surfaces during exposure to radiant and convectively heated environments. In the radiant heating facility, data were obtained over a pressure range from 0.001 to 1.0 atmospheres. Comparison of the predicted and measured values obtained from arc-jet data showed similar results. The resultant predicted thermal conductivity is significantly lower than that of AETB-8 alone and at temperatures above 1,500°R is below that of LI-900.

Assuming equivalent density tiles for both LI-900 and the modified AETB-8, the back-face temperature history of a tile located just forward of the nose wheel door during a typical Earth entry by the shuttle was predicted (fig. 2). The temperature profiles for an LI-900 tile at this location are very similar to the ones predicted for a low-thermal-conductivity k AETB tile. As a result, the performance of a 5.08-cm (2.0-in) -thick low k AETB tile near the front landing gear door of the vehicle would be equivalent to that of an LI-900. The research program therefore has been very successful. Prototypes of both an LI-900/TUF1 tile system have been produced that have substantially improved impact resistance, and a modified AETB/TUF1 has been developed with thermal conductivity equivalent to that of an LI-900.

Point of Contact: Daniel B. Leiser
(650) 604-6076
dleiser@mail.arc.nasa.gov

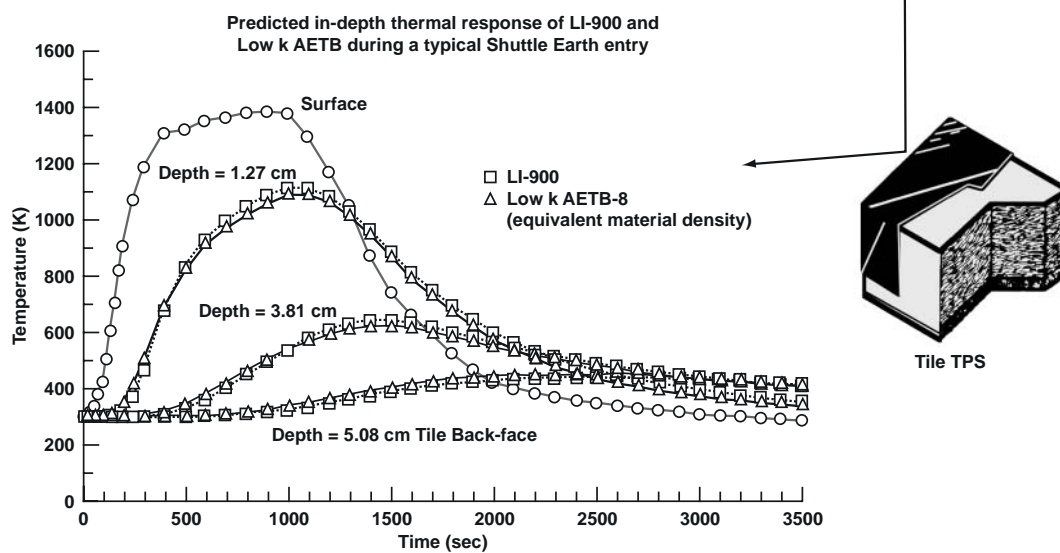


Fig. 2. Proposed high-strength/low conductivity AETB Tile System for shuttle upgrade.

Subsurface Microsensors for Assisted Recertification of Thermal Protection Systems

Frank S. Milos

Integrated Vehicle Health Management (IVHM) is recognized as a critical technology for reducing costs and increasing the safety and reliability of access to space. Ames is the lead Center for development of IVHM technologies for the thermal protection system (TPS). The objective of the Subsurface Microsensors for Assisted Recertification of Thermal Protection Systems (SmarTPS) project is to develop rapid and reliable inspection (health verification) technology applicable to both shuttle upgrades and to future reusable launch vehicles (RLVs). Technology will be developed to automate the detection of both surface and subsurface defects. Most surface defects can be detected from outside the vehicle using precision laser scanning technology. Subsurface defects, however, are difficult to detect without laborious hands-on inspections. For example, for the shuttle, every intertile gap is inspected visually, and TPS disassemblies are required to check for thermal degradation of bonding agents.

Development of an overtemperature microsensor and a noncontact inspection procedure to verify the health of the bond beneath intertile gaps was identified as the highest priority for health management of the TPS. A unified approach to accomplish both objectives is to wed wireless communications with microsensor development. To this end, the prototype microsensor shown in figure 1 was manufactured. The microsensor circuit contains a

thermal fuse, a radio-frequency identification (RFID) microchip, a capacitor, and a coil antenna. The purpose of this microsensor is to indicate the occurrence of excessive temperature at the bond-line between the TPS and the structure of an RLV. The fuse opens at about 288 C, the multiple-use temperature limit of RTV-560, which is a common TPS bonding agent. The rest of the circuit is designed to return the microchip identification code, and a signal for whether or not the fuse is open, to a wireless radio-frequency transceiver such as depicted in figure 2. The microsensor is constructed from high-temperature components that should be able to withstand 10 to 15 minutes of exposure to 345 °C. The microsensor mass is below 0.1 gram; therefore, over 10,000 microsensors can be placed on an RLV at a total mass of under 1 kilogram.

Future plans include thermal, vibration, and other testing as required to qualify the microsensors for possible flight experiments on shuttle or X-vehicles. Microsensors incorporating fuses with different overtemperature limits may be manufactured, depending on the specific requirements of such experiments.

Point of Contact: F. Milos
(650) 604-5636
fmilos@mail.arc.nasa.gov

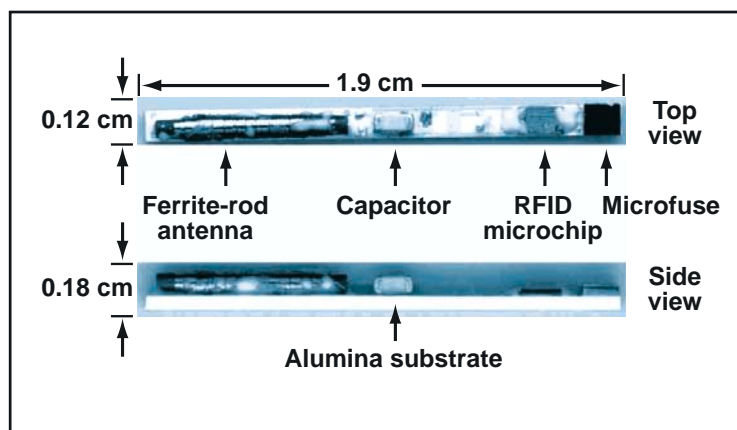


Fig. 1. Microsensor for excessive subsurface temperature.



Fig. 2. Handheld radio-frequency transceiver.

ILab—Parameter Study Tool and IPG Portal

Maurice Yarrow

The ILab tool was specifically written to solve the complex and difficult problems of creating and launching parameter studies. Though today's distributed computational resources are quite capable of running large parameter studies for aerospace problems, users have not had tools available to them that make this process easy and fast. ILab was developed with a host of user-friendly features, so that creating and launching parameter studies can now be accomplished simply and in just minutes.

Within the last year, the ILab tool was given an intuitive user interface. Users can now specify their processes via an advanced computer-aided design (CAD) approach by visually constructing a flowchart-like graphic. ILab's code generator subsequently translates this into appropriate shell scripts, which are then launched onto remote systems and monitored.

Researchers whose parameter studies consist of individual jobs with long-running computational fluid dynamics problems can now take advantage of ILab's unique "restart" capability. This allows users to automatically segment their jobs onto supercomputer scheduling systems and to modify solver parameters for the purpose of steering the computation to a stable solution. Load balancing of jobs is automatically accomplished by restarting the jobs onto supercomputer systems with immediate processing availability. In addition, an advanced Help system has been built into ILab, which users can access from any ILab screen.

Pictured (fig. 1) is the special-purpose parameterization screen (bottom left) which automates the construction of input files for multi-dimension parametric studies. The monitoring screen (upper left) shows the progress of

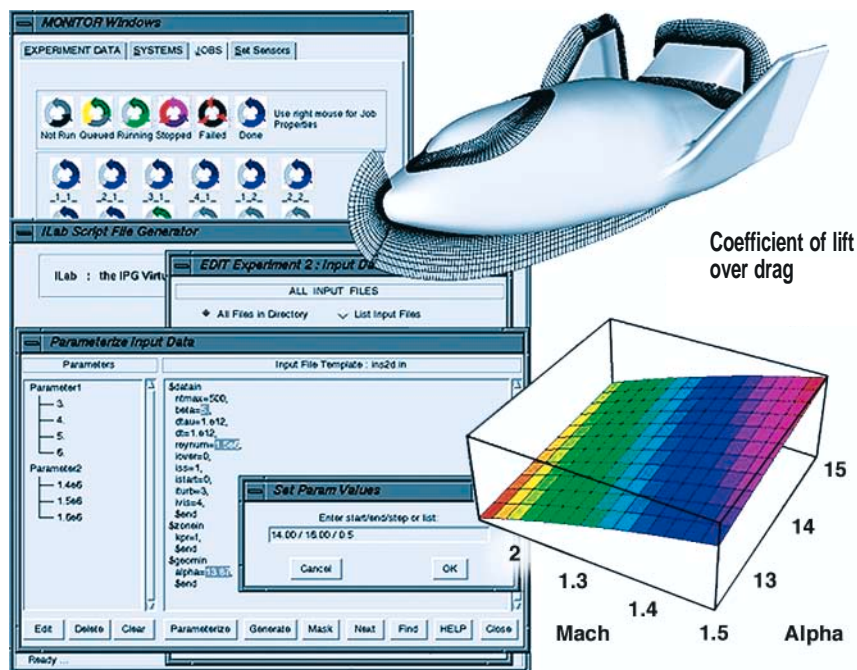


Fig. 1. The ILab Parameter Study Tool and results for the X-38 crew return vehicle.

individual jobs in a parameter study experiment. The NASA X-38 Crew Return Vehicle (upper right) was the subject of a two-dimensional parameter study in Mach number and angle of attack. ILab generated and submitted 192 separate flow-field computations for the requested 16 values of Mach

number and 12 values of angle of attack. Pictured (bottom right) is the surface of coefficients of lift-over-drag for the X-38 at these 192 parameter combinations.

Point of Contact: Maurice Yarrow
(650) 604-5708
yarrow@nas.nasa.gov

Multithreading for Dynamic Unstructured Grid Applications

Rupak Biswas

The success of parallel computing in solving realistic computational applications relies on their efficient mapping and execution on large-scale multiprocessor architectures. When the algorithms and data structures corresponding to these problems are unstructured or dynamic in nature, efficient implementation on parallel machines offers considerable challenges. Unstructured applications are characterized by irregular data-access patterns whereas dynamic mesh adaptation causes computational workloads to grow or shrink at run time. For such applications, dynamic load balancing is required in order to achieve algorithmic scaling on parallel machines. Our objectives were to implement various parallel versions of a dynamic unstructured algorithm and to critically compare their performances in terms of run time, scalability, programmability, portability, and memory overhead.

A multithreaded version of a dynamic unstructured mesh-adaptation algorithm has been implemented on the Cray (formerly Tera) Multithreaded Architecture (MTA). Multithreaded machines can tolerate memory latency and utilize substantially more of their computing power by processing several threads of computation. For example, the MTA processors each have hardware support for up to 128 threads, and are therefore especially well suited for irregular and dynamic applications. Unlike

traditional parallel machines, the MTA has a large uniform shared memory, no data cache, and is insensitive to data placement. Parallel programmability is significantly simplified since users have a global view of the memory, and need not be concerned with partitioning and load-balancing issues. Performance was compared with an MPI implementation on the T3E and the Origin2000, and a shared-memory directives-based implementation on the Origin2000.

A standard computational mesh simulating flow over an airfoil was used for our experiments to compare the three parallel architectures. The initial mesh, consisting of more than 28,000 triangles, was refined a total of five times to generate a mesh 45 times larger, as shown in figure 1. Performance by platform and programming paradigm is presented in figure 2. It is important to note that different parallel versions use different dynamic load-balancing strategies. The multithreaded implementation of the adaptation algorithm required adding a trivial amount of code to the original serial version and had little memory overhead. In contrast, the MPI version doubled the size of the code and required significant additional memory for the communication buffers. The simulation on the eight-processor MTA at San Diego Supercomputing Center using 100 threads per processor was almost ten

times faster than that obtained on 160 processors of a T3E, and more than 100 times faster than that on a 64-processor Origin2000 running a directives-based version. Results indicate that multithreaded systems offer tremendous potential for quickly and

efficiently solving some of the most challenging real-life problems on parallel computers.

Point of Contact: Rupak Biswas
(650) 604-4441
rbiswas@nas.nasa.gov

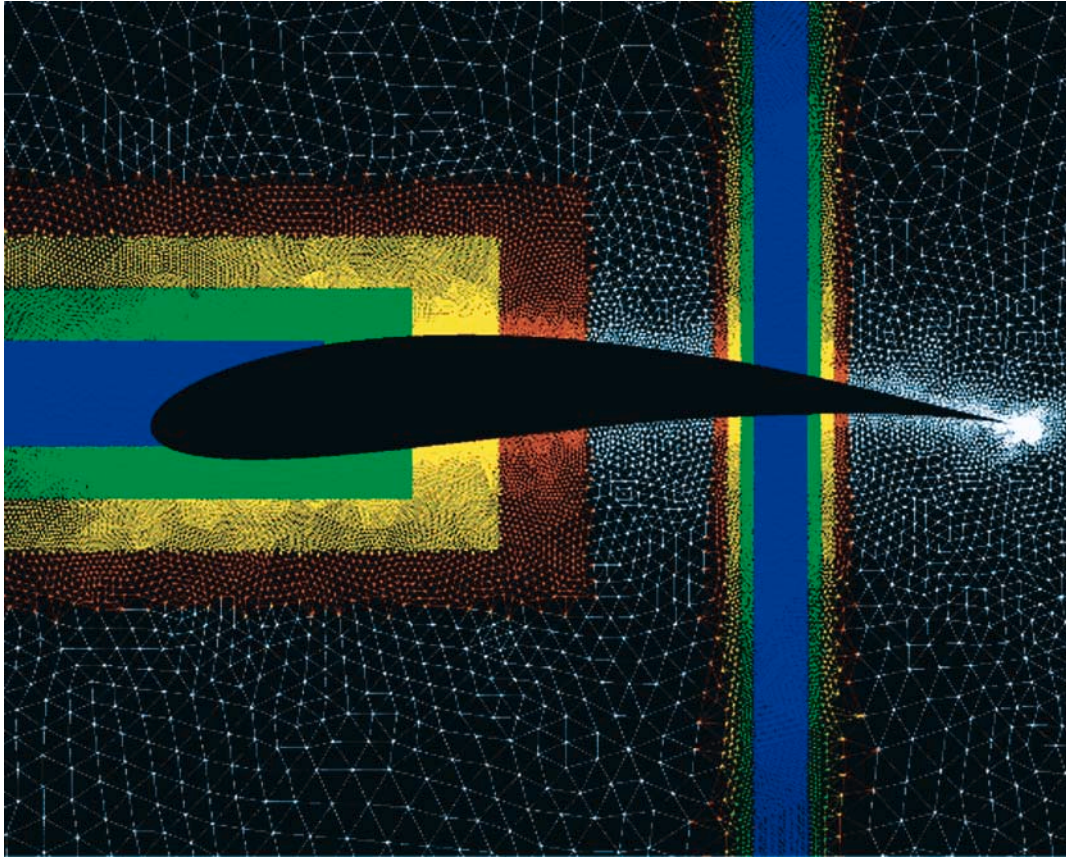


Fig. 1. A close-up view of the computational mesh that was geometrically refined in specific regions to better capture fine-scale phenomena.

Paradigm	System	Code increase	Memory increase	Parallel Performance						
MPI Message-passing	T3E	100%	70%	P	Refine	Overhead		Total		
				8	4.53	14.44		18.97		
				160	0.61	2.39		3.00		
				512	0.14	4.95		5.09		
	Origin 2000	100%	70%	P	Refine	Overhead		Total		
				8	8.31	11.62		19.93		
				64	1.41	3.99		5.40		
Shared-memory directives	Origin 2000	10%	5%	P	Refine	Overhead		Total		
				1	20.8	21.1		41.9		
				8	17.0	22.6		39.6		
				64	42.9	29.6		72.5		
Multi-threading directives	MTA	2%	7%		Threads per processor					
				P	1	40	60	80	100	
				1	150	3.82	2.72	2.22	2.04	
				2		1.98	1.40	1.15	1.06	
				4		1.01	0.74	0.64	0.59	
				8		0.55	0.41	0.37	0.35	

Fig. 2. Performance of the dynamic unstructured mesh-adaptation algorithm by platform and programming paradigm. All times are in seconds; the fastest times are highlighted.

Overset Grid-Generation Software Package

William Chan, Stuart Rogers

In computer simulations of flows about an object, a computational grid is used to model the object's geometry. The Chimera overset-grid method is currently one of the most computationally cost-effective options for obtaining accurate simulations of flow involving complex geometry configurations, viscous fluid dynamics, and bodies in relative, dynamic motion. Considerable success has been achieved in applying this method to a wide variety of problems. The objective of the current work has been to develop a comprehensive set of software tools for performing pre- and post-processing of overset grids for complex-geometry simulation problems, for both static and dynamic cases. These tools have been packaged together in the Chimera Grid Tools software.

The Chimera Grid Tools package allows a user to create overset computational grids, and to

perform geometry processing, grid diagnostics, solution analysis, and flow-solver input preparation. This package has been requested by and distributed to over 200 U.S. organizations under nondisclosure agreements, and has been utilized in aerospace, marine, automotive, environmental, and sports applications. The software consists of a hierarchy of modules together with documentation and examples. At the lowest level are libraries containing commonly used functions such as input/output routines for data files, stretching functions, projection routines, and many others. At one level above the libraries are about 30 independent programs that can be used in batch mode. Capabilities offered by these programs include editing, redistribution, smoothing and projection of grids, hyperbolic and algebraic surface and volume grid generation, and Cartesian grid generation. At the highest level is a graphical user interface called OVERGRID.

The primary function of OVERGRID is to provide a single graphical interface environment for performing a wide range of operations prior to running the flow solver. These operations typically include checking and processing the input geometry, generating the surface and volume grids, analyzing the grid quality using various diagnostics, and creating input parameter files for the domain connectivity program and the flow solver. OVERGRID is used to create structured grids from a geometry description composed of multiple panel networks or triangles. Many of these operations are performed by the various individual modules of Chimera Grid Tools, and OVERGRID serves as a focal point from which these modules can be accessed.

The most recent addition to OVERGRID assists the user in preparing inputs for the

OVERFLOW and OVERFLOW-D flow solvers. For dynamic simulations involving bodies in relative motion, the OVERFLOW-D input file may require up to 100 global parameters and about 70 to 90 parameters for each grid, depending on the numerical scheme chosen. Preparing such an input file for a complex configuration can be a formidable task, especially for a new user. The interface offered in OVERGRID provides a simplified set of commonly used and self-explanatory options for the user to choose from. Many parameters, such as topological boundary conditions, are automatically selected. Numerous error checks are also built in to ensure that a consistent and valid input file is created. An example using the Space Shuttle Launch Vehicle is shown in figure 1, which illustrates the kind of simulations that can be prepared

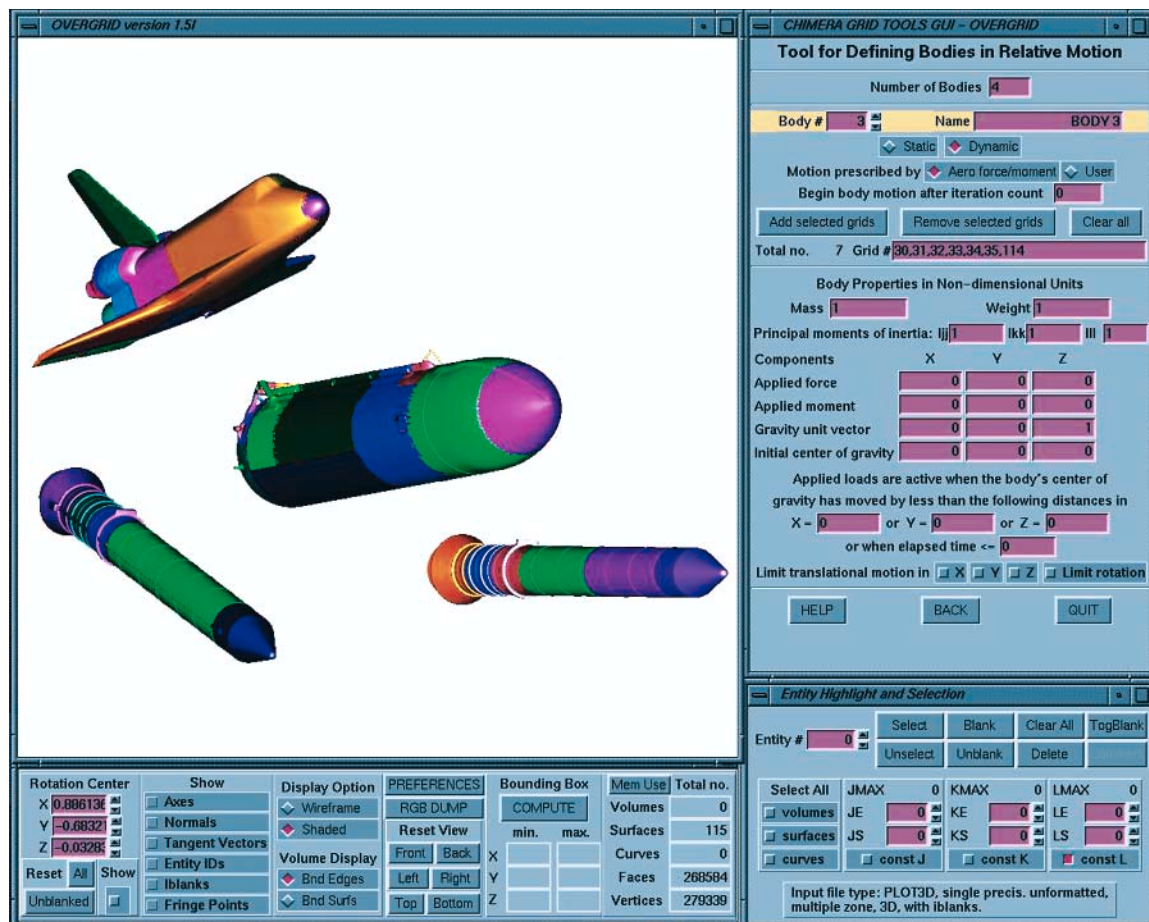


Fig. 1. An example Space Shuttle Launch Vehicle separation procedure.

using the new OVERFLOW-D interface in OVERGRID. Simple widgets allow the user to define the different bodies and to specify their attributes such as mass, moments of inertia, center of gravity, and applied loads.

Point of Contact: William Chan
(650) 604-6607
wchan@nas.nasa.gov

Multi-Level Parallel Computations of Unsteady Turbopump Flows

Cetin Kiris, Dochan Kwak

The objective of this effort was to provide a computational framework for the design and analysis of the entire fuel supply system of a liquid rocket engine, including high-fidelity unsteady turbopump flow analysis. This capability is needed to support the design of pump subsystems for advanced space-transportation vehicles that are likely to involve liquid propulsion systems. To date, computational tools for the design and analysis of turbopump flows are based on relatively lower fidelity methods. An unsteady, three-dimensional viscous flow analysis tool involving stationary and rotational components for the entire turbopump assembly has not been available for real-world engineering applications. The present effort provides developers with information such as transient flow phenomena at start up, the effect of nonuniform inflows, system vibration, and the effect on the structure.

In order to compute the flow on grids with moving boundaries, the overset-grid scheme was incorporated with the flow solver such that new connectivity data are obtained at each time step. The overlapped-grid scheme allows subdomains to move relative to each other, and provides a general flexibility when the boundary movement creates large displacements. Figure 1 shows the model for boost pump and the steps taken in the simulation procedure.

A parallel version of incompressible Navier-Stokes solver (INS3D) was developed by using

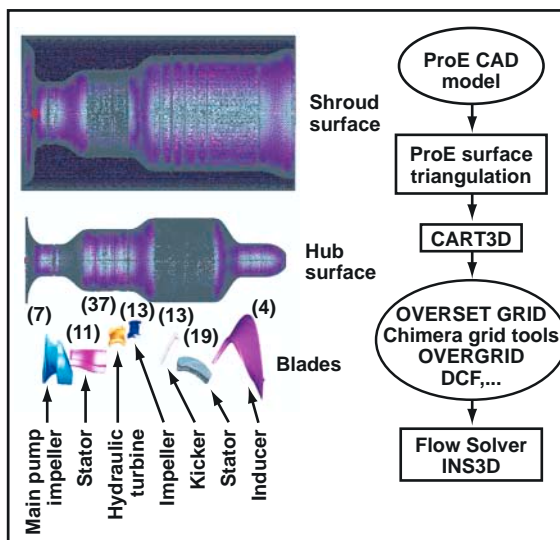


Fig. 1. Boost pump model and steps taken in the simulation procedure.

a Multi-Level Parallel (MLP) approach. This approach differs from the Message Passing Interface (MPI) approach in a fundamental way in that it does not use messaging at all. The coarsest level parallelism is supplied by spawning of independent processes via the standard UNIX fork. The boundary data for the overset-grid system is archived in the shared memory arena by each process. Other processes access the data from the arena as needed. Figure 2 shows INS3D-MLP performance versus computer processing unit (CPU) count for the 19.2 million-grid-point Space Shuttle Main Engine (SSME) impeller model.

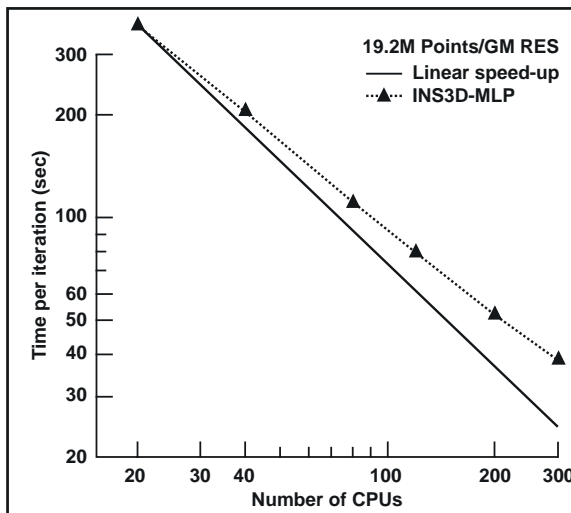


Fig. 2. INS3D-MLP performance versus CPU counts for Origin 2000.

The MLP version of code shows 73% of the linear speed-up performance. When MLP performance is compared with MPI performance, 19% more speed-up is observed by using the MLP version of the code. With pin-to-node implementation in the MLP version of the code, an additional 40% speed-up is obtained. The resulting code was applied to compute unsteady flow through the SSME turbopump, which contains 114 zones with 34.5 million grid points. Velocity magnitude contours during the pump start-up procedure is plotted in figure 3.

Point of Contact: Cetin Kiris
(650) 604-4485
kiris@nas.nasa.gov

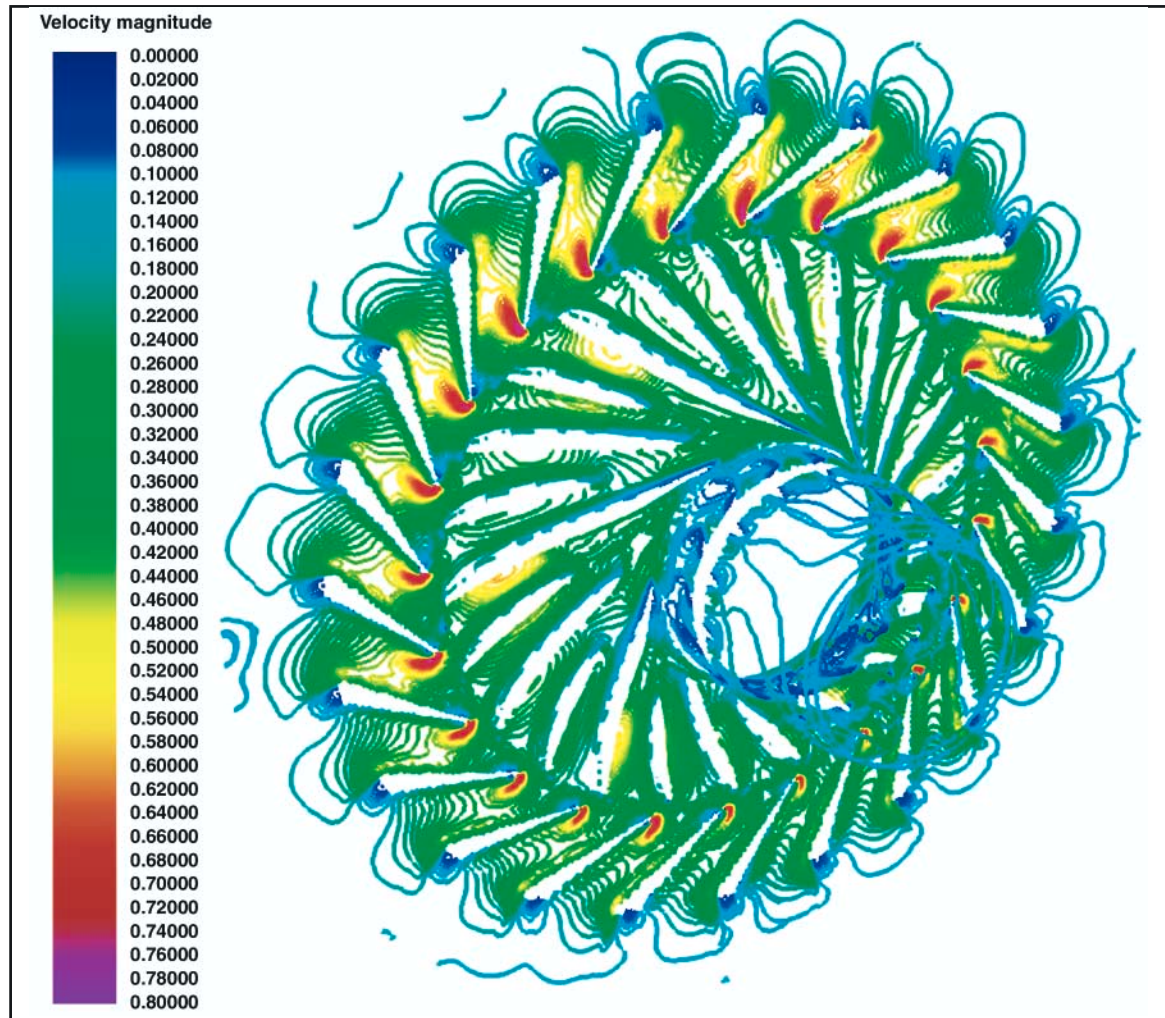


Fig. 3. Velocity magnitude contours during the pump start-up.

PIONEER TECHNOLOGY INNOVATION

Flight Control Design for an Unmanned Rotorcraft Program with a Rapid Development Schedule

Jason D. Colbourne, Mark B. Tischler

Rotorcraft unmanned air vehicle (RUAV) programs are generally developed with small budgets and in time frames that are measured in months rather than in years. Unlike piloted vehicles, unmanned air vehicle (UAV) programs do not have the luxury of long design cycles with multiple iterations. The Northrop Grumman/Ryan Aeronautical Center-led program successfully developed a prototype RUAV (fig. 1) to bid on the U.S. Navy's VTOL (vertical takeoff and landing) Tactical UAV (VTUAV) program. With no remote piloted reversion mode, with no envelope expansion, and with only 4 months to design and develop the flight control systems (FCS), the prototype vehicle successfully flew an 18-minute mission for its first autonomous flight. To complete this program, design tools and methods that develop fast, accurate designs and simulation models were needed.

Over the past 3 years, Ames has been developing the Control and Simulation Technologies for the Autonomous Rotorcraft (COSTAR) program. The COSTAR initiative adapts design tools and methods developed for piloted aircraft to the RUAV platform. The three key

design tools in COSTAR are (1) CIPHER,[®] which facilitates system identification to produce linearized dynamics models from frequency sweeps; (2) CONDUIT,[®] which optimizes flight control laws to meet a given set of design criteria; and (3) RIPTIDE, which builds rapid configuration of real-time workstation-based simulations.

The flight control work began only 4 months prior to the first autonomous flight. Piloted flight testing was performed at the Schweizer Aircraft Corporation's facility in Big Flats, New York, to validate the basic performance of the air vehicle and to generate a flight-test database from which accurate dynamic models could be identified. Piloted frequency-sweep flight tests of the vehicle included three 100-second frequency sweeps at hover, 50, and 100 knots, and two 15-second doublets of each of the four axes.

A six-degree-of-freedom hover state-space model generated in the system identification process used the equations for a rigid body. The stability and control derivatives were tuned by CIPHER so that the responses of the model matched those derived from the flight-test data. The good agreement between the flight data and the model responses and the physically reasonable stability and control derivatives, along with low Cramer-Rao percentages (the latter indicating good confidence in the identified parameters) indicated that the identified model was a valid representation of the aircraft dynamics and that it was suitable for control-law analysis and development. Identification of the hover model was completed just 2 months after the piloted frequency sweeps were performed and a month before the first autonomous flight.



Fig. 1. Northrop Grumman's Prototype (VTUAV).

A classic proportional integral derivative (PID) architecture attitude-command/attitude-hold flight control system was used to stabilize the vehicle. Eleven design parameter gains in the control laws were initially set to values based on classical design methods. CONDUIT adjusts the design parameters to optimize the performance of the control laws against 21 design specifications. The final flight-control laws were optimized in CONDUIT just 5 days before the first flight. The final design represents a good balance between stability and performance without overdriving the actuators.

The first unmanned flight of this vehicle was flown on 12 January 2000—less than 4 months after the first frequency-sweep flight data were collected for mathematical model development. This first unmanned vehicle flight consisted of an 18-minute flight over a 2-mile course. The aircraft flew a simple four-sided racetrack pattern with a ground speed of 9 knots at an altitude of 100 feet above ground level (AGL). The flight was fully autonomous from engine startup to engine shutdown including an autonomous takeoff and landing. No buildup flights were flown prior to this autonomous flight, and the vehicle had no reversion mode for ground pilot control.

Although no open-loop control doublets were performed during the tests (stability augmentation system on at all times), several moderately abrupt control transitions were observed as part of normal flight. Comparison of the simulation models with the flight data shows an excellent

agreement. Figure 2 shows a pitch input that was made into the inner-loop control laws during this flight. Feeding the control input signals into the simulation model produces the response shown by the dashed curve in figure 2. The quality of the agreement shows the value of using a good simulation model in the design of RUAVs. The vehicle flight-test performance and the agreement of the flight-test data with the simulation model indicated that no further improvements to the hover low-speed FCS design were warranted.

Northrop Grumman was awarded the contract on 8 February 2000 with immediate go-ahead. First flight of an EMD vehicle is scheduled for late 2001.

Point of Contact: Jason D. Colbourne
(650) 604-6194
jcolbourne@mail.arc.nasa.gov

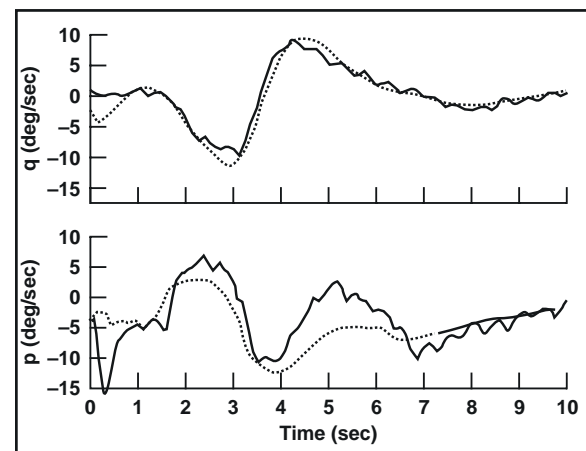


Fig. 2. Comparison of flight-test data to simulation model.

Vertical Lift Technology and NASA Revolutionary Concepts Program

Larry A. Young, John F. Madden, Khanh Q. Nguyen

Ames Research Center is a key team member on two NASA Revolutionary Concepts (REVCON) Phase I aeronautics projects, which focus on vertical lift technologies. The REVCON program is a Dryden Flight

Research Center-led initiative that emphasizes the development and demonstration of high payoff aeronautics technologies that can be quickly taken from concept to flight. The REVCON projects are broken into two phases:

a Phase I \$300,000, 8-month-long, system analysis and overall concept-feasibility assessment study, and a Phase II effort which encompasses the actual vehicle/technology development and flight demonstration. Contractors for both Phases are competitively selected. Only Phase I projects are considered for Phase II award. Proposals for the Phase I effort were solicited by means of a NASA Research Announcement (NRA).

One of the two vertical-lift technology projects that Ames is participating in is the Advanced Technology, Incorporated (ATI) Swashplateless Flight project (fig. 1). This project seeks to demonstrate, on an unmanned air vehicle (UAV), ultralight helicopter flight-test platform primary flight control (rotor blade pitch angle, collective, and cyclic) using embedded flaps on the rotor blades, driven by advanced electromagnetic actuators and power electronics. (Primary flight control for conventional rotorcraft is provided by a complex assembly of mechanical components which make up the rotor control system—the chief component of which is the swashplate.) These same rotor-blade electromagnetic actuators—in addition to providing primary flight control—will be used to demonstrate high frequency (greater than once-per-blade revolution) active rotor control for noise and vibration reduction. Successful demonstration of this technology could yield an elegant design approach for rotorcraft flight control that will reduce helicopter parasite drag, improve range and endurance, improve reliability and safety of operation, and at the same time reduce noise and vibration. The team members for the Swashplateless Flight project are ATI, Diversified Technologies Incorporated (DTI), Science Applications International Corp. (SAIC), the U.S. Army Aeroflightdynamics Directorate, the NASA Ames and Langley Research Centers, and the Dryden Flight Research Center.

The second vertical-lift REVCON project in which Ames is involved is Sikorsky Aircraft's



Fig. 1. ATI swashplateless flight project.

Variable-Diameter Tilt Rotor (VDTR) UAV demonstrator project (see fig. 2). The VDTR concept promises significant performance and safety advantages over conventional tilt rotors. The rotor blades of a VDTR aircraft telescope and retract radially along the blade span such that the rotors are at a larger diameter for hover and low-speed helicopter mode than they are in airplane-mode cruise. This rotor diameter change allows the VDTR aircraft to optimize its rotor disk loading and performance, for each flight condition. The comparatively lower VDTR rotor disk loading (compared with that of a conventional tilt-rotor aircraft) in low-speed helicopter mode allows for improved autorotation characteristics in case of an aircraft power loss. The team members for the VDTR project are Sikorsky, the U.S. Army Aeroflightdynamics Directorate, the NASA

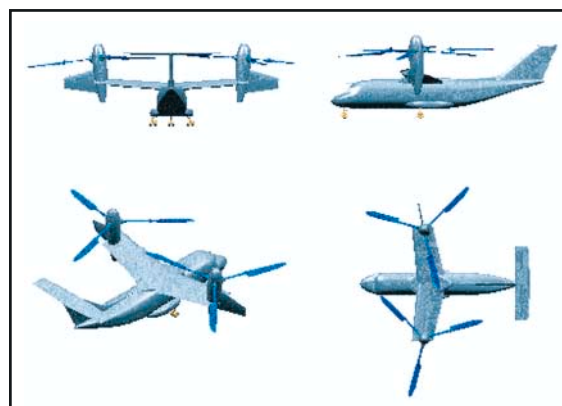


Fig. 2. Sikorsky Aircraft's Variable Diameter Tilt Rotor (VDTR) UAV Demonstrator Project.

Ames, Langley, and Glenn Research Centers, and the Dryden Flight Research Center.

Phase I work for both projects has been completed and final reports submitted.

Selection and award of the REVCON Phase II projects will be made by the end of FY01.

Point of Contact: Larry A. Young
(650) 604-4022
layoung@mail.arc.nasa.gov

Mars Exploration Using Vertical-Lift Planetary Aerial Vehicles

Larry A. Young, Michael R. Derby, Edwin W. Aiken

Despite the thin, cold, carbon-dioxide-based atmosphere of Mars, recent work at Ames Research Center has suggested that vertical-lift planetary aerial vehicles (based on rotary-wing technology) could potentially be developed to support Mars exploration missions. The use of robotic vertical-lift planetary aerial vehicles would greatly augment the science-return potential of Mars exploration, but their development presents many technical challenges.

Why vertical-lift vehicles for planetary exploration? For the same reason that these vehicles provide such flexible aerial platforms for terrestrial exploration and transportation: their ability to hover and fly at low speeds and to take off and land at unprepared remote sites. Further, autonomous vertical-lift planetary aerial vehicles would have the following specific advantages and capabilities for planetary exploration:

- Hover and low-speed flight for aerial surveys
- Remote-site sample return to lander platforms, or precision placement of scientific probes
- Soft-landing capability for vehicle reuse and remote-site monitoring
- Greater range, speed, and access to hazardous terrain than a rover

- Better resolution of surface details than from an orbiter
- Could act as “astronaut agents”

Martian autonomous rotorcraft by their nature will have large lifting-surfaces and will be required to have ultralightweight construction. This in turn will pose a challenge in making them sufficiently robust to operate in the Martian environment. A number of vertical-lift aerial vehicle configurations for Mars exploration are being examined at Ames, including coaxial helicopters, quad-rotor helicopters, and tilt rotors (see fig. 1). Propulsion options include electric motors, powered by fuel cells or batteries, or an Akkerman hydrazine reciprocating engine.

Work to date has consisted mostly of conceptual design studies. NASA and Sikorsky Aircraft jointly sponsored the Year 2000 American Helicopter Society Student Design Competition for the design of a Martian autonomous rotorcraft. Excellent design proposals resulted from that competition. Many of the conclusions of the in-house work at Ames were supported by the independent design work done at the universities. Moreover, a considerable amount of enthusiasm was generated in academia and the industry for possible follow-on collaborative work.

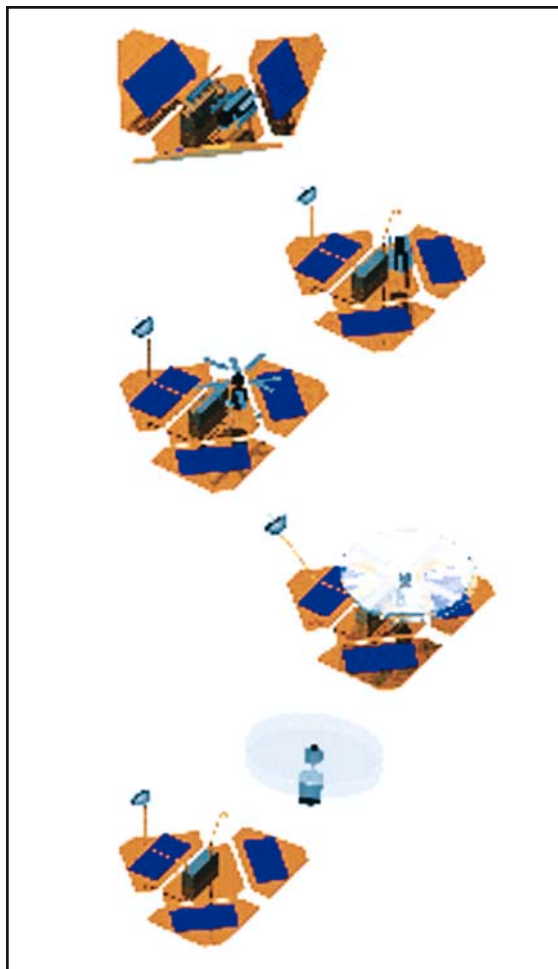


Fig. 1. National Mars Coaxial Helicopter.



Fig. 2. Rotor and hover test stand for testing in simulated Mars atmosphere.

A baseline rotor and hover test stand for testing at Mars atmospheric densities has been developed (fig. 2). Initial proof-of-concept rotor hover testing will commence before the end of FY01.

Point of Contact: Larry A. Young
(650) 604-4022
layoung@mail.arc.nasa.gov

Ultrafast Beam Self-Switching by Using Coupled VCSELs

Peter M. Goorjian, Cun-Zheng Ning

The objective of this work was to develop directional beam switching through the use of two coupled vertical-cavity surface-emitting lasers (VCSELs). The simulation results show directional switching at a speed of about 40 gigahertz (GHz) and between directions about 8 degrees apart.

Dynamic beam switching of VCSELs has important applications for switching and

routing in optical interconnect networks. VCSEL arrays of various kinds have been quite extensively researched for tailoring and engineering near- and far-field patterns. We propose a new method of directional beam switching by using two coupled VCSELs as follows. When two VCSELs are coupled by a small inter-VCSEL separation, and biased at the same steady current near threshold, then the resulting light output is dynamic at an

extremely high frequency. As shown in the figure, the resulting far-field pattern shows two lobes that are oscillating out of phase and producing beam switching.

Our model was based on an approximation to the semiconductor Maxwell-Bloch equations. The time evolution of the spatial profiles of the laser and carrier density is obtained by using a finite-difference algorithm to solve the coupled partial differential equations that govern their evolution. The algorithm is fairly general; it can handle devices with one or multiple active regions of any shapes, which can be either gain- or index-guided. There is no a priori assumption about the type or number of modes. The physical modeling includes the effects of nonlinear carrier dependence and dispersion, with respect to wavelength, on the optical gain and refractive index. The modeling of the optical susceptibility is based on first-principles and includes device details such as a quantum-well structure and many-body effects. Temporal dynamics as fast as on a scale of a picosecond can be resolved.

The simulation is for coupled VCSELs operating at 980 nanometers with circular current apertures of 5.6 microns in diameter. The two VCSELs are operating near threshold current injection. The figure shows snapshots of the far-field beam-intensity patterns, from a top view, within a cycle of modulation. The boundary between the white and black regions is the value of intensity halfway between the maximum and minimum values of one of the peaks during a cycle of oscillation. As shown, the higher far-field peak oscillates between two directions separated by about 8 degrees, and the frequency is at 42 GHz. The near-field pattern also showed two spots that were oscillating in relative intensity. However, they were oscillating 90 degrees out of phase with respect to the oscillation in the far-field pattern.

Point of Contact: Peter M. Goorjian
(650) 604-5547
goorjian@nas.nasa.gov

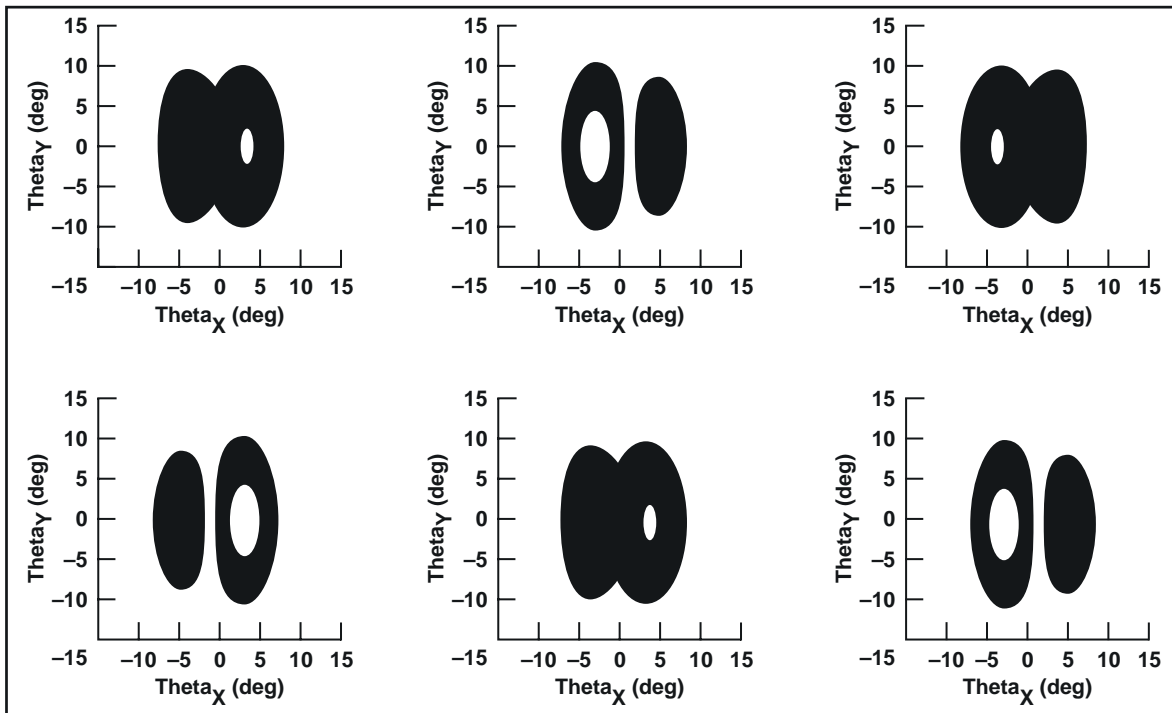


Fig. 1. A top view of the far-field beam intensity over one and one-half cycles of beam switching. The switching speed is 42 GHz and the beams are separated by about 8 degrees.

Multiscale Large-Eddy Simulation

Alan A. Wray

The objective of this research was to improve existing turbulent flow simulations by more correctly modeling the energy transfer between very dissimilar scales. NASA will benefit from this research through improved simulation of fluid flows in and around aerospace vehicles and in astrophysical objects such as stellar interiors and atmospheres and protoplanetary disks.

Turbulent fluid flow contains a complex set of interacting submotions, or “eddies,” which can be characterized by their individual sizes and kinetic energies. In typical turbulent flows, these sizes and energies span a wide range of values, the ranges being larger for flows of larger Reynolds number. Simulations of turbulent flow therefore become increasingly expensive for increasing Reynolds number and at some point are no longer feasible on available computers. To proceed, one must adopt approximations, or models, of some parts of the fluid motion, so that the remaining flow features can still be simulated at reasonable cost. The modeled motions are normally those of smallest size, and simulations incorporating such models are called large-eddy simulations. The missing, modeled eddies are referred to as unresolved.

The models of the small eddies, which are called sub-grid-scale models, incorporate dimensional and plausible-physics arguments to express the effect of these eddies on those still resolved. Typically, a dimensionless parameter is left to be fitted from experimental data or simulation results. Reasonable accuracy is obtained as long as the parameter-fitting and simulated flows are similar, or if “dynamic” models, which determine the free parameter “on-the-fly” based on current local flow conditions, are used; however, some flow types and features are not simulated well with these methods.

The flawed assumption in these models is that even the smallest eddies should have some perceptible, viscous-like effect on all other eddies. The models currently used in large-eddy simulations contain this effect implicitly, and this has been considered a correct modeling of the exact physics. However, recent very large-scale simulations have shown, on the contrary, that small eddies have essentially no direct effect on much larger ones: their effects are felt only indirectly through those of intermediate size.

Researchers at Stanford University and Ames Research Center have developed and tested a “multiscale” large-eddy simulation technique, which consists of applying the small-eddy model only to those eddies near in size to the unresolved ones, but including full interaction between these directly affected eddies and all others. Dramatically improved results are obtained both for fixed and dynamic model types. Figure 1 shows a comparison between a 256^3 direct numerical simulation of decaying isotropic turbulence and three 64^3 large-eddy simulations. The quantity being compared is the kinetic energy dissipation rate for all eddies resolved by a 64^3 grid, as a function of time; this quantity is particularly sensitive to the

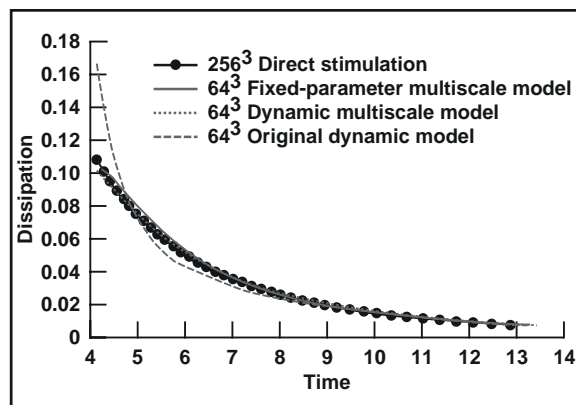


Fig. 1. Total resolved energy dissipation as a function of time, comparing three models with a direct numerical simulation.

accuracy of the simulation of the small-scale motions. It is clear that the dissipation rate is more accurately captured by the fixed-parameter multiscale model than by the original (non-multiscale) dynamic model, and that the dynamic multiscale model provides yet a further improvement in accuracy. The large initial error in the value as computed by the original dynamic model is quickly adjusted for by an overly large dissipation of the smallest resolved eddies, which reduces the dissipation rate to more nearly correct values at the cost of

less accurate simulation of those eddies. The multiscale models do not suffer from this large initial error and do not apply excessive dissipation to the small eddies. Later, as the flow evolves, the small eddies decay away, lessening the need for sub-grid-scale modeling; as a result, all methods become quite accurate.

Point of Contact: Alan Wray
(650) 604-6066
wray@nas.nasa.gov

Unstructured Large-Eddy Simulation Code for Simulation of Reacting Flows in Complex Geometries

K. Mahesh, G. Constantinescu, S. Apte, G. Iaccarino, P. Moin

A large-eddy simulation (LES) unstructured mesh code for high-fidelity simulation of turbulent reacting flows has been developed. The code is designed to run on massively parallel supercomputers. It can handle complex geometries and is being used to compute the flow and associated combustion phenomena in an industrial gas turbine combustor in collaboration with Pratt and Whitney (P&W). LES is chosen because of its demonstrated superiority in predicting turbulent mixing over Reynolds-averaged Navier-Stokes (RANS) formulation. Accurate simulations of chemically reacting flows are critically dependent on the ability to accurately simulate turbulent mixing.

The numerical algorithm allows for the use of hybrid grids. It is a conservative non-dissipative formulation—second-order accurate on uniform grids. The energy-conserving properties of the algorithm allow us to obtain a robust method without the need to introduce numerical dissipation, as is generally done in RANS codes. Keeping the numerical dissipation at

very low levels is essential to maintaining the accuracy of LES simulations. The code solves the incompressible flow equations or the low-Mach-number variable-density equations, the latter being used in simulations of reacting flows.

The dynamic LES model developed at the Center for Turbulence Research (CTR) is used to represent the subgrid stresses. The dynamic formulation offers many advantages when used in unstructured grid formulations, including dynamically computing the model coefficient (no empirical constants), eliminating the need for damping functions near solid surfaces, and eliminating the need for computing the distance to the wall.

Considerable effort was devoted to making the design of the code efficient. The code is fully parallel and uses Message Passing Interface. A novel algorithm was developed for grid-ordering, with the aim of minimizing processor-to-processor communication. The code was ported to several platforms (e.g., Origin2000, IBM SP2, ASCI RED-Intel) and was

shown to scale well for computations using hundreds of processors, provided that the grid partition is such that each processor partition contains at least 5,000 nodes.

Validation simulations in the combustor geometry (a 1/18-combustor sector corresponding to one injector) provided by P&W are under way (see fig. 1). In particular, a special

P&W cold-flow combustor rig, for which detailed experimental data are available, will serve as the key validation test for complex geometries.

Point of Contact: Parviz Moin
(650) 604-5127
moin@rft33.nas.nasa.gov

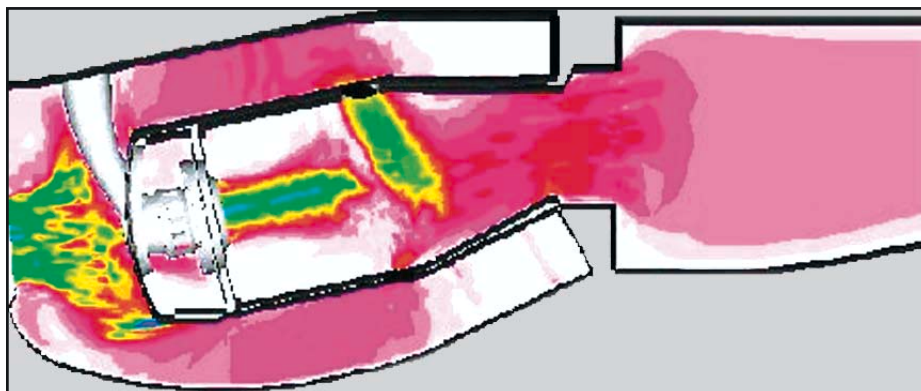


Fig. 1. Section through the PW6000 combustor (plane cutting through the injector symmetry plane). The simulation shows a 20-degree sector of the combustor that corresponds to one injector. Periodic boundary conditions are used on the lateral walls. Reynolds number based on the diffuser inlet section is $Re = 36,000$. The figure shows contours of velocity magnitude. The color scale is 0 (white) to 400 feet per second (dark blue), 40 contours. The results are from a 1.2-million node simulation. The grid is hybrid combination of tets, hexes, and pyramids.

Physics and Models for Optoelectronics Simulation

J. Li, S. H. Cheung, C. Z. Ning

Semiconductor optoelectronics delivers an integrated, reliable, and ultrafast solution to the ever-increasing bandwidth demand in information technology (IT). The objective of the current project at Ames Research Center is to develop the capability from first principles of physics to understand, design, and optimize optoelectronic devices, in order to meet the IT needs of NASA and the public. The project posted significant accomplishments in the area of comprehensive semiconductor laser simulation in FY00.

The research has increased knowledge across several fronts by (1) studying in more detail the role of many-body effects, or Coulomb interaction between charged carriers, in a semiconductor laser device; (2) clarifying the role of plasma heating in the operations of lasing devices; and, more important, (3) developing a hydrodynamic model for spatial inhomogeneous semiconductor lasers from first principles of microscopic physics.

Specifically, the following results were achieved. First, the researchers found that a

law that is believed to be universal for the semiconductor band-gap shrinkage owing to Coulomb interaction in quasi-two-dimensional quantum wells is rather dimension-dependent, and that many-body effects play a nontrivial part in the accurate description of the device, both quantitatively and qualitatively. Second, plasma heating modifies the lasing operations of the device, such as spatial and temporal modulation of the gain and refractive index profile. This in turn alters laser beam quality and dynamics. Third, spatial inhomogeneity-induced diffusion processes increase the injection threshold current, reduce the lasing efficiency, and adversely influence the

dynamical response of the laser when subject to injection current modulation.

These results have been included in the comprehensive simulation code for vertical cavity surface emitting lasers (see fig. 1). The benefit and effect of the research constitutes not only an apparently improved simulation tool for design and optimization, but also a successful step toward the long-term commitment for establishing a microscopic-physics-based benchmark for the optoelectronics industry.

Point of Contact: Jianzhong Li
(650) 604-4410
jianzhng@nas.nasa.gov

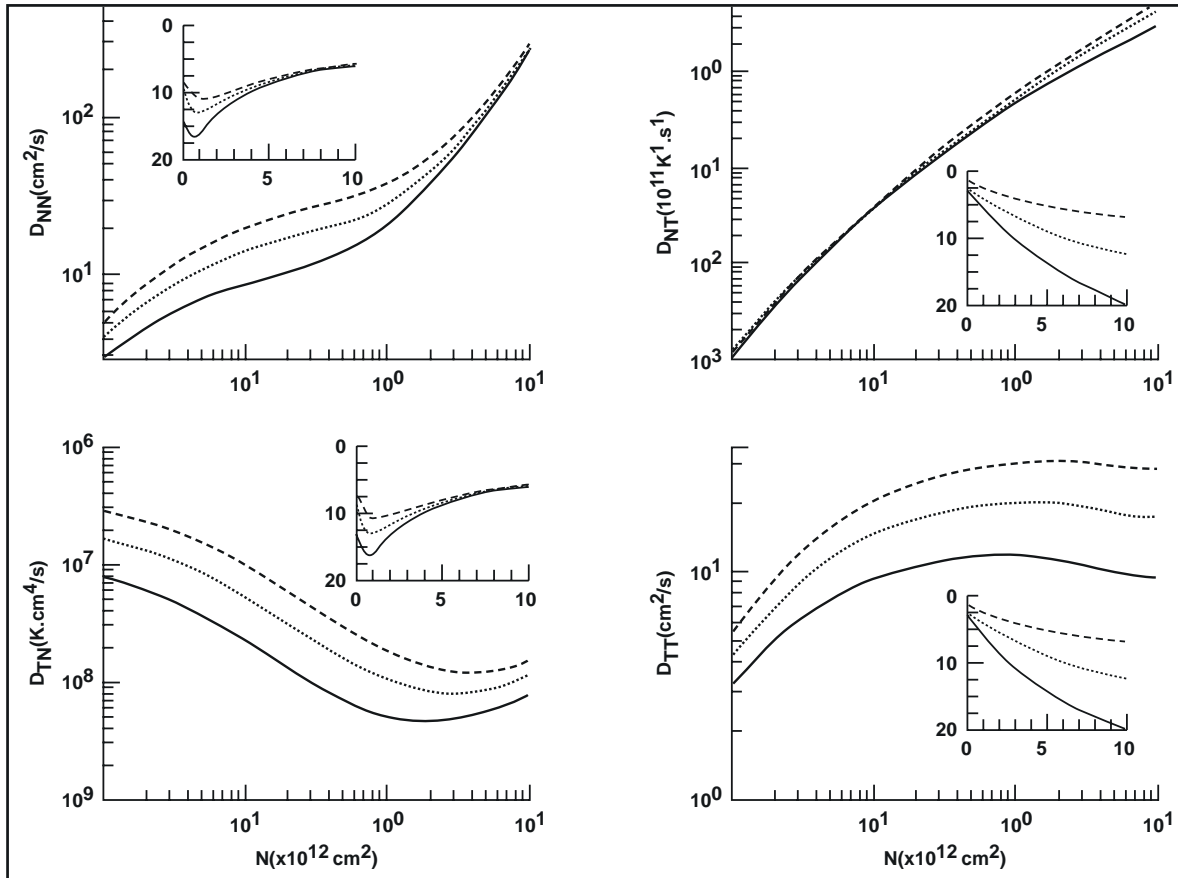


Fig. 1. The carrier-density and temperature dependence of the diffusion coefficients formulated in the hydrodynamic model developed in this project. The results are shown in log-log scale. Insets (in XY scale) show the percentage change in the coefficients as a result of the many-body effects. The solid-line curve is 200 K; the dotted-line curve 300 K; and the dot-dashed curve is 400 K.

Quantum Electronic Device Simulation in Two-Dimensions

A. Svizhenko, M. P. Anantram, T. R. Govindan

The objective of this work is to create a general purpose quantum device simulator capable of computing electric current through nanoscale transistors and molecules. Our code utilizes a fully quantum mechanical approach which is fundamentally different from the traditional approaches adopted in industry.

Successful advancement of solid-state electronics for the last 30 years has been a result of the constant miniaturization of its building blocks—transistors and diodes. Smaller transistors will perform faster and consume less power, which will make electronics, containing millions of such transistors, better and cheaper. It is not clear however whether the functionality of nanoscale (one billionth of a meter) transistors will remain at the same level. Although it is projected that production of nanoscale transistors will begin in 5 to 10 years, there is no theoretical proof that such devices will actually perform better. The reason for this uncertainty is the onset of the quantum mechanical nature of electrons. Commercial simulators, all of which are based on classical laws of physics, fail to predict electric current correctly when transistor size becomes less than 0.1 micron. Thus a new approach is needed.

In the quantum mechanical approach, electrons form minibands of allowed energy, each acting as a path along which an electron can travel. In real space, which affects electric current, these minibands (fig. 1) are bent. Such a behavior is due to the effect of quantum confinement.

Figure 2 shows how the electron flow is squeezed in the channel of the nanoscale field-effect transistor. It is the formation of the minibands and their behavior under applied electric bias that is a key to an understanding of the physics of a nanoscale transistor; that was missing in all previous work in this area.

An important consideration in the design of small transistors is standby power losses. The probabilistic nature of electrons allows them to tunnel through a huge barrier, something that never happens in the classical world. As it turns out, tunneling is a primary reason for parasitic currents flowing through a tiny transistor even when it is turned off. By using our simulator, we were able to design a better transistor and achieved an order-of-magnitude decrease of leakage without compromising overall device performance.

Point of Contact: Alexei Svizhenko
(650) 604-3985
svizhenk@nas.nasa.gov

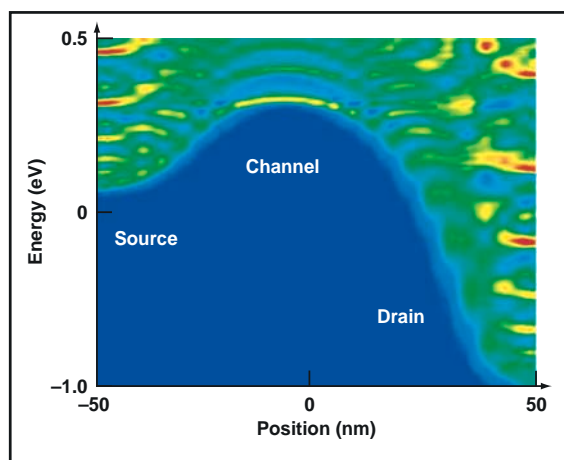


Fig. 1. Density of electron states in nanoscale field-effect transistor as a function of position and energy. Bright stripes in the middle show a formation of minibands of energy in the channel.

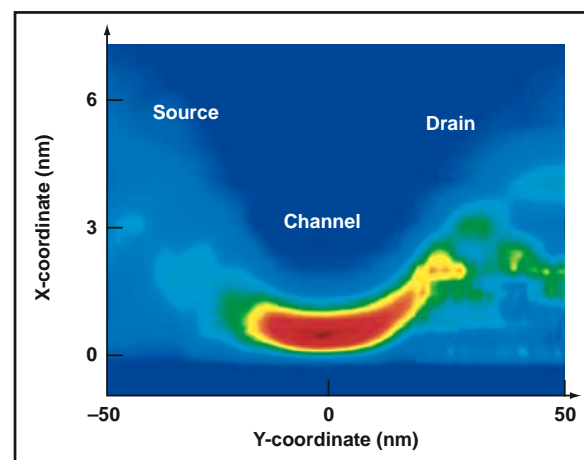


Fig. 2. Electric current flow as a function of position. Electrons are confined to a small region in the channel.

Genetic Algorithm Aerodynamic Shape Optimization

Terry L. Holst, Thomas H. Pulliam

The objective of this work was to explore the use of genetic algorithms in performing optimizations on engineering and science problems of importance to NASA. In particular, a method for aerodynamic shape-optimization using a genetic algorithm (GA) has been developed and used to optimize a number of aerodynamic shapes. In contrast to gradient-based methods, design-space-search methods such as GAs offer an alternative approach with several attractive features.

The basic idea associated with the GA approach was to search for optimal solutions using an analogy to the theory of evolution. During solution iteration (or “evolution” using GA terminology) the decision variables or “genes” are manipulated using various operators to create new design populations, that is, new sets of “chromosomes.” Once established, each new design or chromosome is evaluated using an objective-like “biological fitness function” to determine survivability. The fittest individuals are retained and evolve while the least fit individuals die off.

Constraints can easily be included in this approach either by direct inclusion in the fitness function or by preprocessing the candidate design. For example, if a design violates a constraint, its fitness is set to zero, that is, it does not survive to the next evolution level. Because GA optimization is not a gradient-based optimization technique, it does not need sensitivity derivatives; theoretically, it works well in non-smooth design spaces containing several, or perhaps many, local extrema. It is also an attractive method for multi-objective design applications, offering the ability to compute simultaneous optimal solution sets instead of the limited single-design-point approach traditionally employed by other methods.

Computational results demonstrating the use of GA optimization are presented in figures 1(a) and 1(b) for a typical transonic wing. The design space discretization for this wing optimization problem consists of 10 free parameters, or genes. Eight of the genes are associated with the wing upper-surface thickness—four thickness variables at two span

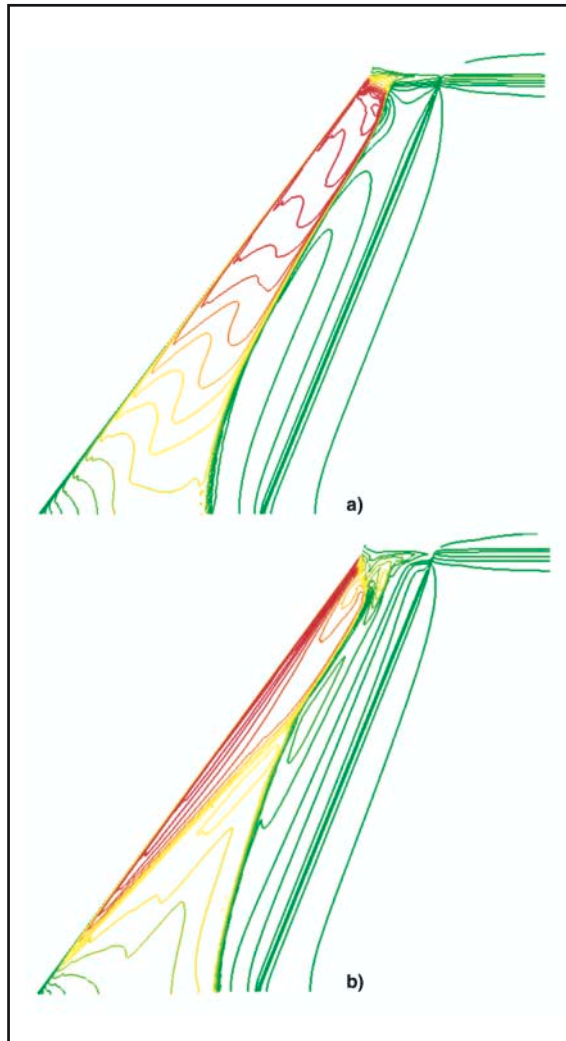


Fig. 1. Mach number contours plotted on the upper wing surface. (a) Baseline solution; (b) optimized solution.

stations each, wing root and tip. The value of wing twist at the root and tip are the two remaining genes. In this optimization, different gene combinations are sought to optimize the wing's lift-to-drag ratio with a constraint on lift.

Figures 1(a) and 1(b) show Mach number contours from the upper wing surface before and after optimization. Note that the optimization has produced a solution with significantly reduced shock strength, especially on the outboard part of the wing. In addition, the single-shock characteristic of the baseline solution has been replaced with a weaker two-shock pattern in the optimized solution. For this optimization, the lift-to-drag function was increased by 14.7% and the drag was reduced by 34%.

Figure 2 presents the effect of population size, that is, the number of chromosomes used, on GA convergence in terms of the number of function evaluations (that is, number of wing flow solutions). The four curves correspond to GA optimizations that utilize 10, 20, 50, and 100 chromosomes, respectively. For this 10-gene problem it is clear that the use of a smaller number of chromosomes (10–20) produces superior GA convergence, which is achieved in about 500 function evaluations. The 50-chromosome case is only slightly

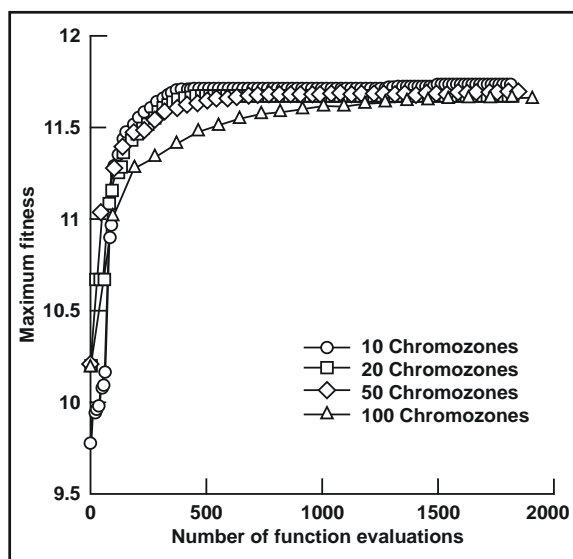


Fig. 2. Effect of number of chromosomes on GA performance.

inferior, but the 100-chromosome case is significantly slower.

A GA procedure suitable for performing aerodynamic shape optimizations has been developed. Results indicate that the GA is easy to implement, flexible in application, and extremely reliable, being relatively insensitive to design space noise.

Point of Contact: Terry L. Holst
(650) 604-6032
tholst@mail.arc.nasa.gov

Contributors to Three-Dimensional Perception of Sound

Durand R. Begault, Elizabeth M. Wenzel

A study was conducted to evaluate the role of individualized head-related transfer functions (HRTF) for localization accuracy and the experience of realism in using auditory displays. Realistic auditory displays that emulate free-field auditory sound sources are required for the efficient and effective design of virtual reality systems for real-world applications, including teleconferencing and interacting with

virtual systems. A number of studies have evaluated humans' abilities to localize aural signals delivered via headphones in a virtual space. The results suggest that optimal localization performance and perceived realism result from inclusion of factors that emulate those typical of everyday spatial hearing experiences (for example, head position effects, a realistically diffuse field or

reflections, and head-related transfer function specific to the listener). Our current work described here directly compares the relative contributions of these factors to localization accuracy and perceived realism using realistic, meaningful acoustic stimuli.

A laboratory study was performed at Ames using headphone-delivered virtual speech stimuli, rendered by means of HRTF-based acoustic auralization software and hardware. The relative advantages of individualized versus generic HRTFs were evaluated because they have been shown to improve localization accuracy and externalization while reducing front-back reversal errors. Virtual speech was presented with (1) no reflections; (2) a few HRTF-filtered “early reflections”; or (3) “full auralization” reverberation. This latter factor has been shown to influence whether or not a headphone-delivered sound is perceived as being external to the listener, but has not been studied in the presence of the other factors under consideration. On half of the trials, the sounds were updated in real time to reflect the listener’s head position based on output from a head-tracker. Nine naïve male and female volunteers participated in the study after being instructed how to make azimuth, elevation, distance, and realism judgments using the interactive, self-paced software (see fig. 1).

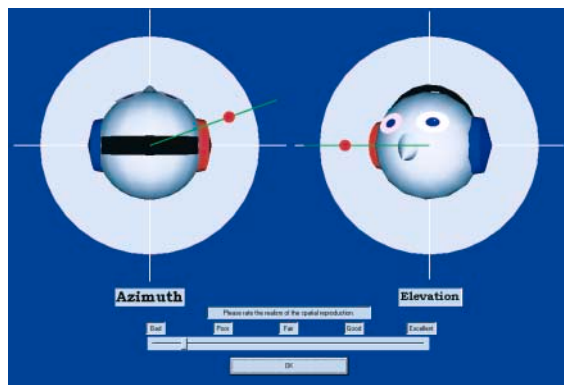


Fig. 1. Response screen graphic. Subjects indicate azimuth and distance on left view, elevation on right view, perceived realism on slider.

The results were evaluated to defined system requirements for improved virtual acoustic simulation. Overall, it appears that auditory signals that include reverberation yield lower azimuth errors and higher externalization rates (here, by a ratio of about 2:1), but at the sacrifice of elevation accuracy. The presence of only 80 milliseconds of early reflections, as opposed to a full auralization, was sufficient to achieve the benefit (fig. 2). Head-tracking did not significantly increase externalization rates, nor did it yield more accurate judgments of azimuth.

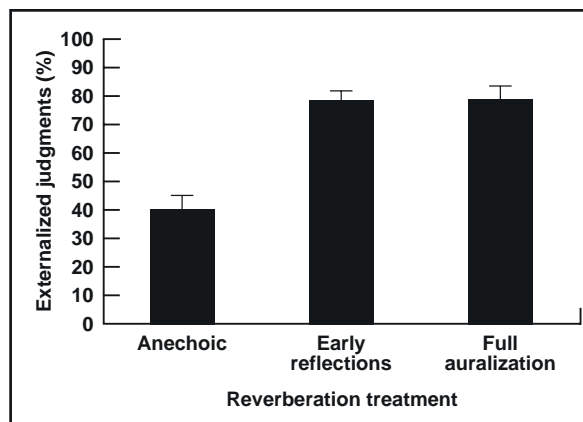


Fig. 2. Externalized judgments: main effect for reverberation. Mean values and standard error bars shown.

It was surprising that the presence of reverberation caused the accuracy of azimuth estimation to improve by approximately 5 degrees. By contrast, the inclusion of head tracking significantly reduced reversal rates, also by a ratio of about 2:1, a phenomenon explained by the differential integration of interaural cues over time, but did not improve localization accuracy or externalization. These findings contrast with previous results indicating that head movements enhance source externalization. Except for the interaction of head tracking and HRTF for azimuthal error, there is no clear advantage to including individualized HRTFs for improving localization accuracy, externalization, or reversal rates, within a virtual acoustic display of speech. For speech, unlike earlier results for

non-speech signals, no dramatic improvement in reversals was found with individualized HRTFs. The fact that individualized HRTFs did not significantly increase azimuthal accuracy was not surprising given the spectral characteristics of speech.

The results taken as a whole suggest that a complete, high-fidelity emulation of all

free-field sound characteristics is not required for an effective spatialized auditory display.

Point of Contact: Durand R. Begault
(650) 604-3920
dbegault@mail.arc.nasa.gov

Bioelectric Keyboard and Joystick for Computer Control

Kevin Wheeler, Chuck Jorgensen

The shrinking size of personal computer systems now makes it possible to wear a functional computer with display goggles available for visualization, but data entry requires the use of keyboards and mice. Our work has focused on eliminating keyboards and joysticks by monitoring the electrical activity in the muscles known as Electromyograms (EMG). We have created software that translates the EMG signals into computer commands such as keystrokes and joystick movement. This software works in a way similar to speech recognition. When a gesture from a fixed set of gestures is performed, the resulting EMG signals are recognized and the computer command corresponding to that gesture is issued to the computer.

We have demonstrated two uses of this technology. The first demonstration involved using the virtual joystick interface to control a class IV flight simulation to land a 757 transport aircraft at San Francisco airport. This activity represents coarser grained movements. The acting pilot reached into the air, pretended to hold and manipulate a joystick. Four movements were used: banking to the left, banking to the right, pitching up, and pitching down. These gestures could be held for an arbitrary amount of time so that rolls could be performed. The strength of the gesture was

translated into the rate of the banking and pitching movements.

To demonstrate finer grained gestures we measured finger movements involved in pretending to type on a number pad. We then were able to “type” on the surface of a table and even on our pants. Figure 1 depicts typing on the participant’s knee as if it were a numerical keypad, the resulting numbers are shown on the screen.

This technology was demonstrated using movements similar to those that computer users are familiar with from day to day such as



Fig. 1. Demonstration of bioelectric keypad using wet electrodes. The left computer screen shows the recognized keystrokes, the right screen shows the raw EMG signals.

typing and moving joysticks. Obviously the ideal interface should evolve away from the qwerty keyboard and into one that is more natural and incorporates speech recognition. However speech alone is not adequate. For example consider rotating and zooming a three dimensional complex object, or numerical entry applications such as inventory. In

particular we are focusing on applications specific to NASA such as being able to perform data entry while constrained by a space suit, controlling remote robotics, and focusing on wearable computing applications.

Point of Contact: Kevin Wheeler
(650) 604-3807
kwheeler@mail.arc.nasa.gov

Center for Turbulence Research: 2000 Summer Program

P. Moin, N. N. Mansour, W. C. Reynolds

A volume of research reports of the Center for Turbulence Research (CTR) Summer Program has been published. The eighth Summer Program of the CTR took place in the 4-week period, 2 July to 27 July 2000. This was the largest CTR Summer Program to date, involving 40 participants from the United States and nine other countries. Twenty-five Stanford and NASA Ames staff members facilitated and contributed to most of the Summer projects.

Several new topical groups were formed, which reflects a broadening of the CTR's interests from conventional studies of turbulence to the use of turbulence analysis tools in applications such as optimization, nanofluidics, biology, and astrophysical and geophysical flows. The CTR's main role continues to be in providing a forum for the study of turbulence and other multiscale phenomena for engineering analysis. The effect of the Summer Program in facilitating intellectual exchange among leading researchers in turbulence and closely related flow-physics fields is clearly reflected in the proceedings.

The development of the dynamic procedure at the CTR has continued to generate renewed interest in large-eddy simulation (LES) over the past decade. During the Program, new averaging strategies, new equations, and decompositions of the flow field using

wavelets were evaluated and tested. In addition, efforts continued in modeling the near-wall turbulence, which remains a pacing item, and in evaluating LES in predicting flow-generated noise. The combustion group continued to attract researchers from around the world. Work on the development and assessment of combustion models was supplemented this year by a large effort to evaluate the use of LES in industrial applications.

The Reynolds-averaged Navier-Stokes (RANS) modeling group continued its effort in developing models that capture the effects of rotation and stratification on turbulence. The ability of RANS models to predict transition was also evaluated. The program benefited from the infusion of novel new ideas from deterministic and stochastic optimization for flow control. These ideas were tested in optimizing microfluidic channels (fig. 1). A novel application of these optimization techniques was the use of evolutionary algorithms in developing strategies for the destruction of aircraft trailing vortices.

The astrophysical group concentrated on protoplanetary disk modeling and simulation. New ideas and transformations of the governing equation promise new advances in this field in the near future. The geophysics group used direct numerical simulation to study sediment

transport on a wavy wall and the propagation of internal waves in the upper ocean thermocline. Finally, two new research topics were introduced to the CTR Summer Program, nanofluidics and biology. The biology work on the life cycle of phytoplankton where turbulence plays a key role is a natural extension of CTR's expertise. The work on nanofluidics, which is based on molecular dynamics, is

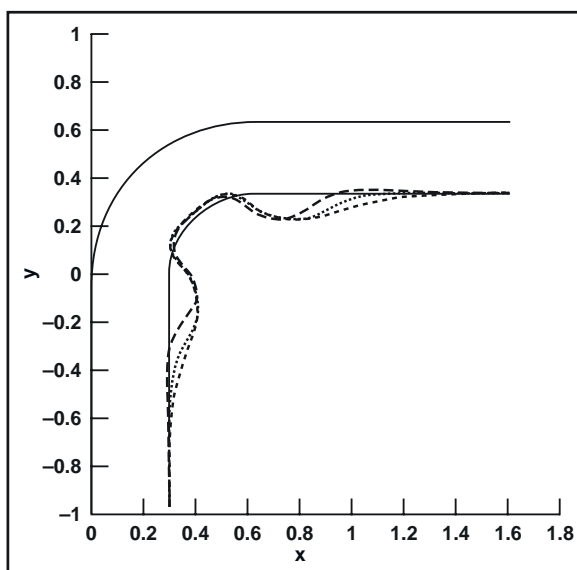


Fig. 1. Design of fluidic channels using a novel shape-optimization algorithm. The various lines show shapes obtained under the same optimization conditions for three admissible spaces with minimum required regularity for the shape. (See <http://ctr.stanford.edu/summer00/mohamadi.pdf> for a detailed report.)

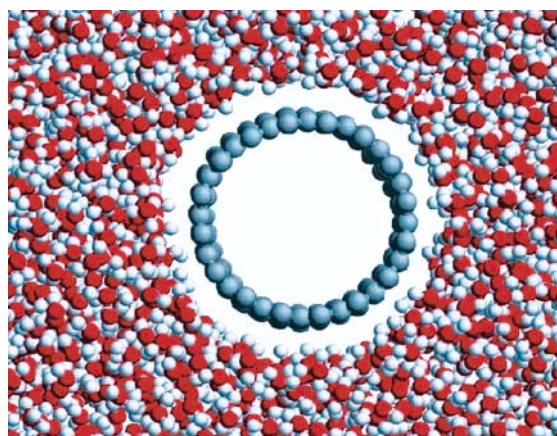


Fig. 2. Snapshot of the atoms from the simulation of a single carbon nanotube in water. (See <http://ctr.stanford.edu/summer00/walther.pdf> for a detailed report.)

an outgrowth of CTR's expertise in using advanced algorithms and large-scale simulations. Carbon nanotubes in water (fig. 2), and flow in a nanometer-scale channel were simulated during the Summer Program.

There are 29 papers in the proceedings, grouped in six areas. Each group is preceded by an overview provided by its coordinator. The entire proceedings of the 2000 Summer Program are available on the World Wide Web (<http://ctr.stanford.edu>).

Point of Contact: Parviz Moin
(650) 604-5127
moin@rft33.nas.nasa.gov

The Effects of Turbulence on Phytoplankton

S. Ghosal, M. Rogers, A. Wray

Phytoplankton are photosynthesizing microscopic organisms that inhabit the upper sunlit layer (euphotic zone) of almost all oceans and bodies of fresh water. They are agents for "primary production," the incorporation of carbon from the environment into living organisms, a process that sustains the aquatic food web. Phytoplankton thus control the

biogeochemical cycles in aquatic environments and thereby exert a dominant influence on life on Earth. This work is directed at understanding the effects of turbulence on the distribution of phytoplankton and extends earlier modeling efforts through a combination of analysis and computer simulation. The purpose is to better understand the principal qualitative aspects of

the physical/biological coupling of this natural system.

Turbulence influences this process in three important ways. First, essential mineral nutrients are transported from the deeper layers to the euphotic zone by turbulence. Second, turbulence helps to suspend phytoplankton in the euphotic zone, since in still water the phytoplankton, especially the larger species, tend to settle out of the sunlit layers. Third, turbulence also transports phytoplankton from the surface to dark sterile waters, an important mechanism of loss. Thus, stable phytoplankton populations are maintained through a delicate dynamic balance between the processes of turbulence, reproduction, and sinking.

A simplified model of a phytoplankton population in isotropic turbulence was considered. The phytoplankton population growth is assumed to be limited by the available light intensity and not by the nutrient supply. The phytoplankton density is controlled by (1) turbulent advection, (2) the reproduction rate associated with the light intensity at a given depth, (3) the sinking speed of the particular phytoplankton being considered, and (4) the loss rate resulting from natural deaths and “grazing” by higher animals. For this simplified model, analysis indicates the possibility of a stable phytoplankton population for certain regions of a two-dimensional parameter space, these parameters being the dimensionless reproduction rate and the dimensionless height of the sunlit “euphotic” zone for clear water (these quantities being normalized by the turbulent phytoplankton diffusivity and the sinking speed in still water).

Several direct numerical simulations of this simplified model problem have been generated using a pseudospectral numerical method. The various simulations correspond to different conditions in the above-described dimensionless parameter space. Parameters below the critical curve result in decaying unsustainable phytoplankton distributions, and those above

the curve yield sustained populations. The simulation results for the horizontally averaged phytoplankton concentration as a function of water depth increase toward the theoretically predicted profile as time evolves, indicating good agreement with the theoretical analysis (fig. 1).

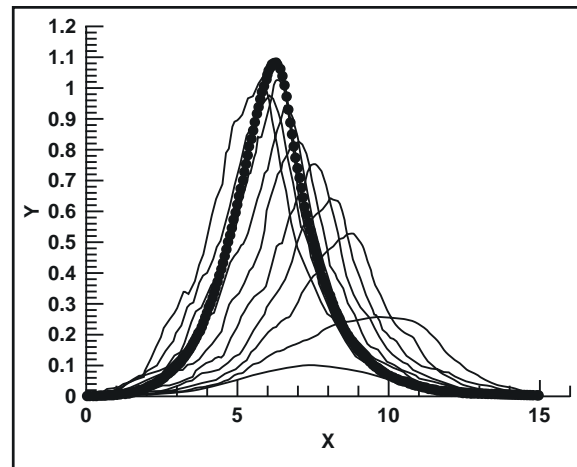
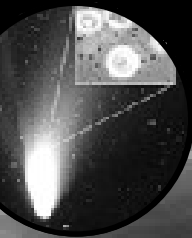


Fig. 1. The time evolution of the horizontally averaged plankton concentration as a function of water depth. The symbols represent the theoretically predicted profile.

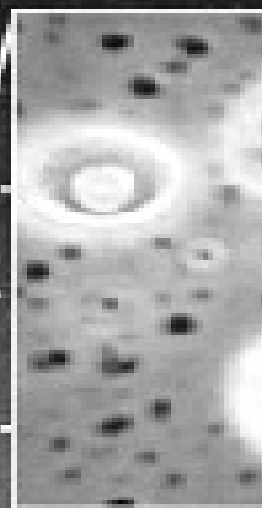
Comparing the numerical simulations and the theory suggests that an eddy-diffusivity model for turbulent transport is adequate for the purpose of predicting the mean phytoplankton concentration. The simulations also confirm that the analytical mean phytoplankton profile is globally stable in the appropriate region of the parameter space.

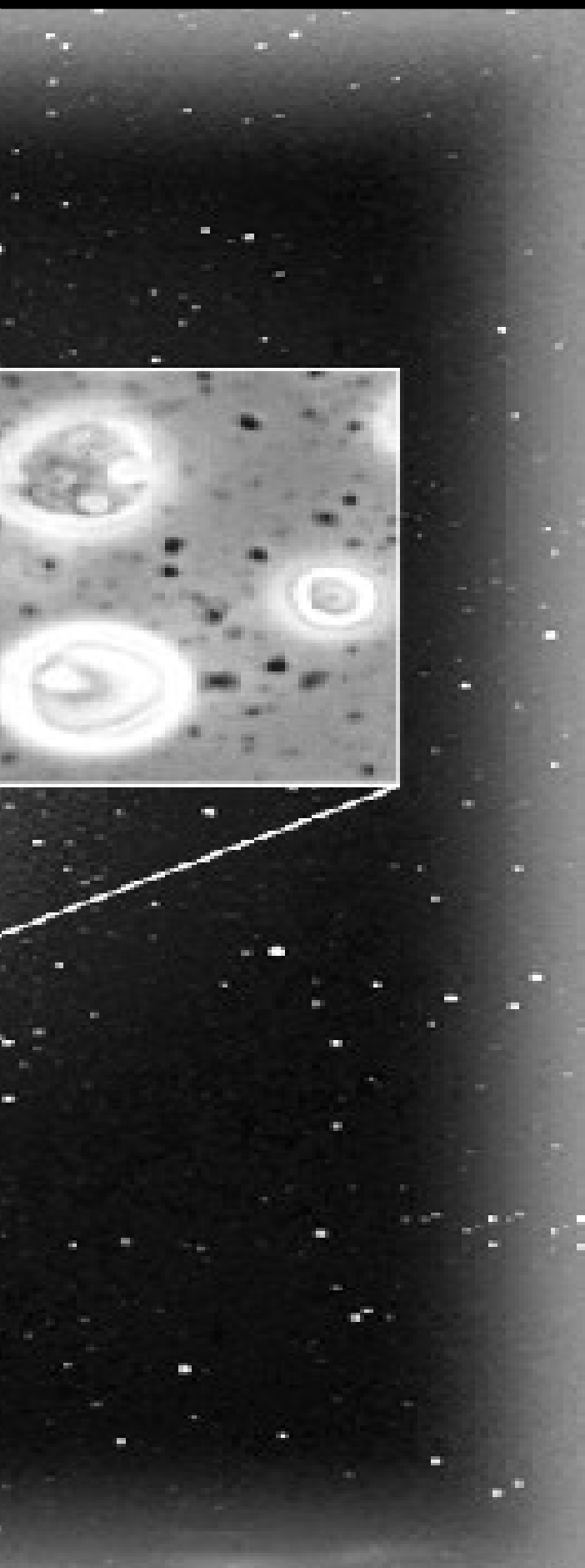
The current model assumes that the plankton distribution is statistically homogeneous in the horizontal direction. This neglects the rich and varied horizontal structure seen in satellite images of plankton. The horizontal structure of phytoplankton concentrations and the manner in which the steady-state distribution in the above model gets established are subjects for future investigations.

Point of Contact: Mike Rogers
(650) 604-4732
mrogers@nas.nasa.gov



Space Science Enterprise





Overview

Scientists in NASA's Space Science Enterprise seek to answer fundamental questions about the origin and evolution of life and celestial objects (planets, planetary systems, stars, galaxies, etc.) in the universe.

Research at ARC implements Space Science Enterprise goals through four elements dealing with astrophysics, planetary systems, exobiology, and space technology. Because the unifying theme for these elements is the origin and evolution of stars, planets, and life, the total research effort is a major thrust in the Space Science Enterprise Astrobiology program.

Astrophysics research addresses Enterprise goals and objectives that deal with understanding how the structure in the universe emerged, the dynamical evolution of galaxies and stars, and the exchange of matter and energy among stars and the interstellar medium. Planetary systems research addresses Enterprise goals and objectives that deal with understanding star formation, the evolution and distribution of volatile and organic material, the origin and distribution of planetary systems, rings, and primitive bodies, and planetary atmosphere evolution. Exobiology research addresses Enterprise goals and objectives that deal with understanding the origin, evolution, and distribution of life by conducting research on the cosmic history of biogenic compounds, prebiotic evolution, the early evolution of life, computational astrobiology, and extreme environments in which living organisms can exist. Finally, space technology efforts address Enterprise goals and objectives that deal with the development of advanced technologies to enable future astrophysics missions, as well as robotic and human solar-system exploration missions.

Ames Research Center is recognized as a world leader in astrobiology, the study of life in the universe and the chemical and physical forces and adaptations that influence its origin, evolution, and destiny. In pursuing our primary mission in astrobiology, Ames performs pioneering basic research and technology development to further fundamental knowledge about the origin, evolution, and distribution of life within the context of cosmic processes. For example, research and technology developments are currently conducted to:

- Study the mechanisms of the origin, evolution, and distribution of life in the universe;
- Determine the abundance and distribution of the biogenic compounds that are conducive to the origin of life;
- Identify locations on bodies within our solar system where conditions conducive to life exist or have existed;
- Explore the other bodies (planets, comets, asteroids) of our solar system;
- Locate planets and planet-forming regions around other stars;
- Study extrasolar matter such as interstellar gas and dust.

This report highlights accomplishments in the four key research thrusts at Ames that support the goals and objectives of the Space Science Enterprise: astrophysics, planetary systems, exobiology, and space technology.

Astrophysics

As NASA's lead in airborne astronomy, scientists at Ames pioneered the field of astrophysics. Study topics range from star-forming regions and processes to interstellar photochemistry to protoplanetary disks.

Understanding cosmic processes—the evolution of the universe itself—is a vital part of the Origins initiative.

Ames astronomers and astrophysicists utilize a wide variety of methods. Ground-based telescopes such as the Keck and Mount Lemmon Observatories are regularly employed for observations of celestial objects and processes. Development continues on the SOFIA, an infrared telescope to be carried aboard a Boeing 747 aircraft specially modified for the task. Space-based observations are also made through instruments such as the Hubble Space Telescope (HST) and other observatories and missions. Computer modeling and laboratory analogs of chemical processes enhance the observational astronomy performed.

Highlighted in this section of the report are a wide variety of accomplishments in astrophysics, including:

- Production and testing of the world's largest echelle grating necessitated to meet the requirements for wavelength range and resolution demanded by the desired measurements of the far-infrared spectral lines of molecules and atoms originating in the interstellar medium;
- Completion of the design and engineering model of the water-vapor monitor for SOFIA, which is critical for the proper calibration of the 3-meter class telescope mounted in a Boeing 747 aircraft;
- The development of a new interstellar simulation chamber, unique within NASA, to directly simulate gaseous molecules and ions at the low temperature and pressure conditions of interstellar space to permit determination of spectroscopic properties of large interstellar aromatic molecules and ions under conditions that precisely mimic interstellar conditions.

Space Technology

To support the Space Science Enterprise in conducting future space science and exploration missions, Ames scientists and engineers develop and validate technologies and instruments, develop calculation-based and modeling algorithms, and refine analytical methods.

Highlighted in this section of the report are a wide variety of accomplishments in space technology, including:

- Development and manufacture of the guide-star telescope detectors for the Gravity Probe B Project, the purpose of which is to test Einstein's theory of general relativity;
- Development of a lightweight, high-efficiency pulse tube cryocooler designed to meet NASA's future requirements for zero boil-off propellant storage needed for developing reusable space transportation vehicles for both Earth-to-orbit and long-duration missions;
- Development of state-of-the-art cryogenic readouts, with improved sensitivity, which are the critical electronics for infrared detector arrays, and in most instances, the dominant source of noise in such detection systems.

Planetary Systems

Scientists in the Space Science Enterprise are interested in how and where planets form in the universe, and the geophysical, geochemical, and atmospheric processes that have occurred over the lifetime of a planet. Further, understanding the dynamics between planetary processes and the origin and evolution of life will help us understand the distribution of life in the universe.

Highlighted in this section of the report are a wide variety of accomplishments in planetary systems, including:

- The production of interactive search and geometrical visualization utilities, as part of the Ames Planetary Data System's Rings Node, to assist Cassini scientists in planning observations of the rings of Saturn during the upcoming tour mission (2004–2008);
- Development of theoretical models for star and planetary formation that have been used to determine requirements for future missions such as the Stratospheric Observatory for Infrared Astronomy (SOFIA) and the Space Infrared Telescope Facility (SIRTF);
- Discovery of a correlation between high stellar metallicity and the detected presence of an extrasolar planet that has been exploited to find extrasolar planets with less effort, thus saving large amounts of time on instruments such as the Keck Telescope.

Exobiology

Ames' Exobiology Program is a key element of NASA's Astrobiology Initiative, and Ames serves as NASA's lead center in exobiology. Research in exobiology at Ames ranges from studying the mechanisms of the origin of living systems to the processes governing the evolution of life to the distribution of life on other planets. When coupled with Ames' pioneering research on the dynamics of galaxies, molecular gases and clouds, planetary systems, and the solar system, our study of life is facilitated by understanding the cosmic environment within which life originates and evolves.

Molecules of exobiological significance are ubiquitous in the universe. It is important to understand the sources and interactions of these building blocks and how living systems emerge from prebiotic molecular chaos.

Highlighted in this section of the report are a wide variety of accomplishments in exobiology, including:

- Establishment of a greenhouse facility to maintain field-collected microbial mats in an environment where human scientists and intelligent agents work together to perform experiments;
- Definitive identification of sugars in meteorite samples, for the first time, indicating that these compounds—central components of contemporary nucleic acids—were available for incorporation into the first living organisms on the primitive Earth;
- Construction of computer simulations that model the structure and function of membranes, a critical component for the origin of cellular functions, and that explore the capacity of membrane structures to function as primitive catalysts.

ASTROPHYSICS

Identifying Polycyclic Aromatic Hydrocarbons in Space

Jesse Bregman, Pasquale Temi

Polycyclic aromatic hydrocarbon (PAH) molecules are the most abundant family of molecules in the interstellar medium after molecular hydrogen and carbon monoxide, and they contain about 10% of all the interstellar carbon. Extremely tough PAH molecules are a component of meteorites, and thus were likely delivered to the early Earth where they may have played an important role in the formation of life. Until recently, the only way to study PAHs in the interstellar medium was by examining their emission spectrum. PAHs fluoresce when present near sources of bright ultraviolet radiation such as exits in planetary nebulae and HII (ionized hydrogen) regions. PAH absorption spectra have been measured in laboratory studies, but these spectra cannot be directly used to determine the mix of PAHs that occurs in the interstellar medium without using complex models. Enough unknowns exist in the models that definitive statements about the exact nature of the interstellar PAHs have so far been impossible.

Recently, a spectral database has become available from the Infrared Space Observatory that contains objects in which the C-H PAH

stretch feature (near 3.26 microns (μm)) has been found in absorption. If the database of isolated neutral PAHs generated by the Ames Astrochemistry Laboratory is used, the interstellar feature can be matched fairly well with a mixture of PAH molecules. However, the mixture is not unique and does not indicate which particular PAHs are present in space. This fact is demonstrated in the figure, which shows two fits to the absorption observed toward the protostellar source S140. The laboratory database contains only a few PAHs as large as those expected to survive the rigors of the interstellar medium, so it is perhaps not surprising that a precise match is still not possible. Techniques for obtaining lab spectra of larger PAHs exist, but making large PAHs for lab studies is very difficult. As soon as such lab data exist, being able to directly compare lab and interstellar spectra without using uncertain models could provide the first identification of individual PAHs in space.

Point of Contact: J. Bregman
(650) 604-6136
jbregman@mail.arc.nasa.gov

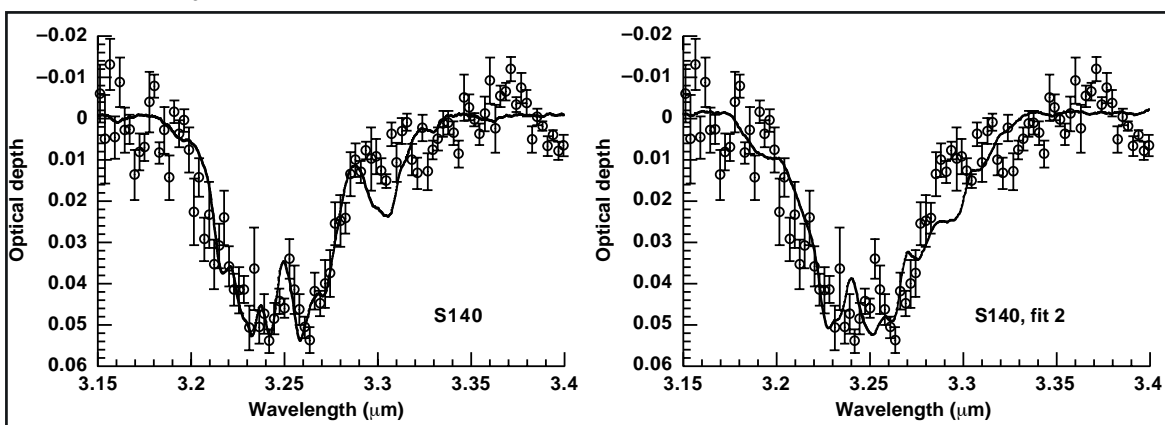


Fig. 1. The spectrum of S140 has been divided by an estimate of the continuum to allow direct comparison with laboratory data of PAHs. The two panels show different mixtures of laboratory PAHs (solid lines) plotted on top of the S140 data points.

The AIRES Far-Infrared Detector Array

Edwin Erickson, Jessie Dotson, Jam Farhoomand, Christopher Mason

A unique, state-of-the-art array of detectors is being developed as part of AIRES, the airborne infrared echelle spectrometer for SOFIA (the Stratospheric Observatory for Infrared Astronomy). SOFIA is a Boeing 747 that will carry a 2.7-meter telescope to operating altitudes up to 45,000 feet. It is under development by NASA and the DLR (the German aerospace center). SOFIA is scheduled to begin operations at Ames Research Center in late 2004. AIRES—which is being built at Ames—is the facility spectrometer for SOFIA; it will measure atomic and molecular spectral lines at far-infrared wavelengths, approximately 30 to 400 times the wavelengths of visible light, to probe physical characteristics of astronomical sources such as star-forming regions and our galactic center.

Highlights of the AIRES detector development include the following: Infrared light collected by the SOFIA telescope will be distributed by the optical system of AIRES to its semiconductor detectors so as to permit simultaneous separation of different wavelengths in each of 24 imaging picture elements (pixels) viewing the sky. The detectors will be arranged in a 16 x 24 rectangular grid with pixels spaced eight-hundredths of an inch apart. Each detector is a chip of antimony-doped germanium mounted in an integrating cavity and fed with light from the spectrometer by a conical light collector, shown in figure 1.

The AIRES optical system and detector assembly will be cooled in a cryostat to a few degrees kelvin, as required to achieve the highest possible sensitivity to the infrared radiation collected by the SOFIA telescope. The detectors convert the light from the spectrometer into electrical signals, which are amplified and multiplexed by adjacent integrated circuits that route the signals to the data system outside the cryostat.

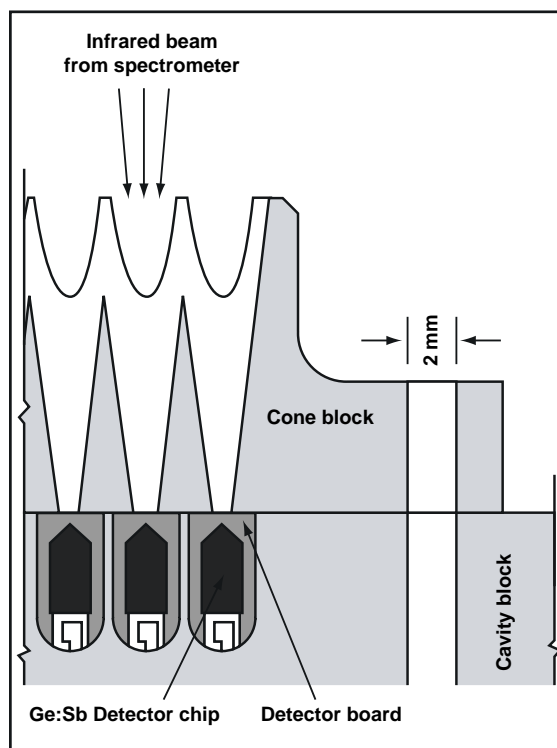


Fig. 1. Detail of the AIRES far-infrared detector geometry.

These unique multiplexing amplifiers were designed specifically for AIRES by industrial specialists collaborating with AIRES team members. The device technology was originally developed for the Space Infrared Telescope Facility, but the new circuits are tailored for the wider range of infrared backgrounds expected on SOFIA. They feature externally programmable gains to accommodate different observing conditions, and so will be suitable for a variety of SOFIA instruments as well as some spaceborne instruments. The AIRES team pioneered this development, and has tested several devices, confirming that their cryogenic noise and gain performance meets AIRES needs.

The entire detector package—detectors, amplifiers, and array assembly—is custom

designed and built, with much of the work done at Ames by the AIRES team. In previous tests, the detector configuration sketched in figure 1 was shown to work well. During FY00, testing of the amplifiers and design and fabrication of a 2 x 24 protoflight detector module have made great progress. This

unique detector system, essential for the success of AIRES, is well on its way to achieving its design performance.

Point of Contact: E. Erickson
(650) 604-5508
erickson@cygnus.arc.nasa.gov

The World's Largest Grating

Michael R. Haas, James A. Baltz, Edwin F. Erickson, Emmett I. Quigley, David C. Scimeca

The airborne infrared echelle spectrometer (AIRES) is a high-resolution grating spectrometer under development as a facility science instrument for the Stratospheric Observatory for Infrared Astronomy (SOFIA). An echelle is a grating used at a steep angle of incidence relative to the incoming light beam. The spectral resolution of a grating spectrometer is directly proportional to the projected length of its grating along this beam and inversely proportional to the wavelength of light being analyzed. AIRES is designed to measure far-infrared (long-wavelength) spectral lines of molecules and atoms originating in the interstellar medium. Therefore, AIRES requires a grating significantly longer than any previously made. In fact, the wavelength range and resolution planned for AIRES demands the world's largest grating!

Further, the entire AIRES optical system must be operated at a few degrees kelvin (near absolute zero). To minimize problems associated with thermal contraction in this cryogenic environment, to facilitate diamond machining, and to ensure long-term stability, a monolithic aluminum blank was chosen. This blank was manufactured from 152-millimeter (mm)-thick, aluminum alloy 6061-T651, Type 200 tooling plate. The final blank is 102 mm thick, 267 mm wide, and 1067 mm long with the corners removed to provide a near-elliptical planform.

The blank was light-weighted by cutting triangular-shaped slots with a wire-electric-discharge machine, which builds less stress into the blank than conventional milling and has the ability to cut deep slots with small corner radii. The resulting truss-like structure is symmetric, provides good specific stiffness, and is 70%-light weighted. Before final machining, the blank was heat-treated at 375 degrees Centigrade (°C) for 2 hours and then thermally cycled 7 times between -200°C and 100°C to obtain the required stability.

A groove spacing of 980 microns, an apex angle of 90 degrees, and a blaze angle of 76 degrees were selected to optimize the packaging and optical performance of the grating at the wavelengths of interest. This combination of parameters maximizes the spectral resolution for the 63- and 145-micron neutral oxygen, 157-micron singly ionized carbon, and 205-micron singly ionized nitrogen transitions arising from the interstellar medium, without adversely affecting performance for other high-priority transitions.

The grating was ruled under contract with Hyperfine, Incorporated, of Boulder, Colorado, with a fly cutter using a single-point diamond turning on a custom ruling engine. The completed grating is shown in figure 1. The light-weighting truss structure is evident along its



Fig. 1. The AIRES echelle is the largest monolithic, fully phased grating in the world.

front edge. Two reflections of the technician are visible; the front reflection originates on the long, 14-degree groove facets, and the rear reflection originates on the steep, 76-degree groove facets.

To achieve the desired optical performance, the AIRES optical system must have a total root-mean-square (rms) wave-front error (WFE) less than 1.5 microns. A detailed error analysis apportioned 0.8-micron rms WFE to the echelle grating. This WFE includes contributions from both absolute and periodic errors in groove position, shape, straightness, and fanning, as well as gross deflections of the blank due to self-weight, tool forces, and

variations in thermal contraction. Interferometric tests of the completed grating measure a WFE of 0.3-micron rms—much better than required. This result implies that the surface is flat to about one part in 7 million. Other optical tests confirm that the efficiency and scattered light properties of this grating are acceptable for use in AIRES. The world's largest echelle grating has been successfully ruled and tested; the associated opto-mechanics, cryostat, detectors, and software for AIRES remain under development.

Point of Contact: M. Haas
(650) 604-5511
mhaas@mail.arc.nasa.gov

The SOFIA Water-Vapor Monitor

Thomas L. Roellig, Robert Cooper, Brian Shiroyama, Regina Flores, Lunming Yuen, Allan Meyer

The Stratospheric Observatory for Infrared Astronomy (SOFIA), a 3-meter class telescope mounted in a Boeing 747 aircraft, is being developed for NASA by a consortium consisting of the University Space Research Association, Raytheon E-Systems, and United Airlines. This new facility will be a replacement for the retired Kuiper Airborne Observatory that used to fly out of Moffett Field. As part of this development, Ames Research Center is providing an instrument that will measure the integrated amount of water vapor seen along the telescope line of sight. Because the presence of water vapor strongly affects the astronomical infrared signals detected, such a water-vapor

monitor (WVM) is critical for proper calibration of the observed emission. The design and engineering model development of the WVM is now complete, and the hardware to be used in the flight unit is being fabricated and tested.

The SOFIA WVM (figure 1) measures the water-vapor content of the atmosphere integrated along the line of sight at a 40-degree elevation angle by making radiometric measurements of the center and wings of the 183.3-gigahertz (GHz) rotational line of water. These measurements are then converted to the integrated water vapor along the telescope line of sight. The monitor hardware consists of three physically distinct subsystems:

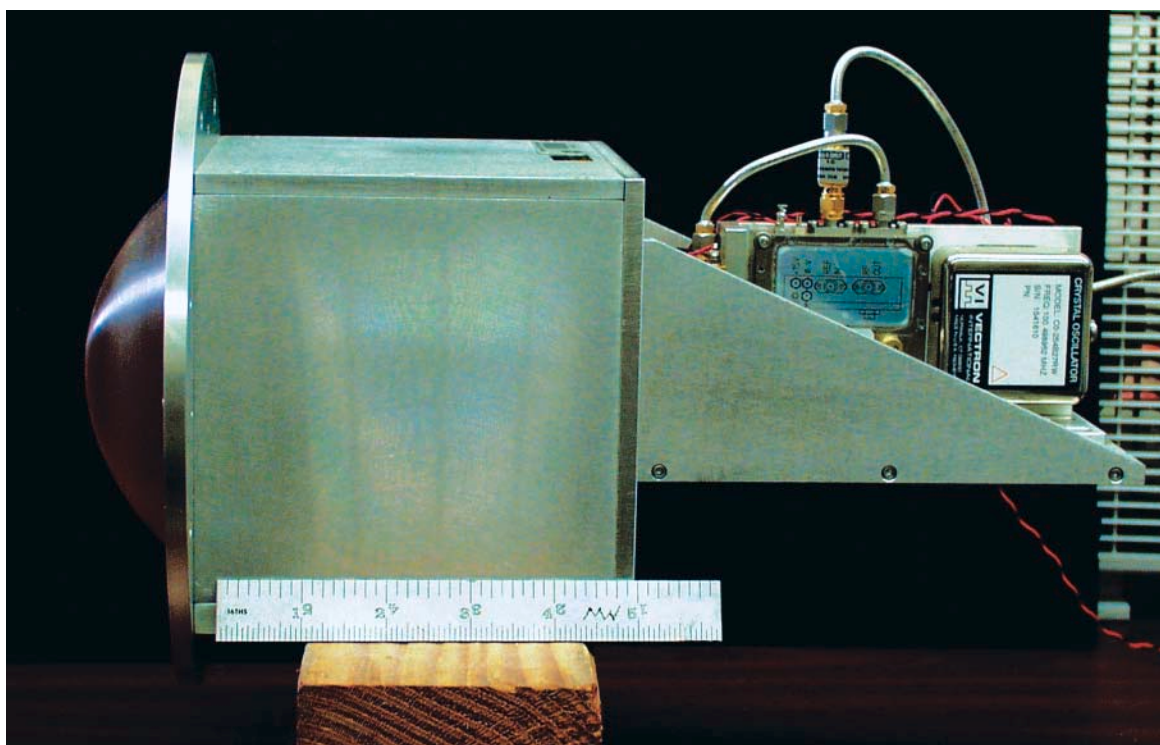


Fig. 1. The SOFIA water-vapor monitor 183-GHz radiometer assembly.

1. The radiometer head assembly, which contains an antenna that views the sky, a calibrated reference target, a radio-frequency (RF) switch, a mixer, a local oscillator, and an intermediate-frequency (IF) amplifier—all these components are mounted together and attached to the inner surface of the aircraft fuselage, so that the antenna can observe the sky through a microwave-transparent window. The radiometer and antenna were ordered from a commercial vendor and modified at Ames to include an internal reference calibrator. Laboratory tests of this subassembly have indicated a signal-to-noise performance over a factor of two better than required.

2. The IF converter box assembly, which consists of IF filters, IF power splitters, RF amplifiers, RF power meters, analog amplifiers, analog-to-digital (A/D) converters, and an RS-232 serial interface driver—these electronics are mounted in a cabinet just under the radiometer head and connected to both the radiometer head and a dedicated WVM computer (CPU). All the flight electronic boards have been fabricated and have been shown

through testing to meet their requirements. A small microprocessor that handles the lowest-level data collection and timing has been programmed in assembly language to collect and co-add the radiometer data and communicate with the software residing in the WVM CPU.

3. A dedicated WVM CPU that converts the radiometer measurements to measured microns of precipitable water and communicates with the rest of the SOFIA Mission and Communications Control System (MCCS)—a nonflight version of this computer hardware has been procured for laboratory testing and the flight software is under development, with approximately 60% of the software coded and unit tested. Proper command and data communications between the WVM and the SOFIA MCCS have been demonstrated using an MCCS simulator that was developed by the SOFIA Project and is located on site at Ames.

Point of Contact: T. Roellig
(650) 604-6426
troellig@mail.arc.nasa.gov

New Interstellar Simulation Chamber Cavity Ring-Down Spectroscopy of Interstellar Organic Materials

Farid Salama, Ludovic Biennier, Robert Walker, Lou Allamandola, Jim Scherer, Anthony O'Keefe

A major milestone has just been achieved at Ames Research Center: a new facility has been developed to directly simulate gaseous molecules and ions at the low temperature and pressure conditions of interstellar space. This laboratory facility—which is unique within NASA—combines the techniques of supersonic free-jet expansion spectroscopy (JES) with the techniques of cavity ring-down absorption spectroscopy (CRDS). The principal objective is to determine the spectroscopic properties of

large interstellar aromatic molecules and ions under conditions that precisely mimic interstellar conditions. The aim of this research is to provide quantitative information to analyze astronomical spectra in support of NASA's Space Science and Astrobiology missions, including data taken with the Hubble Space Telescope.

Understanding the origin, physical properties, and distribution of the most complex organic

compounds in the universe is a central goal of Astrophysics and Astrobiology. Achieving this understanding requires the generation and maintenance of large carbon-containing molecules and ions under interstellar-like conditions with simultaneous measurement of their spectra under these conditions (that is, in the gas phase at very low densities and at very low temperature). As an aside, these organic structures are those that constitute the building blocks of carbon nanotubes. This process has been accomplished by combining three advanced techniques: free supersonic jet expansion, low-temperature plasma formation, and the ultrasensitive technique of cavity ring-down spectroscopy. The new facility thus comprises a pulsed-discharge, supersonic slit-jet source mounted in a high-flow vacuum chamber and coupled to a cavity ring-down spectrometer. Under these experimental

conditions, a beam of argon or helium gas seeded with polycyclic aromatic hydrocarbon molecules (PAHs) is expanded in the gas phase into the cavity ring-down chamber. When the expanding beam is exposed to a high-voltage ionizing electronic discharge, positively charged ions are formed that are characterized by very low, interstellar-like, rotational and vibrational temperatures (temperatures of the order of 10 and 100 kelvin (K), respectively, are achieved this way, as shown in figure 1). The cavity ring-down signal is a direct measurement of the absolute absorption by the seeding molecules and ions. This fact is illustrated in figure 2, which shows the spectrum of the PAH naphthalene ion ($C_{10}H_8^+$). This unique experimental facility has been developed in collaboration with Los Gatos Research through a Small Business Innovative Research contract.

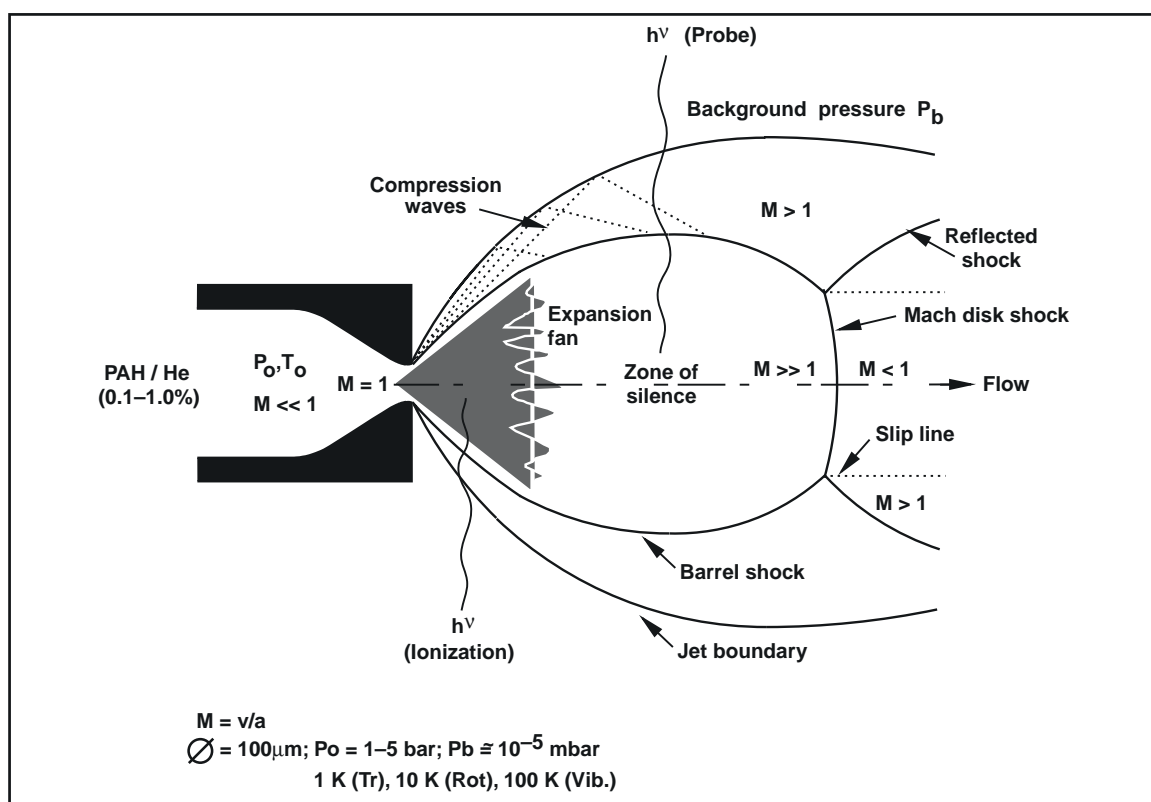


Fig. 1. Location of the "zone of silence" in a supersonic free jet expansion. The physical conditions within the boundaries of the "zone of silence" approach interstellar conditions.

The data shown in figure 2 can now be used to analyze the astronomical spectra. For example, the absorption band of the PAH ion ($C_{10}H_8^+$) shown in figure 2 can be directly compared to the absorption spectrum of the diffuse interstellar bands. These bands, which contribute to the global interstellar extinction, were discovered 80 years ago and remain an enigma to this day.

For the first time, the absorption spectrum of large organic molecules and ions can be measured under conditions that mimic entirely the interstellar conditions.

Point of Contact: F. Salama
(650) 604-3384
fsalama@mail.arc.nasa.gov

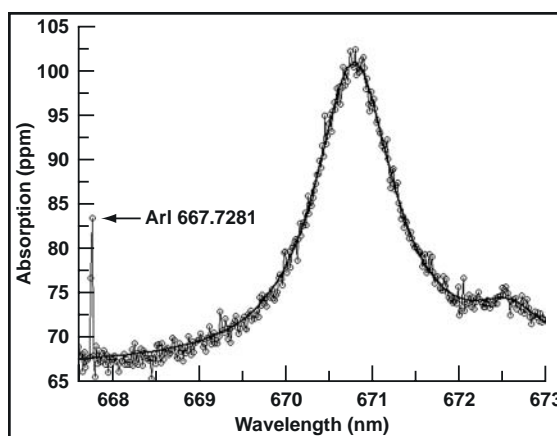


Fig. 2. The CRDS absorption spectrum of the naphthalene cation ($C_{10}H_8^+$) under simulated interstellar space conditions. The spectrum is obtained when an argon free jet expansion seeded with naphthalene is exposed to a high-voltage discharge. Note the absorption line of metastable argon that is used for internal wavelength calibration.

SPACE TECHNOLOGY

Carbon Nanotube Deposition and Growth Technique

Lance Delzeit

Carbon nanotubes (NTs) possess electrical, mechanical, and physical properties that make them ideal for applications in nanotechnology. A major constraint to the realization of many of these applications is the ability to produce nanotubes in an industrially viable method with the characteristics desired for the given application. These characteristics include quantity, chirality, size, density, distribution, and purity of the nanotubes produced. The research described here focuses on the production of NTs with the desired density, distribution, and purity for the application to industrially viable products.

A catalyst deposition and growth technique has been developed that allows for the controlled growth of either single- or multiwalled carbon nanotubes. This technique uses ion-beam sputtering to deposit the catalyst. By changing the catalyst formula and the growth conditions, either single- or multiwalled carbon nanotubes

can be grown. Furthermore, by adjusting the conditions used to produce single-walled nanotubes, the density of the nanotubes grown can be controlled from a sparse distribution of individual single-walled nanotubes to dense mats of single-walled nanotube “ropes.” “Ropes” are an association of individual nanotubes that form a larger structure—just as individual fibers make up a normal rope. The conditions for the growth of multiwalled nanotubes have been optimized for the growth of “towers.” A “tower” is a structure in which the nanotubes grow in the vertical direction because of the high density of the nanotubes in that region. Each of these different structures has applications to a variety of devices.

A further advantage of this technique is the ability to pattern the catalyst onto the surface. If the application requires the nanotubes to be grown in a confined area, then the ability to restrict the deposition of the catalyst to those

areas is critical. By using this process with standard shadow-masking and lithography techniques, such patterned catalyst deposits can be created for the development of applications.

Finally, for most applications, the nanotubes need to be produced free of impurities and contamination. The two major sources of contamination in the growth of carbon nanotubes are the buildup of amorphous carbon from the extraneous decomposition of carbon feed gas and contamination by an extraneous

metal catalyst. The elimination of the extraneous metal catalyst is currently being accomplished by optimizing the catalyst formula, thus reducing the quantity of “inactive” catalyst. The removal of the amorphous carbon is being realized by the use of etching gases that preferentially remove the amorphous carbon while not damaging the carbon nanotubes.

Point of Contact: L. Delzeit
(650) 604-0236
ldelzeit@mail.arc.nasa.gov

Low-Temperature Multiplexing Readouts for Airborne Astronomy

Jam Farhoomand

Cryogenic readouts are the critical electronics for infrared (IR) detector arrays and, in most instances, the dominant source of noise in an IR detection system. Various designs have been developed and perfected over years to minimize the read noise and optimize the circuitry for particular detector arrays for which the readouts are intended to be used. The present effort in this area—to develop readouts that operate at 2 kelvin and achieve improved sensitivity—is driven by the NASA charter to provide state-of-the-art IR technology to the astronomical community at large.

The simplest unit-cell design is the source follower per detector, which employs a single metal-oxide-semiconductor field-effect transistor (MOSFET) in the source follower configuration to read the detector signal. Although the simplicity of this design is attractive in terms of fabrication, minimal use of electronics real estate, and operation, it suffers from the inherent drawback that the integrated charge at the MOSFET gate debiases the detector and thereby degrades the detector linearity. In extreme cases, it can significantly diminish the detector photocurrent. Detector debiasing

could pose severe limitations for detector arrays that require low bias levels, such as those used in the far-IR. A capacitive transimpedance amplifier (CTIA) is one possible solution. This design uses a transistor in an amplifier mode and includes a capacitor in the feedback loop. The feedback capacitor serves as the integrator and, by virtue of the negative feedback, pins the detector node to a constant voltage.

The first generation of CTIA readouts, CRC-696, was manufactured by Hughes/Santa Barbara Research Center for the multiband infrared photometer (MIPS) for the Space Infrared Telescope Facility (SIRTF) instrument. This device was a 1 x 32, single-gain, DC-coupled multiplexer, optimized for low photocurrents. A few of these devices, with and without IR detectors, were tested in the lab at Ames. The success of the CRC-696 led to the development of the next generation of these devices—the SB-190—with added features to expand and enhance their performance. The SB-190 is a 1 x 32, multigain, AC-coupled CTIA designed to accommodate a broad range of IR flux (including photocurrent levels

consistent with airborne astronomy applications) (fig. 1). The multiple gain is achieved by having several integrating capacitors in the feedback loop that can be enabled in eight possible combinations.

These devices have been designed, developed, and characterized; their first application is intended to be for the far-IR detector array of the airborne infrared echelle spectrometer (AIRES), a facility instrument for the Stratospheric Observatory for Infrared Astronomy (SOFIA). To date, several of these devices have been tested; they showed adequate performance, although better performing devices are expected when the processing is refined and better controlled. The typical read-noise at the highest gain setting and with correlated double sampling is about 250 electrons. Further tests are under way, and this readout will be integrated with a 1 x 24 prototype Ge:Sb array in the near future.

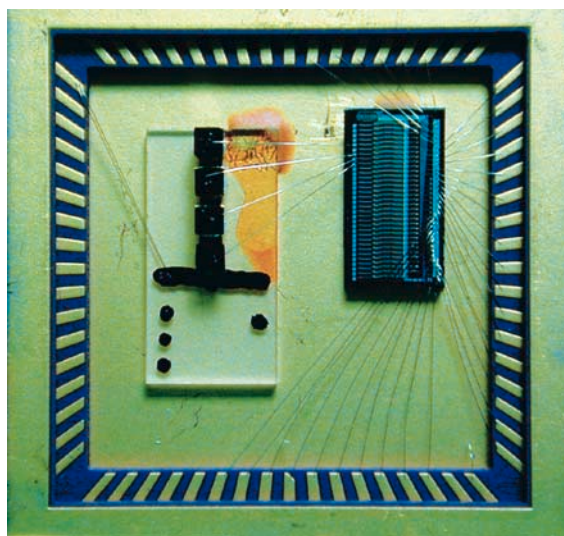


Fig. 1. A prototype 1 x 32 SB-190 multiplexer bonded to 4 Ge:Ga far-infrared detectors.

Point of Contact: J. Farhoomand
(650) 604-3412
jfarhoomand@mail.arc.nasa.gov

Guide Star Telescope Detector Assembly for Gravity Probe-B

John H. Goebel

Because of extensive experience in low-temperature detector and readout technology and the challenging technical and programmatic requirements, Ames is continuing to lead the development and manufacture of the guide star telescope detectors of the Gravity Probe-B (GP-B) Project. GP-B is a Stanford University/Lockheed Martin/Marshall Space Flight Center Physical Science mission. The scientific purpose of GP-B is to test Einstein's theory of General Relativity, which has been only partially verified and is one of the least tested of all physical theories.

The GP-B fine motion guide star tracking system uses a 5.6-inch-aperture, all-fused quartz telescope attached to a quartz block assembly containing the relativistic effect-sensing gyroscopes. The guide star telescope rotates about its central axis, thereby providing

a constant pointed reference direction to a star that is fixed on the celestial sphere. This setup provides the critical inertial reference frame for the spacecraft. The satellite that contains this assembly, scheduled to be launched late in 2002, will be in a polar orbit about the Earth. The precession rate of the sensed gyroscope directional output from the inertial reference frame is a possible indication of a general relativistic deviation from that expected by Newtonian gravitational theory. A precession rate is expected to occur at a scale of a few arcseconds per year (arcsec/year), and it is expected to be measured with an accuracy of about 0.2 milliarcsec/year. For comparison, the apparent angular diameters of the few nearest stars, visible to all but the largest telescopes as points of light, are less than 10 milliarcseconds.

Progress in FY00 has been significant. The GP-B telescope subsystem, with which Ames personnel has significant involvement, has been demonstrated to function in ground tests with sensitivity levels commensurate with the design, and adequate for all mission requirements. The detector module assembly is shown in figure 1. The real-time pointing accuracy of the x-axis and y-axis detector pairs achieve sensitivities limited by noise levels of 8 and 10 milliarcseconds/ $\sqrt{\text{hertz}}$, respectively. The mission requirement is 10 milliarcseconds/ $\sqrt{\text{hertz}}$, which is set by the theoretical shot-noise-limited photon arrival rate. Hence, during the 3-minute period of the spacecraft roll, the pointing accuracy is limited to about 80 microarcseconds of angle on the sky. Also being investigated are the possible interfering effects that may degrade the performance during the mission, whether they arise from astronomical, atmospheric, terrestrial, or spacecraft factors.



Fig. 1. Detector module assembly for GP-B.

A picture of the quartz telescope with the attached light detectors is shown in figure 2. The telescope is standing on its base plate. Light enters from above, is reflected into the upper structure, the knife edge divider assembly, where the beam is divided equally between a total of eight photodiodes. The equality of this division determines the error signal that is sent back to the control circuits that readjust the spacecraft orientation. Four detectors are



Fig. 2. GP-B quartz telescope assembly.

needed for complete control; the other four are identical, but redundant. The detectors are at the top of the figure. Signals are conveyed via flexible printed circuits to connectors that interface the detectors thermally and electrically to a low-thermal-conductivity cable bundle (not shown) that is part of the science instrument assembly.

Point of Contact: J. Goebel
(650) 604-3188
jgoebel@mail.arc.nasa.gov

Lightweight, High-Efficiency Pulse Tube Cryocooler

Peter Kittel, Louis J. Salerno

A lightweight, high-efficiency (LWHE) pulse tube cryocooler (LHEC) has been developed through an Ames, Air Force, and TRW partnership. This cooler is designed to meet NASA's future requirements for zero boil-off (ZBO) propellant storage. Such ZBO systems will meet NASA challenges for developing reusable space transportation vehicles for both Earth-to-orbit and long-duration missions. In addition to ZBO, LWHE coolers can be used with heat exchangers for sizing In-Situ Consumable Production (ISCP) liquefiers for production and storage of propellants and breathable gases during human and robotic exploration missions. Other space applications include a ZBO system for storing liquid nitrogen for shuttle/station astrobiology experiments. As an example, one such experiment stored samples in a 12-liter liquid nitrogen Dewar for periods of up to 12 days. To date, samples required preparation several weeks in advance, necessitating replenishment with liquid nitrogen until loading on the shuttle for launch. A ZBO system would not only alleviate this requirement but would also allow sample storage for longer time periods. Finally, this cooler can be used for Space Science and Earth Science instruments.

The cryocooler is a flight-type pulse tube cryocooler with a design point of 10 watts (W) of cooling at 95 kelvin (K) (-178 degrees Centigrade ($^{\circ}\text{C}$)). This cooler has an efficiency of 12 W of input power for each watt of cooling at 95 K. This efficiency is nearly a third better than that of the previous design. It weighs 3.6 kilograms (7.9 pounds), about a factor of three less than previous design. The operating lifetime goal of this cooler is 10 years. The cryocooler is shown in figure 1, and the thermal performance of the cooler is illustrated in figure 2.



Fig. 1. The lightweight, high-efficiency pulse tube cryocooler. The scale at the bottom is 2 centimeters. The cold plate is the block near the middle of the vertical column.

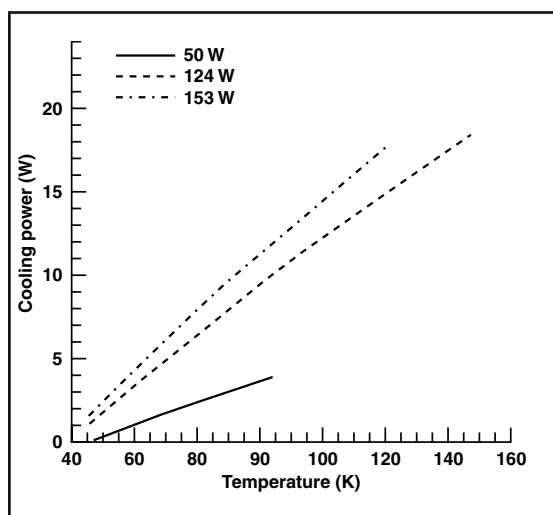


Fig. 2. The performance of the LHEC for three different input powers.

For ZBO space transportation systems, coolers near 95 K are needed for storage of oxygen and methane. Coolers will also be required near 20 K for liquid hydrogen storage. For space applications, less complex coolers such as pulse tubes, which offer the advantage of having no moving parts at the cold head, are presently favored for these cooling requirements from an operating simplicity, reliability, and lifetime standpoint. From a versatility standpoint, 20 K coolers developed for transportation could also be used as first stages for instrument coolers that employ dilution refrigerators or adiabatic magnetization refrigerators as a second stage.

The cooler described here will be delivered to Ames in 2001 for performance testing. Then it will go to Glenn Research Center to be incorporated into a ZBO test in 2002. The ZBO test involves a partnership of three NASA centers: Ames, Glenn, and Marshall. The test will demonstrate the ZBO storage of liquid nitrogen in a 1400-liter (50-cubic-foot) tank.

Point of Contact: P. Kittel
(650) 604-4297
pkittel@mail.arc.nasa.gov

Protein Nanotechnology

Jonathan Trent

Because of NASA's efforts to make missions "faster, better, and cheaper," there is a growing need for the development of smaller, stronger, and "smarter" scientific probes compatible with space exploration. The necessary breakthroughs in this area may well be achieved in the revolutionary field of nanotechnology. This technology is on the scale of molecules, and it holds the promise of creating devices smaller and more efficient than anything currently available. While much exciting research is developing around carbon nanotube-based nanotechnology, researchers at Ames are exploring biologically inspired nanotechnology.

The biological "unit," the living cell, may be considered the ultimate nano-scale device. Cells that are constructed of nano-scale components are extremely sensitive, highly efficient environmental sensors capable of rapid self-assembly, flawless self-repair, and adaptive self improvement—not to mention their potential for nearly unlimited self-replication. Ames is focusing on a major component of all

cells (proteins) that are capable of self-assembling into highly ordered structures. A protein known as HSP60, which spontaneously forms nano-scale ring structures (fig. 1a, end view; 1b, side view), that can be induced to form chains (fig. 1c) or filaments (fig. 1d), is currently being studied.

With thermostable HSP60s, highly efficient methods have been developed for purifying large quantities of these proteins; their composition and structure-forming capabilities are being currently modified by using the "tools" of molecular biology. For example, if a small fragment of the HSP60 protein is removed, protein rings are produced that do not form chains or filaments, but continue to form rings that spontaneously assemble into highly ordered hexagonally packed arrays (fig. 2a). If these proteins are modified to bind metal atoms, they can be used as a template to create an ordered pattern of metal on a surface with nanometer spacing. Ultimately the hope is to use such ordered arrays of metal to manufacture nano-scale electronic devices. Similarly,

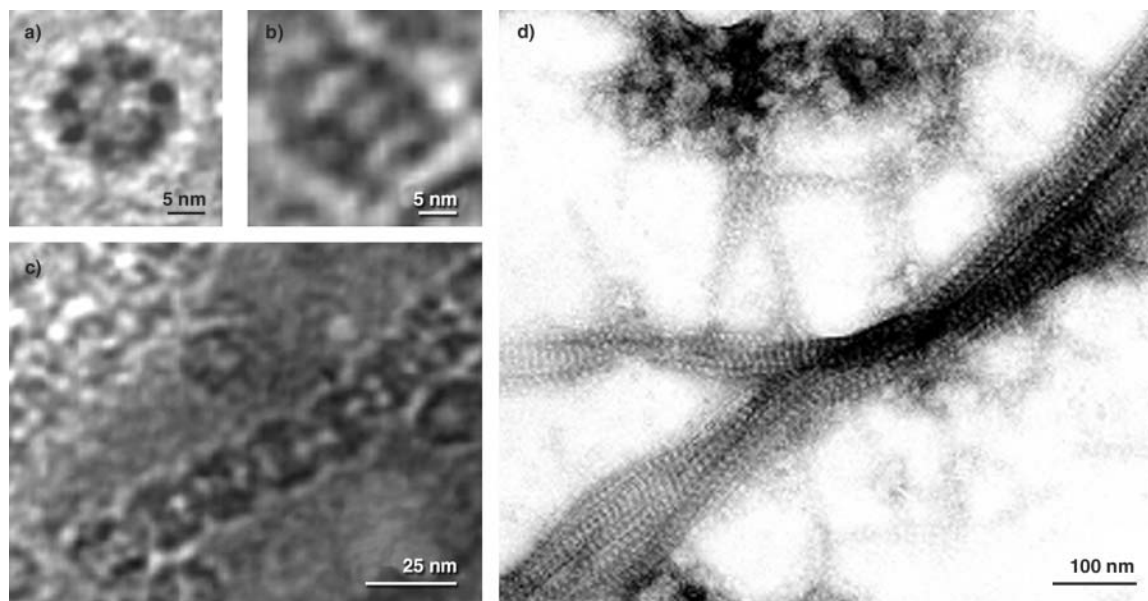


Fig. 1. Protein rings (a, end view, and b, side view), chains of rings (c), and bundles of chains (d) that can be used in nanotechnology.

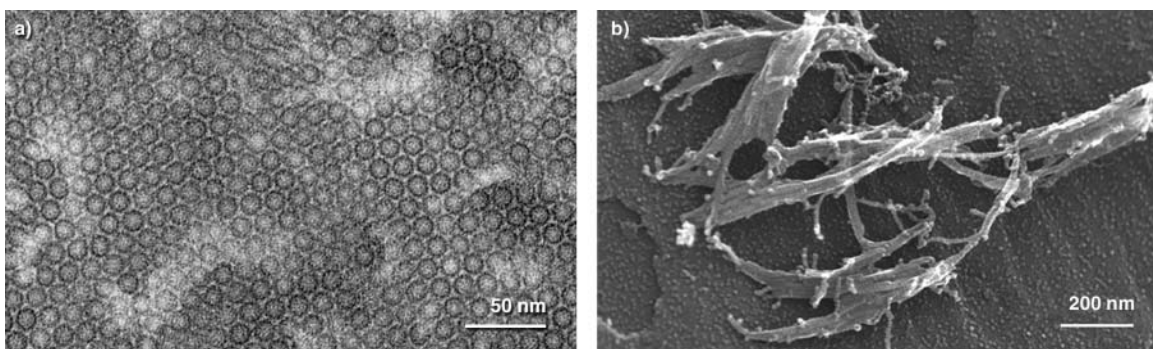


Fig. 2. Modified proteins form hexagonally packed rings (a) or metal-containing protein filaments (b).

metal binding to proteins that form filaments (fig. 2b) may be used to create self-assembling nano-scale wires, which may someday be used to produce self-assembling circuits.

Potential applications abound for protein-based nanotechnology applicable to the production of smaller, stronger, and “smarter” probes for NASA, or more generally for applications in electronics and medicine. The combination of nanotechnology, information technology, and biotechnology at Ames Research Center provides an excellent research environment for biologically inspired nanotechnology. Analytical capabilities in nanotechnology provide

essential tools for determining structure and function of protein-based systems. Supercomputing in information sciences provides capabilities essential for molecular simulations and biomolecule visualizations. Biotechnology provides the methodological basis for the genetic engineering essential for modifying and functionalizing protein structures. The goal is to establish the feasibility of creating useful protein-based nanostructures with applications for NASA and other critical areas of technology.

Point of Contact: J. Trent
(650) 604-3686
jtrent@mail.arc.nasa.gov

PLANETARY SCIENCE

The Radiative Signature of Europa Ice

Galina M. Chaban, Timothy J. Lee, Winifred M. Huo

Recent observations from the Galileo satellite indicate that three of the Jupiter moons, Europa, Gandymede, and Callisto, may have subsurface oceans. Because water is an essential ingredient of life, the possible existence of the subsurface ocean and the nature of its composition is of great interest to planetary scientists and astrobiologists. Of the three moons, Europa has attracted the most attention. Data from the Galileo near-infrared mapping spectrometer (NIMS) indicate the possibility of hydrated salts on Europa's surface. The combination of a subterranean ocean, internal heat from tidal flexing, salt, and possible prebiotic materials from comet and meteorite impact may provide a possible condition for the formation and evolution of life. So far, the existence of both a subsurface ocean and hydrated salts is based on indirect

evidence. The analysis of the NIMS spectra, for example, is based on the change of the water absorption spectra in hydrated salts in the 1.0 to 2.5-micron (μm) region. The assignment is by no means unique.

To search for a frequency range that can pinpoint the presence of salt more definitively, large-scale quantum chemistry calculations of hydrated magnesium sulfate, $\text{MgSO}_4 \cdot n\text{H}_2\text{O}$, $n = 1-3$, were made using second-order many-body perturbation theory and with a basis set of Gaussian functions at the triple zeta + polarization level. The configuration of the lowest electronic states of $\text{MgSO}_4 \cdot 2\text{H}_2\text{O}$ and $\text{MgSO}_4 \cdot 3\text{H}_2\text{O}$ are shown in figures 1 and 2. The wavelengths and intensities of infrared absorption for the SO_2 stretch modes are tabulated in Table 1.

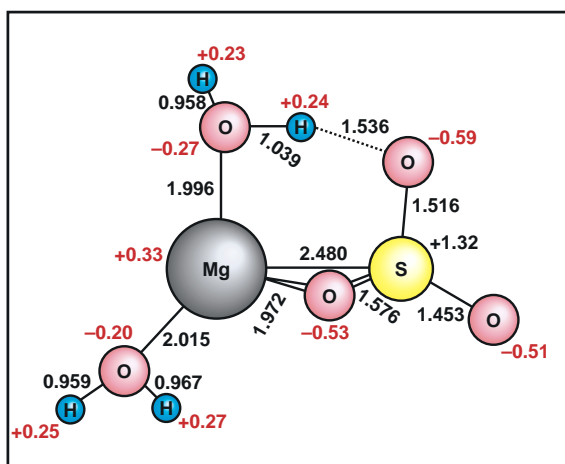


Fig. 1. Configuration of the lowest electronic state of $\text{MgSO}_4 \cdot 2\text{H}_2\text{O}$.

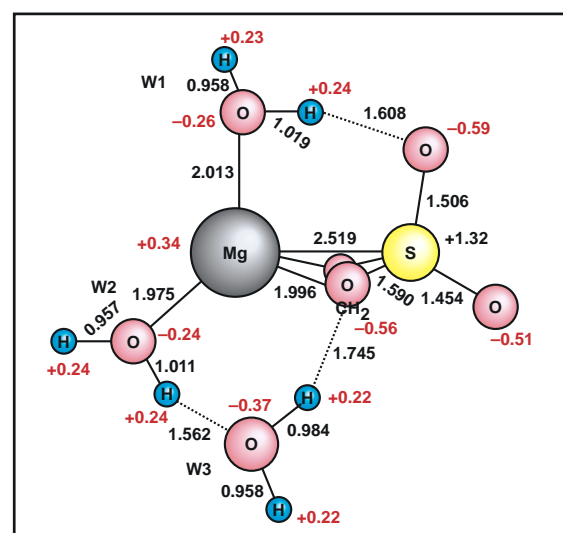


Fig. 2. Configuration of the lowest electronic state of $\text{MgSO}_4 \cdot 3\text{H}_2\text{O}$.

Table 1. Wavelength and intensity of the SO₂ stretch modes for MgSO₄•nH₂O, n = 1–3.

Molecule	Vibrational mode	Absorption wavelength, μm	Intensity, $\text{Db}^2/\text{A}^2 \text{ amu}$
MgSO ₄	Asymmetric SO ₂ stretch	7.424	7.01
	Symmetric SO ₂ stretch	8.569	6.33
MgSO ₄ •H ₂ O	Free SO ₂ stretch	7.502	8.90
	Bonded SO ₂ stretch	9.911	10.95
MgSO ₄ •2H ₂ O	Free SO ₂ stretch	7.576	9.00
	Bonded SO ₂ stretch	9.804	10.80
MgSO ₄ •3H ₂ O	Free SO ₂ stretch	7.593	8.48
	Bonded SO ₂ stretch	9.372	9.00

The SO₂ stretch modes occur at longer wavelengths than the infrared absorption modes of water. They can serve as a unique identifier for the presence of magnesium sulfate salts. Interesting results were obtained on the infrared spectra of water bonded to magnesium sulfate. These results can be used to design a

better detector for possible salts on the surface of Europa.

Point of Contact: W. M. Huo
(650) 604-6161
whuo@mail.arc.nasa.gov

Particle-Gas Dynamics in the Protoplanetary Nebula

J. N. Cuzzi, R. C. Hogan, A. R. Dobrovolskis

“Primitive” or unmelted asteroids, from which the planets were built, are represented in the meteorite record as a vast dataset that has had little context for interpretation. The accretion of these primitive bodies from small grains and millimeter-sized, melted “chondrules” almost certainly occurred in the presence of gas. Study of this stage is complicated by the feedback effects of the gas on the particles, and vice versa. Ames’ efforts focus on numerical modeling of particle-gas interactions in turbulent flows, and understanding meteorite properties in the light of theoretical models.

The Ames “turbulent concentration” theory (TC), introduced several years ago, shows how particles of a specific size/density combination are concentrated by orders of magnitude in weak nebula turbulence. The theory makes specific predictions as to the relative abundance distribution of the concentrated particles. Predictions of the shape of the size distribution are in very good agreement with observed particle size distributions in primitive chondrites, thus revealing the fingerprints of TC. A multifractal theory has been developed to predict the magnitude of turbulent

concentration at much higher Reynolds numbers than achievable numerically, but the concentration factor can be so large that the local particle mass density can exceed that of the gas, and the feedback effect of the particle phase on damping the gas turbulence must be considered before further modeling efforts can proceed. A cascade model of a process that is capable of reproducing the way concentrations of particles emerge as energy flows down the turbulent cascade, or inertial range, is being developed to better understand the effects of heavy mass loading on turbulence and TC. The cascade model is parameterized by partition functions or “multipliers” that are only statistically defined, but whose probability distribution function can be fit to present numerical results for mass-loaded turbulent fluids. In other words, the multipliers appropriate for densely particle-enriched regions where the turbulent kinetic energy and/or vorticity might be damped could be different from the multipliers in “normal” regions where mass loading is negligible. The dependence of these multipliers on the local gas and/or particle density properties is now being determined by making extensive use of new runs of a scalar field particle code (rather than the previous Lagrangian particle code) on the Ames Origins 2000 facility.

In FY00, Ames researchers also developed a scenario to help explain a new phenomenon found in chondritic meteorites by collaborators at Stanford University and the University of Hawaii. The observation is of an abundant class of iron/nickel metal grains with chemical and crystallographic properties that define their growth and cooling times simultaneously. The scenario developed visualizes a very hot, early, perhaps inner stage of the protoplanetary nebula, rather different from the environment in which more familiar chondrites form. In this dense, hot region, strong convection plumes rise toward the surface of the nebula, cooling and condensing small metal and silicate particles much as raindrops or hailstones condense in upwelling thunderstorm plumes on Earth. Some fraction of these objects are dispersed outward to cooler regions before being downdrafted again to their destruction. Although the theory adequately explains some properties of these unique meteorites, it is clear that deeply puzzling aspects remain unexplained.

Point of Contact: J. Cuzzi
(650) 604-6343
cuzzi@cosmic.arc.nasa.gov

Planetary Rings

J. N. Cuzzi, I. Mosqueira, M. Showalter, F. Poulet

In addition to the natural curiosity inspired by their exotic appearance, planetary rings present a unique dynamical laboratory for understanding the properties of collisional particle disks that might aid in the understanding of the accretion of the planets. Ames scientists are involved in numerous different aspects of planetary-ring studies.

An ongoing Hubble Space Telescope (HST) program to observe the rings while they “open up” as seen from Earth over the last five years (see figure) has produced over 100 images in a variety of filters. Analysis of these images using a newly developed surface-scattering code has led to the conclusion that the increasing redness of the rings that has been found to

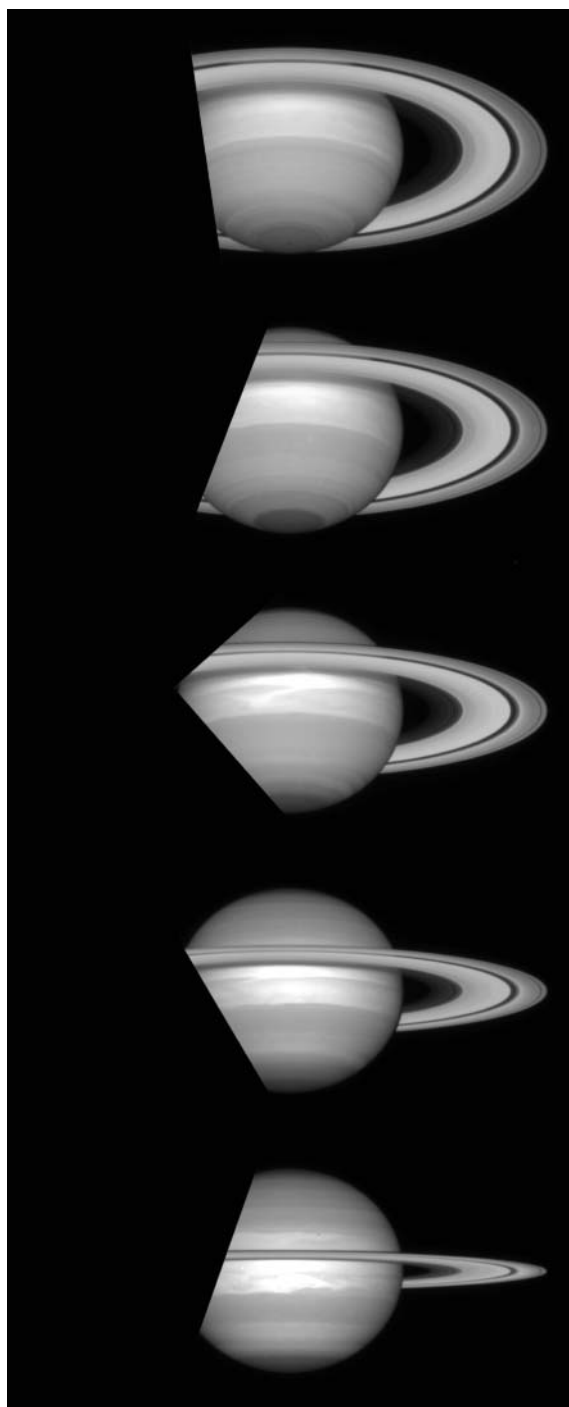


Fig. 1. HST observations of Saturn since 1996, during which time the ring opening angle has increased from about 4 degrees to about 24 degrees. The time sequence begins in the bottom image. Data of this quality are available in over eight color filters. Voyager data are of higher spatial resolution, but only three filters are available—fortunately they are nearly identical to three of the HST filters.

occur as the angle between the Sun and the Earth increases is caused by unusually rough surfaces on the ring particles. This theory supports the concept that a ring “particle” is actually an ensemble or aggregation of smaller “particles”—a lumpy snowman-like fractal structure. Further analysis will give insight into how this structure varies across the rings, on scales that can never be observed directly (tens of meters or less). In addition, this modeling and analysis has established that the abrupt brightening of the rings as the Sun-ring-Earth angle gets very small, which has been previously ascribed to the disappearance of shadows, is more likely due to optical interference effects within the grainy surface of individual particles. This result helps reconcile the brightening with dynamical expectations that the ring particles are collapsed into a fairly thin, dense layer because of inelastic collisions rather than being many particles thick as had been previously thought. This study also examined a discrepancy between Voyager and HST color observations of the rings, tracing it to an incorrect Voyager calibration. A direct comparison of Voyager and HST color data reveals that the two datasets are in very good agreement from the standpoint of spatial color variations. Variations of color, which trace out particle compositional variations, vary with radius and ring opacity in a way that is quite unusual and will be addressed in future analysis.

The systems of large (and small) regular moons that orbit the gas giant outer planets have always been cited as “solar systems in miniature,” but their own origin has remained a puzzle. One recent area of interest is the two outer Galilean moons of Jupiter (Ganymede and Callisto), which are of very similar mass and size, yet have very different internal structures. A two-stage accretion scenario has been developed that postulates a long-lived, secondary accretion stage only for Callisto

involving debris that forms in a very extended disk of material that extends far out beyond the boundaries of the current satellite system. A small amount of gas remaining in this disk causes solid material to drift slowly inward onto the outermost moon, accreting without providing much heating. In addition, a study of the thermal internal evolution of a realistic Callisto was carried out, including ice-phase-change boundaries and plastic ice convection, showing that a sufficiently slow accretion rate would indeed preclude melting of the icy component and prevent complete differentiation of the icy and rocky material.

Ames maintains the Planetary Data System Rings Node (<http://ringmaster.arc.nasa.gov/>), which archives and distributes ring data from

NASA's spacecraft missions and from Earth-based observatories. The entire archive of images from the Voyager missions to the giant planets is now on line, with catalogs to help users find the images they need. Interactive search and geometrical visualization utilities are also available to assist Cassini scientists in planning observations of the rings during the upcoming tour (2004–2008). Ames also provides the Cassini project with the Interdisciplinary Scientist for Rings and Dust, who chaired the Rings Discipline Working Group this year as it worked through initial ring science sequence planning.

Point of Contact: J. Cuzzi
(650) 604-6343
cuzzi@cosmic.arc.nasa.gov

Vortex Evolution in a Protoplanetary Disk

Sanford Davis

The theory that planets form from a thin disk of dust and gas was first proposed in the 18th century and is now a generally accepted fact. The process by which planets actually emerge from this tenuous state is a subject of intense current study. Recent research points to vortex motion as a possible intermediary where dust particles are captured, concentrated, and finally accumulated by gravitational attraction. These mass accumulations gradually grow to kilometer-sized objects (planetesimals) and ultimately to full-sized planets. With the assumption that the disk can support a turbulent flow, it was shown that vortices arise naturally and persist as long as turbulent energy is present. Other possibilities are that vortices arise from certain instabilities in the rotating disk or from external impacts of clumpy infalling gas. In either case, coherent vortices could lead to important and far-reaching processes in the protoplanetary disk.

A research study is under way to determine the effect of vortices on the wave structure in a typical disk, which may also play a role in the planet-formation process. It is well-known that discrete vortices in a sheared flow do not retain their coherence. This coherence time depends on the local shear rate, the strength, and the size of the vortex. During the shearing epoch, and depending on the nature of the medium, a vortex can emit a variety of wave systems. In this study, the equations of motion have been simulated using a high-resolution numerical method to track Rossby and acoustic/shock waves. Rossby waves are slowly moving waves of vorticity generated in flows with large-scale vorticity gradients. Acoustic waves are waves of expansion and contraction that occur in all compressible media. The protoplanetary disk is a rotating compressible gas with a radially variable rotation rate. It can support both wave systems.

A typical result from the simulation is given in figure 1, which shows a sequence of snapshots of the perturbed vorticity defined as the difference between the total vorticity and the baseline flow. This baseline flow is a Keplerian flow (Rotational velocity = Constant \times (Radius) $^{-1/2}$), and the initial vortex is shown in the third quadrant in figure 1(a). The vortex becomes elongated about its initial location at $r = 4$ (blue-red streaks on the white circle in fig. 1(b)), and both inward- and outward-bound

counterclockwise spiral vorticity waves are spawned. The outward-bound waves evolve to an axisymmetric wave pattern (circularization) with shock waves (fig. 1(d)). It is interesting that the vortex-induced waves can induce a supersonic radial flow. Another wave system (Rossby waves) appears in the region $r < 10$. The shock waves are axisymmetric, whereas the Rossby waves have a cosine angular dependence. Each wave system has a characteristic radial speed.

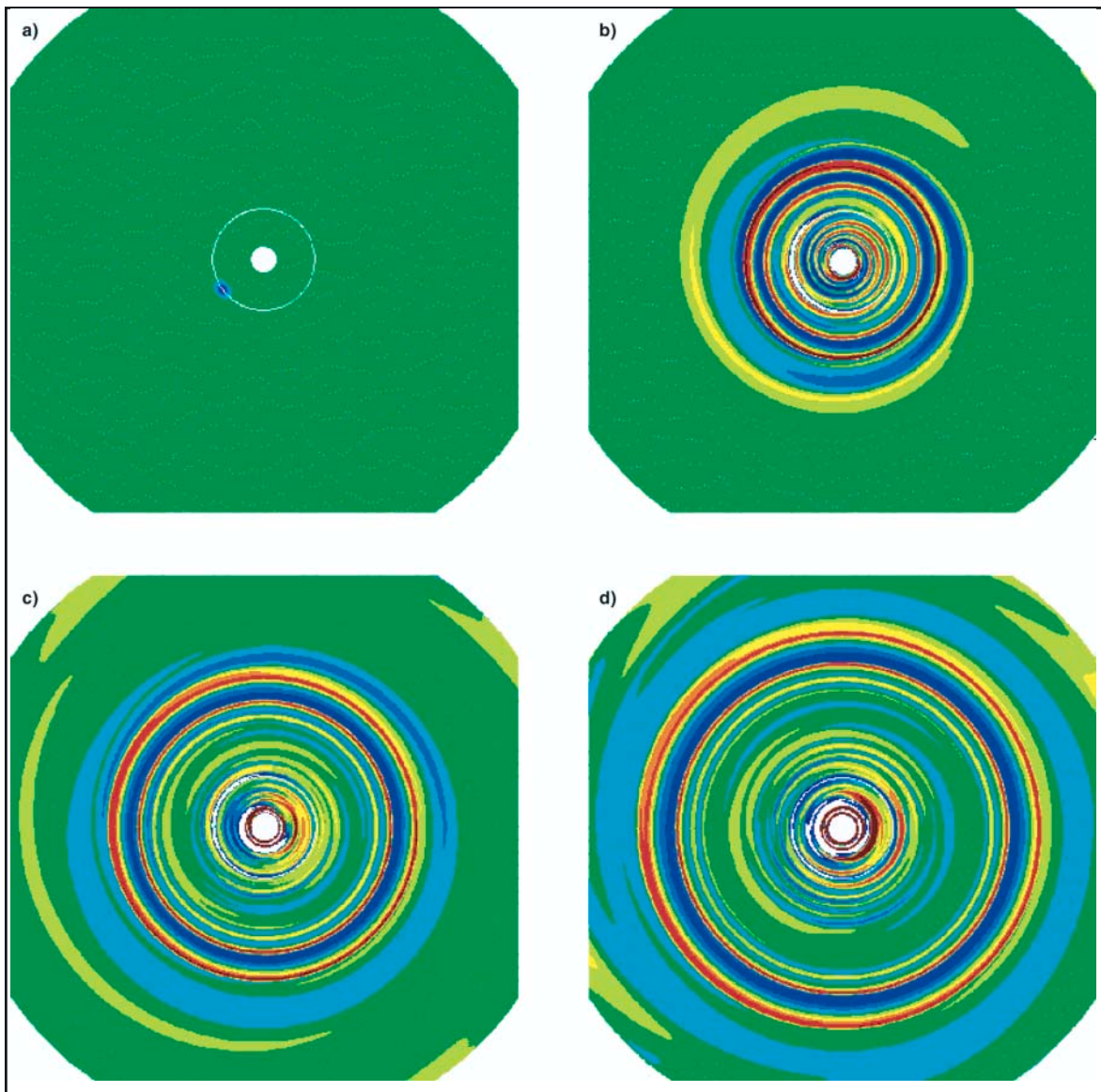


Fig. 1. Perturbation vorticity bitmaps showing density (shocks) and Rossby waves. (a)–(d): 0, 16, 32, and 48 vortex revolutions, respectively.

Follow-up work will augment the numerical simulations with particle and/or granular gas models to examine the effect of these vorticity-induced waves on particle migration, accumulation, and (possibly) planetesimal formation.

Point of Contact: S. Davis
(650) 604-4197
sdavis@mail.arc.nasa.gov

Liquid Water on Present-Day Mars?

Robert M. Haberle

Near-surface environmental conditions on Mars today are generally considered inadequate to permit liquid water to exist in equilibrium with the atmosphere. Mean annual temperatures are about 50–60 kelvin (K) below the melting point, and mean annual surface pressures are very close to the triple point. Yet there are localized regions where, for a few hours of the day at the right time of year, surface temperatures and pressures meet the minimum requirements for the existence of liquid water: pressures and temperatures above the triple point of water but below the boiling point.

That such conditions do exist was determined using a validated General Circulation Model. The model predicts where and for how long liquid water could exist each Martian year. For pure liquid water, the model predicts that liquid water might occur in five regions: between 0 and 30 degrees North in the plains of Amazonis, Arabia, and Elysium; and in the Southern Hemisphere impact basins of Hellas and Argyre. The combined area of these regions represents 29% of the surface area of the planet. In the Amazonis region, these requirements are satisfied for a total integrated time of 37 sols each Martian year. In the Hellas basin, the number of degree-days above 0 is 70, a number that is well above those experienced in the dry valley lake region of Antarctica.

Whether liquid water ever forms in these regions depends on the availability of ice and heat, and on the evaporation rate. The latter is poorly understood for low-pressure CO₂ environments, but is likely to be so high that melting occurs rarely, if at all. However, even rare events of liquid-water formation would be significant because they would dominate the chemistry of the soil, and would have biological implications as well.

Interestingly, these regions are remarkably well correlated with the location of impact craters that appear to have been filled with lakes at some time in the past. Approximately 86% of the more than 100 impact crater lakes lie within the model-predicted regions where conditions for liquid water are favorable. The lakes do not exist today, but appear to have existed within the last several billion years, and some appear to have existed within the last several hundred million years. The reason for this amazing correlation is not known.

Point of Contact: R. Haberle
(650) 604-5491
haberle@humbabe.arc.nasa.gov

Measurement of Meteor Impact Experiments Using Three-Component Particle Image Velocimetry

James T. Heineck, Peter H. Schultz

The study of hypervelocity impacts has been aggressively pursued for more than 30 years at Ames as a way to simulate meteoritic impacts. Development of experimental methods coupled with new perspectives over this time has greatly improved the understanding of the basic physics and phenomenology of the impact process. These fundamental discoveries have led to novel methods for identifying impact craters and features in craters on both Earth and other planetary bodies. Work done at the Ames Vertical Gun Range led to the description of the mechanics of the Chicxulub crater (a.k.a. K-T crater) on the Yucatan Peninsula, widely considered to be the “smoking gun” impact that brought an end to the dinosaur era.

This is the first attempt in the world to apply three-component particle image velocimetry (3-D PIV) to measure the trajectory of the entire ejecta curtain simultaneously with the fluid structure resulting from impact dynamics. The science learned in these experiments will build understanding in the entire impact process by simultaneously measuring both ejecta and atmospheric mechanics. Furthermore, it will aid in the interpretation of the data coming from the Deep Impact Space Probe, due to be launched in 2004.

The work has implications not only to geologists but also to space transportation engineers. Micrometeorites that impact space vehicles may have catastrophic effects on those ships. Modeling these impacts has been an active field of study as well. As a matter of course, the experimental methods developed for the planetary geologist have been applied to the study of impactor effects on space vehicles and vice versa.

The first goal was to develop the PIV technique as applied to hypervelocity impacts and prove the concept. The second objective was to observe an impact, both to visualize and to quantify the extremely complex ejecta-gas interaction resulting from an oblique impact in an atmosphere.

The system was set up at the Ames Vertical Gun Range. As shown in figure 1, two cameras are mounted in a stereo arrangement above the target. A laser light sheet, 5 millimeters thick, was projected from the side and was oriented 3.5 inches above and parallel to the target surface. The laser creates two short-duration pulses with a controllable time interval (on the order of microseconds) between the pulses. The cameras record separate images of the ejecta as illuminated by the two laser pulses. The resulting image pairs from each camera were cross-correlated to determine both the direction and the magnitude of the displacements of the ejecta in the plane of the laser. The perspective difference of each

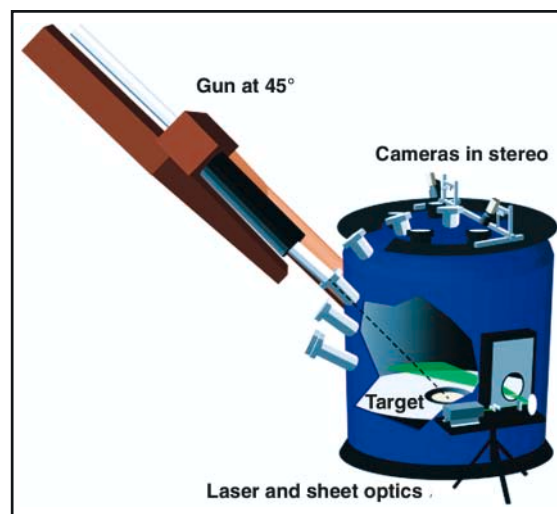


Fig. 1. Illustration of the PIV system, the target, and the vacuum chamber of the Vertical Gun Range.

camera view permits the derivation of the third component of velocity. Tracer particles were added to the target to follow the gas dynamics, thus permitting simultaneous cross-correlation with the ejecta.

The implementation of 3-D PIV yielded excellent results. Figure 2 shows a typical flow pattern derived from the PIV measurements. This vector and contour plot represents both the speed and direction of the impact dynamics resulting from a one-eighth-inch copper sphere traveling 2.2 miles per second. It impacted the surface of the sand target at 45 degrees. The atmosphere above the target was nitrogen at a pressure of approximately 7.5 pounds per square inch. The lengths of the arrows are

directly proportional to the velocity of the particles in the data plane. The color represents a contour of the velocity component that is perpendicular to the data plane. The blue regions are moving away from the viewer; the orange regions are moving toward the viewer. Note that the ring of ejecta is distorted because of the angular impact. The downrange particles are moving significantly faster than other portions of the curtain. In addition to the ejecta ring, the fluid mechanics associated with the wake of the impactor are clearly shown.

Point of Contact: J. T. Heineck
(650) 604-0868
jheineck@mail.arc.nasa.gov

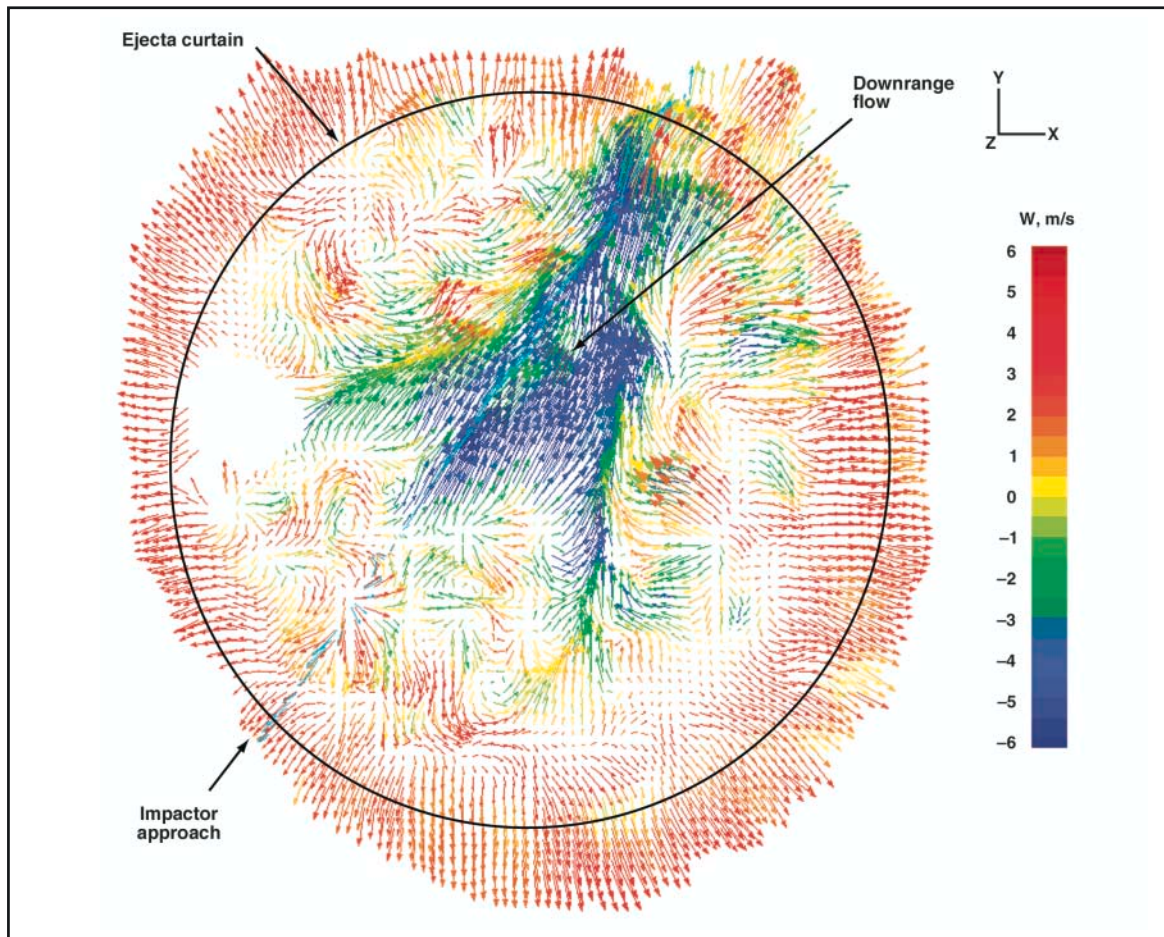


Fig. 2. Vector plot of the in-plane velocities of impact ejecta and atmospheric interaction. The contour colors are of the out-of-plane velocities.

The Center for Star Formation Studies

D. Hollenbach, K. R. Bell, G. Laughlin

The Center for Star Formation Studies, a consortium of scientists from the Space Science Division at Ames and the Astronomy Departments of the University of California at Berkeley and Santa Cruz, conducts a coordinated program of theoretical research on star and planet formation. Under the directorship of D. Hollenbach (Ames), the Center supports postdoctoral fellows, senior visitors, and students; meets regularly at Ames to exchange ideas and to present informal seminars on current research; hosts visits of outside scientists; and conducts a week-long workshop on selected aspects of star and planet formation each summer.

In June 2000, the Center worked together with researchers from the Arcetri Observatory (Florence, Italy) to hold an international workshop entitled "High Mass Star Formation: An Origin in Clusters." The week-long workshop, held in Volterra, Italy, had approximately 175 attendees, and included an invited talk by D. Hollenbach on "Star Formation and the Fluctuating Ultraviolet Field in the Galaxy."

One focus of the NASA Ames portion of the research work in the Center in FY00 involved the effect of ultraviolet radiation from young massive stars on the interstellar medium of a galaxy. The interstellar medium of a galaxy is the gas and dust that lie between the stars. Most of the gas is hydrogen; the dust mass is only about 1% of the gas mass. The gas and dust reside in various components, often characterized by the gas density in the component. The densest and coldest component is the molecular clouds; this component forms stars. Diffuse clouds are less dense than molecular clouds; they are primarily cold atomic hydrogen. The warm medium consists of neutral and ionized gas at very low density and relatively

high temperature. The star formation rate in a galaxy depends on the rate at which molecular clouds can be formed, because only this component forms stars. The molecular clouds are thought to form by the coalescence of diffuse clouds into opaque, self-gravitating clouds. However, high rates of star formation lead to high populations of massive stars that radiate copious ultraviolet flux. The ultraviolet flux in turn heats up the diffuse clouds in the interstellar medium and transforms them into a warm medium. Because a warm medium is unlikely to form molecular clouds, the lack of diffuse clouds cuts off the supply of molecular clouds in a galaxy, thereby cutting off the star formation rate. This scenario then provides a self-regulation mechanism that controls the rate of star formation in a galaxy.

Another focus of the Ames portion of the Center research in FY00 involved a collaborative theoretical study of the conditions that determine whether a collapsing molecular cloud core of gas and dust gives rise to a single star surrounded by planets or to a binary star system. This work focused on the realization that the molecular cloud cores that precede star formation can have equilibrium configurations that are nonaxisymmetric (lopsided). An analytical study carried out by the Center reported on the discovery and the properties of a sequence of these unusual egg-shaped equilibrium configurations. The analysis shows that these configurations can collapse in a way that may naturally produce either binary or single stars, depending on the initial degree of distortion.

The theoretical models of the Center have been used to interpret observational data from such NASA facilities as the Infrared Telescope Facility (IRTF), the Infrared Astronomical Observatory (IRAS), the Hubble Space

Telescope (HST), and the Infrared Space Observatory (ISO, a European space telescope with NASA collaboration), as well as from numerous ground-based radio and optical telescopes. In addition, they have been used to determine requirements for future missions such as the Stratospheric Observatory for

Infrared Astronomy (SOFIA) and the Space Infrared Telescope Facility (SIRTF).

Point of Contact: D. Hollenbach
(650) 604-4164
hollenbach@ism.arc.nasa.gov

The Formation and Dynamics of Planetary Systems

Gregory Laughlin

Progress was made in FY00 in numerous areas bearing on the overall problem of the formation and evolution of planetary systems. Specific topics of research have ranged from the earliest stages of star formation through the long-term fate of the Earth, and they are described in four peer-reviewed research papers.

In the present-day solar system, the sun contains 99.9% of the mass, whereas the planets contain the bulk of the system angular momentum. The clouds of gas and dust that collapse to form star-planet systems, however, are essentially in uniform rotation. One of the major unsolved puzzles in the theory of star and planet formation thus involves the detailed mechanism by which mass is transported inward onto the protostar while angular momentum is simultaneously pushed outward. It is believed that spiral gravitational instabilities play a key role in eliciting angular momentum transport, but a full description of how spirals grow and operate on a global scale (that is, throughout the entire protoplanetary disk) is not understood. Considerable theoretical progress was made in this area by performing a stability analysis of idealized singular isothermal disks. This research, carried out and published in collaboration with researchers at the University of California at Berkeley, Arcetri (Italy), and UNAM (Mexico), has clearly explained the role of the corotation

amplifier in allowing spiral waves to grow. This in turn gives us a clearer theoretical picture of the very earliest stages of star and planet formation.

A second line of inquiry has developed a way to constrain the conditions under which our own solar system formed. The outer giant planets in our solar system all have nearly coplanar, circular orbits. This orderly configuration indicates that the sun and the planets have always existed in relative isolation. If another stellar system had passed within several hundred astronomical units of the sun, gravitational perturbations would have scattered the outer planets (particularly Neptune) into highly eccentric, inclined orbits. An extensive set of Monte Carlo star-planet scattering calculations has shown that the solar system likely formed in an aggregate containing fewer than 1500 stars, and thus was not born in a dense stellar cluster (resembling, say, the Trapezium region in Orion). Primitive meteorites, however, contain daughter products of extinct radioactive elements that have half-lives of one million years or less. In order to explain the presence of such short-lived isotopes in meteorites, it has been proposed that either (1) the presolar nebula was enriched by a nearby supernova explosion, or alternately that (2) x-ray flares associated with the nascent sun were able to create radioactive atoms via

processes such as spallation. The new research strongly favors scenario (2), because the presence of a nearby supernova would imply that the sun formed in a very massive aggregate of stars, and this possibility is effectively ruled out by the Monte Carlo calculations.

A third focus of the research effort examined the emerging correlation between high stellar metallicity and the detected presence of an extrasolar planet. Now that more than 70 extrasolar planets have been found, it is possible to evaluate the emergence of statistical trends. An analysis of volume-limited samples of stars in the solar neighborhood demonstrated that stars with metal content >50% higher than solar are 10 times more likely to harbor a

short-period planet than the average star in the solar neighborhood. This finding can be exploited to find extrasolar planets with less effort, thus saving large amounts of time on instruments such as the Keck Telescope. A catalog of 200 highly metal-rich stars was compiled, and within 6 months, 5 planets have been detected in this catalog. Two were found by the Marcy group, two were found by Swiss researchers, and one was found by Ames researchers (HD 20675b, to be confirmed and announced in late 2001).

Point of Contact: G. Laughlin
(650) 604-0125
gpl@acetylene.arc.nasa.gov

Stability of Upsilon Andromedae's Planetary System

Jack J. Lissauer, Eugenio Rivera

The objectives of this project are to study the dynamical properties of planetary systems that are consistent with the observational data on the three-planet system orbiting the nearby main sequence star Upsilon Andromedae. Results show that systems with the planetary masses and orbital parameters that provide the best fit to stellar radial velocity observations made at Lick Observatory through either February 2000 or July 2000 are substantially more stable than systems with the parameters originally announced in April 1999. Simulations using the February 2000 parameters are stable for planetary masses as much as four times as large as the observational lower bounds (which are obtained by assuming that

the solar system lies in the orbital plane of the Upsilon Andromedae planetary system). In relatively stable systems, test particles (which can be thought of as representing asteroids or Earth-like planets that are too small to have been detected to date) can survive for long times between the inner and middle planets as well as several astronomical units or more exterior to the outer planet, but no stable orbits were found between the middle and outer planets.

Point of Contact: J. Lissauer
(650) 604-2293
lissauer@ringside.arc.nasa.gov

The Organic Refractory Material in the Diffuse Interstellar Medium: Mid-Infrared Spectroscopic Constraints

Yvonne J. Pendleton, Louis J. Allamandola

An analysis was made of the 4000- to 1000-cm⁻¹ (2.5- to 10-micron) region of the spectrum of diffuse interstellar medium (DISM) dust compared with the spectra of 13 laboratory-produced chemical candidates that serve as analogs to the interstellar material. Results indicate that the organic refractory material in the DISM is predominantly hydrocarbon in nature, possessing little nitrogen or oxygen, with the carbon distributed between the aromatic and aliphatic forms. Long alkane chains H₃C-(CH₂)_n- with n much greater than 4 or 5 are not major constituents of this material.

Spectral analysis of the DISM allows us to place significant constraints on the likelihood of the proposed materials to be present in it. The spectra of candidate materials are evaluated using four spectral characteristics based on the interstellar data. Comparisons to laboratory analogs indicate that the DISM organic material resembles plasma-processed pure hydrocarbon residues much more so than energetically processed ice residues, which were previously thought to be relevant analogs. This result is consistent with a birth site for the carrier of the 3.4-micron band in the outflow region of evolved carbon stars, rather than in the icy mantles of dense cloud dust.

The organic signatures of extragalactic dust, carbonaceous chondritic material, and *E. coli* bacteria have also been compared because they have been discussed in the literature as relevant to the DISM. The organic material extracted from the Murchison carbonaceous meteorite and the spectrum of *E. coli* bacteria reveals spectral features in the 5–10 micron region that are absent in the DISM. Although the presence of unaltered circumstellar components in the Murchison meteorite has been established through several lines of evidence, it is unclear whether or not the aliphatic component that gives rise to the 3.4-micron band is in that category. With respect to the complete 2–10 micron wavelength region, no spectral evidence exists for a biological origin of the 3.4-micron interstellar absorption band. The similarity of the aliphatic CH stretch region of dust from our own galaxy to that of distant galaxies suggests that the organic component of the interstellar medium is widespread and may be an important universal reservoir of prebiotic organic carbon.

Point of Contact: Y. Pendleton
(650) 604-4391
ypendleton@mail.arc.nasa.gov

Theoretical Predictions of the Opacity of Methane

David Schwenke

The goal of the present work is to predict the infrared (IR) spectrum of methane (CH_4), which is of great interest to many areas in the Space Science Enterprise. These areas include the study of the atmospheres of Jupiter-like planets and the study of brown dwarfs.

The IR spectrum of methane has been studied extensively in the laboratory, but the complexity of the spectrum has severely hampered its study. Only the stronger bands arising from low-lying vibrational levels have been analyzed, and these data are insufficient for Space Science applications.

In principle, most of the problems of experimental studies can be circumvented by theoretical results, but theory must overcome many new problems. The main difficulty lies in obtaining results that are of useful accuracy. Many theoretical studies of the energy levels of CH_4 have been performed, all using a quartic expansion of the potential energy surface (PES). In all cases, the quartic PES parameters were determined either by ab initio electronic structure calculations or by least-square fitting to experimental energy levels.

The present study examined the question as to whether or not a quartic PES is sufficient to predict uncharacterized energy levels. Ab initio electronic structure calculations of an octic PES for CH_4 were made and compared with the results of the PES truncated to a quartic expansion. These calculations advance the state of the art in theoretical spectroscopy in two respects. First, they were the first calculations to compute an octic PES for a molecule containing five atoms. Electronic structure calculations were made at nearly 8000 geometries using a high-level theoretical technique. Second, the vibrational calculations were the first to use an accurate kinetic energy operator.

Thus for the first time it was possible to make predictions of the energy levels of CH_4 with confidence.

The study produced several major conclusions. The quartic representation of the PES only qualitatively represents the octic PES in the low energy regime. As the energy goes up, the quartic expansion can be grossly in error. In addition, the errors in previous theoretical studies based on second-order perturbation treatments of the vibrational energy levels were found to be commensurate with the errors in the quartic PES. Thus it is consistent to use a quartic PES with second-order perturbation theory to estimate low-lying energy levels. However, using the quartic PES with a more accurate determination of the vibrational energy levels is not consistent. In particular, optimizing the quartic PES to match observed energy levels should not yield reliable predictions of uncharacterized energy levels. Finally, the ab initio octic PES produced energy levels that agreed well with all characterized experimental energy levels. Although the present accuracy is not yet sufficient to satisfy the Space Science Enterprise needs, significant progress is quite possible in the near future.

A detailed account of the present work can be found in D. W. Schwenke and H. Partridge, *Spectrochimica Acta*, vol. 57, page 887-895 (2001).

Point of Contact: D. Schwenke
(650) 604-6634
schwenke@pegasus.arc.nasa.gov

Cratering Rates on Synchronously Rotating Satellites

Kevin Zahnle, Paul Schenk

Impact cratering of synchronously rotating satellites is expected to occur faster on the leading hemisphere than on the trailing hemisphere because the orbital velocity of the satellite around the planet is generally large compared to the space velocities of comets and asteroids. The relationship between comets and moons is broadly akin to that between flies and windshields. As it is with cars, the predicted asymmetry is large, with cratering rates at the apex of motion (the center of the leading hemisphere) typically 30–80 times greater than at the antapex. However, the expected asymmetry is at best poorly expressed on actual satellites, with the alarming exception of Triton, where the observed asymmetry is apparently too great. The failure to observe the seemingly inevitable suggests that some of these satellites have led, and may still be leading, interesting lives.

This study used a suite of Monte Carlo simulations to better determine how cratering rates vary across the surfaces of synchronous satellites. The method generates orbits randomly from ancestral distributions that arguably are isotropic, or nearly so; assigns to each orbit an impact probability and a possible impact site and appropriate crater diameter; while also allowing practical treatment of many effects that would be dauntingly difficult to treat analytically. An empirical fit to the suite of numerical experiments is that the cratering rate is

$$\dot{N} \propto \left(1 + \frac{v_{\text{orb}}}{\sqrt{2v_{\text{orb}}^2 + v_{\infty}^2}} \cos \beta \right)^{2.0+0.47\gamma}$$

where v_{orb} refers to the circular orbital velocity of the satellite and v_{∞} refers to the characteristic encounter velocity of the ecliptic comet with the planet; the angle β is the angular

distance measured from the apex of motion; and the parameter γ is the power law exponent describing the assumed cumulative size distribution of the impactors, $N(> d) \propto d^{-\gamma}$, where d is diameter. The expression works well for $1 < \gamma < 4$; real solar-system populations typically have $1.5 < \gamma < 3$.

As noted previously, the predicted cratering asymmetries are not seen, in fact. Most synchronous satellites are effectively saturated with impact craters, for which no signature of a leading/trailing cratering asymmetry is to be expected. The three interesting exceptions are Ganymede and Europa, moons of Jupiter, and Triton, chief moon of Neptune. Europa has few impact craters and no obvious leading/trailing asymmetry. But this is not surprising, because Europa's icy shell is decoupled from the interior by a liquid water ocean: it would be relatively easy for the shell to rotate nonsynchronously. Ganymede is a more interesting case. Careful analysis reveals that Ganymede does preserve a fourfold asymmetry between fore and aft. This asymmetry is much less than the 60-fold asymmetry expected, but it is in the right direction; a possible interpretation is that Ganymede once rotated nonsynchronously but no longer does. This finding in turn implicates a once-thicker liquid water ocean for Ganymede, a conclusion in harmony with other clues that Ganymede was once much more like Europa than it is now.

Finally, Triton revolves in a retrograde orbit around Neptune. It appears to be a captured comet that melted as its orbit tidally evolved from a highly eccentric ellipse to a circle. Triton has very few craters. Its surface is obviously geologically young, probably no older than Europa's. Essentially all its impact craters are on its leading hemisphere. In particular, a lack of craters near $\beta = 90$ degrees

appears to be real, because this region (facing Neptune) was the part of Triton seen best by the Voyager 2 spacecraft. This cratering pattern is too asymmetric to be accounted for by comets or other objects that orbit the sun. Required, rather, are objects in prograde orbit around Neptune. Such objects would strike Triton mostly head-on, and the resulting craters would be confined mostly to the leading hemisphere. The origin of the implied swarm

of prograde, Neptune-orbiting debris is an open question. The alternative explanation is that Triton has been capriciously resurfaced so as to appear, from the one viewpoint of the Voyager 2, as if it had run face-first into a swarm of debris.

Point of Contact: K. Zahnle
(650) 604-0840
kzahnle@mail.arc.nasa.gov

EXOBIOLOGY

A Greenhouse Co-Laboratory

Brad Bebout, Richard Keller

The Ames Microbial Ecology/Biogeochemistry Research Lab, in combination with the ScienceDesk team, has made significant progress in realizing a greenhouse “co-laboratory,” which will be shared by members of the NASA Astrobiology Institute’s Early Microbial Ecosystems Research Group (EMERG). (See figure 1.) The greenhouse facility is being used to maintain and perform manipulations of field-collected microbial mats. Microbial mats, extant representatives of Earth’s earliest ecosystems, are highly dynamic communities of microorganisms that exhibit extremely high rates of metabolic processes. Maintaining the structure and function of these communities outside the natural environment is, therefore, a challenge. Using the greenhouse constructed on the roof of Building N239, mats that resemble naturally occurring communities have been maintained over a year after field collection. In FY00 it was determined that the greenhouse-maintained mats sustain natural rates of biogeochemical processes. This facility, therefore, is useful to support continued measurements of the rates and conditions under which various trace-gases are emitted and/or consumed by microbial mats and

stromatolites. The greenhouse mats will be used to investigate the effects of early Earth environmental conditions on the rates of trace-gas production and consumption in the microbial mats, a period of Earth’s history no longer available to us for direct measurement. These measurements are also relevant to the search for life on extrasolar planets, where the most promising search strategy involves the detection of possibly biogenic gases using infrared spectrometry. Space-based interferometers, such as the Terrestrial Planet Finder, should be able to resolve the spectra of several biologically important trace gases in the atmospheres of extrasolar planets, possibly within 10–15 years.

The greenhouse represents a unique facility and a unique resource to be shared among EMERG team members. The scientific objectives of the team require multiple collaborators to conduct and analyze measurements of mat parameters on a frequent basis over many weeks. However, pragmatics and funding constraints inhibit the productivity of the distributed team and prevent full utilization of the greenhouse. The construction of a

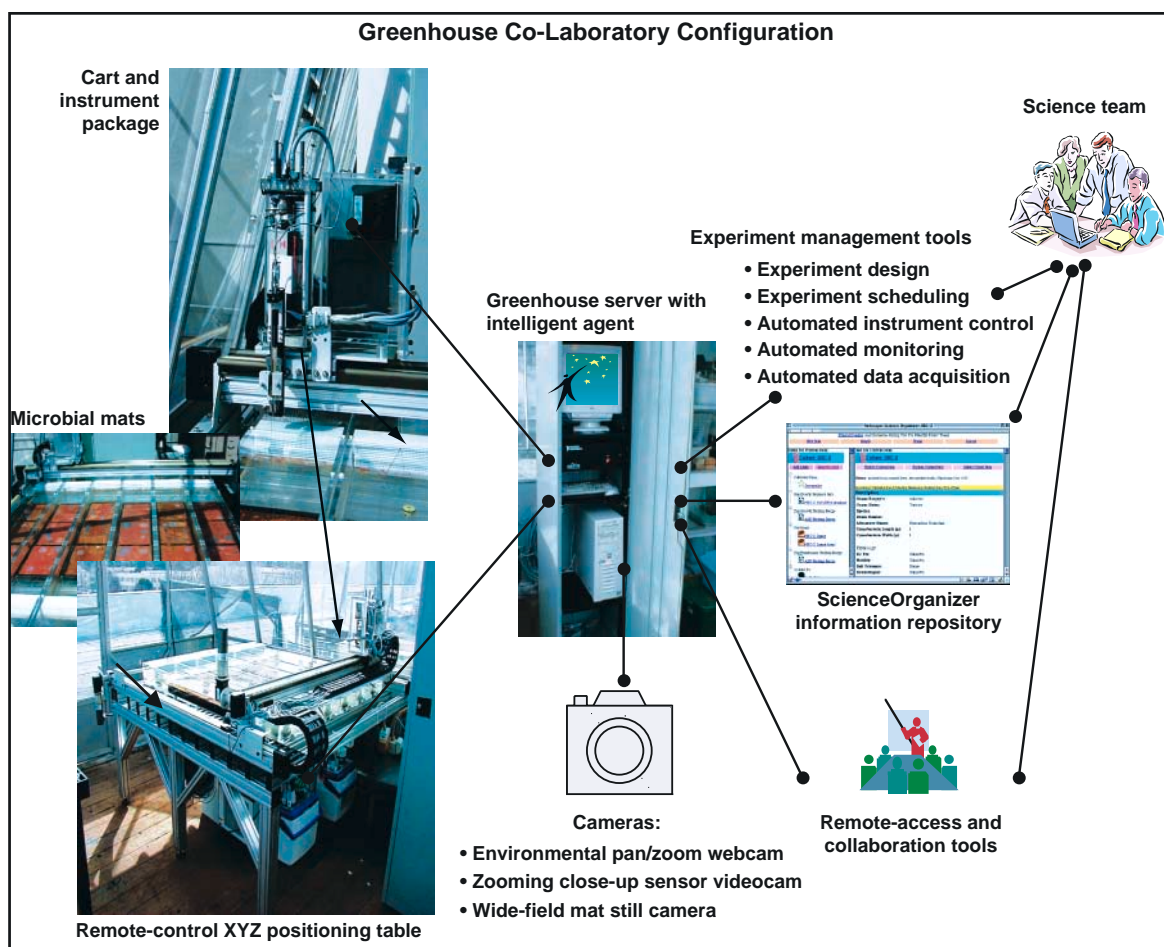


Fig. 1. Diagrammatic representation of the greenhouse co-laboratory with photographs of the hardware already in place.

co-laboratory—in which human scientists and intelligent software agents work together to perform experiments—will alleviate demanding proximity and time requirements that affect productivity. Rather than placing the burden solely on local team members, a co-laboratory will enable an entire distributed investigator team to share responsibility for experimentation and data collection.

This motivation has led to construction of a co-laboratory designed to enable the geographically distributed group of EMERG scientists to plan greenhouse experiments, operate scientific equipment, take experimental measurements, share results, and collaborate in real time with remote colleagues. Intelligent

software agents will assist in the experimentation process, controlling the hardware, recording results, and interacting with the scientists via e-mail. As part of the initial hardware development for the co-laboratory, an X,Y,Z positioning table that is capable of automatically positioning sophisticated instruments at any location in the mats has been constructed. The instrument package currently includes microelectrodes, a light sensor, a chlorophyll fluorometer, a surface-detection device, and a fiber-optic spectrometer. The positioning system and the instrumentation package are viewable over the Internet (<http://greenhouse.arc.nasa.gov>) via a webcam hooked up to a computer located in

the greenhouse. Next implementation steps involve controlling the positioning table and equipment remotely over the Internet.

Point of Contact: B. Bebout
(650) 604-3227
bbebout@mail.arc.nasa.gov

CHEMIN: A Mineralogical Instrument for Mars Exploration

David F. Blake

The identification of the types of rocks on Mars that may harbor evidence of present or past life (that is, biomarkers) will require *in situ* mineralogical analysis. In order to establish the conditions under which a rock formed, the identity of each mineral present and its amount must be determined. In terrestrial laboratories, x-ray diffraction and x-ray fluorescence (XRD/XRF) are the techniques of choice for such characterizations.

Recent progress in x-ray technology allows the consideration of simultaneous x-ray diffraction (XRD: mineralogic analysis) and high-precision x-ray fluorescence (XRF: chemical analysis) in systems scaled down in size and power to the point at which they can be mounted on landers or small robotic rovers. The CHEMIN XRD/XRF instrument, which simultaneously collects XRD and XRF data, has been proposed in the past for a variety of solar-system missions and is presently proposed for three separate Mars scout missions, including a precision lander, a penetrator, and a lander equipped with a drill.

NASA was awarded a patent in 1996 (U.S. Patent No. 5,491,738) for the CHEMIN concept. The instrument received a commercial "R&D 100 award" as one of the top 100 innovative technologies of 1998. A SBIR (Small Business, Innovative Research) phase II proposal has been awarded to Moxtek, Inc. to build and commercialize a laboratory version of CHEMIN.

CHEMIN is a charged-coupled device (CCD)-based simultaneous XRD/XRF instrument. The device is designed to characterize the elemental composition and mineralogy of small fine-grained or powder samples. The name CHEMIN refers to the combined CHEMical and MINeralogic capabilities of the instrument.

Diffraction and fluorescence data are obtained simultaneously by operating the CCD in single-photon counting mode. Energy discrimination is used to distinguish between diffracted primary beam photons and fluorescence photons. Diffraction data are obtained in transmission mode, and resolution is presently sufficient on the prototype instrument to allow application of the Rietveld refinement method to the diffraction data. X-ray fluorescence data will be obtained for all elements, $4 < Z < 92$.

A diagram of the proposed CHEMIN flight instrument is shown in figure 1. In operation, the carousel of the instrument (which is the only moving part) is rotated to place one of 40 collection grids in a position to receive a soil sample or a sample of drill cuttings from a rock. The carousel is then rotated to place the grid in the analysis position between the x-ray source and the CCD. A combination of carousel rotation and 1- to 2-millimeter motion along the x-axis allows the entire substrate to be sampled sequentially by the x-ray beam. An intelligent systems program determines the location of sample material suitable for analysis and supervises data collection.

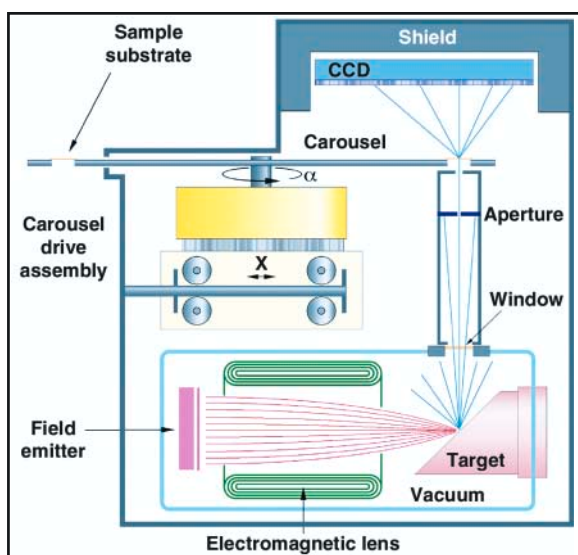


Fig. 1. Cross-sectional diagram of the proposed CHEMIN flight instrument.

A prototype of the CHEMIN instrument has been operable since July 1996. After optimization of the x-ray source collimation, later in 1996, diffraction data of sufficient quality to be used with advanced diffraction data analysis methods such as Rietveld refinement were obtained. Various sample handling systems are presently being pursued, and designs have been proposed for terrestrial use in commercial laboratories, in the International Space Station, and in the proposed Mars Sample Return Handling Facility.

Point of Contact: D. Blake
(650) 604-4816
dblake@mail.arc.nasa.gov

Sugar-Related Compounds in Meteorites

George Cooper, Novelle Kimmich, Josh Sarinana, Katrina Brabham, Laurence Garrel, Warren Belisle

A goal of NASA is to understand the origin and evolution of life. Carbonaceous meteorites provide the only record yet available for the laboratory study of organic compounds that were synthesized very early in the solar system and delivered to the planets. Until now, sugars and related compounds (polyols), one of the most critical classes of compounds necessary for all current life forms, had not been definitively identified in extraterrestrial samples. Ribose and deoxyribose, five-carbon sugars, are central to the role of contemporary nucleic acids, deoxyribonucleic acid (DNA) and ribonucleic acid (RNA). Glycerol, a three-carbon sugar alcohol, is a constituent of all known biological membranes. Part of the scientific research performed at Ames is directed toward determining whether or not such compounds are part of the organic content

of meteorites. This report describes the results of the search for such compounds.

Results are reported from analysis of water extracts of the Murchison and Murray carbonaceous meteorites. The means of identification of compounds was gas chromatography-mass spectrometry (GC-MS). Compounds were prepared for GC-MS as their trimethylsilyl and/or tertiary butyl-dimethylsilyl derivatives. Present analyses of Murchison and Murray extracts show that a variety of polyols are present in carbonaceous meteorites (figure 1). The identified compounds include a sugar, dihydroxy acetone; sugar-alcohols; sugar mono-acids; sugar di-acids; and "deoxy" sugar acids (or "saccharinic" acids). In general, the compounds follow the abiotic synthesis pattern of other meteorite classes of organic compounds: decreasing abundance with increasing

	Sugars	Sugar Alcohols	Sugar Acids	Dicarboxylic Sugar Acids	Deoxy Sugar Acids			
3C	$\begin{array}{c} \text{CH}_2\text{OH} \\ \\ \text{C}=\text{O} \\ \\ \text{CH}_2\text{OH} \end{array}$ Dihydroxyacetone	$\begin{array}{c} \text{CH}_2\text{OH} \\ \\ \text{H}-\text{C}-\text{OH} \\ \\ \text{CH}_2\text{OH} \end{array}$ Glycerol	$\begin{array}{c} \text{CO}_2\text{H} \\ \\ \text{H}-\text{C}-\text{OH} \\ \\ \text{CH}_2\text{OH} \end{array}$ Glyceric acid	—				
4C	— Erythritol & Threitol	$\begin{array}{c} \text{CH}_2\text{OH} \\ \\ \text{H}-\text{C}-\text{OH} \\ \\ \text{H}-\text{C}-\text{OH} \\ \\ \text{CH}_2\text{OH} \end{array}$ Erythritol & Threitol	$\begin{array}{c} \text{CO}_2\text{H} \\ \\ \text{H}-\text{C}-\text{OH} \\ \\ \text{H}-\text{C}-\text{OH} \\ \\ \text{CH}_2\text{OH} \end{array}$ Erythronic & Threonic acid	$\begin{array}{c} \text{CO}_2\text{H} \\ \\ \text{H}-\text{C}-\text{OH} \\ \\ \text{HO}-\text{C}-\text{H} \\ \\ \text{CO}_2\text{H} \end{array}$ Tartaric & Mesotartaric acid	$\begin{array}{c} \text{CO}_2\text{H} \\ \\ \text{H}_3\text{C}-\text{C}-\text{OH} \\ \\ \text{CH}_2\text{OH} \end{array}$ 2-Methyl glyceric acid	$\begin{array}{c} \text{CO}_2\text{H} \\ \\ \text{H}-\text{C}-\text{H} \\ \\ \text{H}-\text{C}-\text{OH} \\ \\ \text{CH}_2\text{OH} \end{array}$ 3, 4 Dihydroxy butyric acid	$\begin{array}{c} \text{CO}_2\text{H} \\ \\ \text{H}-\text{C}-\text{OH} \\ \\ \text{H}-\text{C}-\text{H} \\ \\ \text{CH}_2\text{OH} \end{array}$ 2, 4 Dihydroxy butyric acid	$\begin{array}{c} \text{CO}_2\text{H} \\ \\ \text{H}-\text{C}-\text{OH} \\ \\ \text{H}-\text{C}-\text{OH} \\ \\ \text{CH}_3 \end{array}$ 2, 3 Dihydroxy butyric acid (and diastomer)
5C	— Ribitol + Isomers	$\begin{array}{c} \text{CH}_2\text{OH} \\ \\ \text{H}-\text{C}-\text{OH} \\ \\ \text{H}-\text{C}-\text{OH} \\ \\ \text{H}-\text{C}-\text{OH} \\ \\ \text{CH}_2\text{OH} \end{array}$ Ribitol + Isomers	$\begin{array}{c} \text{CO}_2\text{H} \\ \\ \text{H}-\text{C}-\text{OH} \\ \\ \text{H}-\text{C}-\text{OH} \\ \\ \text{H}-\text{C}-\text{OH} \\ \\ \text{CH}_2\text{OH} \end{array}$ Ribonic acid + Isomers	$\begin{array}{c} \text{CO}_2\text{H} \\ \\ \text{H}-\text{C}-\text{OH} \\ \\ \text{H}-\text{C}-\text{OH} \\ \\ \text{H}-\text{C}-\text{OH} \\ \\ \text{CO}_2\text{H} \end{array}$ 2, 3, 4-Trihydroxy Pentanedioic acid	$\begin{array}{c} \text{CO}_2\text{H} \\ \\ \text{H}-\text{C}-\text{H} \\ \\ \text{H}-\text{C}-\text{OH} \\ \\ \text{H}-\text{C}-\text{OH} \\ \\ \text{CH}_2\text{OH} \end{array}$ 2-Deoxyribonic acid + Isomer			
6C	* Glucitol & Isomers	$\begin{array}{c} \text{CH}_2\text{OH} \\ \\ \text{H}-\text{C}-\text{OH} \\ \\ \text{HO}-\text{C}-\text{OH} \\ \\ \text{H}-\text{C}-\text{OH} \\ \\ \text{H}-\text{C}-\text{OH} \\ \\ \text{CH}_2\text{OH} \end{array}$ Glucitol & Isomers	$\begin{array}{c} \text{CO}_2\text{H} \\ \\ \text{H}-\text{C}-\text{OH} \\ \\ \text{HO}-\text{C}-\text{OH} \\ \\ \text{H}-\text{C}-\text{OH} \\ \\ \text{H}-\text{C}-\text{OH} \\ \\ \text{CH}_2\text{OH} \end{array}$ Gluconic acid & Isomers	$\begin{array}{c} \text{CO}_2\text{H} \\ \\ \text{H}-\text{C}-\text{OH} \\ \\ \text{HO}-\text{C}-\text{H} \\ \\ \text{H}-\text{C}-\text{OH} \\ \\ \text{H}-\text{C}-\text{OH} \\ \\ \text{CO}_2\text{H} \end{array}$ Saccharic acid & Isomers	$\begin{array}{c} \text{CO}_2\text{H} \\ \\ \text{H}-\text{C}-\text{H} \\ \\ \text{H}-\text{C}-\text{OH} \\ \\ \text{H}-\text{C}-\text{OH} \\ \\ \text{H}-\text{C}-\text{OH} \\ \\ \text{CH}_2\text{OH} \end{array}$ 2-Deoxygluconic acid + Isomer			

Fig. 1. Polyols identified in the Murchison and Murray carbonaceous meteorites. Compounds were identified by gas chromatography-mass spectrometry as their trimethylsilyl and/or tertiary butyl-dimethylsilyl derivatives. *6-C sugar monomers were not seen but may be present in bound forms.

carbon number within a class of compounds and many, if not all, possible isomers are present at a given carbon number.

A plausible synthetic origin for at least some of the polyols in Murchison and Murray is the photolysis of interstellar gases on interstellar grains. Another possible origin is the condensation of alkaline aqueous solutions of formaldehyde—which is known to produce polyols. Formaldehyde is a relatively abundant and ubiquitous molecule in interstellar space and comets. Extracts of Murchison and Murray show that the aqueous solution on the parent body(ies) was slightly alkaline. When produced, further chemistry under alkaline and/or oxidation can oxidize sugars to a variety of acids of the type in figure 1.

The fact that a suite of related sugar derivatives and dihydroxyacetones are present in meteorites makes it likely that more sugars were, at one time, also present. Other bodies (comets or asteroids), perhaps in different stages of aqueous alteration or oxidation, may have delivered intact sugars to planets in the early solar system. However, dihydroxyacetone alone is capable of producing larger sugars in aqueous solution. The finding of these compounds in some of the oldest objects in the solar system suggests that polyhydroxylated compounds were, at the very least, available for incorporation into the first living organisms.

Point of Contact: G. Cooper
(650) 604-5968
gcooper@mail.arc.nasa.gov

Effects of Disturbance on Microbial Communities

Ken Cullings

This research addresses the Astrobiology objective regarding ecosystem responses to disturbance. A result of both absolute species numbers in any ecosystem and interactions among members of the community, functional biodiversity plays a pivotal role in the resilience of ecosystems to disturbance and environmental change. Ecosystem reliability can increase when the number of species per functional group increases, thus illustrating the value of functional redundancy or similarity in an ecosystem. On the other hand, gains or losses of species that perform different functions can cause ecosystem processes to be significantly altered. Thus, a controversial aspect of functional diversity is whether species exhibiting similar function are actually redundant, and thus expendable.

This research targets microbes, and a common view is that the potential for redundancy or similarity among microbial species is high. The focus is on one pivotal mutualistic interaction, the ectomycorrhizal (EM) symbiosis, a plant/fungal interaction that controls both carbon and nitrogen cycles in forest ecosystems. This research has two steps: first, to assess changes in the EM community in response to disturbance; and second, to determine if there are functional changes in the ecosystem that result from any changes.

Artificial Defoliation, a manuscript in press at *Oecologia*, describes the first study of the effects of altered carbon available to roots in systems comprising more than a single tree species. Results indicated no significant effect on either EM colonization or species richness. However, the relative abundance of EM of the two tree species shifted from a ratio of approximately 6:1 without treatment (lodgepole EM:spruce EM), to a near 1:1 ratio after

treatment. In addition, EM species composition changed significantly after defoliation. Species of EM fungi associating with both lodgepole pine and Engelmann spruce were affected, indicating that alteration of the photosynthetic capacity of one species can affect mycorrhizal associations of neighboring nondefoliated trees. Finally, although some fungal species may exhibit consistent specificity patterns (for example, *Suillus tomentosus* to *P. contorta*), other fungal species shift host preference in response to the change in source of fixed carbon induced by defoliation.

A study made of the effects of litter addition on a stand of pure lodgepole pine, *P. contorta*, is complete. Molecular analyses indicate that litter addition significantly increases EM infection levels in the topsoil layer, directly adjacent to the added litter. No change is seen with perlite addition. Thus, this response is due solely to nutrient changes imposed by litter. The molecular analyses also indicate that the EM community is altered significantly by litter addition. Species dominant in controls may be lost in response following treatment, and some species increase only in response to litter—not to perlite—further illustrating the role of changes in nutrient status.

Results of molecular analyses of the effects of litter removal on a mixed lodgepole pine/Engelmann spruce (*P. engelmannii*) indicate that litter removal significantly decreased EM fungal species richness, from 3.0 to 1.5 species/core; as expected from previous studies that indicate that increased nitrogen in litter can inhibit EM infection, litter removal induced a significant increase in EM infection, from a mean of 228 EM/core in controls to 326 in treatments; and furthermore, although many basidiomycete fungal species are common to

both treatments and controls, the ratio of basidiomycetes to ascomycetes changed significantly in response to litter removal, from a ratio of 12:1 of basidiomycete to ascomycete EM to a ratio of 3:1.

Together, these results indicate that these disturbances can cause changes in the EM fungal community. Because different species may perform different functions, these results

indicate that it is now necessary to assess changes to pivotal ecosystem functions. Thus, the next step of this study will be to perform assessments of changes in enzyme systems that are responsible for controlling both nitrogen and carbon cycles in forest ecosystems.

Point of Contact: K. Cullings
(650) 604-2773
kcullings@mail.arc.nasa.gov

Structure and Functions of Protocells

Andrew Pohorille, Michael A. Wilson

This research studies the origin of cellular functions, with a long-term objective to explain how protocells performed functions essential for their survival and evolution utilizing only molecules that may have been available in the protobiological milieu. Simple models of several protocellular functions have been developed, and computer simulations have been carried out using molecular dynamics (MD) computer simulations. In MD simulations, Newton's equations of motion are solved for all the atoms in the system under study, providing a complete time history of the system. Properties of interest are computed from the trajectory using classical statistical mechanics.

Probably the first cell-like structures were vesicles—closed, spheroidal assemblies of organic material enclosing an aqueous medium. The walls of vesicles are built of amphiphilic molecules that have water-soluble (hydrophilic) and water-insoluble (hydrophobic) groups at opposite ends. These molecules are arranged in bilayers such that the hydrophilic head groups point toward water and the hydrophobic tails form the interior of the bilayer. In this respect, vesicle walls resemble modern cell membranes. Under proper conditions, vesicles form spontaneously from an

aqueous solution of amphiphiles. Vesicles became the precursors to true cells—protocells—by acquiring the capabilities needed to survive and reproduce. Protocells had to transport ions and organic matter from the environment across their walls, capture and utilize energy, and synthesize the molecules necessary for self-maintenance and growth. The identity of molecules that performed these functions is open to debate. Because most metabolic functions in modern organisms are carried out by proteins, the most parsimonious assumption is that their protobiological precursors were peptides. Their protocellular potential is illuminated by the fact that a wide range of simple, naturally occurring or synthetic peptides can spontaneously insert into membranes and assemble into channels capable of transporting material across cell walls.

The stability of monomers and dimers of a peptide consisting of leucine (L) and serine (S) in a heptad repeat arrangement of (LSLLSL)₃ has been investigated in a membrane-like system consisting of an octane layer between two water layers. Both the transmembrane and parallel, in-plane orientations of the monomer correspond to stable states, with the parallel orientation being more stable. However, conversion between the two requires crossing a

large free energy barrier and a substantial structural rearrangement of the water molecules on both sides of the membrane.

Although a transmembrane dimer was found to be stable, a dimer oriented parallel to the interface was found to be unstable. This finding implies that the predominant state of an equilibrium distribution of peptides is a monomer parallel to the interface. Under the application of an external electric field, the monomers rotate into the transmembrane orientation, where they can aggregate into dimers and tetramers. Experiments in other laboratories have demonstrated that tetramers can function as channels for transporting protons across the membrane.

One goal of this research project is to construct multimeric, transmembrane structures that can function as primitive catalysts. In the present case, the peptide does not possess interactions that are specific enough to maintain a rigid structure that could contain a catalytic site because the transmembrane dimer structure, as shown in the figure, is much less rigid than a coiled-coil structure. It has been observed more generally that transmembrane proteins are not simply “inside-out” analogues of water-soluble proteins. Consequently, specific residues must be modified to achieve the packing that is typical of water-soluble coiled coils.

Point of Contact: A. Pohorille
(650) 604-5759
pohorill@raphael.arc.nasa.gov

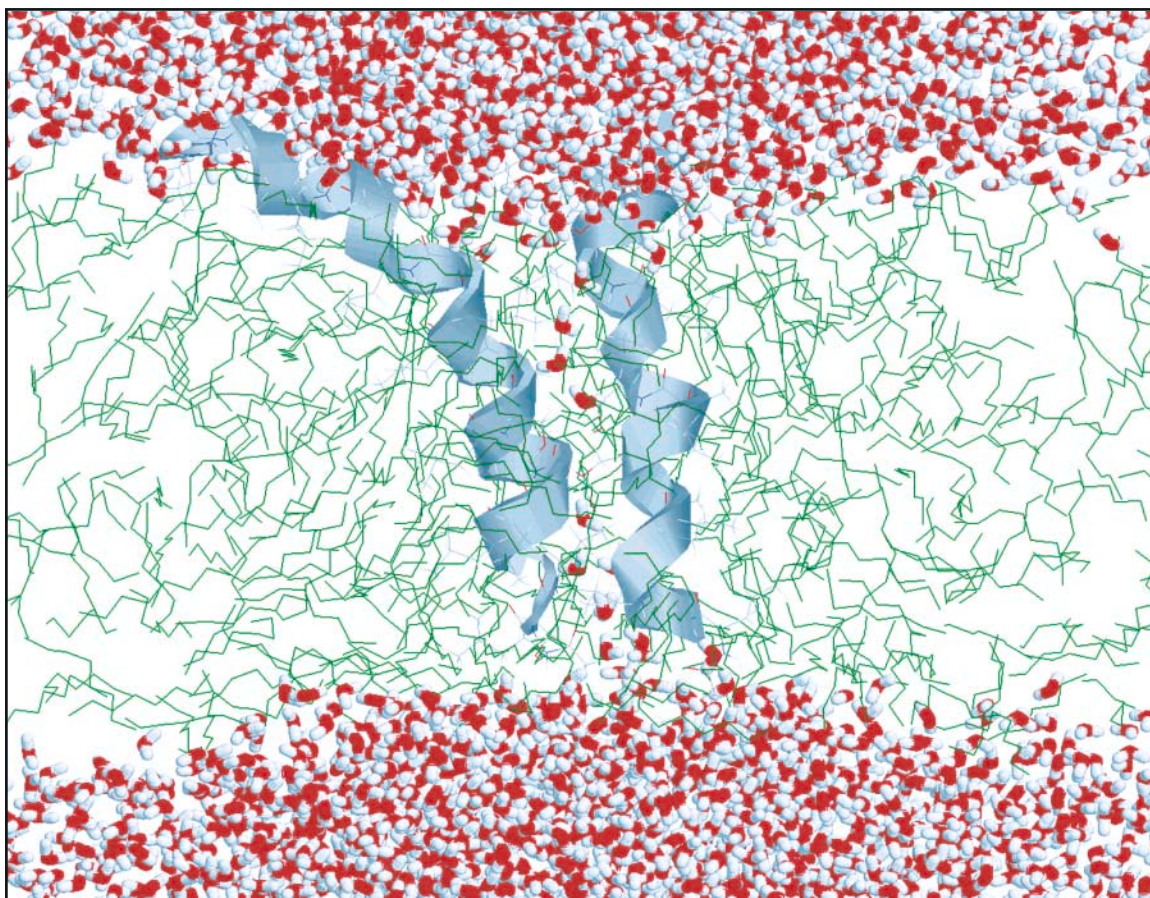


Fig. 1. Transmembrane dimer of (LSLLSL)₃. The peptide molecules are shown as gray helices, the octane is green, and the water is red and white. The disorder is evidenced by the separation of the helices and the significant water penetration into the membrane interior.

Microbial Ecosystem Structure

Lee Prufert-Bebout

The Ames Geobiology and Ecosystem Structure Laboratory is a new facility established in FY00. The research goals of this laboratory are to contribute to our understanding of the spatial distribution of microbes in biofilms, microbial mats, and stromatolites, and to understand how these distribution patterns are recorded in the rock record. Spatial distribution of microbes is of critical importance in facilitating the transfer of gaseous and dissolved compounds between both microorganisms and their environment.

Because microorganisms are motile and can in effect position themselves where conditions are most advantageous, their distribution patterns offer key clues as to how these ecosystems function. The old adage is that “everything is everywhere, but the milieu selects.” Understanding how microbes react to the milieu via their physical distribution is, therefore, key to interpreting modern, ancient, and extraterrestrial microbial ecosystems.

However, most microbial ecology research approaches are not designed to address this issue. Microbes cultivated as single-organism populations in a test tube will not behave in the same manner as those in mixed microbial population assemblages in natural environments. In natural environments, microbial populations experience fluctuations in irradiance, water flow, and chemical environment that are seldom, if ever, seen in a laboratory environment. Monitoring of natural ecosystems offers clues as to how ecosystems function, but the large number of variables operating at any given time prohibit rigorous scientific manipulation and testing. The goal is to bridge this gap by conducting controlled, mixed microbial ecosystem experimentation.

The first series of experiments in the Geobiology and Ecosystem Structure Laboratory has documented that given an initial, homogeneous distribution, within carbonate sediments, four different cyanobacterial isolates will repeatedly segregate themselves with distinctly different distribution patterns. However, the actual distribution patterns observed are a function of speed of water flow, permeability of sediments, availability of nutrients, and irradiance conditions. Hence it is possible to control the degree and pattern of lamination that occurs in these sediments. The cyanobacteria used in these experiments are cultures isolated from modern stromatolites. This approach provides a powerful tool for interpreting the distribution patterns of these cyanobacteria in their natural environment, which to a great extent causes the formation of the laminated fabric of actively lithifying stromatolites. Some of these microbes act as binding agents that hold sediments together, while others are active agents in the precipitation of new mineral components that convert the biological ecosystem into a lithified structure that can be preserved in the rock record. Understanding the controls of formation of these laminated fabrics in modern stromatolites is a first step in improving the interpretation of lamination biosignatures in ancient stromatolites from Earth and potentially laminated rocks from extraterrestrial sources.

Point of Contact: L. Prufert-Bebout
(650) 604-3826
lbebout@mail.arc.nasa.gov

Ringdown Cavity for Isotopic Ratio Measurements of Carbon and Oxygen

Todd Sauke, Joe Becker

Molecular and isotopic spectroscopy in the midinfrared (3–7 micrometer wavelength) has been extremely useful for many quantitative gas-detection applications in fields as diverse as astrobiology, geology, atmospheric science, pollution control, environmental monitoring, and industrial process control. Variations in isotopic ratios of $^{12}\text{C}/^{13}\text{C}$ and $^{16}\text{O}/^{18}\text{O}$ in Martian soil samples could be important clues to the planet's geologic and biologic history. Such variations would be expected to be generated in a sample by any process of elemental transfer whose rate-limiting step is diffusion controlled, including past or present volcanism, freeze/thaw cycles, incorporation of carbon dioxide into the soil from the Martian atmosphere, enzymatic reactions, or respiration. Isotopic variability could also be caused in a sample by its having been mixed with other reservoirs of carbon or oxygen.

The typically strong absorption lines in the midinfrared spectral region allow for sensitive detection without the need for complex, alignment-sensitive, multipass sample absorption cells. The diode laser light sources used for spectroscopy in this spectral region typically require cryogenic cooling, making them difficult, cumbersome, and expensive, and thus limiting their usefulness. On the other hand, in the near-infrared at 1.3- and 1.55-micrometer wavelengths, where inexpensive room-temperature laser sources are readily available, the molecular absorption lines are orders of magnitude weaker than those in the midinfrared, and they can be used only with long-path multipass absorption cells. Typical long-path multipass cells, such as White cells, Harriot cells, etc. are large, cumbersome, and alignment sensitive. The relatively new technique of ringdown cavity spectroscopy affords

another solution to the problem of achieving very long effective absorption path lengths.

Laser spectroscopy offers important advantages over conventional mass spectrometry for measurements on the surface of a planet. Importantly, because of the high spectral resolution of the laser spectrometer, the detailed and complex sample preparation and purification required for reliable mass spectrometry is unnecessary, because contaminant gases do not interfere with the measurement. The goal is to develop a prototype instrument for laser spectroscopic isotope analysis of planetary soils and ices on possible missions to Mars and/or Europa.

This project uses a ringdown cavity to provide the ultra-long effective path length needed for spectroscopy with weak infrared absorption lines, but will achieve high light throughput and high spectral resolution by locking the ringdown cavity to the narrow spectral line-width of a diode laser source.

A near-infrared spectrometer consisting of a 1.6-micrometer near-infrared room-temperature diode laser, an optical isolator, a spatial filter, and a tuned ringdown cavity has been designed and constructed. The spectrometer will ultimately be frequency locked to the continuous-wave laser source, affording both high spectral resolution of isotopic absorption lines and high optical throughput for high-sensitivity measurements.

Point of Contact: T. Sauke
(650) 604-3213
tsauke@mail.arc.nasa.gov

Prebiotic Peptide Synthesis

Arthur L. Weber

About four billion years ago on the primitive Earth, chemical processes yielded molecules that had the ability to make copies of themselves (self-replicate). Over evolutionary time, these replicating molecules developed into the deoxyribonucleic acid (DNA) protein-replicating system of modern life. Although the DNA molecule has a structure that makes it an excellent self-replicating molecule, its structure is too complex to have been synthesized by chemical processes on the early prebiotic Earth. This difficulty with the prebiotic synthesis of DNA has led to a search for simpler replicating molecules. One of the best candidates for a primitive replicating molecule is a small protein, called a peptide. Peptides are considered good candidates because they are constructed from very simple building blocks—activated amino acid molecules—that could have been made by chemical processes on the primitive Earth. To understand the prebiotic processes on the early Earth that could have generated replicating molecules, such as peptides, this study has examined plausible prebiotic chemical processes that have the potential to yield peptides and other replicating molecules from very simple chemical ingredients such as formaldehyde and derived sugars, and analyzed the thermodynamics of carbon chemistry to establish which types of organic reactions are energetically favorable or unfavorable under mild aqueous conditions.

Because earlier studies have indicated the involvement of amino acid and peptide thioesters in prebiotic peptide synthesis, a new, very simple method for preparing peptide

thioesters was developed; this method involves the reaction of a thiol molecule with amino acids activated by reaction with the commercially available reagent (carbonyldiimidazole). This synthetic method was used to prepare peptide thioesters from three and eight amino acids in length for several different amino acids. Chromatographic techniques were developed that allow measurement and purification of the peptide thioesters. This new synthetic method provides an uncomplicated way to generate peptide thioesters for studies of peptide replication.

To identify and understand the chemistry that could have been involved in the origin of the earliest replicating molecule under mild aqueous conditions, the energy values for the chemical changes that occur in carbon groups undergoing redox reactions and carbon-carbon bond cleavage reactions were calculated. Results indicate that the energy of redox reactions involving hydrogen transfer between carbon groups is determined mainly by the type of functional group that donates the hydrogen equivalents, with the energy becoming less favorable in the order: aldehydes, formic acid, alcohols, and hydrocarbons. In addition, results indicate that the cleavage energy of carbon-carbon bonds is determined primarily by the type of functional group that donates the shared electron-pair during cleavage, with the cleavage energy becoming less favorable in the order: carbonyls (ketones, aldehydes), carboxylic acids, alcohols, and hydrocarbons; and that the cleavage energy is more favorable when the shared electron-pair is transferred from a more oxidized to a more reduced carbon group,

except for bonds between a carbonyl group and a carboxylic acid group where the reverse transfer is more favorable. From the energy of each cleavage reaction, the energy of its corresponding synthesis (or reverse) reaction that has an energy equal to the negative of the cleavage energy was estimated. Results indicate that the chemistry of the origin of life and the structure of metabolism are constrained

and limited by the strong dependence of the energy of carbon group transformations on the type of functional group(s) participating in the transformations.

Point of Contact: A. Weber
(650) 604-3226
aweber@mail.arc.nasa.gov



Biological & Physical Research Enterprise

2.5 Meter Diameter Centrifuge

Life Sciences Glovebox

Habitat Holding Rack 1

Service System

Habitat Holding Rack 2

Thermomodule
Water Treatment System
Gas Exchanger
Pump

Filtration System

Aquarium Feeder

Cooling System

Power Supply Unit

UV Lamp

Drive Unit

Sensor Box

Control Unit

Biotelemetry System

Optical Visualization System

Lamp System

Aquarium Package

Supply

Aquarium



tem
Rack 2
ort Unit



quarium

Overview

The mission of the Office of Biological and Physical Research (OBPR) Enterprise is to conduct basic and applied research to support human exploration of space and to take advantage of the space environment as a laboratory for scientific, technological, and commercial research. Ames supports this mission by conducting research and managing spaceflight projects; by operating ground facilities which facilitate applied research; and by developing advanced biomedical technologies. In concert with the OBPR research themes, Ames researchers are involved in cross-disciplinary research programs involving biology, physics, and chemistry, along with engineering and operations support to facilitate both 0-gravity (0-g) and hypergravity (>1-g) implementation of such research.

Ames has also established inter-Center activities with the Johnson and Kennedy Space Centers, to share data in development of their research disciplines in fulfillment of OBPR goals, which include the following:

- Enable Exploration: Conduct research to enable safe and productive human habitation of space;
- Science: Use the space environment as a laboratory to test the fundamental principles of physics, chemistry, and biology;
- Outreach: Use space research opportunities to improve academic achievement and the quality of life on Earth;
- Ground research: Conduct research to enable safe and productive human habitation of space.

Though OBPR funding supports activities in two directorates at Ames, the research reported in this year's report represents only the Astrobiology and Space Directorate.

With the International Space Station (ISS) in operation and discussions of Mars exploration, NASA continues to move toward ever-longer-duration space missions. A safe, habitable environment with assurances of the most efficient means of providing life support is mandatory as we extend human space exploration. Ames researchers have addressed development of a waste-processing incinerator for life support, which incorporates efficient combustors to reduce the combustion fluctuation and achieve cleaner burning. The system will “close the loop” on carbon in the life-support system. Research is presented which addresses the next-generation spaceflight water recovery system—the Vapor Phase Catalytic Ammonia Removal system. This process is significant in achieving 98% recovery and no re-supply requirements for minimally 3 years.

One of the major issues both on the ISS and on other future space missions is the need to reduce re-supply mass and to limit power use. Ames researchers are assessing reduction of the mass of oxygen needed when traveling beyond Earth’s atmosphere by tapping into the recovery of oxygen from the carbon dioxide produced by man during the processes of living. Development of equipment to attain

such goals is described. Power issues are being addressed by creating energy integration techniques for application to life-support problems. For example, what are the potential savings in energy and cooling in creating balance models?

Engineering, science, and operations elements are joining forces at Ames to develop a virtual glove box (VGX). The VGX can be used on the ground and in microgravity to facilitate crew training and maximize the efficiency of glove-box experiment planning, operations, training, and troubleshooting for the International Space Station.

From our experiences with both human and nonhuman animal models over the last 40 years, we know that space travel induces bone and muscle loss. What associated facts are we learning? Through use of salt-sensitive and salt-resistive rat models, Ames researchers are studying the correlation of calcium and sodium levels in the body and the resultant potential osteoporosis conditions. Other studies with humans are providing insight into the relationship between age, activity levels (runners vs. nonrunners), and bone density.

Dietary Salt Sensitivity and Bone in a Spaceflight Model

Sara B. Arnaud

It is well known that the amount of salt in the diet affects blood pressure. Eight to thirty percent of patients who develop hypertension can be described as “salt-sensitive” because they manifest high blood pressure when consuming salt-rich diets. High salt diets affect not only the cardiovascular system but are also thought to worsen osteoporosis unless the amount of calcium in the diet is also relatively high. This is because there is an obligatory excretion of calcium in amounts proportional to the amount of sodium in the diet. Using a rat model for human hypertension (the Dahl salt-sensitive and salt-resistant strains), Dr. Thierry-Palmer from the Morehouse School of Medicine has found no differences in the amount of calcium excreted in the urine that seemed to relate to the level of dietary salt, but has found some differences in vitamin D metabolism magnified by the level of dietary salt. Vitamin D is a component of the calcium endocrine system that functions to facilitate the transport of calcium in and out of the kidney, intestine, and bone. In the absence of differences in the renal handling of calcium, we collaborated to explore the possibility that the vitamin D abnormalities might be connected to some differences in bone.

Static and dynamic studies were made of the femurs in Dahl salt-sensitive and salt-resistant rats. The static studies involved measurements of mineral content and strength in the bones of animals fed normal amounts of dietary salt (0.4%). No differences were found in the mineral content or strength of bones from salt-

sensitive or salt-resistant male or female juvenile rats. The dynamic studies used the same measurements to evaluate the responses of bone to a spaceflight model in female rats fed high or low levels of dietary salt. Females were studied because the vitamin D differences were found in females only. Salt-sensitive rats tended to grow more rapidly than salt-resistant animals and weighed more than the resistant species. Given that bone mineral content of weight-bearing bones is related to body weight, the values in the salt-sensitive animals tended to be higher than in the salt-resistant animals. This additional mineral in the larger rats did not influence the response to skeletal unloading. Unloaded femurs showed 9% decreases in sensitive and 10% decreases in the resistant forms. The responses in femoral strength are illustrated in figure 1 on the next page. It shows the results of torsion testing of femurs with an instrument developed by T. Cleek and R. Whalen. Torque, Newton-meters squared (Nm^2), was consistently less in the femurs unloaded for 4 weeks than in the femurs bearing normal body weight. There were no observable differences between the salt-sensitive and salt-resistant juveniles. We plan to continue these observations in mature females. For the present we have been unable to connect the differences in vitamin D metabolism with a specific bone response in male or female juveniles of the species.

Point of Contact: S. Arnaud
(650) 604-6561
sarnaud@mail.arc.nasa.gov

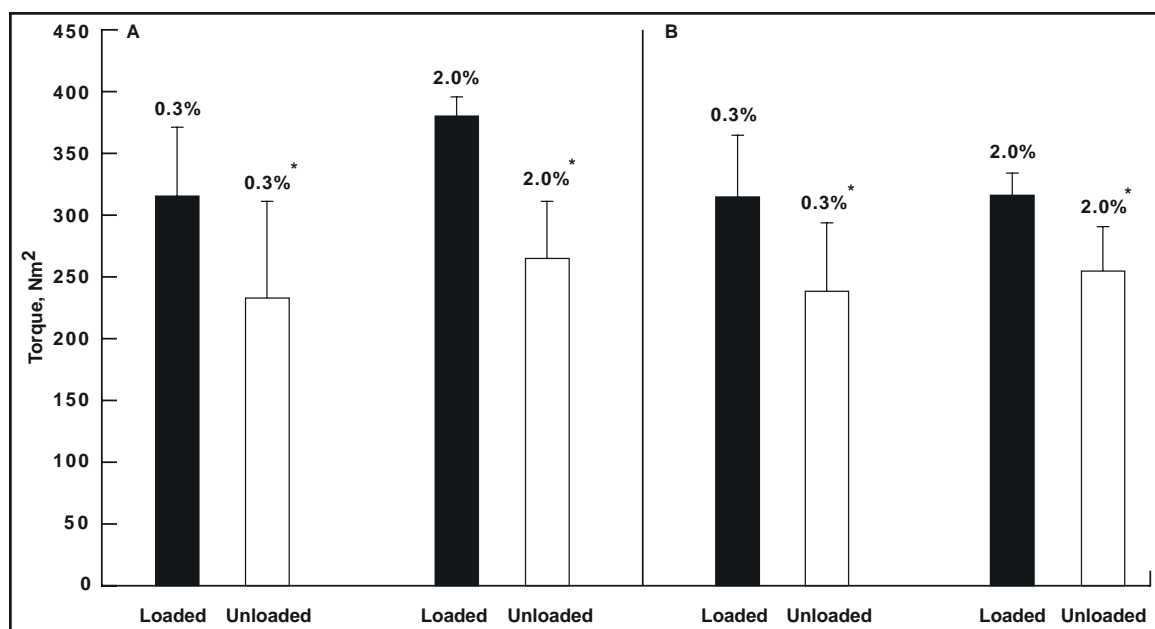


Fig. 1. The results of torsion testing of the left femur after either 4 weeks of ambulation or 4 weeks of unloading in a spaceflight simulation model in rats fed either 0.3% (low) or 2% (high) levels of dietary salt. Panel A shows the results in the Dahl salt-sensitive rats with body weights averaging 238 grams (gr), and panel B shows the results in Dahl salt-resistant rats with body weights averaging 200 grams. The asterisk indicates statistically significant differences at $p < 0.05$. There do not appear to be differences in the response of femurs of salt-sensitive and salt-resistant rats to unloading.

Effect of Age and Activity Level on Bone Mass and Distribution

Tammy Cleek, Robert Whalen

The objective of this study was to gain a better understanding of the relationship between age, activity level (as indicated by runners and non-runners), and site specific bone mass and long bone structural parameters related to long bone cross-sectional geometry. We hypothesized that bone mass measurements and long bone structural properties would be decreased with age but would be enhanced by a higher activity level.

Currently, the most widely used and accepted method of noninvasive skeletal assessment is dual energy x-ray absorptiometry (DXA) which measures regional and whole body changes in bone mineral content (BMC) and areal bone mineral density (BMD). However,

whole bone stiffness and strength are not solely dependent on bone mass, but also upon its cross-sectional shape and distribution.

Bone densitometry has been previously used to obtain cross-sectional properties of bone in a single scan plane. In a new approach using three noncoplanar scans, this technique was extended to obtain the principal moments of inertia and orientations of the principal axes of each scan cross-section. This method has been validated using aluminum phantoms and cadaveric long bones. The method was used in this study to investigate structural properties in the long bones of the lower limb as a function of age and activity level in women.

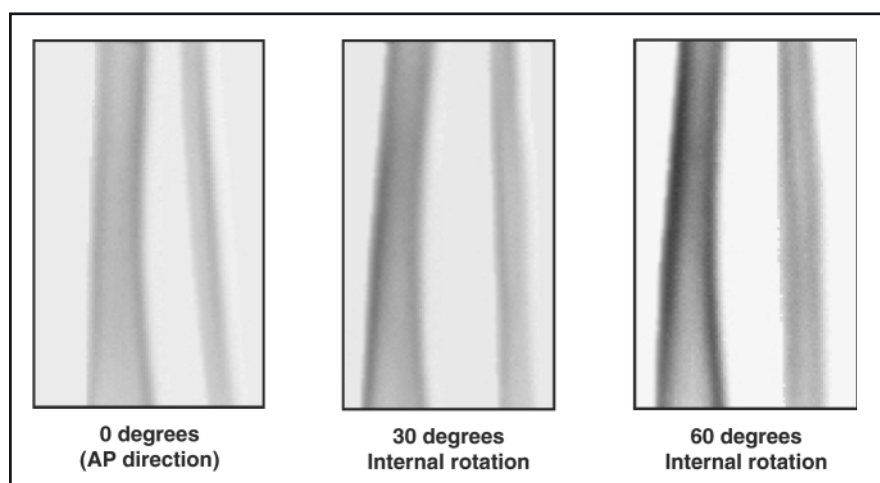


Fig. 1. Typical scan images of the lower leg at three different angular orientations.

Twenty-six women were studied using the Hologic QDR-1000/W DXA bone densitometer. The women were recruited in two age groups, 25-35 (Y, $n = 14$) and 60+ (E, $n = 12$). Within the age groups were runners, considered high loaders (HL), and nonrunners, considered low loaders (LL). Three non-coplanar scans were taken of the middle third of the lower right leg of each subject. Between each scan, the right leg was rotated internally 30 degrees to obtain a different axial view of the same region of the lower leg. The first figure shows the resulting three bone images. Notice that in each of the three images the tibia and fibula are visibly separated. Thus, it is possible to process the bones independently.

Cross-sectional area (A), principal moments of inertia (Imax, Imin), and polar moment of inertia (J) were determined at each scan line for the tibia and fibula along the middle third of the lower leg. Tibia and fibula principal moments for one of the subjects is shown in Figure 2.

Bone mass is reflected by A, while Imax, Imin and J also account for bone mass distribution. Measurements were scaled by appropriate parameters to account for subject body size differences. Area was divided by normalized body weight (BW/BW_{mean}), and Imax, Imin and J were divided by normalized body weight

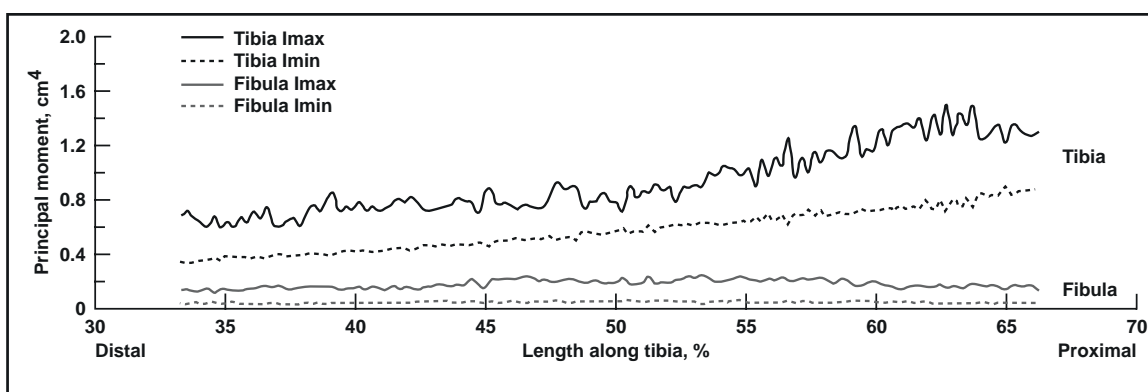


Fig. 2. Typical principal moment data for the tibial and fibular midshaft in a YLL subject.

(BW/BW_{mean}) and tibia length (l/l_{mean}), according to the axial force or moment generated about the tibial midshaft by the ground reaction force. Scaled values were averaged over the entire middle third section for each subject, and group means were calculated and are reported in the table.

In the tibia, the mean A*, I_{max}* and J* values were significantly higher in runners for both age groups. There was no dependence on age for any of the measurements. Interestingly, the

fibula did not show corresponding changes. We postulate that high loads associated with running lead to increased bone structural parameters to support axial loads (A), bending (I_{max}), and torsion (J) in the tibia.

Point of Contact: T. Cleek/R. Whalen
(650) 604-0519/3280
tcleek@mail.arc.nasa.gov
rwhalen@mail.arc.nasa.gov

TABLE 1. MEAN VALUES FOR TIBIA AND FIBULA

Tibia						Fibula			
Group	n	A* (cm ²)	I _{max} *(cm ⁴)	I _{min} *(cm ⁴)	J* (cm ⁴)	A* (cm ²)	I _{max} *(cm ⁴)	I _{min} *(cm ⁴)	J* (cm ⁴)
EHL	5	^a 2.548	^a 1.764	0.763	^a 2.527	0.528	0.129	0.031	0.160
ELL	7	1.991	1.094	0.594	1.688	0.492	0.101	0.028	0.129
YHL	5	^a 2.556	^a 1.549	0.748	^a 2.297	0.550	0.117	0.023	0.140
YLL	9	2.004	1.113	0.593	1.706	0.523	0.135	0.026	0.163

*Indicates scaled values; ^aP < 0.05.

BIOASTRONAUTICS RESEARCH

NASA Virtual GloveboX (VGX):Advanced Astronaut Training and Simulation System for the International Space Station

Jeffrey D. Smith, Richard Boyle

In the coming years, the International Space Station (ISS) will provide a permanent micro-gravity laboratory for biological research in space. From this orbital laboratory, astronaut crews will carry out complex life science experiments designed to answer long-standing questions concerning life’s ability to adapt and respond to the space environment. Many of these experiments will require the use of the Life Sciences Glovebox (LSG). Within the LSG, astronauts must manipulate scientific

instruments, perform experimental assays, collect tissue specimens and record biological data—all under highly controlled conditions and within strict time constraints. These experiments often demand extensive training and knowledge of instrumentation, anatomy, and specific scientific objectives. Furthermore, astronauts must remain highly proficient but, due to scheduling constraints, they can receive only limited Earth-based training with LSG mock-ups and real experiment specimens.

Also, the Earth-based training that astronauts receive may occur months prior to the mission, and they can never fully practice these procedures under microgravity conditions. These difficulties place very high demands on astronaut crews and also a very high level of risk on LSG experiment success.

The NASA Virtual GloveboX (VGX), being developed at Ames Research Center, combines state-of-the-art software and technology to provide astronauts and support crews with a realistic simulation environment for performing biological research in space. The VGX, shown in the first figure, is modeled after the Life Sciences Glovebox, making it fast and easy to plan experiments, develop procedures, and train and troubleshoot various experimental scenarios that astronauts may encounter when aboard the ISS. The VGX integrates off-the-shelf hardware with new real-time simulation technologies to make this realistic training and simulation tool possible. Two ultra-high resolution projectors run in synchronization with stereo glasses to produce a detailed three-dimensional scene within the glovebox work area, as shown in the second figure. Astronauts or technicians use a variety of three-dimensional tracking and/or force feedback devices to interact with computer-generated objects in the virtual environment. Moving experimental equipment in and out of the work area can be done at the click of a button; or, in a simulated experiment, the operator may be required to unlock door latches and open compartments to move equipment or experimental specimens in and out. Using the VGX, experiment developers can determine the optimal layout of experimental equipment, and quickly refine protocols by simulating experiments many times without the need for repeated set-up and break-down. Once procedures have been developed, astronauts can use the VGX as a training tool to practice a variety of tasks quickly and easily. They may also use it

to train on off-nominal situations and to refresh themselves on critical experimental procedures when time is short or when other training facilities are unavailable.

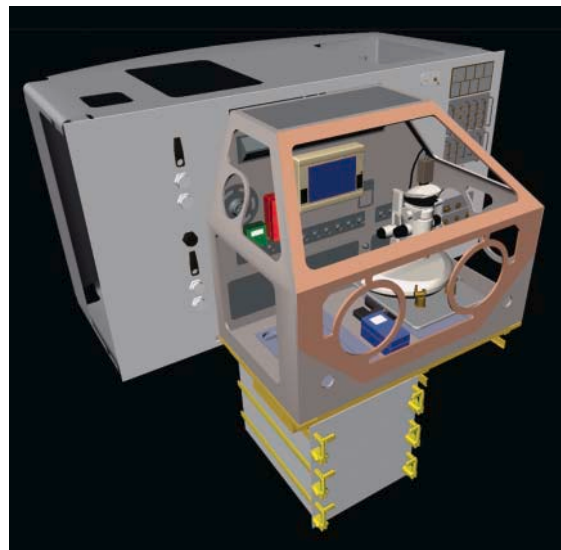


Fig. 1. The NASA Virtual GloveboX (VGX) combines virtual environment technologies and simulation engines to produce a realistic engineering experiment development and astronaut training tool for biological research in space. The VGX is shown here deployed from the Life Sciences Glovebox rack with an animal habitat attached below. A microscope and experimental equipment are placed inside the glovebox work area.

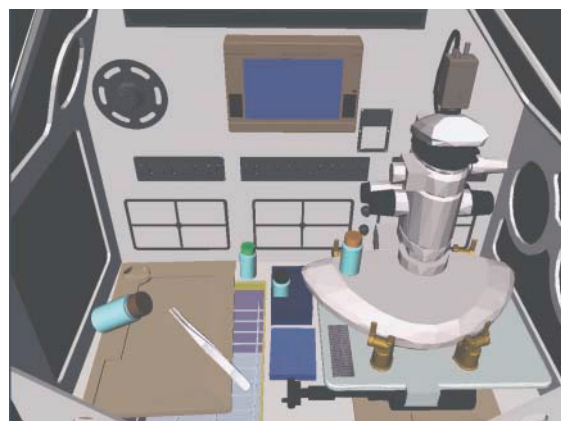


Fig. 2. Experiment development and simulation within the glovebox allows for manipulation of high-resolution models of actual equipment and supplies that will be used for biological research in space. A stereo microscope with CCD camera attached and several vials, tweezers, and a pad of gauze are shown in this depiction. The door to the animal habitat attached below the glovebox is pushed aside to reveal a portion of the habitat cage.

The VGX will maximize the efficiency of glovebox experiment planning, operations, training, and trouble-shooting for astronauts and support crews, thus greatly reducing the risks associated with Space Station glovebox experiment success. With the realistic simulation environment of the VGX, gravity can be turned on and off, allowing astronauts to practice experiments in a simulated real-time microgravity environment while still on Earth. This represents a significant advancement over current training methods which must be developed and practiced entirely on Earth under its constant unit gravity acceleration.

In a continuing effort to improve the VGX, many new advances in virtual environment computing and technologies are also being developed which push NASA to the forefront in real-time visual/haptic simulation and computing research. The resulting VGX simulation system helps solve NASA's

glovebox development and training requirements, but at the same time, it provides a generalized simulation engine for any immersive environment application, such as biomedical/surgical procedures for interactive scientific or engineering applications. For NASA, the Virtual Glovebox can not eliminate the need for training on LSG mock-ups using real experiment equipment and real biological specimens; however, the VGX streamlines these processes and provides astronauts with a means to keep their skills sharp both on Earth and in space. With better ways to engineer, develop, and train for the many complex life science experiments that astronauts will perform onboard the ISS, Ames Research Center is paving the way to successful biological research in space.

Point of Contact: Jeffrey Smith
(650) 604-2586
jdsmith@mail.arc.nasa.gov

ADVANCED LIFE SUPPORT

Advanced Life Support Power Reduction

Cory K. Finn

This research involves modeling of the power and energy usage of regenerative life support systems suitable for exploring the Moon and Mars. System energy integration and energy reuse techniques are being investigated, along with advanced control methods for efficient distribution of power and thermal resources. The high power requirements associated with food production and overall closed regenerative system operation remain a critical technological challenge. Optimization of individual processors alone will not be sufficient to produce an optimized system; system studies must be used in order to improve the overall efficiency of life support systems.

Designs are being developed that match sources of waste heat—crop lighting and solid waste processing systems—with processes that can use this waste heat—water processing, food processing, food preparation, and heating water for showers, for washing dishes, and for washing clothes. Using energy integration techniques, optimal system heat exchange designs are being developed by matching hot and cold streams according to specific design principles. For various designs, the potential savings for power, heating and cooling are being identified and quantified, and estimates are being made of the emplaced mass needed for energy exchange equipment.

Advanced control system designs are also being developed that allow for more efficient distribution of resources, such as system cooling water or electrical power in order to reduce system power requirements. More efficient energy usage can be achieved by allocating power and thermal resources in a dynamic fashion. Advanced control techniques, such as market-based control, can be used in order to smooth out system thermal and power loads. Reductions in peak loading will lead to lower overall requirements. The controller dynamically adjusts the use of system resources by the various subsystems and components in order to achieve the overall system goals. A typical system goal would be the smoothing of power usage and/or heat rejection profiles, while maintaining adequate reserves of food, water, oxygen, etc., and not allowing excessive build-up of waste materials. Initially, computer simulation models are being used to test various control system designs. The most promising of these will be tested using a laboratory-scale, life-support-system testbed at Ames Research Center.

Energy balance models are being developed to support both the energy integration and the dynamic resource allocation work. These models leverage off of existing mass flow models of regenerative life support systems developed at Ames. The heat exchange designs and control schemes developed as part of this NRA research will be provided to Johnson Space Center for use in the development of the ALS Systems Integrated Test Bed (also known as BIO-Plex) and in the design of flight hardware for Moon or Mars missions.

Currently, energy integration techniques are being applied to the life support problem. Several potential designs that would be suitable for various Mars missions have been selected for application of the energy integration analysis. Life support data have been collected, and an optimized heat exchange design has been developed for each scenario. For each design, the potential savings in energy and cooling have been estimated.

In addition to the energy integration work, advanced control system designs are being developed that allow for more efficient distribution of electrical power. A dynamic model of the BIO-Plex air loop has been created and serves as a platform for the development of active power management strategies. Several resource allocation objectives have been defined and tested. One objective that was considered was to reallocate power as needed to the various life support processors to eliminate surges in power usage over time; however, the reallocation of power was subject to constraints. For example, material storage levels needed to be maintained, as well as atmospheric conditions within the life support chambers. This power management system has been demonstrated using the simulation model, and has performed reasonably well. A second objective that has been and continues to be investigated is to smooth the demand for power throughout the system over time.

Point of Contact: C. Finn
(650) 604-1027
cfinn@mail.arc.nasa.gov

Solid-State Compressor for Space Station Oxygen Recovery

John Finn

At present, the life support system on the International Space Station *Alpha* vents overboard the carbon dioxide (CO_2) produced by the crew members. Recovering the oxygen contained in the CO_2 has the potential to reduce resupply mass by 2000 pounds per year or more, a significant weight that could be used for experimental payloads and other valuable items. The technologies used to remove CO_2 from the air and to recover O_2 from CO_2 are flight-ready; however, the interface between the devices is a problem for the Space Station system. Ames Research Center has developed a new technology that solves the interface issue, possibly allowing closure of the oxygen loop in a spacecraft for the first time.

The relevant part of the air revitalization system is shown in figure 1. CO_2 produced by the crew is removed in the Carbon Dioxide Removal Assembly (CDRA). This device effectively produces a pure CO_2 stream, but at a very low pressure. Elsewhere, the oxygen generation system which makes O_2 by electrolyzing water produces a hydrogen stream. In principle the CO_2 and H_2 can react to form methane and water over a suitable catalyst. Water produced in this methane-formation reactor can be returned to the water

electrolyzer, where the O_2 can be returned to the cabin; however, the methane-formation reactor requires CO_2 at a much higher pressure than that produced by the CDRA. Furthermore, the CO_2 and H_2 are often not available at the same time, due to power management and scheduling on the space station. In order to get the CO_2 to the reactor at the right pressure and at the right time, a device or assembly that functions as a vacuum pump, compressor, and storage tank is required.

One solution to this problem is to use a mechanical vacuum pump/compressor combined with a high-pressure buffer tank. However, this has implementation problems: (1) the rapidly moving parts of a mechanical compressor wear out relatively quickly, requiring frequent maintenance or replacement; (2) the mechanical compressor can add noise and vibration to the sensitive station environment, unless large amounts of insulating material are provided; (3) there is so little space available for the buffer tank that the compression ratio would have to be quite high; and (4) the power required to compress the CO_2 to high pressure is considered very high for the power-limited Space Station.

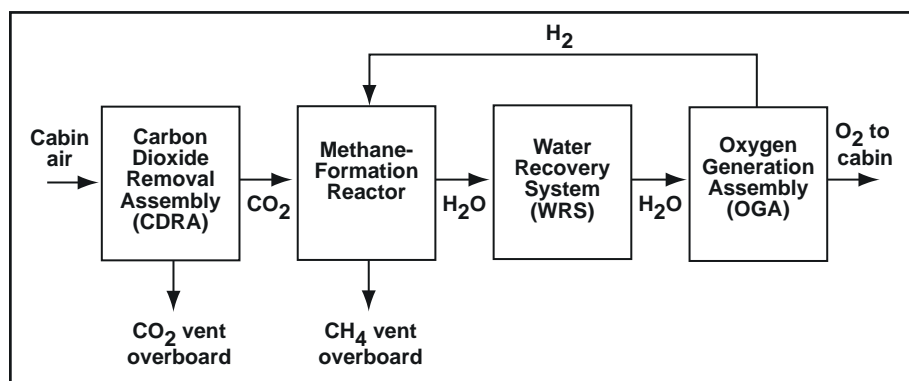


Fig. 1. Carbon dioxide removal, carbon dioxide reduction, and oxygen generation planned for the International Space Station (methane-formation is not yet implemented). The compressor would be placed between the carbon dioxide removal and methane-formation reactor assemblies.

The solution being developed by Ames engineers uses a technique that was originally developed for compressing the very low-pressure Mars atmosphere so that it could be used in an in situ propellant production plant. The compressor uses a temperature-swing adsorption cycle and has no rapidly moving parts. Low-pressure CO₂ from the CDRA is adsorbed in a cool cylinder containing a sorbent material that has a high capacity for CO₂. In this step, the device acts like a vacuum pump. Next, the cylinder stays in a standby mode until the CO₂ is required; that is, the device acts like a storage tank. Finally, the cylinder is heated and the CO₂ is driven off the sorbent, producing CO₂ at a high pressure. The compressed CO₂ flows into the methane-formation reactor. Coolant from the Space Station's thermal control system cools the cylinder back to its initial state, and the process is repeated. Several such cylinders are combined in the device. They operate out of phase from each other, so that there is always a "vacuum pump" and a "compressor" available whenever they are needed by the processors on either side.

A single-bed prototype solid-state compressor was built at Ames and successfully tested with a high-fidelity CDRA at Marshall Space Flight Center in FY00 (figure 2). The temperature-swing adsorption compressor uses less power than the mechanical compressor system and has fewer parts. Its lifetime is estimated at ten years. It is free of vibration and noise, and is also smaller and lighter than its counterpart.

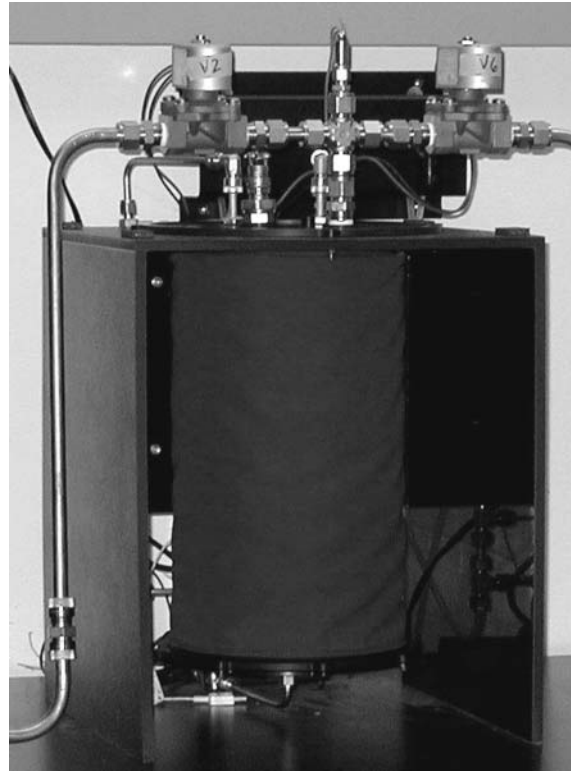


Fig. 2. Single-bed prototype of an Ames solid-state compressor.

Point of Contact: J. E. Finn
(650) 604-1028
jfinn@mail.arc.nasa.gov

Development of a Waste Processing Incinerator for Life Support

John W. Fisher

As space missions become longer, waste treatment on a spacecraft transitions from storage to reclamation of items such as activated carbon and carbon dioxide (CO₂). Activated carbon and CO₂ can be reclaimed from hydrocarbon wastes such as paper, food scraps, and inedible plant biomass. Inedible plant biomass is produced when plants are grown in space to produce food. Growing plants consume CO₂, and burning the inedible parts of a plant produces CO₂ that can be used to grow more plants. Unfortunately the process of burning (combustion) produces some toxic byproducts. One of the objectives of Ames' research on waste processing is to develop technology to burn waste and reclaim CO₂ without releasing toxic materials into the spacecraft.

The combustion process generally does well at completely oxidizing biomass to CO₂ and water. This is obvious from observation of the results of a typical wood fire—only a small residue of inorganic substances, ash, is left in a fireplace after burning wood. The process of combustion of biomass in an incinerator operates in a similar way; the biomass is converted to gaseous products and inorganic ash. Combustion in a fireplace, however, typically takes place with wide fluctuations in temperature and composition as a function of time and position in the burning zone. Efficient combustors reduce the combustion fluctuation and achieve cleaner burning.

Fluidized combustion is a technology that provides good control of the combustion process and minimizes contaminants due to incomplete combustion. A fluidized bed consists of a bed of solid particles such as sand that behaves as a fluid. The fluidization occurs

because a gas such as air is blowing up through the bed and causing the particles of the bed to float. Because sand is much denser than air, the bed holds much more heat energy than an equivalent amount of air. The heat energy held by the bed buffers the combustion process against the wide fluctuations in temperature that cause incomplete combustion.

Even in the best of combustors, however, some unoxidized material remains. In addition, some contaminants such as nitrogen and sulfur oxides are necessarily formed. In recent years, the research at Ames has focused on means to eliminate these byproducts. One approach has been to use reductive catalytic systems to convert the nitrogen and sulfur oxides to nitrogen and elemental sulfur—innocuous materials at room temperature. Oxidative catalysts can then oxidize the remaining hydrocarbon contaminants to very low levels.

In collaboration with university and corporate organizations, Ames has developed and tested an integrated incineration system that utilizes a fluidized bed combustor followed by a catalytic cleanup system. This system has demonstrated the ability to burn inedible biomass and produce a very clean CO₂ product. The concentration of contaminants in the gas exiting the incinerator is generally less than a few parts per million. Except for the CO₂ itself (toxic to humans at high concentrations), the exit stream from the incinerator will be able to meet the Space Maximum Allowable Contaminant (SMAC) standards for clean air in a spacecraft.

When this system has been optimized for reliability and energy efficiency, it will be ready for testing in an advanced life support system that “closes the loop” on carbon.

Carbon will travel in the system from plant to person to incinerator and back to the plant without ever becoming a stored waste.

Point of Contact: J. Fisher
(650) 604-4440
jfisher@mail.arc.nasa.gov

Development of the Vapor Phase Catalytic Ammonia Removal Process

Michael Flynn, Bruce Borchers

The Vapor Phase Catalytic Ammonia Removal (VPCAR) system technology represents the next generation in spaceflight water recovery systems. Water is the single largest resupply requirement associated with human space flight, accounting for 87% by mass of an astronaut's daily metabolic requirement. The VPCAR system achieves a mass metric almost an order of magnitude better than the current state-of-the-art water processors. (Mass metric is a technique used to compare candidate technologies by reducing all performance parameters into a single equivalent launch mass metric.) Incorporating the VPCAR technology into human space flight missions could potentially save hundreds of millions of dollars in resupply costs, depending on the specific mission scenario. As a result, a human-rated version of the VPCAR technology has been authorized for development.

The human-rated system is being developed under contract to Water Reuse Technology (NAS2-00089). This is an external contract for the development and testing of the next generation VPCAR technology. We are currently about 1/2 way through a two-year contracted development program. This activity is funded

through Advanced Life Support program funds and a NASA peer reviewed NRA (00-HEDS-01).

Process Description. The VPCAR process is a two-step distillation-based water processor. The current configuration of the technology is shown in Figure 1. A process flow diagram is



Fig. 1. Vapor Phase Catalytic Ammonia Removal (VPCAR) water recycling system.

provided in Figure 2. The VPCAR process is characterized by the use of a wiped-film rotating-disk vacuum evaporator to volatilize water, small molecular weight organics, and ammonia. This vapor stream is then oxidized in a vapor phase catalytic reactor to destroy any contaminants. The VPCAR process uses two catalytic beds to oxidize contaminants and decompose any nitrous oxide (N_2O) produced in the first bed. The first catalytic bed oxidizes organics to carbon dioxide and water, and ammonia to N_2O and water. This oxidation reactor contains 1% platinum on alumina pellets and operates at about 523 K. The second catalytic bed reduces the N_2O to nitrogen and oxygen. This reduction catalyst contains 0.5% ruthenium on alumina pellets and operates at about 723 K. The reactor and distillation functions occur in a single modular

process step. The process achieves between 97-98% water recovery and has no scheduled maintenance or resupply requirements for a minimum of three years.

The VPCAR activity is significant in that it represents the development of the next generation of life support water recovery technology. Ames Research Center's involvement has spanned from the first principle definition to the model development, bench-scale and lab-scale prototype development, and most recently, contract management of the development of a human-rated version of the technology for evaluation for spaceflight application.

Point of Contact: M. Flynn
(650) 604-1163
mflynn@mail.arc.nasa.gov

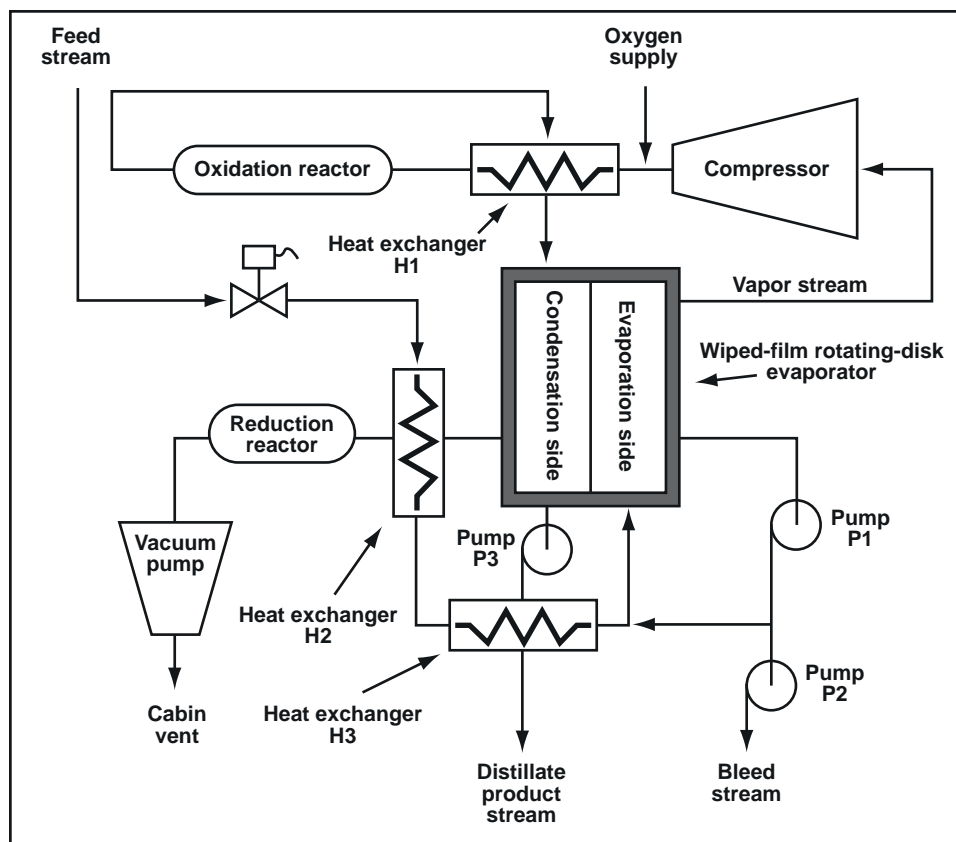
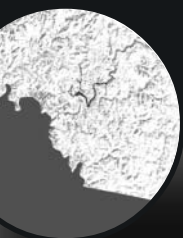
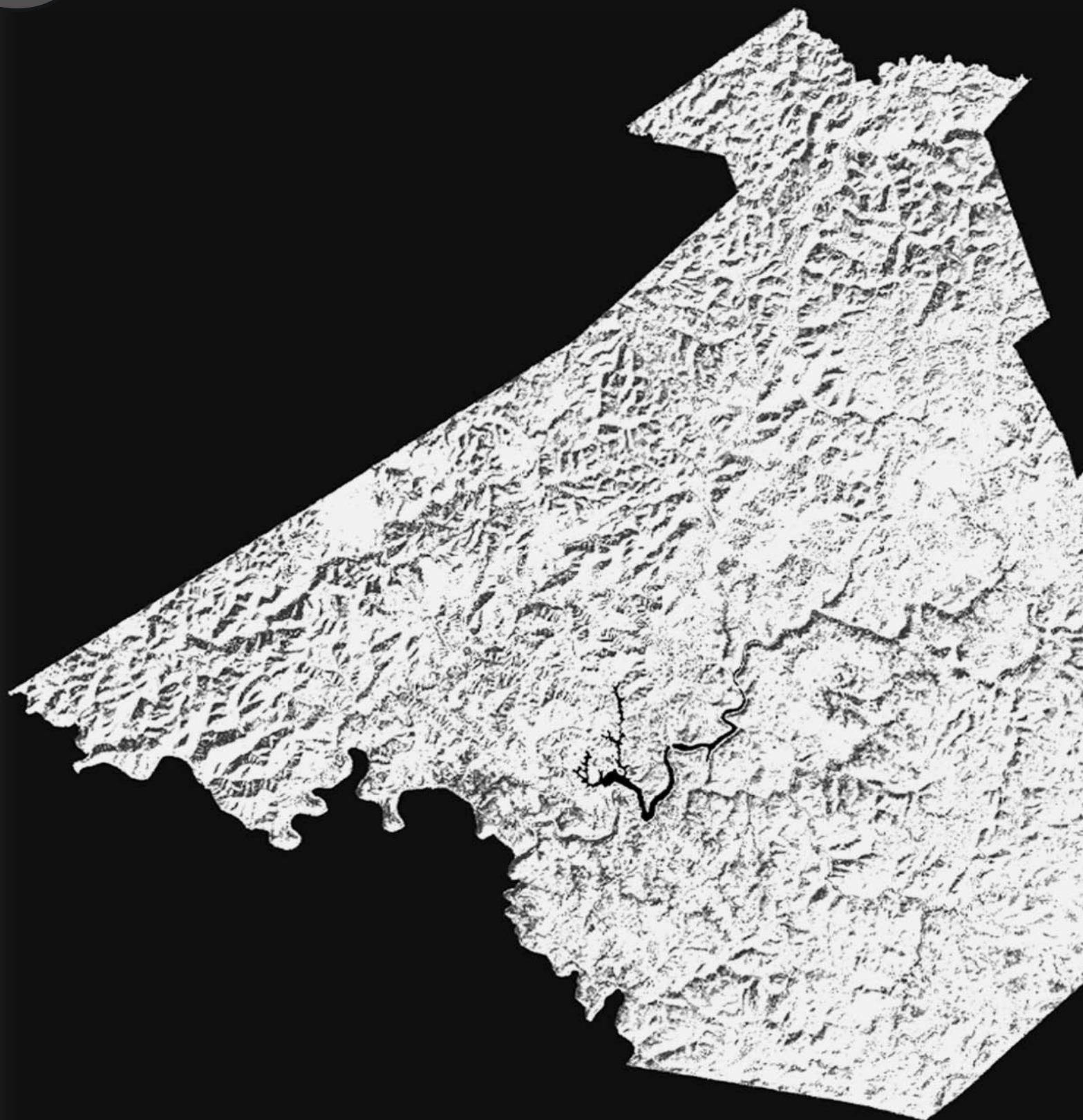
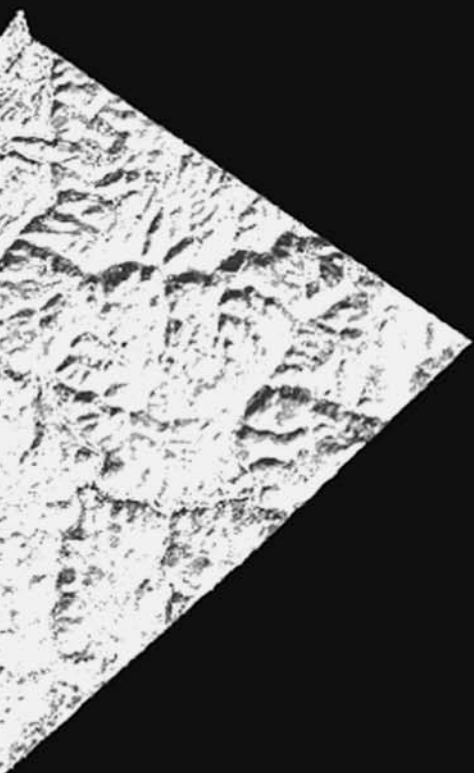


Fig. 2. VPCAR Flow Diagram.



Earth Science E n t e r p r i s e





Overview

The Earth is an oasis in the vastness of space. The natural environment of the Earth is the basis from which life, as it is known, is derived and upon which all life depends for its existence. Without it, human civilizations cannot succeed and thrive. Humans and all life on Earth depend on the natural environment for uncontaminated air, water, food and the other necessities of life such as energy and shelter. As the human population continues to grow, the demands for nature's resources continue to escalate and the Earth's life-sustaining systems are taxed more than ever before. It is critical to understand the natural world, how it is changing, and how humans can help sustain it.

NASA's Office of Earth Science (OES) studies the total Earth environment—atmosphere, ice, oceans, land, biota, and their interactions—in order to understand the effects of natural and human-induced near-term changes on the global environment, and to lay the foundation for long-term environment and climate monitoring and prediction. During FY2000, numerous research and technology efforts were accomplished, the results of which address the major goals of the OES Enterprise:

- Observe, understand, and model the Earth system to learn how it is changing, and the consequences for life on Earth.
- Expand and accelerate the realization of economic and societal benefits from Earth science, information, and technology.
- Develop and adopt advanced technologies to enable mission success and serve national priorities.

Ames Research Center supports the OES by conducting research and by developing technology with the objective of expanding the knowledge of the Earth's atmosphere and its ecosystems. These are also goals of the Agency's Astrobiology research and technology efforts, which are led by Ames. A complementary objective is to apply the knowledge gained to practical everyday problems, and to transfer the technology and knowledge to users outside NASA.

Key components of the Earth Science Division's research programs include the study of the physical and chemical processes of biogeochemical cycling; the dynamics of terrestrial ecosystems; the chemical and transport processes that determine atmospheric composition, dynamics, and climate; and the physical processes that determine the behavior of the atmosphere on the Earth and other solar system bodies.

Earth scientists at Ames engage in research related to four of the NASA strategic enterprises.

The Earth Science Enterprise

NASA Headquarters Code Y

Terrestrial ecology and atmospheric assessments, airborne instrument development, applications, Astrobiology, and Information Technology

The Human Exploration and Development of Space Enterprise

NASA Headquarters Code U

Application of technology to issues of human health

The Aeronautics and Space Transportation Technology Enterprise

NASA Headquarters Code R

Environmental assessments of aircraft operation, remotely piloted aircraft (RPA) sensor development, and science demonstration

The Space Science Enterprise

NASA Headquarters Code Y

Planetary atmospheres study

Research efforts include environmental concerns related to stratospheric ozone depletion, perturbations in the chemical composition of the atmosphere, and climatic changes resulting from clouds, aerosols, and increasing amounts of greenhouse gases in the Earth's atmosphere. Numerous state-of-the-art instruments are flown successfully each year, and critical data are collected for stratospheric and tropospheric research.

At Ames, scientists and technical personnel design, develop, and perform both remote sensing and in situ experimental measurements. In addition they perform computer simulations of atmospheric processes and ecosystems processes to understand exchanges between the biosphere and the atmosphere using both airborne and satellite sensor data. The scientists conceive and develop advanced instrumentation to satisfy the measurement requirements of all supported enterprises emphasizing both airborne and selected spacecraft sensors. Project managers and project scientists provide science mission management and science leadership for major NASA science programs and other agency science programs. Staff scientists conceive and develop applications programs utilizing proven and developing technology. Additionally, they transfer developed scientific knowledge and

technology to commercial and private interests, national and international governmental agencies and ministries, other disciplines, and educational institutions.

The Airborne Sensor Facility (ASF) within the Earth Science Division provides remote sensing support for OES investigations, and for calibration and validation studies for the Earth Observing System (EOS). It is tasked with maintaining and operating a suite of OES facility sensors that are made available to the science community at large through the NASA flight request process. The sensors are flown on various NASA, U.S. Department of Energy, and other aircraft, as required.

The ASF does data processing, flight operations, sensor calibration, systems development, and data telemetry. Current activities are centered around the Moderate Resolution

Imaging Spectrometer (MODIS) and the Advanced Spaceborne Thermal Emission and Reflection Radiometer (ASTER) airborne simulators (the MODIS Airborne Simulator, MAS, and the MODIS ASTER instrument, MASTER), which are being used to characterize calibration sites and develop algorithms for the new Terra (EOS AM-1) satellite systems. These data are processed into a calibrated Level-1B product at the ASF, and delivered to the instrument science teams via the EOS Distributed Active Archive Centers.

Research results and technology developments are published in the scientific literature. Additionally, many of these results are disseminated to the commercial and educational communities contributing to a better public understanding of the Earth Science Enterprise within NASA.

Automated Processing of Terrestrial Satellite Imagery Using Bayesian Methods

Chris Hlavka, Peter Cheeseman, John Stutz, Robert Slye

The typical approach to developing land cover/land use maps with satellite imagery involves defining spectral classes by clustering the image data and making assignment of classes to pixels. AutoClass, a general-purpose Bayesian classifier, was tested in terms of integration into the land cover map-making procedure and improved information content compared to products using other classifiers. Landsat Thematic Mapper (TM) images, ancillary data for interpreting and evaluating AutoClass results, were provided by the United States Geological Survey (USGS) offices in Menlo Park, California and the USGS in Reston, Virginia.

The current version of AutoClass is the product of years of development and refinement. It has been successfully used in several application areas from astronomy to biology. The LISP version of AutoClass was tested with Landsat data (a 1000 x 1000 pixel image). The results were promising in that tightly-defined classes were defined that were related to identifiable features of the scene, but not rigorously evaluated with "ground truth." Also, because the program was computationally intensive, the analysis took many hours on a massively parallel computer, a Thinking Machines Corporation Connection Machine (Model 2).

A newer, faster version of AutoClass written in C was tested on a moderate speed platform, a Sun Ultra 30. Software was written to convert imagery in a standard format used in remote sensing into the binary format used for AutoClass input. AutoClass-C was modified to classify image output in standard formats, enabling map product development and assessment with commercial remote sensing

image analysis software. It was further modified to write class parameters in an ASCII file to enable maximum likelihood (ML) classification of a full image with classes defined by AutoClass on a pixel subset. The clustering/ML combination was implemented to allow AutoClass to be applied to mapping larger data sets.

Land cover products were developed for three sites—two small (~500 x 500 pixel, ~15 x 15 kilometers (km)) sites in Western Texas, and Nicholas County, West Virginia (2.2 million pixels, about 1,700 km²). The small site maps were developed by clustering and classifying all pixels with AutoClass. The Nicholas County map (Fig. 1) was developed by clustering a sub-sample (every third row in every third column, or 1/9th of the pixels) with AutoClass to define spectral classes, followed by maximum likelihood classification of the full image. Aerial photography was used to relate spectral classes to cover types (road, developed areas, agricultural areas or crop types, types of natural vegetation, water) and assess map product quality. In addition, Centers for Disease Control ground observations in forested areas were used to assess the Nicholas County product, and to compare the AutoClass product to a USGS map product.

The AutoClass map products showed good definition of land-cover types associated with human activity. Discrimination among forest types was complicated by their occurrence in areas of topographic relief. The USGS map products were produced using a combination of Landsat TM and geographic information layers (maps of roads and slope/aspect), whereas the AutoClass maps were produced from Landsat TM alone, therefore a definitive comparison

between the performance of AutoClass (clustering based on probabilistic considerations) relative to a more traditional classifier (clustering based on distance) cannot be made yet. However, the AutoClass map products appear to provide more accurate maps in areas of low relief, and definition of subtle distinctions in vegetation types. Susan Benjamin,

U.S. Geological Survey, Menlo Park, California, and Jim Falcone, U.S. Geological Survey, Reston, Virginia, collaborated in this research.

Point of Contact: Chris Hlavka
(650) 604-3328
chlavka@mail.arc.nasa.gov

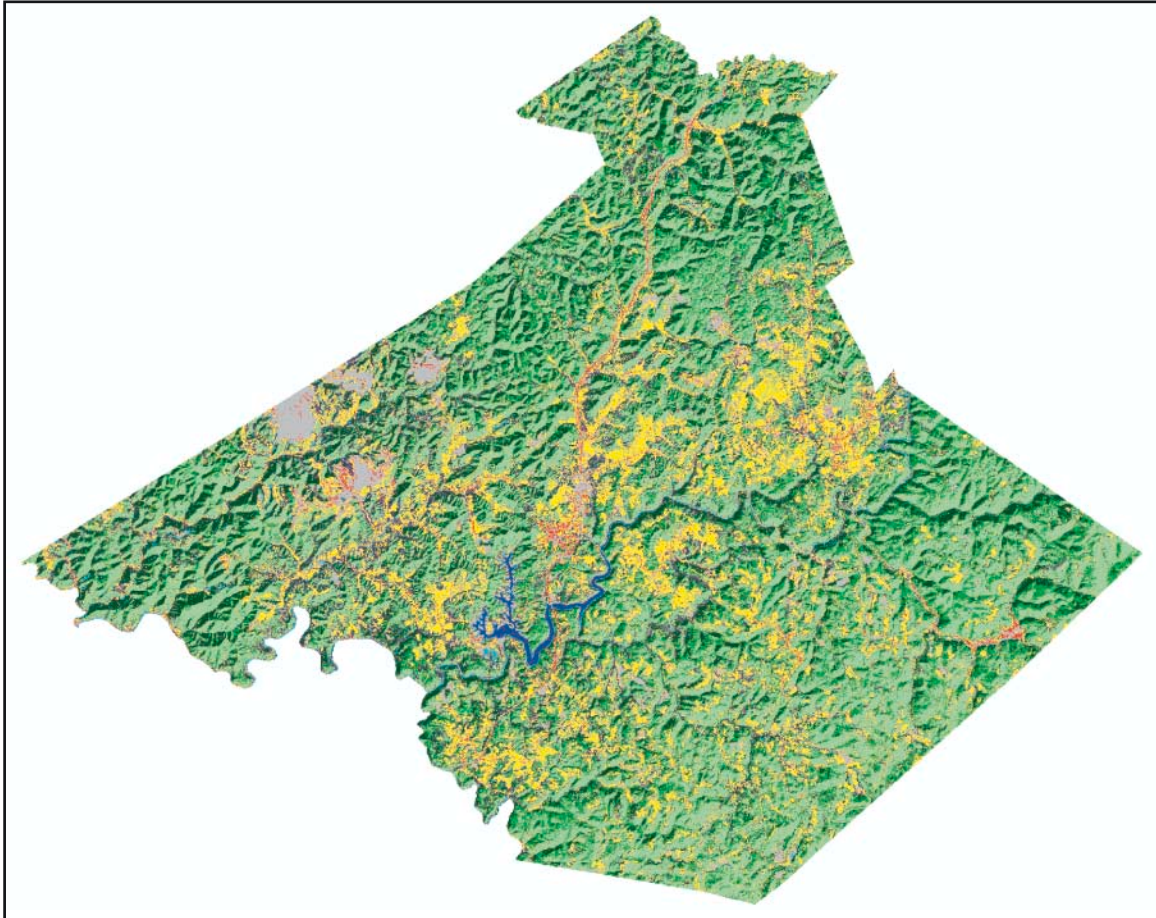


Fig. 1. Map of Nicholas County, West Virginia, produced by using AutoClass-C to process Landsat-7 Thematic Mapper imagery. [Color Code: hemlock forest - dark green; pine forest - purple; mixed forest - medium green; deciduous forest - light green; crops/pasture - yellow; towns/mines - gray; road/pavement - red; water - blue]

Biomass Burning Losses of Carbon Estimated from Ecosystem Modeling and Satellite Data Analysis for the Brazilian Amazon Region

Christopher Potter, Vanessa Brooks Genovese, Steven Klooster, Matthew Bobo, Alicia Torregrosa

To produce a new daily emissions record of carbon from biomass burning events in the states of the Brazilian Legal Amazon, the staff has used vegetation greenness estimates from satellite images as inputs to a terrestrial ecosystem production model. This carbon allocation model generates new estimates of regional vegetation biomass at eight kilometer resolution. The modeled biomass product is then combined for the first time with fire pixel counts from the Advanced Very High Resolution Radiometer (AVHRR) to overlay regional burning activities in the Amazon.

Results from this analysis indicate that carbon emission estimates from annual region-wide sources of deforestation and biomass burning in the early 1990s are apparently three to five times higher than reported in previous studies for the Brazilian Legal Amazon, i.e., studies which implied that the Legal Amazon region tends toward a net-zero annual source of

terrestrial carbon. In contrast, this analysis implies that the total net source fluxes from the Legal Amazon region range from 0.2 to 1.2 petagrams (Pg) of carbon annually, depending strongly on annual rainfall patterns. The reasons for the higher burning emission estimates are (1) use of combustion fractions typically measured during Amazon forest burning events for computing carbon losses, (2) more detailed geographic distribution of vegetation biomass and daily fire activity for the region, and (3) inclusion of fire effects in extensive areas of the Legal Amazon covered by open woodland, secondary forests, savanna, and pasture vegetation. The total area of rainforest estimated annually to be deforested did not differ substantially among the previous analyses and this one.

Point of Contact: Christopher Potter
(650) 604-6164
cpotter@mail.arc.nasa.gov

New Technology Developed and Tested for Disaster Management and Mitigation

James Brass, Vincent Ambrosia, Robert Higgins

Disasters are costly both in human life and loss of homes. Yearly, these disasters result in 133,000 deaths and 140 million homeless worldwide. Current technology for monitoring fires has relied on instrument designs that are 15 to 20 years old; these systems are large, heavy, and usually have not been designed for fire characterization and mapping.

Through a government and industry partnership, new technology has been built and tested specifically for fire monitoring. "FireMapper," a multispectral microbolometer has been built by Space Instruments, Inc. through a Small Business Innovative Research (SBIR) program sponsored by the United States Forest Service (USFS) Pacific Southwest Riverside Fire Lab.

This new technology offers a small highly calibrated instrument for use in aircraft and uninhabited airborne vehicles.

The NASA-USFS Environmental Initiative and NASA's Office of Earth Science Natural Hazards Program sponsored the development of an instrument package to meet the needs of the disaster community. Requirements and specifications summarized by many user workshops and conferences resulted in the microbolometer being integrated with two visible/near infrared digital cameras to provide vegetation (fuel) and fire data.

The Brazil deployment provided a unique opportunity to test and evaluate this new technology. To characterize the variability found in savanna and tropical forest fires, and to map forest clearing, this system was flown over prescribed fires and forests of central

Brazil. For the first time, this system provided calibrated multispectral data of fire activity resulting in fire temperature and intensity information. The data from FireMapper will allow scientists to compare fire behavior over differing ecosystems and vegetation types. This information will provide a better understanding of the importance of fire in greenhouse gas generation and ecosystem succession. Other collaborators in this research were P. Riggan and R. Lockwood, USFS; J. Hoffman, Space Instruments, Inc.; J. A. Pereira, IBAMA, Brazil; E. Stoner, U.S. Aid for International Development; H. Miranda and A. Miranda, University of Brasilia, Brazil; T. Krug, Brazilian Space Institute, Brazil.

Point of Contact: James A. Brass
(650) 604-5232
jbrass@mail.arc.nasa.gov

VINTAGE: Viticultural Integration of NASA Technologies for Assessment of the Grapevine Environment

L. Johnson, V. Vanderbilt, M. Bobo

The quality of wine grapes is influenced by such factors as ratio of fruit weight to vine leaf area, amount of sunlight directly intercepted by grape clusters, and water stress levels. Vineyard canopy density (leaf area index (LAI)) is thus a key variable of interest. California premium winegrowers are making increasing use of optical remote sensing as an additional tool for monitoring canopy density and managing vineyards. In particular, prior NASA research has demonstrated the use of high spatial resolution (two meters) vegetation index imagery for subdividing individual fields ("blocks") for harvest based upon end-of-season vigor, as inferred by canopy density. Block segmentation can result in more uniformly mature wine "lots" and, ultimately, in some cases, in improved wine quality. The

VINTAGE project is a public-private partnership dedicated to the further development of geospatial technologies and process modeling as vineyard management tools. Project investigators continue to examine relationships among vine stress, canopy development, and resulting wine quality by combining remote sensing with an agro-ecosystem process model.

Ground-based measurements of LAI were made on 50 vineyard plots (~405 hectares) located on two different Napa Valley ranches owned and operated by the Robert Mondavi Winery. The LAI2000 Plant Canopy Analyzer (LI-COR, Inc., Lincoln, Nebraska) was calibrated with destructive harvest of 12 grapevines (i.e., measurement of fruit, leaf and stem weights, leaf area). Global positioning system (GPS) measurements were made of all 50 plots

for accurate positioning with respect to the imagery. Two-meter multispectral images were collected above the two sites with an airborne ADAR-5500 digital camera system (Positive Systems Inc., Whitefish, Montana, USA). A reasonably strong relationship was found between aerial image Normalized Difference Vegetation Index (NDVI) and the LAI estimated from the ground ($r^2 = 0.61$). This result is encouraging, as it suggests that the simple NDVI is useful for estimating canopy cover over vineyard blocks of differing planting density, age, and trellis type.

Several additional field measurements were made during the last growing season. Eight sample plots, representing a variety of trellis systems, planting density, age, and plant variety were selected for one-dimensional (1-D) model validation. LAI measurements were taken at these plots every 7-10 days beginning shortly after budbreak, based on a relationship between shoot length and shoot leaf area to shoot length. Leaf water potential and soil moisture were measured periodically at each plot. Digital soils data were acquired for all of Napa County from the U.S. Department of Agriculture Natural Resources Conservation Service/Soil Survey Geographic (NRCS/SSURGO) data base, which is the finest resolution and detail data base available. These data were projected to the State Plane coordinate system, which is the projection of choice for Mondavi and most of the winegrowing community. A 10-meter digital elevation model was downloaded from USGS and projected to State Plane coordinates. An independent vendor created and delivered a high-resolution (1.5 meter) Digital Elevation Model (DEM) for the study area. A software procedure was written to automatically download weather data from Napa Valley weather stations on a daily basis. Irrigation quantities were recorded weekly at each site. Sub-surface measurements of soil depth and

moisture were taken with a ground penetrating radar. As a result of the work, project staff are now positioned to conduct 1-D validation runs of the BioGeochemical (BGC) model (see below). This effort will give the first indication of goodness of fit, and may expose areas of weakness that call for model alteration or enhanced data collection.

An ecosystem process model was adapted for use in the agricultural setting. The model, called Agricultural BioGeochemical Cycling (Ag-BGC) is customized with physiological parameters obtained from literature on grape physiology. A prototype user interface was developed for the model allowing the input of LAI estimates derived from satellite or aircraft data. Additionally, the model can now be run with different timesteps (daily to yearly). An irrigation function was incorporated to compute timing and amount of irrigation needed to maintain vines at a prescribed target leaf water potential (water stress level). Using the LAI, soil and daily weather data, the model will calculate evapotranspiration and soil moisture on a daily basis. The spatial resolution depends on the availability of LAI data and terrain information. The model was tested on a vineyard block of Mondavi Winery. LAI (estimated from aircraft imagery) was combined with soil maps and daily weather data. As a demonstration, the model was run to estimate irrigation requirements for this particular block to maintain the vines at -1.5 mega pascals (Mpa). Results are currently under evaluation.

Another demonstration of Ag-BGC was performed to show the effect of vine spacing on water use. Transpiration and leaf water potential were simulated for a hypothetical year representing the average climate observed from 1985-1997. The onset of water stress as a function of LAI (row/vine spacing) was examined, as was the amount of irrigation needed to maintain vines at a target leaf water

potential (-1.2 Mpa). The results are being evaluated.

Vestra Resources, Inc., an Ames' partner, is developing a hardware, software, and data structure for viewing the VINTAGE model results using a mobile field geographic information system (GIS)-based solution. The portable solution will allow multispectral imagery, VINTAGE model output, and other GIS data layers to be viewed and manipulated under field conditions.

The following individuals and companies collaborated with Ames researchers on this

project: R. Nemani and M. White, University of Montana; Robert Mondavi Winery, Oakville, California; Vestra Resources, Inc., Redding, California; Bay Area Shared Information Consortium (BASIC), San Jose, California; Y. Rubin, University of California, Berkeley; S. Hubbard, Lawrence Berkeley Laboratory, Livermore, California.

Point of Contact: L. Johnson
(650) 604-3331
ljohnson@mail.arc.nasa.gov

ATMOSPHERIC CHEMISTRY AND DYNAMICS BRANCH

Airborne Tracking Sunphotometry

Philip B. Russell, Beat Schmid, John M. Livingston, Jens Redemann, Robert Bergstrom, James Eilers, Richard Kolyer, Duane Allen, Dawn McIntosh, Jill Bauman

Sunphotometry is the measurement of the transmission of the solar beam through the atmosphere. Such measurements, made in several narrow bands of ultraviolet, visible, and infrared radiation, provide valuable information on the properties of aerosols and important trace gases such as water vapor and ozone. Atmospheric aerosols (suspensions of particles comprising hazes, smokes, and thin clouds in the troposphere and stratosphere) play important roles in influencing regional and global climates, in determining the chemical composition of the atmosphere, and in modifying transport processes. In all these roles, aerosols interact with trace gases through processes such as evaporation and condensation, photochemical reactions, and mutual interactions with the radiation field. Using a single technique, sunphotometry, to study both aerosols and trace gases is often an advantage in understanding their properties and these interactions.

The objective is to provide unique measurements of aerosols, water vapor, and ozone that address current scientific issues by taking advantage of the three-dimensional mobility of aircraft and other platforms.

Recent advances in understanding climate change, photochemistry, and atmospheric transport and transformation processes have emphasized the need for better knowledge of atmospheric aerosols and their interactions with trace gases. As a result, national and international bodies have called for increased efforts to measure aerosol and trace gas properties and effects, as a means of improving predictions of future climate including greenhouse warming, ozone depletion, and radiation exposure of humans and other organisms.

A fundamental measure of any aerosol or trace gas is how much it attenuates radiation of various wavelengths. This attenuation is often

described in terms of the quantity optical depth. The dependence of optical depth on wavelength is the optical depth spectrum. The Ames airborne sunphotometers determine the optical depth spectrum of aerosols and thin clouds, as well as the amounts of water vapor and ozone in the overlying atmospheric column. They do this by pointing detectors at the sun, locking onto the solar beam (i.e., tracking the sun), and measuring the (relative) intensity of the solar beam in several spectral channels. The tracking head of each instrument mounts external to the aircraft cabin, so as to increase data-taking opportunities relative to in-cabin sunphotometers and to avoid data contamination by cabin-window effects.

In FY00, the focus was on improvements of the 6- and 14-channel Ames Airborne Tracking Sunphotometers (AATS-6 and AATS-14), their integration on two aircraft where they had not previously flown, and many flights in two major field campaigns. In particular, AATS-6 was integrated on the Navajo aircraft of the Navy Space and Warfare Center (SPAWAR) and made 21 flights in the Puerto Rico Dust Experiment (PRIDE) in July 2000, and AATS-14 was integrated on the CV-580 of the University of Washington and made 24 flights in the Southern African Regional Science Initiative (SAFARI 2000) in August and September 2000. Analysis of AATS data from PRIDE and SAFARI is now under way. The Ames sunphotometer AATS-6 was used in the October 2000 Water Vapor Intensive Experiment of the Department of Energy Atmospheric Radiation Measurement (DOE-ARM) Program.

Results obtained with AATS-6 and AATS-14 in two previous experiments were also published in FY00. AATS results from the Second Aerosol Characterization Experiment (ACE-2, June-July 1997) were published in a collection

of 7 papers in *Tellus*, and results from the Tropospheric Aerosol Radiative Forcing Observational Experiment (TARFOX, July 1996) were published in 6 papers in the second TARFOX special issue of *J. Geophys. Res.*

The AATS-14 data sets are also being used in continuing studies of several techniques for separating aerosol and ozone contributions to solar-beam attenuation. The goal of these studies is to provide insights into aerosol-ozone separation for the Stratospheric Aerosol and Gas Experiment (SAGE II and SAGE III) spaceborne sensors, particularly when their measurements extend downward from the stratosphere into the troposphere. Also, project personnel combined SAGE II measurements with those by the Cryogenic Limb Array Etalon Spectrometer (CLAES) to develop maps and histories of stratospheric aerosol properties before and after the Pinatubo volcanic injection to the stratosphere.

The Ames investigators on this project collaborated with the following academic and research institutions: NASA Goddard Space Flight Center and NASA Langley Research Center; National Oceanic and Atmospheric Administration; Lawrence Berkeley National Laboratory; University of Washington; California Institute of Technology; University of California at Los Angeles; State University of New York; Naval Postgraduate School; University of Miami; San Jose State University; Stockholm University; United Kingdom Meteorological Research Flight; Max Planck Institute of Chemistry, Germany; University of Science and Technology of Lille, France; and TNO Physics and Electronics Laboratory, Netherlands.

Point of Contact: Philip B. Russell
(650) 604-5404
prussell@mail.arc.nasa.gov

Analysis of Polar Stratospheric Clouds from Advanced Very-High-Resolution Radiometer Measurements

Kathy L. Pagan, R. Stephen Hipskind

Polar stratospheric clouds (PSCs) play an important role in stratospheric ozone destruction under cold polar conditions. The current PSC measurement record comes from a variety of in situ measurements, lidar observations, and limb-viewing satellite data. Although these measurements offer many advantages, including good vertical resolution and the ability to characterize a variety of physical and optical PSC properties, they offer little information concerning PSC spatial and temporal distributions.

The advanced very high resolution radiometer (AVHRR) is a 5-channel nadir-viewing cross-track scanning radiometer. A series of AVHRR sensors onboard the TIROS-N/NOAA polar-orbiting satellites have been collecting data over both polar regions of the Earth since 1979. The horizontal resolution of AVHRR depends on view angle and ranges from 1.1 kilometer (km) at nadir to ~6 km at the steepest view angles. AVHRR is an operational weather sensor and was not designed specifically for PSC detection; however, because the AVHRR archive provides excellent spatial and temporal coverage of the polar regions, the use of AVHRR data for detecting PSCs has been investigated with the goal of producing a long-term, high-resolution PSC climatology.

PSCs form during the polar winter and early spring, when little or no sunlight is present. Prior to this study, conventional wisdom held that PSCs could not be detected in AVHRR imagery because they are too optically thin and there is insufficient thermal contrast between PSCs and the cold polar surfaces. This is true for Type I (nitric acid trihydrate or liquid ternary aerosol) PSCs. However, using the two AVHRR thermal infrared channels, channel 4

(10.3–11.3 micrometer (μm)) and channel 5 (11.5–12.5 μm), project personnel have developed methods to discriminate ice PSCs from other clouds using a combination of channel 5 brightness temperatures and the brightness temperature difference (BTD) between channels 4 and 5.

It was found that the optically thickest ice PSCs can be detected in AVHRR by color contouring channel 5 brightness temperatures. Ice PSCs form at or below ~188 kelvin (K). However, these clouds are not opaque and will transmit upwelling radiation, making the cloud top temperature appear warmer from a nadir view. Because surface and tropospheric temperatures are typically warmer than 195 K in most polar regions, pixels with AVHRR channel 5 brightness temperatures at or below 195 K can be classified as ice PSCs. Although this approach is relatively straightforward, only a small percentage of PSCs can be detected using this method.

Most ice PSCs are optically thin and can be easily confused with tropospheric cirrus clouds using only AVHRR channel 5 brightness temperatures. In this study a radiative transfer model using AVHRR channel 4–5 BTDs to discriminate optically thin PSCs from underlying cirrus has been developed. A suitable range of effective radii and volume densities were chosen to represent both cirrus and ice PSCs. Signals were then simulated using ice refractive indices for a range of PSC and cirrus cloud temperatures and background brightness temperatures. AVHRR pixels are categorized as ice PSCs when the BTD is greater than the maximum cirrus BTD. AVHRR pixels are categorized as probable ice PSCs when the BTD is greater than the average cirrus BTD.

Thresholds provided by the radiative transfer model have been incorporated into a classification algorithm for mapping PSCs. This algorithm inputs surface and tropospheric temperature estimates and employs look-up tables for cirrus average and maximum BTD values for various underlying conditions. To start, each pixel with AVHRR channel 5 brightness temperature at or below 195 K is classified as ice PSC. Then, if each pixel does not meet this criterion, the channel 4–5 BTD for it is checked against modeled cirrus average and maximum BTDs, given the pixel's underlying surface and tropospheric temperatures, and classified accordingly. After PSCs are identified in AVHRR imagery, it is possible to estimate the PSC optical depth, effective radius, temperature, and ice water path. Maps of these PSC characteristics can then be produced.

Work is ongoing to validate the model results with Polar Ozone and Aerosol Measurement

(POAM) II and III ice PSC data and lidar PSC data. Future plans include applying the model to moderate resolution imaging spectroradiometer (MODIS) data. This recently launched satellite instrument offers measurements in 36 spectral channels, 16 of them in the thermal infrared range. It is anticipated that the greater number of channels, narrower bandwidths, and greatly improved calibration of MODIS will permit the development of a more robust ice PSC detection algorithm and better estimates of ice PSC cloud properties.

M. E. Hervig, University of Wyoming, and P. G. Foschi, San Francisco State University, collaborated with the Ames investigators on this project.

Point of Contact: Kathy L. Pagan
(650) 604-0713
pagan@cloudl.arc.nasa.gov

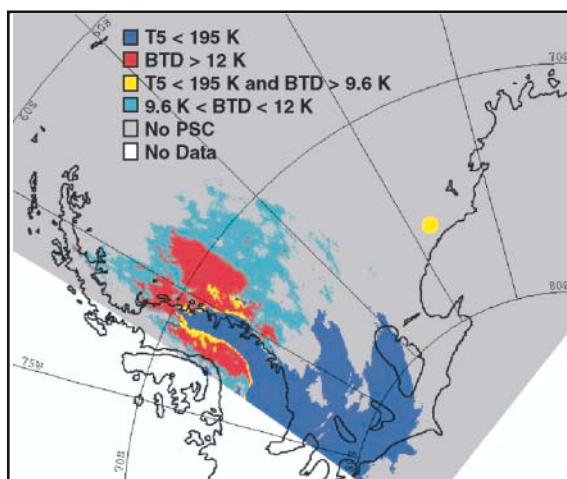


Fig. 1. Ice PSCs identified in the 18:35 Coordinated Universal Time (UTC) AVHRR imagery on July 21, 1992, in West Antarctica. A radiative transfer model was used to calculate AVHRR channel 4–5 BTDs for a range of cirrus and ice PSC conditions. A classification algorithm was then used to map the PSCs. Each pixel with AVHRR channel 5 brightness temperature (T_5) at or below 195 K was classified as ice PSC (dark blue). Failing this criteria, a pixel was classified as ice PSC if the channel 4–5 BTD was greater than the modeled maximum cirrus BTD based on the underlying surface and tropospheric temperature (red) of the pixel. Finally, a pixel was classified as probable ice PSC if the channel 4–5 BTD was greater than the modeled average cirrus BTD (cyan). A small amount of pixels were both colder than 195 K and had AVHRR channel 4–5 BTDs greater than the modeled average cirrus BTD (yellow). Pixels that were not identified as PSC represent tropospheric cloud, sea ice, or snow and ice land surfaces (gray). No AVHRR data were available for some regions (white). The location of the nearest radiosonde station is noted (yellow dot).

Asian Pollution at the California Coast, and African Plumes in the Mid-Pacific: High Resolution CO Simulations Reveal Unexpectedly Long Transports

Robert B. Chatfield

One facet of this work highlights the origins of pollution flowing into the American West Coast. Figure 1 shows a feature discovered for the first time in the interpretation of NASA's broad airborne survey, Pacific Exploratory Mission-Tropics B (PEM-Tropics B). The map shows a general description of the pollution of the global troposphere by a pollutant

normally associated with automobile exhaust and wintertime, carbon monoxide (CO). CO has a variety of pollution sources, including biomass burning, and as a chemical reaction product in the atmosphere of the oxidation of methane and isoprene, which have biological sources.

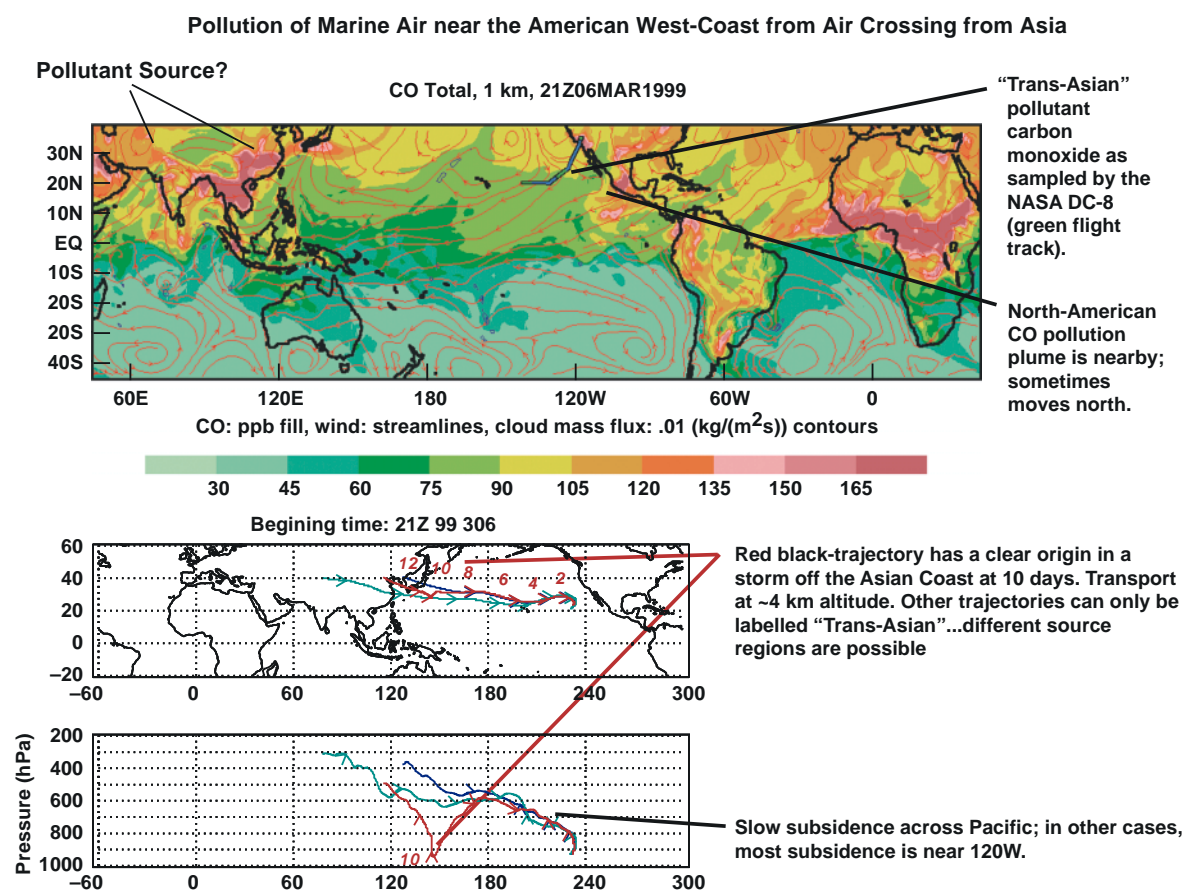


Fig 1. Carbon monoxide pollution of the Northern hemisphere and its flow into the clean Pacific as sampled during the PEM-Tropics B intensive airborne investigations of the Global Tropospheric Experiment. Note especially the large yellow region off the coast of Western North America in this map of simulated CO at 1 km. The air in a larger region off the coast of Southern California has moved rapidly from Asia, or points upwind, and then subsided. Red figures indicate number of days' journey along a back trajectory. Meanwhile, a partially separated region of CO pollution off the Mexican Coast has moved slowly westward from sources in Mexico, the southern United States, and possibly mixed with burning pollution from tropical countries to the east.

Both pollutant and natural sources of CO are concentrated over continents. In the figure, the southern part of the yellow area off the coast of the Americas, southwest from Mexico, comes from pollution processes in nearby Mexico and the southeastern USA. Consequently, CO levels of ~90 parts per billion (sampled by NASA's DL-8 and P-38 aircraft in an extensive sampling mission), about twice the clean-atmosphere background off the coast from California, were thought to originate from such nearby land areas. Instead, this near-coastal pollution appears to follow a much longer path leading over the coast of East Asia, and typically arriving by sinking from a high altitude (~6 km). Meteorological trajectories tracing individual "parcels" indicated this, but could not tell the origin of the air or describe quantitatively what sources produced the observed CO. This higher level of understanding is required as scientists attempt to predict the future of the globe. These simulations with the chemistry model, nicknamed Global-Regional Atmospheric Chemistry Event Simulator (GRACES), and the weather simulation system, called mesoscale model 5 (MM5), confirmed the general origins: Air had passed over Asia. In addition, these techniques quantified mixing by fine-scale motions in the lowest kilometers near the sampling region, and lofting of pollution through clouds and storms over Asia.

Is Asia partly to blame for polluting the air entering the West Coast, exacerbating slightly the native smog problems of the United States? The simulations indicate that this is often the case. Also they suggest that Asian pollution emissions may be underestimated in the published data, because the model produces credible peaks, but at too low a level.

Even longer-distance transport is the result shown in the second figure. Occasionally, the air reaching the western shores of the United States has not been influenced by pollution over Asia. Instead, trajectories and analyses of maps such as the second figure suggest origins even further upwind. Exact attributions over these long distances are still difficult to make. Our analyses indicate origins from pollution, mostly tropical biomass burning, over northern subtropical Africa and South America. This is a surprise, and is indicated only by models with highly detailed spatial resolution. Both MM5 and GRACES have simulation grid points at ~100 kilometers (60 miles) resolution.

More theoretical studies that are referenced by a large variety of airborne sampling studies have also aided Ames' research. Work with Dalhousie University, Nova Scotia, has helped unravel the processes of ozone in the upper troposphere. Not only NO_x (reactive nitrogen oxides, NO + NO₂) but also a supply of active photochemical species, radicals like hydroxy radical (OH) and hydroperoxy radical (HO₂), are required to describe the ozone and oxidation chemistry of the upper troposphere.

An analysis of the chemical effects of compounds such as acetone, hydrogen peroxide, and other peroxides on the chemistry of the upper troposphere has been done. These compounds are active radical sources, and they tend to ignite the fuse of a photochemical reaction chemistry that determines ozone levels in the upper troposphere. The analyses have shown that acetone sources should do this but also decrease the available NO_x to much lower quantities. The peroxide compounds were found to have a particularly important role in determining ozone. This finding has helped interpret the situational modeling and global

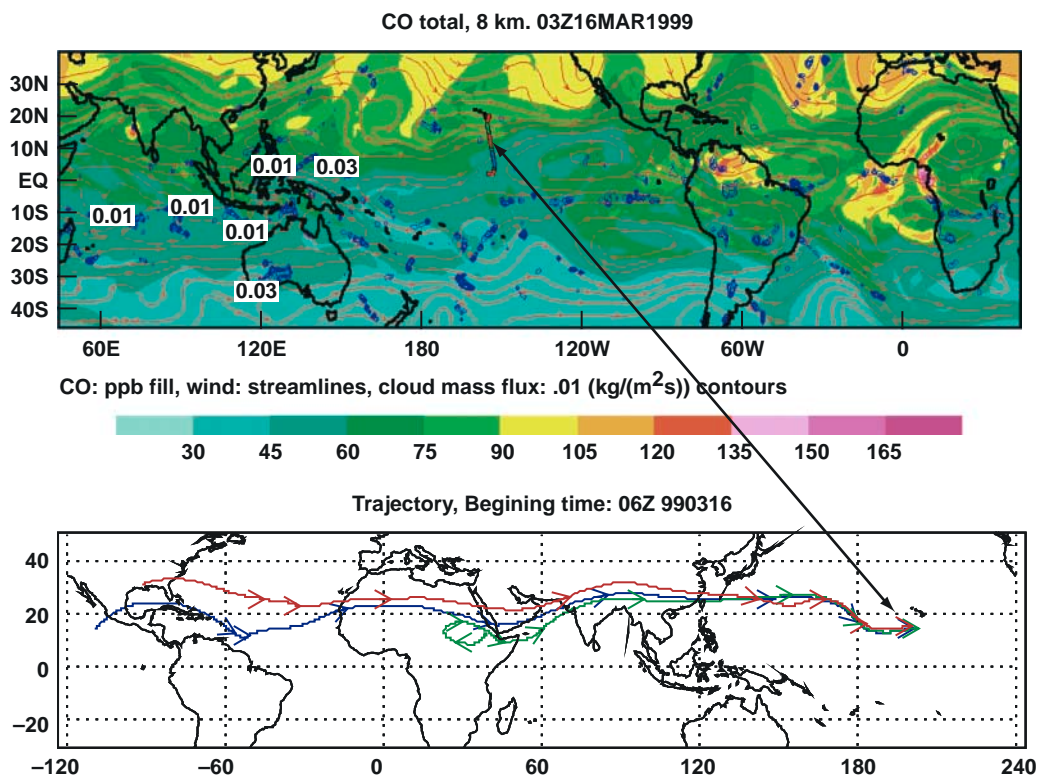


Fig 2. Carbon monoxide pollution of the North Pacific originating from a "subtropical global plume" originating in Africa. (a) A map of CO at 8 km on March 16, 1999, showing several northern subtropical plumes extending from South America, Africa, and perhaps South Asia at a high point in the Northern Hemisphere spring burning season. Comparisons were made between data and simulation, with good results. (b) Back trajectory calculations made from the 8.2 km level at the approximate DC-8 position. No cloud lofting was apparent along these paths over Asia, though some trajectories encountered light convection as they passed through the meridian ~160 E in the Pacific. The trajectories and maps suggest the possibility that the southern portions of the northern hemispheric CO maximum (light green, >75 parts per billion (ppb) CO) could be influenced by northern subtropical plume stranding together with broader patterns of Northern Hemisphere pollution. Strands of the subtropical pollution plume are clearly visible over Asia.

analysis simulations. Such studies have broader implications. Ozone in this region has its strongest role as a greenhouse gas, but responds slowly to many influences. I. Folking of Dalhousie University collaborated with the Ames' investigators.

Point of Contact: Robert B. Chatfield
(650) 604-5490
chatfield@clio.arc.nasa.gov

Dominant Presence of Oxygenated Organic Species in the Remote Southern Pacific Troposphere

H. Singh and Y. Chen

Oxygenated organic species are intimately involved with the fate of nitrogen oxides (NO_x) and hydrogen oxides (HO_x), which are necessary for tropospheric ozone formation. A recent airborne experiment (March–April, 1999) focused over the Southern Hemisphere (SH) Pacific Ocean (Pacific Exploratory Mission–Tropics B (PEM–Tropics B)) provided a first opportunity for a detailed characterization of the oxygenated organic composition of the remote Southern Hemisphere troposphere. Three co-located multichannel airborne instruments measured a dozen key oxygenated species (carbonyls, alcohols, organic nitrates, organic peroxides, peroxides) along with a comprehensive suite of C_2 – C_8 nonmethane hydrocarbons (NMHC). Analyses done in FY00 on these measurements reveal that in the tropical SH (0° – 30°S), oxygenated chemical abundances are extremely large and collectively are nearly five times those of NMHC. Even in the northern hemisphere remote atmospheres, their burden is equal to or greater than that of NMHC. Therefore the

global extent of oxygenated chemicals is greater than was previously thought. The relatively uniform global distribution of oxygenates is indicative of the presence of large natural and distributed sources. A global three-dimensional model, reflecting the present state of knowledge, is unable to correctly simulate the atmospheric distribution and variability of several of these species. More research is needed to discover the sources and transport mechanisms associated with these findings before global models can be improved to reflect this new information.

This research was performed in collaboration with A. Staudt and D. Jacob, Harvard University, Cambridge, Massachusetts; D. Blake, University of California, Irvine, California; B. Heikes and J. Snow, University of Rhode Island, Narragansett, Rhode Island.

Point of Contact: Hanwant Singh
(650) 604-6769
hsingh@mail.arc.nasa.gov

ER-2 and DC-8 Meteorological Measurement Systems

T. Paul Bui, Stuart W. Bowen, Cecilia Chang, Jonathan Dean-Day, Leonhard Pfister, Antonio A. Trias

The Meteorological Measurement System (MMS) provides high-resolution, airborne meteorological parameters (pressure, temperature, turbulence index, and the three-dimensional (3-D) wind vector). The MMS consists of three major systems: (1) an air-motion sensing system to measure the air velocity with respect to the aircraft, (2) an aircraft-motion sensing system to measure the aircraft velocity with respect to the earth, and (3) a data-acquisition system to sample,

process, and record the measured quantities. Since much of the instrumentation is attached to the aircraft at judiciously chosen locations, the MMS is a platform-specific instrument that cannot be transported from one aircraft to another.

The MMS is uniquely qualified to investigate atmospheric mesoscale (gravity and mountain lee waves) and microscale (turbulence) phenomena. An accurate characterization of the

turbulence phenomenon is important for the understanding of dynamic processes in the atmosphere, such as the behavior of buoyant plumes within cirrus clouds, diffusions of chemical species within wake vortices generated by jet aircraft, and microphysical processes in breaking gravity waves. Accurate temperature and pressure data are needed to evaluate chemical reaction rates and to determine accurate mixing ratios. Accurate wind-field data establish a detailed relationship between the various constituents, and the measured wind also verifies numerical models used to evaluate air-mass origin. Since the MMS provides quality information on atmospheric state variables, MMS data have been extensively used by many investigators to process and interpret the in situ data from various instruments aboard the same aircraft.

In FY00, the MMS instrument for the ER-2 successfully completed the Stratospheric Aerosol and Gas Experiment (SAGE)-III Ozone Loss and Validation Experiment (SOLVE) deployed to Kiruna, Sweden. The

instrument team produced accurate basic atmospheric state variables that contribute to a broad spectrum of research and investigations. The thermodynamic data provided important measurement constraint and validation for the microphysical studies of the polar stratospheric cloud particles, a critical link in the chlorine activation leading to the destruction of ozone. These basic state data also regulated directly and indirectly the heterogeneous chemical reactions. The 3-D wind data not only provided the meteorological coordinate of the polar vortex, the data supplied the precision for the investigation of mesoscale temperature perturbations that result from mountain waves. In addition, the MMS accurate geometric altitude registration using differential global positioning system (GPS) (less than 5 meter) coordinates provided a significant breakthrough in the interpretation and comparison with satellite-derived data.

Point of Contact: T. Paul Bui
(650) 604-5534
pbui@mail.arc.nasa.gov

Open Path Diode Laser Hygrometer (DLH) Instrument for Tropospheric and Stratospheric Water Vapor Studies

James R. Podolske

The diode laser hygrometer (DLH), developed by NASA's Langley and Ames Research Centers, has flown on the NASA DC-8 on several field missions including Subsonic Aircraft: Cloud and Contrail Effects Special Study (SUCCESS), Vortex Ozone Transport Experiment (VOTE), Tropical Ozone Transport Experiment (TOTE), Subsonic Assessment (SASS) Ozone and Nitrogen Oxide Experiment (SONEX), Pacific Exploratory Mission-Tropics A and B (PEM-Tropics A and B), and the recently completed SAGE III Ozone Loss and Validation Experiment (SOLVE) campaign of 1999-2000. The optical layout of this sensor consists of the compact

laser transceiver mounted to a DC-8 window port and a sheet of retro-reflecting "road sign" material applied to the DC-8 engine enclosure that completes the optical path. The advantages of this sensor approach include compactness, simple installation, fast response time (50 millisecon (msec)), no wall or inlet effects, and wide dynamic measurement range (several orders of magnitude).

Using differential absorption detection techniques similar to those described in the literature, gas-phase water ($H_2O(v)$) is sensed along a 28.5 meter (m) external path. For dry conditions (generally altitudes above 6 kilometers (km)), the diode laser wavelength is locked

onto a strong, isolated line at 7139.1 centimeters (cm),⁻¹ while for altitudes typically below 6 km the laser wavelength is locked onto a weaker line at 7133.9 cm⁻¹. By normalizing the laser differential absorption signal with the laser power signal, the H₂O(v) measurement is unaffected by clouds, haze, plumes, etc., thereby enabling high spatial resolution measurements in and around clouds. The H₂O(v) mixing ratio is computed by an algorithm from the differential absorption magnitude, ambient pressure and temperature, and

coefficients derived from laboratory calibration of the sensor. These calibrations are conducted prior to each field mission, and they involve measuring the sensor response to known H₂O(v) concentrations flowing through a 3 meter-long chamber at pressures ranging from 100 to 1000 hecto Pascals. Glen Sachse, NASA Langley Research Center, collaborated with the investigator on this study.

Point of Contact: James Podolske
(650) 604-4853,
jpodolske@mail.arc.nasa.gov

The Argus Instrument

Max Loewenstein, Hansjürg Jost, James Podolske, Jeff Greenblatt

The Argus instrument is a lightweight, infrared (3- to 5-micrometer wavelength) diode-laser spectrometer. It was designed for measuring the atmospheric nitrous oxide (N₂O) and methane (CH₄) tracer fields in situ from balloons and aircraft. The instrument can return atmospheric measurements over the altitude range of 5 to 30 kilometers (km).

In preparation for the winter 1999-2000 SAGE III Ozone Loss and Validation Experiment/Third European Stratospheric Experiment On Ozone (SOLVE/THESEO 2000) Arctic ozone campaign, Argus was integrated on the ER-2 high-altitude research aircraft during the summer and fall of 1999. Thermal calculations and engineering modifications of Argus were undertaken at Dryden Flight Research Center (DFRC), home of the ER-2, for the successful completion of this task, which also required several test flights to tune up the thermal conditioning system of the instrument. Several Argus improvements were also made to enhance data quality for this mission. These included installing a longer optical-path gas sampling cell, improving laser temperature control, streamlining the data analysis code, and adding an in-flight gas calibration system.

The ER-2 component of the SOLVE/THESEO 2000 Arctic ozone study began in January of 2000 with ferry flights from DFRC through Westover Air Force Base, Massachusetts, and then to Kiruna, Sweden, at 67° N. In 12 flights originating in Kiruna, from January through March of 2000, regions both inside and outside the winter polar vortex were sampled by the instruments onboard the ER-2. The research was supported by additional aircraft-, balloon- and ground-based instruments from both the NASA SOLVE and European THESEO elements of the field campaign. The overall purpose of the campaign was to achieve a detailed understanding of the chemistry and the spatial extent and intensity of ozone loss inside the winter polar vortex. Polar Stratospheric Clouds (PSCs) that form during the cold Arctic polar night in the lower (10 to 20 kilometers (km)) stratosphere greatly enhance destruction of ozone by human-caused emissions of chlorine and bromine. The presence of these PSCs is fundamental to the formation of the well-known Antarctic ozone hole, though the amount of Arctic ozone destruction is not as great as that observed annually in the early austral spring over the Antarctic.

The Argus instrument specifically contributed to SOLVE by measuring the long-lived chemicals N_2O and CH_4 , which act as dynamical tracers of the vortex motion. Two aspects of vortex dynamics are of importance: subsidence of the vortex due to strong radiation cooling in the polar night, and formation of a vortex edge marking the boundary between the subsiding region and the midlatitude atmosphere, defined by the strong circumpolar wind jet enclosing and isolating the polar night region. The N_2O and CH_4 tracers move, chemically unmodified, with the atmospheric motion, thus acting as constant metrics against which to measure ozone destruction activity in moving air masses. Several other instruments on the ER-2 and on balloons launched during the campaign period measure the same tracers as Argus, reflecting the great importance of knowing the tracer fields accurately.

On the ER-2 the Argus instrument is the smallest and lightest of four instruments that measure tracers by using different measurement principles. In order to validate tracer measurements, the four ER-2 instruments entered into a detailed intercomparison of their N_2O measurement results on all ER-2 flights. N_2O plays a special role as a tracer because of its very long (greater than 100 years) atmospheric lifetime. A result of this effort was to

merge three of the N_2O datasets into a “unified” dataset formed by performing a weighted average of the three sets. The fourth set of much lower data rate, but of the highest accuracy, was used as a quality check on the unified set. This set, recorded on the SOLVE data archive, then became the canonical N_2O tracer set for use by other experiments on the ER-2, such as integrating measured total inorganic chlorine into a Cl: N_2O rule. N_2O , an easier measurement than chlorine, could then be used to infer total chlorine at other times and locations in the stratosphere.

A postmission workshop was held in Palermo, Italy, in September 2000, where project personnel presented papers and posters. Papers have been submitted for publication with such topics as the unified N_2O data set, vortex subsidence, vortex edge detection, formation of unusually large, rapidly sedimenting PSC particles, ozone loss quantified at 16% over the Arctic stratosphere, and an unprecedented local loss of ozone of 60% at 18-km altitude. Jeff Grose, San Jose State University Foundation, and Margaret Swisher, Foothill/DeAnza Community College District, collaborated with the Ames investigators on this project.

Point of Contact: Max Loewenstein
(650) 604-5504
mloewenstein@mail.arc.nasa.gov

Transport and Meteorological Analysis

Leonhard Pfister, Henry B. Selkirk, Marion J. Legg

The objectives of this work are twofold. First, to provide real-time meteorological satellite guidance to airborne field missions for NASA's Upper Atmosphere Research Program, the Global Tropospheric Experiment, and the Atmospheric Effects of Aviation Project. Extensive meteorological satellite datasets were provided for use by the mission scientist and by the science team. These same data were then archived for postdeployment data analysis by the science team. Second, to provide scientific analysis of the data from the airborne field missions supported. The results of these analyses were made public through peer-reviewed publications.

During FY00, the science field campaigns, for which real-time meteorological support was provided, included the Sage III Ozone Loss and Validation Experiment (SOLVE) mission in Sweden from December 1999 to March 2000, and the Atmospheric Chemistry of Combustion Emissions Near the Tropopause (ACCENT) mission in September 2000. In addition, real-time information on convectively influenced air for mission planning during ACCENT was provided. This technique uses a combination of trajectory modeling and satellite imagery to establish which air masses have been recently influenced by convection. This information is useful for investigating such problems as nitrogen oxides (NO_x) production by lightning, water vapor budgets in the upper troposphere, and emissions by subsonic aircraft in the upper troposphere. This technique for establishing the recent air-mass history is also a useful tool for postprocessing and data analysis in support of other investigators on the missions.

The second objective of this work is scientific analysis of the data from the airborne field

missions supported. Data are divided into four basic areas:

- water vapor and subvisible cirrus clouds in the upper tropical troposphere,
- water vapor in the upper winter arctic troposphere and lower stratosphere,
- gravity waves and turbulence, and
- tropospheric chemistry.

The first of these areas is fundamental to the input of water vapor into the stratosphere, which is an important factor in stratospheric gas-phase chemistry and for the formation of Polar Stratospheric Clouds (PSCs). The chemistry of PSCs, in turn, is responsible for much of the ozone loss due to chlorinated hydrocarbons. The second area, water vapor in the arctic upper troposphere and lower stratosphere, is potentially important in the formation of ice clouds that can have similar chemical effects as the PSCs. Gravity waves are important because (a) they produce turbulence, which can affect vertical mixing of stratospheric trace constituents; (b) they transport momentum upward, driving important features of the stratospheric circulation such as the tropical quasi-biennial oscillation; and (c) they produce temperature deviations that can produce subvisible cirrus clouds. The fourth area involves investigating the effects of convection on tropospheric chemical trace constituents, particularly NO_x (via lightning) and water vapor.

To deal with the four areas of scientific analysis, some important analysis tools have been developed. The most novel of these is the so-called "convective influence" calculation, whereby a calculation is done, using a combination of back trajectories and meteorological

satellite data, the amount and age of recent “convective influence” on an air parcel. This technique has been used in connection with the first area of scientific analysis indicated previously, namely subvisible cirrus clouds in the upper tropical troposphere. An assessment has been done as to whether subvisible cirrus clouds observed during the 1995-1996 Tropical Ozone Transport Experiment/Vortex Ozone Transport Experiment (TOTE/VOTE) were produced by local cooling and ice nucleation, or were a long-lived outflow from convection. It was found that good correspondence exists between the locations of different types of near-tropopause cirrus and the origins of the air, with smooth laminar cirrus clearly the result of local cooling, and lumpier clouds the apparent outflow of convection. Notably, these calculations indicate that some of this convective outflow can last several days. Also of note is the presence of inertia-gravity waves and their characteristics. These waves have a very good correspondence to the sloping cloud shapes, indicating that the cooling associated with these waves is probably responsible for the clouds.

This last result is significant, since it lends support to a hypothesis that is the result of modeling work. This hypothesis suggests that long-period waves produce cirrus clouds, which are then heated and lofted into the stratosphere. As the clouds grow, large particles fall out, dehydrating the air. In effect, this mechanism will move air into the stratosphere and dehydrate it at the same time, possibly resolving a crucial question of how very dry air gets into the lower tropical stratosphere.

The convective influence technique has also yielded insight into some of the results from the ACCENT experiment. As a result of this

technique, it is possible to trace high values of methyl iodide in the upper troposphere over the Gulf of Mexico to convection in the eastern Pacific. The significance of this finding is the ability to understand one component (convection) influencing why air masses have the composition that they do. Developing an understanding of the impact of natural processes (for example, convection) on air masses is certainly a prerequisite for understanding the impact of human influences (for example, aircraft).

With the completion of the SOLVE experiment, some results have been obtained on the second area of scientific analysis, namely water vapor in the lowermost arctic stratosphere. These results, based on observed water vapor and temperature histories, show that during early spring about 15% of air parcels that have ozone values between 300-350 parts per billion by volume (ppbv) (well within the arctic stratosphere) experience ice saturation sometime during a given ten-day period.

This is potentially significant, since ice clouds within the lowermost stratosphere can lead to possible chlorine activation. What may be more significant is that, at the very bottom of the arctic stratosphere (near 100 ppbv of ozone), 30% of parcels in a given ten-day period during early spring experience ice saturation even if their water vapor content is at the prevailing stratospheric value of 5 parts per million by volume (ppmv). This means that the arctic tropopause may act as a major drying mechanism for the upper troposphere during spring, a finding that is important for the Earth’s radiation budget.

Point of Contact: Leonhard Pfister
(650) 604-3183,
pfister@telsci.arc.nasa.gov

Hypervalent Chlorine Nitrates: Implications for Stratospheric Chlorine Chemistry

Timothy J. Lee

It has been known for many years that high levels of chlorine radicals (ClO_x) observed in the polar stratosphere couple with nitrogen oxides (NO_x), resulting in the removal of reactive chlorine species by conversion into temporary reservoir species. Of the various possible reactions between the ClO_x and NO_x families, the association reaction between ClO and NO_2 to produce chlorine nitrate, ClONO_2 , has been considered the most significant:



The suggestion that ClONO_2 could be an important reservoir species was first made by Rowland et al. in 1976. Since then, a significant effort has been expended in elucidating the chemistry of ClONO_2 in the stratosphere. Also, a large number of field measurements have been made to ascertain the abundance of ClONO_2 in the chemically perturbed region of the polar vortex.

Despite the enormous work, there are still discrepancies in balancing the atmospheric chlorine budget. Researchers believe that additional long-time chlorine reservoir species may be involved besides the currently recognized chlorine reservoirs, ClONO_2 and hydrogen chloride (HCl). Attempts to improve the current understanding have led to the conclusion that higher oxides of chlorine heretofore overlooked may account for the missing reservoir of inorganic chlorine in the stratosphere. This speculation arose partly from the ground based measurements that detected extraordinarily high concentrations of OCIO in the polar vortex, which is believed to be produced primarily by the coupling between ClO and bromine oxide (BrO). In addition, the observation of OCIO and NO_3 in the polar stratosphere has strengthened the notion that

many more reactions are possible between the NO_x and ClO_x families. In response to these findings, some effort has been directed at the alternative possibility of gas-phase reservoir species resulting from the reactions of OCIO with NO_3 and ClO with NO_3 .

Friedl et al., in work performed at Jet Propulsion Laboratory (JPL), examined the products of the reaction between OCIO and NO_3 from $T = 220$ to 298 kelvin (K) using a flow reactor and infrared (IR), visible, and ultraviolet (UV) spectroscopic analysis. IR and UV absorption features observed at low temperature (<230 K) were assigned to the novel compound chloryl nitrate, O_2ClONO_2 (fig. 1).

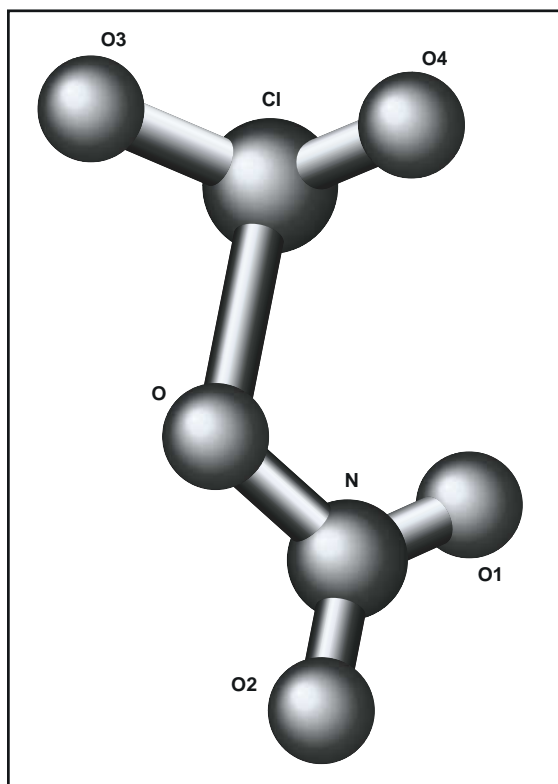
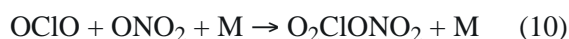
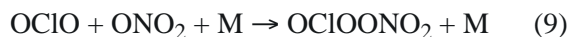
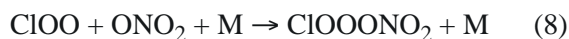
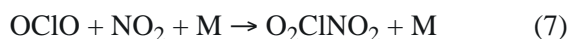


Fig. 1. Novel compound chloryl nitrate, O_2ClONO_2 .

Using a one-dimensional model they deduced that chloryl nitrate may exist in significant concentrations in the “collar” region of the polar vortex, where both the reactants are likely to exist in the nighttime air mass. However, in a later study Boyd et al. found no evidence for the occurrence of the homogeneous reaction $\text{NO}_3 + \text{OCIO} \rightarrow \text{products}$ at room temperature, in disagreement with Friedl et al.

In general, the higher oxides of chlorine nitrate could be important if they are produced in sufficient amounts to act as temporary or long-term reservoirs for both odd chlorine and odd nitrogen species. In particular, the possibility that the hypervalent compounds might act as reservoir species is bolstered by previous studies from our laboratory that have shown their electronic spectra to be shifted to higher energy, thereby ensuring their photostability in the stratosphere. Further, independent of their atmospheric significance, the recombination products are interesting molecules from the viewpoint of structural chemistry. Therefore, it is important to establish the properties of these oxides in order to aid in the interpretation of laboratory and atmospheric observations. In the present study, we have considered the following reactions as the possible pathways for adduct formation:



Using the tools of computational quantum chemistry, we have established that the

OCIONO_2 , O_2ClONO_2 , and ClOOONO_2 compounds are thermodynamically not very stable, if at all, and will, therefore, play no role in stratospheric chlorine chemistry. On the other hand, the ClOONO_2 , ClOOONO_2 , and O_2ClONO_2 compounds are thermodynamically stable enough that they could exist in certain regions of the stratosphere. Their weakest bond energy is computed to be about 7 kcal/mol, indicating that in the upper stratosphere (where it is hotter), these compounds are more likely to dissociate. By comparing our computed IR spectra for O_2ClONO_2 with the experimentally observed one from Friedl et al., we have also shown conclusively that they did indeed observe O_2ClONO_2 from the reaction of $\text{OCIO} + \text{NO}_3$, contrary to the conclusions of Boyd et al. In fact, our thermodynamic analysis of the stability of O_2ClONO_2 is consistent with both the experiments from Friedl et al. and Boyd et al. since the latter were performed at room temperature (298 K) while the former extended down to 220 K.

Other important physical characterization data for the ClOONO_2 , ClOOONO_2 , and O_2ClONO_2 compounds also have been provided, including equilibrium structures, dipole moments, full IR spectra, heats of formation, and bond energies for possible dissociation pathways, in order to aid future experimental, modeling, and field measurement studies involving these compounds. Finally, our computational studies have further established the importance of hypervalent halogen compounds in stratospheric chemistry.

Point of Contact: Timothy J. Lee
(650) 604-5208
tjlee@mail.arc.nasa.gov

ATMOSPHERIC PHYSICS BRANCH

Aerosol Radiative Forcing of Asian Continental Outflow

Rudolf F. Pueschel and Anthony W. Strawa

Anthropogenic aerosols are a major uncertainty in climate prediction. Current estimates of the global annually averaged direct radiative forcing of sulfates, soot (black carbon), mineral dust, and biomass smoke range from -0.3 to -1.0 W m^{-2} , with an uncertainty factor of about two. To reduce this uncertainty via better characterization of aerosol properties, integrated field experiments have been conducted (for example, Smoke, Cloud, and Radiation-A (SCAR-A), Smoke, Cloud, and Radiation-Brazil (SCAR-B), Indian Ocean Experiment (INDOEX), Tropospheric Aerosol Radiative Forcing Observation Experiment (TARFOX), and South African Regional Science Initiative (SAFARI)). Presented here are aerosol radiative forcing data for the western Pacific Ocean region (not covered by any of the above-mentioned deployments) with simulations based on in situ measurements of particle characteristics in elevated Asian outflow.

As an illustration of the findings, figure 1 compares the clear-sky daily averaged aerosol forcing of Asian outflow (column 1) per unit optical depth with other types of forcings, namely biomass burning (ScB and Zam), forcing by dust (Ace2), forcing associated with urban-industrial pollution (Tfox, ScA, Indo), and forcing by enhanced stratospheric aerosol (Pin). Results are presented for solar broadband fluxes at the surface and at the top of the atmosphere, and for infrared broadband fluxes at the top of the atmosphere. It follows from the first figure that (1) the daily averaged forcing varies between -60 and -100 W m^{-2} irrespective of the geographic location of the measurements; (2) the averaged forcing at the top of the atmosphere is usually significantly

smaller than at the surface; and (3) infrared heating at the top of the atmosphere in Asian continental outflow is similar to that of Saharan dust.

In spite of only a relatively small change in the net flux at the top of the atmosphere, generally looked at as a measure of the climatic impact of aerosols, Asian outflow strongly reduces the solar radiation reaching the surface. Possible consequences are dynamical feedbacks (for example, suppressed convection, weakening of the hydrological cycle, and changes in local heating rates.) Heating rates of $+10 \text{ kelvin/d}$ (K/d) (per unit mid-visible extinction) were calculated, mainly they were caused by sub-micron particles. Particles exceeding one micrometer contributed only about 30% to this rate due to reduced solar heating because of infrared cooling. This atmospheric heating by aerosols could cause low-level clouds to evaporate. This is an opposing effect to increase in cloud cover that can be attributable to more cloud condensation nuclei forming smaller drops at higher concentration.

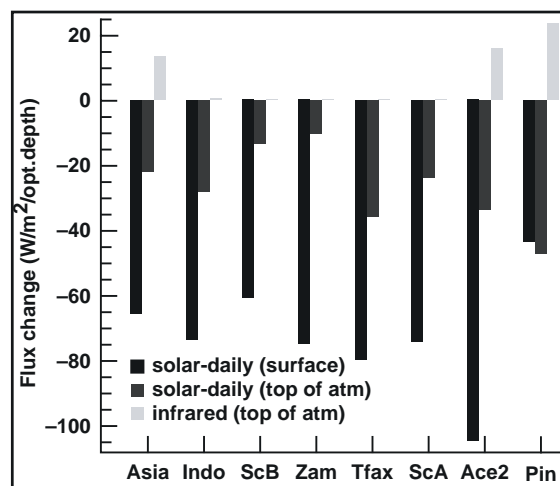


Fig. 1. Scaled aerosol direct forcing comparison.

Although stratospheric background aerosol is nonabsorbing, the particles injected by the Pinatubo volcanic eruption were large enough to cause infrared warming (Fig. 1). In the Arctic stratosphere, the existence of soot aerosol (arguably from aircraft) increases heating rates from a fraction of a degree per day to about two degrees per day, with possible implications to dynamics and chemical reaction rates.

The presence of clouds is critical for an assessment of aerosol forcing. In the presence of clouds at altitudes higher than the aerosol layer, the aerosol forcing is similar to a cloud-free scenario, albeit at a reduced rate. If the

clouds are below the aerosol layer, aerosols primarily reduce cloud-associated solar flux losses such that cooling is not just reduced but can change to warming. Thus the removal of lower-level clouds turned weak net flux gains (warming) into weak net-flux losses (cooling). S. Kinne of NASA Goddard Space Flight Center collaborated with the Ames investigators.

Point of Contact: Rudolf F. Pueschel
(650) 604-5254
rpueschel@mail.arc.nasa.gov

Analysis of SOLVE Observations of PSCs and Implications for the Evolution of the Arctic Vortex

Katja Drdla

In-situ measurements of polar stratospheric clouds (PSCs) made from the ER-2 aircraft during the SAGE III Ozone Loss and Validation Experiment (SOLVE) have revealed new information about the composition and properties of these clouds. Model results have been compared with the ER-2 measurements in order to refine understanding of the cloud microphysics.

Measurements made by the Multiangle Aerosol Spectrometer Probe (MASP) reveal that most particles generally appear to be liquid-phase. Growth of these particles was observed at temperatures near 192 kelvin (K), consistent with the predicted behavior of ternary nitric acid/dihydrogen sulfate/water solutions ($\text{HNO}_3/\text{H}_2\text{SO}_4/\text{H}_2\text{O}$). Even at warmer temperatures, starting as air cools below 196 K, some swelling of the particles is apparent. The correlation of this growth with total available HNO_3 indicates that HNO_3 condensation is responsible. The observations have been compared with predictions of several ternary

solution models with generally good agreement. The presence of liquid-phase particles has implications for the long-term evolution of the Arctic winter. The widespread persistence of liquid particles constrains understanding of freezing processes, especially in air parcels that have experienced extensive denitrification. No significant differences in particle size distributions exist between highly denitrified and less denitrified air parcels, suggesting that very few particles are removed by the processes causing denitrification.

However, a very small fraction ($<0.1\%$) of the particles did freeze during the winter, forming solid-phase HNO_3 -containing particles that were observed both by the MASP and by the NO_y instrument. The presence of these frozen particles cannot be explained by current laboratory data on aerosol freezing, in which freezing occurs only at temperatures several degrees below the ice frost point. Alternative formation mechanisms, in particular homogeneous freezing above the ice frost point and

heterogeneous freezing, have been explored using the microphysical model. Homogeneous freezing at a rate of 10^4 cubic centimeters per second (cm^3s^{-1}) produces particles comparable to observations. However, the PSCs form too frequently (observations often show a lack of solid-phase PSCs well below the nitric acid trihydrate (NAT) condensation point), and the altitude variation is not well captured. For homogeneous freezing to explain the observations, the freezing rate must have a complex dependence upon the local conditions.

On the other hand, PSCs that form by heterogeneous freezing are strongly affected by the winter-long PSC processing; that is, denitrification removes most of the nuclei. The resulting model correlation between denitrification and particle concentration is comparable to the ER-2 observations. In addition to providing an explanation for the occasional absence of solid-phase PSCs, this process also explains why denitrification did not exceed 80%.

To understand the winter-long implications of these findings, the model has been run from November to mid-April, using a large set of trajectories that provided representative coverage of the entire Arctic vortex through the period of PSC formation and ozone depletion. The various possible freezing processes have been shown to have different characteristics in terms of the overall extent of frozen particles, the evolution of the PSCs, denitrification, and dehydration. Scenarios with freezing above the ice frost point lead to widespread denitrification. This denitrification enhances the ozone loss at the end of the winter by up to 30%, as long as the vortex remains stable until late March.

Point of Contact: Katja Drdla
(650) 604-5663
katja@aerosol.arc.nasa.gov

Global Aerosol Climatology Project

Peter Pilewskie, Warren Gore, and Larry Pezzolo

In June and July, 2000, Ames personnel participated in the Puerto Rico Dust Experiment (PRIDE), a multi-agency field study of the radiative, microphysical, and transport properties of Saharan dust. There were two primary objectives: (1) determine the extent to which the properties of dust particles and the spectral surface reflectance of the ocean surface need to be known before remote sensing systems can accurately determine optical depth and flux; and (2) evaluate/validate the skill with which the Naval Research Laboratory's Aerosol Analysis and Prediction System (NAAPS) predicts the long-range transport and vertical distribution of African dust.

The results of these efforts will support U.S. Navy and NASA applied science objectives on satellite validation and the prediction of dust-induced visibility degradation. In addition, secondary efforts of PRIDE will address in situ issues of coarse mode particles and basic research issues on climate forcing, geochemical cycles, and meteorology.

Ames' specific contributions to PRIDE were to provide measurements and analyses of solar spectral fluxes. The Ames Solar Spectral Flux Radiometer (SSFR) was deployed on the Space and Naval Warfare Systems Command (SPAWAR) Navajo aircraft, measuring upwelling and downwelling spectral irradiance

between 300 and 1700 nanometers (nm). A similar SSFR was deployed at a ground site to obtain downwelling irradiance at the surface. The data will be used to determine the net solar radiative forcing of dust and other aerosols, to quantify the solar spectral radiative energy budget in the presence of elevated aerosol loading, to support satellite algorithm validation, and to provide tests of closure with in-situ measurements.

In August/September 2000, Ames personnel participated in the South African Regional Science Initiative (SAFARI 2000), an international science initiative aimed at developing a better understanding of the southern African Earth/atmosphere/human system. The goal of SAFARI 2000 is to identify and understand the relationships between the physical, chemical, biological and anthropogenic processes that underlie the biogeophysical and biogeochemical systems of southern Africa. Particular

emphasis will be placed upon biogenic, pyrogenic, and anthropogenic emissions, their characterization and quantification, their transport and transformations in the atmosphere, their influence on regional climate and meteorology, their eventual deposition, and the effects of this deposition on ecosystems.

During SAFARI 2000, the SSFR was deployed on the NASA ER-2, the University of Washington CV-580, and at a ground site in Kruger National Park. Data will be used to characterize the spectrally dependence of cloud and aerosol radiative forcing.

Maura Rabbette and John Pommier, Bay Area Environmental Research Institute and Steve Howard, Symtech Corporation, collaborated with the Ames investigators on this project.

Point of Contact: Peter Pilewskie
(650) 604-0746
ppilewskie@mail.arc.nasa.gov

In-Situ Measurement of Particle Extinction

Anthony W. Strawa and Rudolf F. Pueschel

Aerosol optical properties are extremely important in assessing climate change. The lack of sufficient knowledge of aerosol optical properties and their variability in the atmosphere have led the Intergovernmental Panel on Climate Change to rate the effect of aerosol as the most uncertain of all parameters considered important to climate change. Currently, these aerosol properties are obtained from filter samples that measure absorption of black carbon aerosols on a time scale of tens of minutes to hours. Aerosol variability causes significant changes in optical properties on the order of seconds, especially when sampled from aircraft. Thus, the research community is very interested in an instrument that can measure the optical properties of all aerosols,

not just black carbon, on a time scale of seconds. The instrument developed by a commercial vendor can meet these expectations and has the capability to revolutionize the measurement of aerosol optical properties.

Ames is working with the vendor to develop an innovative instrument using cavity ring-down absorption spectroscopy (CRDS) to measure the extinction and scattering coefficients of aerosol, and consequently, the single-scatter albedo. The prototype instrument demonstrates: (1) fast and accurate measurement of aerosol extinction, (2) measurement of aerosol scattering in a CRDS system, and (3) simultaneous measurement at two laser wavelengths. The instrument proved capable of measuring

the extinction of ammonium sulfate aerosol typical of the mid- to high-troposphere background aerosol. At the same time, the scattering of the aerosol was measured, and an estimate of its single-scatter albedo could be made. It is expected that continued development of this technology will lead to a flight-ready instrument within the next two years.

T. Owano, Informed Diagnostics, Inc., collaborated on this project.

Point of Contact: Anthony W. Strawa
(650) 604-3437
astrawa@mail.arc.nasa.gov

The Runaway Greenhouse Effect on Earth and Other Planets

Maura Rabbette, Peter Pilewski, Christopher McKay, and Richard Young

Water vapor is an efficient absorber of outgoing longwave infrared radiation on Earth and is, therefore, a primary greenhouse gas. Since the amount of water vapor in the atmosphere increases with increasing surface temperature, and the increase in water vapor further increases the temperature, there is a positive feedback. The runaway greenhouse effect occurs if this feedback continues unchecked until all the water has left the surface and enters the atmosphere. For Mars and Earth, the runaway greenhouse effect was halted when water vapor became saturated with respect to ice or liquid water, respectively. However, Venus is considered to be an example of a planet where the runaway greenhouse effect did occur, and it has been speculated that if the solar luminosity were to increase above a certain limit, it would also occur on Earth.

Satellite data acquired during the Earth Radiation Budget Experiment (ERBE) clear sky conditions shows that as the sea surface temperature (SST) increases, the rate of outgoing infrared radiation at the top of the atmosphere also increases, as expected. Surprisingly, above 300 kelvin (K) the outgoing radiation emitted to space actually decreases with rising SST. Less energy to space implies that more energy is available to heat the surface, leading to a potentially unstable situation. This behavior is a signature of the

runaway greenhouse effect on Earth. However, the SST never exceeds 303 K, thus the system has a natural cap that stops the runaway.

According to Stefan-Boltzmann's law, the amount of heat energy radiated by the Earth's surface is proportional to temperature (T)⁴. However, if the planet has a substantial atmosphere, it can absorb all heat radiation from the lower surface before the radiation penetrates into outer space. Thus, an instrument in space looking at the planet, does not detect radiation from the surface. The radiation that it detects comes from some level higher up in the atmosphere. The effective temperature (T_e) is the temperature of this emitting region within the troposphere; lower levels may have much higher temperatures. On Earth the average temperature of the surface is 288 K, but the effective temperature is only 255 K. The value $T_e = 255$ K corresponds to the middle troposphere, above most of the water vapor and clouds.

Atmospheric instruments and sensors on high-altitude aircraft, radiosonde, and satellite platforms provide direct observations of sea-surface temperatures, outgoing infrared flux to space, and atmospheric humidity and temperature profile measurements. The ERBE data is now being used to model the sea-surface temperature and outgoing flux to space. The aim is that this radiative transfer model will

reproduce the signature of the potential runaway greenhouse effect on Earth (figures 1 and 2). The model will be a link between ERBE measurements and theory and will help us to understand climate evolution and divergent climates of Venus, Earth, and Mars, as well as the inner boundary of the habitable zone in other planetary systems.

The significance of the observed sea-surface temperature at which the outgoing longwave radiation to space begins to decrease, as well as the observed upper limit on the sea-surface temperature, is that both phenomena are relevant to several aspects of paleoclimatology and astrobiology. This model will be used in an attempt to predict the upper limit of sea-surface temperatures for different values of

atmospheric carbon dioxide (CO_2), an objective directly relevant to understanding past and future climate states of the Earth. For example, did these same processes prevent the oceans from evaporating during past climate episodes of enhanced CO_2 ? Evidence suggests that even during past climates SST did not exceed 303 K. The runaway greenhouse effect is thought to be a critical factor in defining the inner edge of the habitable zone of any planetary system, therefore an understanding of the phenomenon on Earth and in our own solar system is of great importance.

Point of Contact: Maura Rabbette
(650) 604-0128,
mrabbette@mail.arc.nasa.gov

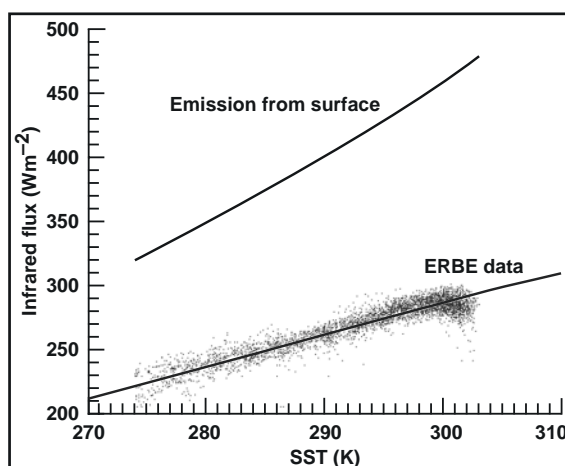


Fig. 1. According to Stefan-Boltzmann's law, the amount of heat energy radiated by the Earth's surface is proportional to $(T)^4$ (upper line). The output from MODTRAN, i.e., the modeled Top of Atmosphere Emission, is also displayed (lower line). The model incorporates user defined atmospheric pressure profiles and temperature profiles based on a moist adiabatic lapse rate as well as relative humidity profiles. Together these profiles give the best modeled fit (up to an SST of 300 K) to the Top of Atmosphere Emission.

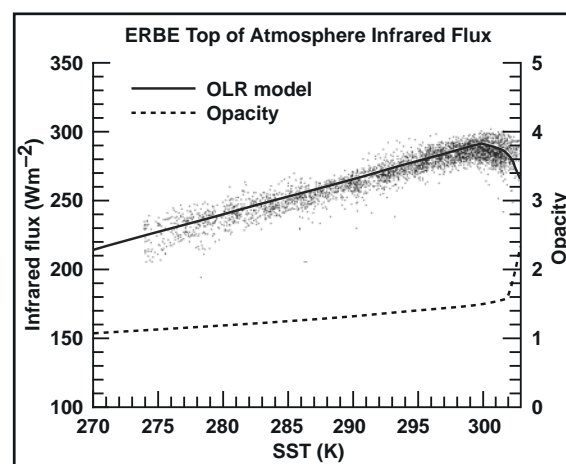


Fig. 2. The radiative transfer model was then used to reproduce the signature of the potential runaway greenhouse effect on Earth. For SST values 301-303 K, much higher concentrations of water vapor were introduced into the atmospheric profile. As a result, a turnaround and decrease in the outgoing longwave radiation model was achieved (solid line through ERBE data points). Also shown is the corresponding sharp increase in atmospheric opacity (dashed line).

Three-Dimensional Simulations of Polar Stratospheric Cloud Formation

Eric Jensen

Clouds composed of water ice and nitric acid form in the stratosphere over the Antarctic and Arctic during wintertime. These clouds have been definitively linked to ozone destruction due to heterogeneous chemical reactions on the particle surfaces. This process leads to the ozone hole over the Antarctic, and several studies have suggested the relatively minor ozone loss over the Arctic may worsen in the future.

A three-dimensional (3-D) model for simulation of these polar stratospheric clouds (PSCs) has been developed. With this model, calculations of the PSC properties and their effects over the entire hemisphere can be made. The model is driven by measured wind fields and temperatures. Microphysical processes are explicitly calculated, with 20 size bins for sulfate aerosols and cloud particles. The figure shows a snapshot of PSCs simulated during the Arctic winter of 1999/2000 during the NASA Stratospheric Aerosol and Gas Experiment (SAGE) III Ozone Loss and Validation Experiment (SOLVE). Validation of the simulations using aircraft and satellite measurements made during SOLVE is being done. The 3-D simulations are being used to calculate the vertical redistribution of nitric acid over the entire Arctic.

Preliminary modeling results suggest that the net removal of nitric acid is relatively insensitive to the threshold conditions for PSC

formation assumed. The 3-D model is also useful for providing a large-scale context for the localized in situ aircraft measurements. This modeling tool is expected to be useful for analysis and interpretation of future satellite measurements of PSCs.

Point of Contact: Eric Jensen
(650) 604-4392
ejensen@sky.arc.nasa.gov

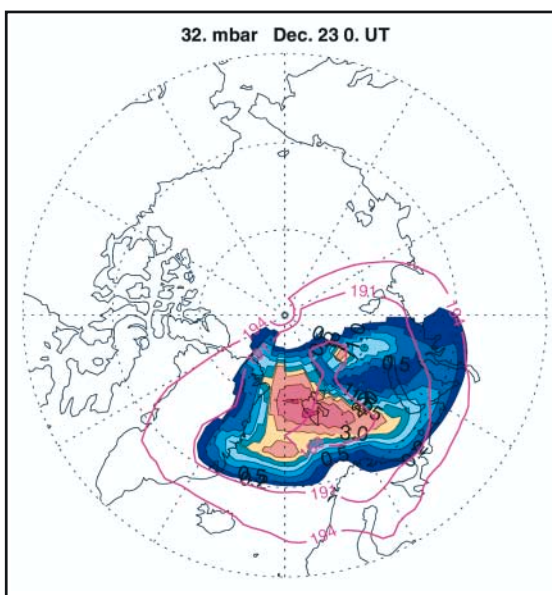


Fig. 1. Results from a three-dimensional simulation of Arctic PSCs during the winter of 1999–2000. Condensed nitric acid mixing ratio (color shading, parts per billion by volume) and temperature (red contours) are shown on the 32 millibar (mbar) pressure level, on December 23. The model indicates a large PSC extending from eastern Greenland over northern Russia.

REPORT DOCUMENTATION PAGE			Form Approved OMB No. 0704-0188	
Public reporting burden for this collection of information is estimated to average 1 hour per response, including the time for reviewing instructions, searching existing data sources, gathering and maintaining the data needed, and completing and reviewing the collection of information. Send comments regarding this burden estimate or any other aspect of this collection of information, including suggestions for reducing this burden, to Washington Headquarters Services, Directorate for Information Operations and Reports, 1215 Jefferson Davis Highway, Suite 1204, Arlington, VA 22202-4302, and to the Office of Management and Budget, Paperwork Reduction Project (0704-0188), Washington, DC 20503.				
1. AGENCY USE ONLY (Leave blank)		2. REPORT DATE June 2002		3. REPORT TYPE AND DATES COVERED Technical Memorandum
4. TITLE AND SUBTITLE Ames Research Center Research and Technology Report 2000			5. FUNDING NUMBERS	
6. AUTHOR(S) Ames Investigators				
7. PERFORMING ORGANIZATION NAME(S) AND ADDRESS(ES) Ames Research Center Moffett Field, CA 94035-1000			8. PERFORMING ORGANIZATION REPORT NUMBER A-0106853	
9. SPONSORING/MONITORING AGENCY NAME(S) AND ADDRESS(ES) National Aeronautics and Space Administration Washington, DC 20546-0001			10. SPONSORING/MONITORING AGENCY REPORT NUMBER NASA/TM-2001-210935	
11. SUPPLEMENTARY NOTES Point of Contact: Dr. Stephanie Langhoff, Chief Scientist, Ames Research Center, MS 230-3, Moffett Field, CA 94035-1000 (650) 604-6213 or contact the person(s) designated as the Point of Contact at the end of each article.				
12a. DISTRIBUTION/AVAILABILITY STATEMENT Unclassified — Unlimited Subject Category 99 Distribution: Standard Availability: NASA CASI (301) 621-0390			12b. DISTRIBUTION CODE	
13. ABSTRACT (Maximum 200 words) This report highlights the challenging work accomplished during fiscal year 2000 by Ames research scientists, engineers, and technologists. It discusses research and technologies that enable the Information Age, that expand the frontiers of knowledge for aeronautics and space, and that help to maintain U.S. leadership in aeronautics and space research and technology development. The accomplishments are grouped into four categories based on four of NASA's Strategic Enterprises: Aerospace Technology, Space Science, Biological and Physical Research, and Earth Science. The primary purpose of this report is to communicate knowledge—to inform our stakeholders, customers, and partners, and the people of the United States about the scope and diversity of Ames' mission, the nature of Ames' research and technology activities, and the stimulating challenges ahead. The accomplishments cited illustrate the contributions that Ames is making to improve the quality of life for our citizens and the economic position of the United States in the world marketplace.				
14. SUBJECT TERMS Aeronautics, Space transportation, Space sciences, Earth sciences, Life sciences, Information technology, Research and technology			15. NUMBER OF PAGES 196	
			16. PRICE CODE	
17. SECURITY CLASSIFICATION OF REPORT Unclassified	18. SECURITY CLASSIFICATION OF THIS PAGE Unclassified	19. SECURITY CLASSIFICATION OF ABSTRACT Unclassified	20. LIMITATION OF ABSTRACT	